QA: QA

Civilian Radioactive Waste Management System
Management & Operating Contractor

Waste Package Degradation Process Model Report

TDR-WIS-MD-000002 REV 00

March 2000

Prepared for:

U.S. Department of Energy
Yucca Mountain Site Characterization Office
P.O. Box 30307
North Las Vegas, Nevada 89036-0307

Prepared by:

TRW Environmental Safety Systems Inc.
1211 Town Center Drive
Las Vegas, Nevada 89144-6352

Under Contract Number
DE-AC08-91RW00134

INFORMATION COPY
LAS VEGAS DOCUMENT CONTROL

WM-11
DF03

DISCLAIMER

This report was prepared as an account of work sponsored by an agency of the United States Government. Neither the United States Government nor any agency thereof, nor any of their employees, nor any of their contractors, subcontractors or their employees, makes any warranty, express or implied, or assumes any legal liability or responsibility for the accuracy, completeness, or any third party's use or the results of such use of any information, apparatus, product, or process disclosed, or represents that its use would not infringe privately owned rights. Reference herein to any specific commercial product, process, or service by trade name, trademark, manufacturer, or otherwise, does not necessarily constitute or imply its endorsement, recommendation, or favoring by the United States Government or any agency thereof or its contractors or subcontractors. The views and opinions of authors expressed herein do not necessarily state or reflect those of the United States Government or any agency thereof.

DRAFT DISCLAIMER

This contractor document was prepared for the U.S. Department of Energy (DOE), but has not undergone programmatic, policy, or publication review, and is provided for information only. The document provides preliminary information that may change based on new information or analysis, and is not intended for publication or wide distribution; it is a lower level contractor document that may or may not directly contribute to a published DOE report. Although this document has undergone technical reviews at the contractor organization, it has not undergone a DOE policy review. Therefore, the views and opinions of authors expressed do not necessarily state or reflect those of the DOE. However, in the interest of the rapid transfer of information, we are providing this document for your information, per your request.

Civilian Radioactive Waste Management System
Management & Operating Contractor

Waste Package Degradation Process Model Report

TDR-WIS-MD-000002 REV 00

March 2000

Prepared by:

V. Pasupathi for JCF — 3/21/00

J.C. Farmer, PMR Lead
Waste Package Materials, LLNL

Date

V. Pasupathi — 3/21/00

V. Pasupathi, Deputy PMR Lead
Waste Package Materials

Date

Checked by:

D.A. Nitti — 3/21/00

D.A. Nitti, Project Manager
Waste Package Department

Date

Approved by:

David Stahl — 3/21/00

David Stahl, Manager
Waste Package Materials

Date

INTENTIONALLY LEFT BLANK

CONTENTS

Page

ACRONYMS AND ABBREVIATIONS xvii

1. INTRODUCTION 1-1
   1.1 OBJECTIVES 1-4
      1.1.1 Objectives of this Report 1-4
      1.1.2 Purpose of the Analysis and Model Reports 1-5
   1.2 SCOPE 1-5
   1.3 PRINCIPAL FACTORS AND OTHER FACTORS CONSIDERED 1-6
   1.4 QUALITY ASSURANCE 1-8
   1.5 WASTE PACKAGE DEGRADATION PROCESS AND ABSTRACTION MODELS 1-8
      1.5.1 Environment on the Surface of Drip Shield and Waste Package Outer Barrier 1-11
      1.5.2 Mechanisms for Early Failures 1-11
      1.5.3 Aging and Phase Stability of Waste Package Outer Barrier 1-11
      1.5.4 General Corrosion and Localized Corrosion 1-12
      1.5.5 Stress Corrosion Cracking 1-13
      1.5.6 Hydrogen Induced Cracking of Drip Shield 1-14
   1.6 SCREENING OF FEATURES, EVENTS, AND PROCESSES 1-14
   1.7 RELATIONSHIP TO OTHER PROCESS MODEL REPORTS AND DOCUMENTS 1-15

2. EVOLUTION OF THE PROCESS MODEL 2-1
   2.1 BACKGROUND 2-1
   2.2 PREVIOUS TREATMENT OF WASTE PACKAGE DEGRADATION MODELING 2-1
   2.3 TOTAL SYSTEM PERFORMANCE ASSESSMENT SITE RECOMMENDATION APPROACH 2-3
   2.4 ISSUES RELATED TO WASTE PACKAGE DEGRADATION 2-5

3. MODELS AND ABSTRACTED MODELS 3-1
   3.1 MODEL DESCRIPTIONS 3-1
      3.1.1 Overview of Waste Package and Drip Shield Design 3-1
      3.1.2 Early Failures 3-2
      3.1.3 Environment on the Surface of the Waste Package and Drip Shield 3-6
      3.1.4 Phase Stability and Aging 3-12
      3.1.5 General Corrosion 3-24

CONTENTS (Continued)

Page

3.1.6 Localized Corrosion 3-42
3.1.7 Stress Corrosion Cracking 3-69
3.1.8 Hydrogen Induced Cracking 3-85
3.1.9 Model Uncertainties 3-92
3.1.10 Model Validation 3-94
3.1.11 Alternative Approaches or Models 3-96
3.2 INTEGRATED MODEL 3-97
3.2.1 Conceptual Model for the Integrated Model 3-98
3.2.2 Abstraction of General Corrosion Models for Waste Package Outer Barrier and Drip Shield 3-102
3.2.3 Abstraction for Manufacturing Defects in Waste Package Closure Welds 3-107
3.2.4 Abstraction of Stress and Stress Intensity Factor Profile in Waste Package Closure Welds 3-109
3.2.5 Nominal Case Analysis of Drip Shield and Waste Package Degradation 3-112

4. RELATIONSHIP TO NRC ISSUE RESOLUTION STATUS REPORTS 4-1
4.1 SUMMARY OF THE KEY TECHNICAL ISSUES 4-1
4.2 RELATION OF THE WASTE PACKAGE PMR TO THE KEY TECHNICAL ISSUES 4-2
4.2.1 Container Life and Source Term 4-2
4.2.2 Total System Performance Assessment and Integration 4-4

5. SUMMARY AND CONCLUSIONS 5-1

6. REFERENCES AND INPUTS 6-1
6.1 DOCUMENTS CITED 6-1
6.2 CODES, STANDARDS, REGULATIONS, AND PROCEDURES 6-4

EXECUTIVE SUMMARY

Containing the waste and keeping water away from the waste package and the waste is a crucial element of the long-term post-closure safety strategy of the potential Yucca Mountain repository system. This report is one of nine Process Model Reports (PMRs) developed to address the technical basis supporting the Total System Performance Assessment (TSPA) model. These PMRs are supported by Analysis and Model Reports (AMRs) that contain the more detailed technical information used in each PMR and in the TSPA.

As a major component of the engineered barrier system, the waste package contributes to isolation of high-level radioactive waste during the preclosure and postclosure periods and it reduces the uncertainties associated with the performance of the repository. As a result, the performance of the waste package and the drip shield have been designated as "Principal Factors" important to the repository safety strategy. The waste package protected by a drip shield will be exposed to degradation processes and conditions in the repository environment that eventually have an impact on its post-closure performance. Some of the important conditions contributing to waste package degradation include: humidity and temperature in the emplacement drift, chemistry of the water dripping on the waste package, and corrosion properties of the waste package outer barrier. Eight process models or analyses, four abstraction models, and two engineering calculations were developed and documented in individual AMRs or Calculations. This PMR provides a summary of each of the process models and the abstraction models and a summary of their utilization in the integrated waste package degradation model contained in the WAPDEG code.

This report also includes discussions on the features, events, and processes (FEPs) relevant to the performance of the waste package materials. The FEPs that are deemed potentially important to repository performance are evaluated, either as components for the TSPA or as separate analyses in the AMR.

In addition to the description of the process models and the abstraction models, this PMR also addresses two of the Key Technical Issues and the related Issue Resolution Status Reports that the Nuclear Regulatory Commission considers important to the repository performance. These issues are the Container Life and Source Term (CLST) and the Total System Performance Assessment (TSPA) and Integration. Several subissues that relate directly to the waste package are discussed in this PMR along with the approach used by the Project to meet the acceptance criteria for each of the Key Technical Issue.

This PMR also addresses related issues identified by other agencies and organizations such as the Nuclear Waste Technical Review Board (NWTRB).

The integrated waste package model incorporated into in the WAPDEG code was used to develop the key results documented in this PMR. The waste package and drip shield degradation analyses have shown that based on the current corrosion model abstractions and assumptions, both the drip shields and waste packages do not fail within the regulatory time period (10,000 years). In particular, the waste package service lifetime is predicted to extend far beyond the regulatory time period (failure beginning at about 50,000 years). The materials selected for the drip shield (Titanium Grade 7) and the waste package outer barrier (Alloy 22) are

highly corrosion resistant and, under the repository exposure conditions, are expected to be immune to the degradation processes that, if initiated, could lead to failure in a shorter time period. Those degradation modes are localized corrosion (pitting and crevice corrosion), stress corrosion cracking (SCC), and hydrogen induced cracking (HIC) (applicable to drip shield only). Both the drip shield and waste package degrade by general corrosion at very low passive dissolution rates. The current experimental data and detailed process-level analyses, upon which the model abstractions incorporated in the WAPDEG analysis are based, have also indicated that the candidate materials would not be subject to those rapidly penetrating corrosion modes under the expected repository conditions, except for possibly the closure-lid welds of the waste package, if SCC were to occur there. To preclude SCC, weld stress mitigation will be implemented on a dual lid waste package closure weld design.

The estimated long life-time of the waste packages in the current analysis is attributed mostly to 1) the depth of the stress mitigation in the dual closure-lid welds and 2) the very low general-corrosion rate of the closure-lid welds which requires a very long time to corrode away the compressive stress zones, thus providing a very long delay time before initiating SCC crack growth.

FIGURES

Page

1-1. Waste Package 1-2
1-2. A View of a Typical In-Drift Placement at Waste Packages 1-3
1-3. Model Confidence Foundation 1-6
1-4. Schematic Representation of the Elements of Process Models Interrelationships among the Process Models and the AMRs Containing These Models 1-10
3-1. Size Distribution for Indicated Frequency of Occurrence for Outer Surface Breaking Flaws in Waste Package Alloy 22 Shell Welds 3-5
3-2. Size Distribution for Indicated Frequency of Occurrence of Outer Surface Breaking Flaws in Waste Package Alloy 22 Lid Welds 3-5
3-3. Deliquescence Point for Sodium Nitrate Solutions 3-9
3-4. Isothermal Time-Temperature-Transformation Diagram for Alloy 22 Base Metal 3-15
3-5. Effect of Thermal Aging at 649°C on the Precipitation of Intermetallic Phases at Grain Boundaries on Alloy 22 3-16
3-6. Time to Reach Various Stages of Precipitation in Aged Alloy 22 Base Metal Plotted on a Log Scale as a Function of Reciprocal Temperature (see Equation 3-5) 3-17
3-7. Graphical Extrapolation of the Curves to Repository-Relevant Temperatures 3-18
3-8. Graphical Extrapolation of the Limited Kinetic Data for Long Range Order in Alloy 22 Base Metal 3-21
3-9. Effect of Thermal Aging for 173 Hours at 700°C on the Corrosion Resistance of Alloy 22 in Simulated Acidic Concentrated Water at 90°C (DEA002 and DEA201) 3-22
3-10. Effect of Thermal Aging for 173 Hours at 700°C on the Corrosion Resistance of Alloy 22 in Simulated Concentrated Water at 90°C (DEA016, DEA202 and DEA203) 3-23
3-11. Schematic Representation of Model for General Corrosion and Localized Corrosion of Drip Shield and Waste Package Materials 3-25
3-12. Schematic Representation Showing Augmentation of Model for General Corrosion and Localized Corrosion to Account for Microbiologically Influenced Corrosion of Drip Shield and Waste Package Materials 3-26
3-13. Regression Analysis of Dry Oxidation Rate Data for Titanium 3-27
3-14. Range of Observed Penetration Rates for Stainless Steels 304 and 316 Shown as Cumulative Probability Distributions 3-29
3-15. Range of Observed Logarithms of Penetration Rates for Stainless Steels 304 and 316 Shown as Cumulative Probability Distributions 3-30
3-16. Range of Localized Penetration Rates for Stainless Steels 304 and 316 3-30
3-17. Comparison of Observed Penetration Rates for Stainless Steels 304 and 316 3-31
3-18. Two-Year General Corrosion Rate Data from Long Term Corrosion Test Facility Based Upon Generic Weight Loss Samples 3-35

FIGURES (Continued)

Page

3-19. Two-Year General Corrosion Rate Data from Long Term Corrosion Test Facility Based Upon Generic Crevice Samples 3-35
3-20. Two-Year General Corrosion Rate Data From Long Term Corrosion Test Facility Based Upon Both Generic Weight Loss and Crevice Samples, Including Those with Apparent Negative Rates 3-36
3-21. Two-Year General Corrosion Rate Data From Long Term Corrosion Test Facility Based Upon Both Generic Weight Loss and Crevice Samples, Excluding Those with Apparent Negative Rates 3-36
3-22. Combination of All General Corrosion Rate Data for Alloy 22 from Long Term Corrosion Test Facility, Including 6-, 12-, and 24-Month Exposures 3-37
3-23. Combination of All General Corrosion Rate Data for Alloy 22 from Long Term Corrosion Test Facility, Including 6-, 12-, and 24-Month Exposures with Negative Rates Excluded 3-37
3-24. General Corrosion of Titanium Grade 16: 12-Month Weight Loss Samples from Long Term Corrosion Test Facility 3-39
3-25. General Corrosion of Titanium Grade 16: 12-Month Crevice Samples From Long Term Corrosion Test Facility 3-40
3-26. Distribution of Positive General Corrosion Rates Based Upon Weight Loss and Crevice Samples 3-40
3-27. Distribution of Positive General Corrosion Rates with Variability Based Upon Weight Loss and Crevice Samples 3-41
3-28. Baseline – Platinum in Simulated Concentrated Water at 90°C (PT001) 3-45
3-29. Type 1– Alloy 22 in Simulated Acidic Concentrated Water at 90°C (DEA002) 3-45
3-30. Type 2 – Alloy 22 in Simulated Concentrated Water at 90°C (DEA016) 3-46
3-31. Type 3 – 316L in Simulated Saturated Water at 100°C (PEA016) 3-46
3-32. Alloy 22 in Various Repository Media – Comparison of Cyclic Polarization Data 3-48
3-33. Potentiostatic Polarization of Alloy 22 in Simulated Concentrated Water at 90°C and 200mV Versus Ag/AgCl 3-48
3-34. Cyclic Polarization Curve for Alloy 22 in 110°C Basic Saturated Water – Thermally Aged at 700°C for 10 Hours (DEA159) 3-49
3-35. Cyclic Polarization Curve for Alloy 22 in 110°C Basic Saturated Water – Thermally Aged at 700°C for 173 Hours (DEA208) 3-49
3-36. Titanium Grade 7 in Simulated Saturated Water at 120°C (NEA031s) 3-50
3-37. Titanium Grade 7 in Simulated Concentrated Water at 90°C (NEA003) 3-50
3-38. Potentials versus Temperature – Stainless Steel 316L in Simulated Acidic Concentrated Water 3-53
3-39. Potentials versus Temperature – Stainless Steel 316L in Simulated Concentrated Water 3-53
3-40. Potentials versus Temperature – Stainless Steel 316L in Simulated Saturated Water 3-54
3-41. Potentials versus Temperature – Alloy 22 in Simulated Dilute Water 3-54

FIGURES (Continued)

Page

3-42. Potentials versus Temperature – Alloy 22 in Simulated Concentrated Water 3-55
3-43. Potentials versus Temperature – Alloy 22 in Simulated Acidic Concentrated Water 3-55
3-44. Potentials versus Temperature – Alloy 22 in Simulated Saturated Water 3-56
3-45. Corrosion and Threshold Potentials of Titanium Grade 7 in Simulated Saturated Water (NEA031s) 3-56
3-46. Corrosion and Threshold Potentials for Titanium Grade 7 in Simulated Acidic Concentrated Water 3-57
3-47. Corrosion and Threshold Potentials for Titanium Grade 7 in Simulated Concentrated Water 3-57
3-48. Corrosion and Threshold Potentials for Titanium Grade 7 in Simulated Dilute Water 3-58
3-49. Effect of Molybdenum on the Critical Pitting Temperature of Stainless Steels in Ferric Chloride Solution 3-58
3-50. Effect of Pit Resistance Equivalence Number on the Critical Pitting and Crevice Corrosion Temperature of Stainless Steels in Ferric Chloride Solution 3-59
3-51. Effect of Hydrogen Peroxide on Corrosion Potential of Alloy 22 in Simulated Acidic Concentrated Water at 25°C 3-60
3-52. Effect of Hydrogen Peroxide on Corrosion Potential of Alloy 22 in Simulated Concentrated Water at 25°C 3-61
3-53. Effect of Chromium Content in Ni-Cr Alloys on Ultimate Crevice pH 3-62
3-54. Concentrations of Dissolved Metals in Stainless Steel 304 Crevice Exposed to 0.1 N NaCl 3-62
3-55. Stainless Steel 316L, 4M NaCl, 200 mV & 23°C – Crevice pH versus Time 3-65
3-56. Alloy 22, 4M NaCl at 23°C – Crevice pH versus Time 3-65
3-57. Determination of Crevice pH for Waste Package Materials 3-66
3-58. Finite Element Model for the Initial WPOB Design and Selected Cross-Sections for Stress Plots 3-74
3-59. Radial Stress - Initial WPOB Outer Lid at 125C 3-74
3-60. Hoop Stress - Initial WPOB Outer Lid at 125C 3-75
3-61. Flaw Orientations for Lid Welds 3-75
3-62. Stress Intensity Factor for Radial Crack in Initial WPOB Outer Lid 3-77
3-63. Schematic and Dimensions for Dual-Lid WPOB Design 3-78
3-64. Measured Hoop Stress with and without Laser Peening Showing Stress Threshold for SCC. (Figure modified from that in the AMR) 3-79
3-65. Calculated Stress Intensity Factor for Hoop Stress with and without Laser Peening. Threshold Stress Intensity Factor for SCC is also Shown. (Figure modified from that in the AMR) 3-79
3-66. A Schematic of the Dual Closure-Lid Design of Waste Package Outer Barrier 3-101

FIGURES (Continued)

Page

3-67. The Variability Cumulative Distribution Functions for the General Corrosion Rate of Waste Package Outer Barrier Using 25%-75%, 50%-50%, and 75%-25% Uncertainty and Variability Partitioning Ratios and 50th Uncertainty Percentile 3-104

3-68. The Variability Cumulative Distribution Functions for the General Corrosion Rate of the Alloy 22 Waste Package Outer Barrier Using 25%-75%, 50%-50%, and 75%-25% Uncertainty and Variability Partitioning Ratios and 25th Uncertainty Percentile 3-104

3-69. The Variability Cumulative Distribution Functions for the General Corrosion Rate of the Alloy 22 Waste Package Outer Barrier Using 25%-75%, 50%-50%, and 75%-25% Uncertainty and Variability Partitioning Ratios and 75th Uncertainty Percentile 3-105

3-70. The Variability Cumulative Distribution Functions for the General Corrosion Rate of the Ti-7 Drip Shield Using 25%-75%, 50%-50%, and 75%-25% Uncertainty and Variability Partitioning Ratios and 50th Uncertainty Percentile 3-105

3-71. The Variability Cumulative Distribution Functions for the General Corrosion Rate of Ti-7 Drip Shield Using 25%-75%, 50%-50%, and 75%-25% Uncertainty and Variability Partitioning Ratios and 25th Uncertainty Percentile 3-106

3-72. The Variability Cumulative Probability Distribution Functions for the General Corrosion Rate of Ti-7 Drip Shield Using 25%-75%, 50%-50%, and 75%-25% Uncertainty and Variability Partitioning Ratios and 75th Uncertainty Percentile 3-106

3-73. Cumulative Probability for the Occurrence of Defects in the Welds of the Outer (25-mm thick) and Inner (10-mm thick) Lids of Waste Package Outer Barrier 3-109

3-74. Conditional Probability Density Functions of Defect Sizes in the Closure Lid Welds for Various Combinations of Values for the Location and Scale Parameters (b & v) 3-110

3-75. Hoop Stress as a Function of Depth in the Alloy 22 Outer-Lid Welds (25-mm thick) at the Reference Location on the Outer-Lid Weld Circumference and the Uncertainty Range 3-113

3-76. Stress Intensity Factor as a Function of Radial Crack in the Alloy 22 Outer-Lid Welds (25-mm thick) at the Reference Location on the Outer-Lid Weld Circumference and the Uncertainty Range 3-113

3-77. Hoop Stress as a Function of Depth in the Alloy 22 Outer-Lid Welds (25-mm thick) at 0°, 90° and 180° Angles Along the Circumference of the Outer-Lid Weld 3-114

3-78. Stress Intensity Factor as a Function of Radial Crack in the Alloy 22 Outer-Lid Welds (25-mm thick) at 0°, 90° and 180° Angles Along the Outer-Lid Weld Circumference 3-114

3-79. Hoop Stress as a Function of the Projected Depth in the Alloy 22 Inner-Lid Welds (10-mm thick) at the Reference Location on the Inner-Lid Weld Circumference and the Uncertainty Range 3-115

FIGURES (Continued)

Page

3-80. Stress Intensity Factor as a Function of the Projected Radial Crack Depth in the Alloy 22 Inner-Lid Welds (10-mm thick) at the Reference Location on the Inner-Lid Weld Circumference and the Uncertainty Range 3-115

3-81. Hoop Stress as a Function of the Projected Depth in the Alloy 22 Inner-Lid Welds (10-mm thick) at 0°, 90° and 180° Angles Along the Circumference of the Inner-Lid Weld 3-116

3-82. Stress Intensity Factor as a Function of the Projected Radial Crack Depth in the Alloy 22 Inner-Lid Welds (10-mm thick) at 0°, 90° and 180° Angles Along the Inner-Lid Weld Circumference 3-116

3-83. The Upper and Lower Bounds, Median, and 95th, 75th, 25th and 5th Percentile Confidence Intervals of the First Breach Profile of Waste Packages with Time 3-121

3-84. The Upper and Lower Bounds, Median, and 95th, 75th, 25th and 5th Percentile Confidence Intervals of the First Breach Profile of Drip Shield with Time 3-121

3-85. The Upper and Lower Bounds, Median, and 95th, 75th, 25th and 5th Percentile Confidence Intervals of the First Crack Breach Profile of Waste Packages with Time 3-122

3-86. The Upper and Lower Bounds, Median, and 95th, 75th, 25th and 5th Percentile Confidence Intervals of the First Patch Breach Profile of Waste Packages with Time 3-122

INTENTIONALLY LEFT BLANK

TABLES

Page

1-1. Principal Factors, Other Factors, and the PMRs Where Addressed 1-7
1-2. Primary FEP Summary for Waste Package and Drip Shield Degradation 1-16
2-1. Key External Issues for the Waste Package Degradation Process Model Report 2-6
3-1. Summary of Estimated Probabilities and Performance Consequences for Various Types of Waste Package Defects 3-7
3-2. Composition of Standard Test Media Based upon J-13 Well Water 3-10
3-3. Initial Basic Saturated Water Solution Recipe 3-11
3-4. Modified Basic Saturated Water Solution Recipes 3-12
3-5. Intermetallic Phases Observed in Alloy 22 with Transmission Electron Microscopy 3-14
3-6. Time Required for Precipitation of Intermetallic and Carbide Particles on the Grain Boundaries of Alloy 22 Base Metal 3-14
3-7. Summary of the Distribution of Rates for General Corrosion of Alloy 22 Samples 3-38
3-8. Summary of Error Analysis for Corrosion Rates Based Upon Weight Loss of Alloy 22 3-41
3-9. Summary of Error Analysis for Corrosion Rates Based Upon Weight Loss of Titanium Grade 16 3-42
3-10. Electrochemical Potentials Determined from Cyclic Polarization of Alloy 22 in Basic Saturated Water 3-47
3-11. Distribution of Localized Corrosion Rates for Alloy 22 3-67
3-12. Distribution of Localized Corrosion Rates for Titanium Grade 7 3-67
4-1. Issue Resolution Status Reports, Subissues, Technical Acceptance Criteria, and PMR Approach 4-6

INTENTIONALLY LEFT BLANK

ACRONYMS AND ABBREVIATIONS

AFM	atomic force microscope or microscopy
AMR	Analysis and Model Report
ASTM	American Society for Testing and Materials
BSW	basic saturated water
BWR	boiling water reactor
CAM	corrosion allowance material
CDF	cumulative distribution function
CLST	container life and source term
CRM	corrosion resistant material
CRWMS	Civilian Radioactive Waste Management System
DIRS	Document Input Reference System
DIS	Data Inventory Sheet
DOE	U.S. Department of Energy
DTN	data tracking number
EBS	engineered barrier system
FEP	features, events and processes
GB	grain boundary
HLW	high-level waste
IRSR	Issue Resolution Status Report
J-13	Water from Well No. J-13
KTI	key technical issue
LC	localized corrosion
LLNL	Lawrence Livermore National Laboratory
LRO	long-range order
M	molarity
MIC	microbiologically influenced corrosion
M&O	Management and Operating Contractor
N	normality
NFE	near field environment
NRC	U.S. Nuclear Regulatory Commission
OCRWM	Office of Civilian Radioactive Waste Management

ACRONYMS AND ABBREVIATIONS (Continued)

PA	Performance Assessment
PMR	Process Model Report
PND	probability of nondetection
ppm	parts per million
QA	Quality Assurance
QARD	Quality Assurance Requirements and Description Document
RH	relative humidity
SAW	simulated acidified water
SCC	stress corrosion cracking
SCW	simulated concentrated water
SDW	simulated dilute water
SEM	scanning electron microscopy
SSW	simulated saturated water
TBD	to be determined
TBV	to be verified
TDMS	Technical Data Management System
TEM	transmission electron microscope
TSPA	Total System Performance Assessment
UNS	Unified Numbering System for Metals and Alloys
UT	ultrasonic testing
WAPDEG	waste package degradation code
WF	waste form
WP	waste package
WPOB	waste package outer barrier
wt. %	weight percent
XRD	X-ray diffraction
YMP	Yucca Mountain Project

1. INTRODUCTION

Containing the waste and keeping water away from the waste package and the waste is a crucial element of the long-term post-closure safety strategy of the potential Yucca Mountain repository system. There are many potential degradation processes that could impact the performance of the engineered barrier system. The role of this PMR is to describe the process models utilized to evaluate the degradation processes that may affect the performance of the repository. To evaluate the postclosure performance of a potential repository at Yucca Mountain, a Total System Performance Assessment (TSPA) will be conducted. A set of nine Process Model Reports (PMR)s, of which this document is one, is being developed to summarize the technical basis for each of the process models supporting the TSPA model. These reports cover the following areas:

- Integrated Site Model
- Unsaturated Zone Flow and Transport
- Near Field Environment
- Engineered Barrier System Degradation, Flow, and Transport
- Waste Package Degradation
- Waste Form Degradation
- Saturated Zone Flow and Transport
- Biosphere
- Disruptive Events.

These PMRs are supported by Analysis and Model Reports (AMRs) that contain the more detailed technical information to be input into each PMR and the TSPA. This technical information consists of data, analyses, models, software, and supporting documentation that will be used to defend the applicability of each process model for its intended purpose of evaluating the postclosure performance of the potential Yucca Mountain repository system. The PMR process will ensure the traceability of this information from its source through the AMRs, PMRs, and eventually to how that information is used in the TSPA.

As described in the *Monitored Geologic Repository Project Description Document*, the recommended waste package design is Enhanced Design Alternative II (CRWMS M&O 1999a).

The Enhanced Design Alternative II waste package design is the reverse of the Viability Assessment design. In Enhanced Design Alternative II, the corrosion-resistant material protects the underlying structural material from corrosion while the structural material supports the thinner more expensive corrosion-resistant material. As shown in Figure 1-1, this design includes a double-wall waste package made from Alloy 22 and 316 stainless placed underneath a protective drip shield made of titanium.

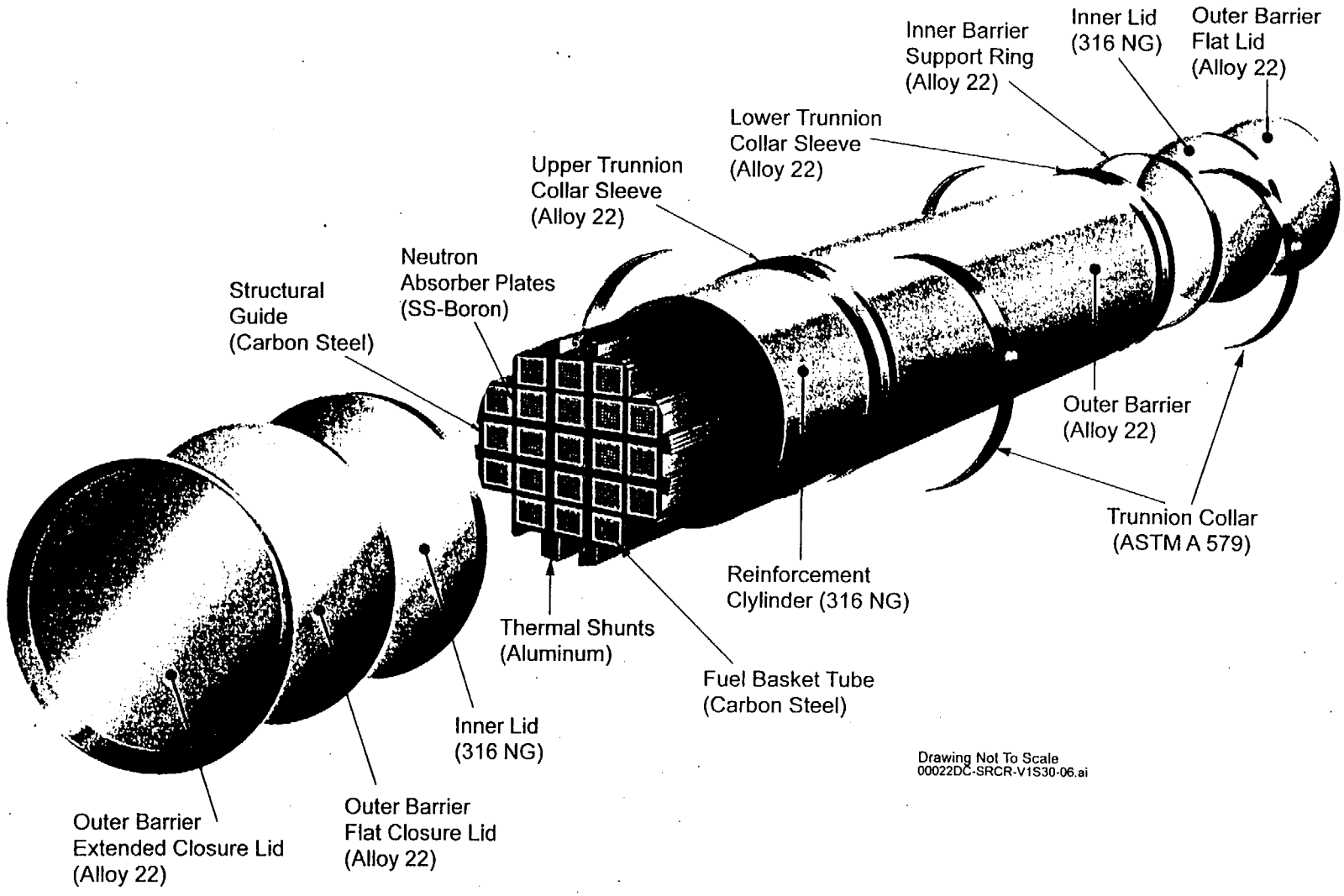

Figure 1-1. Waste Package

Enhanced Design Alternative II uses thermal management features (line loading, ventilation, and blending) to limit peak temperatures of cladding, the waste package shell, and the drift wall. This produces more uniform temperature along the drifts, and margin in meeting requirements for cladding integrity, drift stability, and avoidance of localized corrosion of the waste package materials. Figure 1-2 shows a typical layout of an in-drift placement of three different waste packages. Note that drip shields will be placed over the waste packages just before repository closure to provide protection from water.

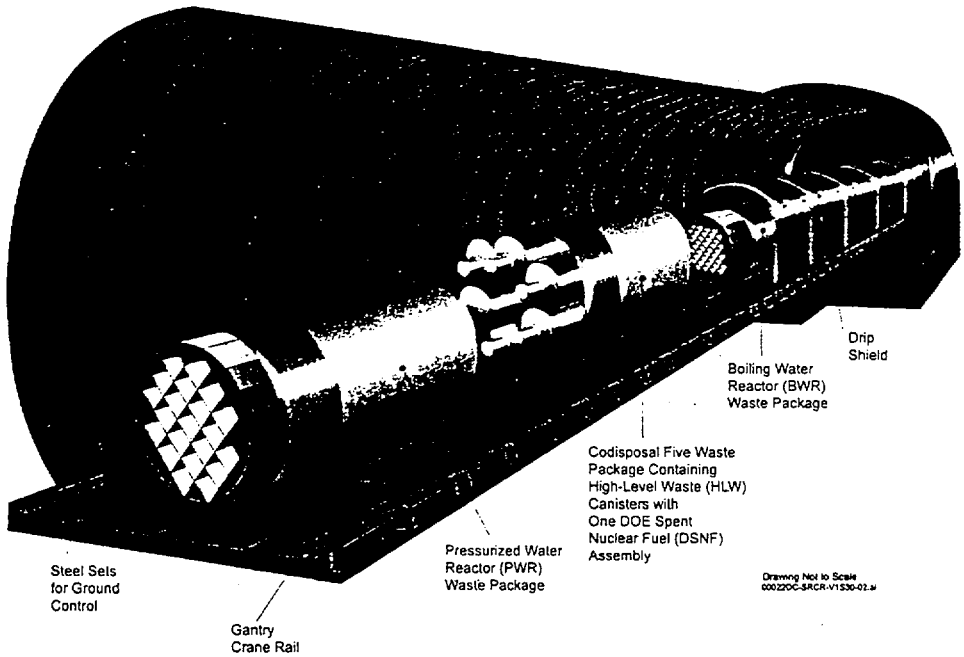

Figure 1-2. A View of a Typical In-Drift Placement at Waste Packages

The purpose of the PMR on waste package degradation is to account for the degradation of the waste package materials under the expected conditions of the Yucca Mountain site, which is being evaluated as a potential site for a geologic repository for the disposal of nuclear waste. The different types of data pertaining to the waste package material degradation are represented in various model reports. Functional summaries of the component models and their respective output are provided in Section 1.4. This report was developed in accordance with the technical product development plan *Development Plan for Waste Package Degradation Process Model Report* (CRWMS M&O 1999b).

Each of the process models of the Waste Package Degradation PMR considers different specific processes of the material degradation and the waste package degradation code (WAPDEG) (CRWMS M&O 2000g) represents an overall synthesis of these process models. Each model was developed using unique methodologies and inputs, and the determination of the models for each of the waste package components is dependent on the functional requirements of that component. This PMR summarizes the individual waste package component degradation models and describes how the component models are related and combined to evaluate the overall waste

package and drip shield performance. A detailed description of each component model is provided in each respective AMR.

In January 2000, the Project modified the repository design. The changes instituted consist of removing the backfill from the reference design and reorienting the drifts to minimize the impacts of the rockfall. Preparation of this PMR and the supporting AMRs has preceded this design change and therefore, do not include their potential impacts. However, a qualitative assessment has been made of their potential impacts on the results of the process models and the respective AMRs. For the waste package PMR, the design change directly affects the following AMRs and the results contained in them.

- Stress Corrosion Cracking of the Drip Shield, the Waste Package Outer Barrier and the Stainless Still Structural Material.
- Abstraction of Models for the Stress Corrosion Cracking of Drip Shield and Waste Package Outer Barrier and Hydrogen Induced Cracking of Drip Shield.
- WAPDEG Analysis of Waste Package and Drip Shield Degradation.

At this time, the AMR on the stress corrosion cracking assumes that the drip shield is protected by backfill from rockfall induced stresses and therefore, stress corrosion cracking. Removal of the backfill may subject the drip shield to localized areas of stresses due to rockfall and increase the susceptibility to stress corrosion cracking. The abstraction AMR on stress corrosion and the WAPDEG analysis AMR are similarly affected. While a more detailed analysis is required to quantify the impact of the design change, preliminary analysis shows that any stress corrosion cracks in the drip shield will not result in the dripping of water on the waste package. This is due to the cracks becoming plugged with corrosion products.

In addition to the increased susceptibility to stress corrosion cracking, the drip shield may also be subjected to increased corrosion due to rockfall induced cold worked regions. Preliminary review of literature indicates that this is not a significant issue. However a more detailed evaluation is necessary.

It is planned to address these issues in the next versions of the AMRs.

1.1 OBJECTIVES

1.1.1 Objectives of this Report

The objectives of this report are to document waste package and drip shield material degradation models with regard to the data input methodologies used to construct the model, uncertainties and limitations of the modeling results, and model validation. This report summarizes the following:

- Sources of data input
- Methodologies used to construct the model components
- Modeling results, uncertainties, and limitations.

Assumptions that are specific to the individual models are listed in Chapter 3. Additional details of model assumptions can be found in Chapter 5 of the individual AMRs.

1.1.2 Purpose of the Analysis and Model Reports

The principal purpose of the Waste Package AMRs is to provide documentation of the degradation process models, under the expected Yucca Mountain environment, for subsequent use in performance assessment modeling, thermal studies, and TSPA studies. The subsequent process models are used to analyze release of radionuclides from the waste package and their transport in the saturated zone and the unsaturated zone. Figure 1-3 shows the model inputs, outputs and the laboratory test information that forms the bases for the confidence in the model results.

1.2 SCOPE

The waste package degradation PMR describes processes that will lead to degradation of the waste package components within the near field environment (NFE). Specific technical information contained in the waste package degradation PMR consists of data, analyses, models, software, and supporting documents. The waste package degradation PMR also provides a technical basis for the applicability of the overall integrated model for its intended purpose of evaluating aspects of postclosure performance of the Yucca Mountain repository system.

The waste package degradation PMR provides information about important environmental factors that affect waste package and drip shield lifetimes such as the thermal, hydrologic, and geochemical processes acting on waste package and drip shield surfaces. The waste package degradation PMR uses inputs from other companion documents, which include those that describe the Engineered Barrier System (EBS) design, the EBS PMR, and the NFE PMR. Inputs also include outputs from the TSPA.

Chapter 2 of this PMR describes the evolution of the waste package degradation model. Details of the individual models and analyses are provided in Chapter 3. Chapter 4 describes the NRC Issue Resolution Status Report relevant to this PMR. Acceptance criteria and responses to these criteria are addressed in this chapter. Summary and conclusions are provided in Chapter 5.

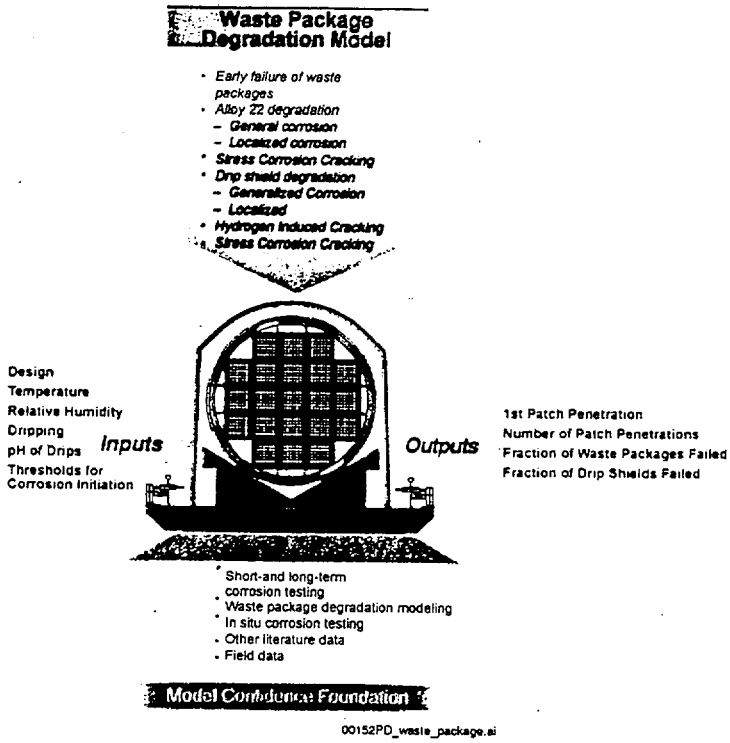

Figure 1-3. Model Confidence Foundation

1.3 PRINCIPAL FACTORS AND OTHER FACTORS CONSIDERED

The magnitude of the YMP and the complexities associated with both the natural and engineered barrier systems dictate that the YMP prioritize its activities and focus on the factors most important to performance, hereafter named the Principal Factors. The Repository Safety Strategy (RSS) (YMP 1999) has identified seven Principal Factors and twenty Other Factors of second-order importance. The selection of the Principal Factors was based on preliminary TSPA analyses and expert judgment, which showed that these factors significantly affected the performance of the potential repository. The Other Factors were deemed to have minimal effects on the repository performance in terms of dose to the accessible environment. Table 1-1 lists the seven Principal Factors, the twenty Other Factors, and the PMRs that address each factor. The WP PMR has the following Principal Factors:

1. Performance of the drip shield
2. Performance of the waste package barriers.

Performance of the drip shield is a principal factor since it represents the diversion of seepage away from the waste package. This factor defines the timing and amount of water transmitted through the drip shield.

Performance of the waste package barriers is a principal factor for the post closure safety case because this factor defines the timing and amount of water transmitted into the waste package and affects the rate of release of radionuclides.

Table 1-1. Principal Factors, Other Factors, and the PMRs Where Addressed

Principal Factor (Nominal Scenario)	Process Model Report
Seepage into drifts	Unsaturated Zone Flow and Transport
Performance of the drip shield	Waste Package Degradation
Performance of the waste package barriers	Waste Package Degradation
Solubility limits of dissolved radionuclides	Waste Form Degradation
Retardation of radionuclide migration in the unsaturated zone	Unsaturated Zone Flow and Transport
Retardation of radionuclide migration in the saturated zone	Saturated Zone Flow and Transport
Dilution of radionuclide concentrations during migration	Saturated Zone Flow and Transport
Other Factors (Nominal Scenario)	
Climate	Unsaturated Zone Flow and Transport
Net Infiltration into the mountain	Unsaturated Zone Flow and Transport
Unsaturated zone flow above the repository	Unsaturated Zone Flow and Transport
Coupled processes - effects on unsaturated zone flow	Unsaturated Zone Flow and Transport
Coupled processes - effects on seepage	Near Field Environment
Environments on the drip shield	Engineered Barrier System Degradation, Flow, and Transport
Environments on the waste package	Engineered Barrier System Degradation, Flow, and Transport
Environments within the waste package	Waste Form Degradation
CSNF waste form performance	Waste Form Degradation
DHLW glass waste form performance	Waste Form Degradation
DSNF, Navy fuel, Pu disposition waste form performance	Waste Form Degradation
Colloid-associated radionuclide concentrations	Waste Form Degradation
In-package radionuclide transport	Waste Form Degradation
Transport through the drift invert	Engineered Barrier System Degradation, Flow, and Transport
Advective pathways in the unsaturated zone	Unsaturated Zone Flow and Transport
Colloid-facilitated transport in the unsaturated zone	Unsaturated Zone Flow and Transport
Coupled processes – effects on unsaturated zone transport	Unsaturated Zone Flow and Transport
Advective pathways in the saturated zone	Saturated Zone Flow and Transport
Colloid-facilitated transport in the saturated zone	Saturated Zone Flow and Transport
Biosphere transport and uptake	Biosphere
Factors For Disruptive Event Scenarios	
To be determined; see Section 3.5 for preliminary considerations (YMP 1999)	Disruptive Events

The general guidelines for addressing these factors are to try to bound the effects of the Other Factors, when possible, and perform analyses that are conservative. Principal Factors will be studied and evaluated more thoroughly, using both the most realistic evaluations, and bounding analyses if this is warranted by other aspects of the site performance.

1.4 QUALITY ASSURANCE

The Quality Assurance program applies to this analysis. All types of waste package designs were classified as Quality Level-1. This report applies to all of the waste package designs included in the Monitored Geologic Repository Classification Analyses. *Classification of the MGR Uncanistered Spent Nuclear Fuel Disposal Container System* (CRWMS M&O 1999c) is cited as an example of a waste package type. The development of this report is conducted under activity evaluation *Analysis Model Reports* (CRWMS M&O 1999d), which was prepared per QAP-2-0, *Conduct of Activities*. The results of that evaluation were that the activity is subject to the *Quality Assurance Requirements and Description* (DOE 2000) requirements.

The Waste Package Degradation PMR was prepared in accordance with AP-3.11Q, *Technical Reports* and reviewed in accordance with AP-2.14Q, *Review of Technical Products*. The AMRs that support this PMR were prepared in accordance with AP-3.10Q, *Analyses and Models*.

The status of the data supporting this PMR are included in the supporting AMRs and in the DIRS database. The data are incorporated in the TDMS. Data verification and qualification were carried out in accordance with procedures AP-3.15Q and AP-SIII.2Q, respectively.

This PMR includes the results from the following software codes used in the supporting AMRs. However, no software codes were used in the development of this PMR. Following statements on the software codes are presented for information only.

ANSYS, Version 5.3 which is a finite element analysis code used for thermal and stress analyses.

pcCRACK, Version 3.1 which is a fracture mechanics code used for stress intensity and crack growth simulation analyses.

WAPDEG, Version 4.0 which is used to determine waste package and drip shield failure fractions as a function of time.

1.5 WASTE PACKAGE DEGRADATION PROCESS AND ABSTRACTION MODELS

The waste package degradation process models consist of several individual process models or analyses and associated abstraction models.

In all, eight (8) process models or analyses and six (6) abstraction models and two engineering calculations were developed and documented in individual AMRs or Calculations. These are listed below.

Process Models or Analyses
Analysis of Mechanisms for Early Waste Package Failures, Document Identifier DI # ANL-EBS-MD-000023 (CRWMS M&O 2000m)
Environment on the Surface of Drip Shield and Waste Package Outer Barrier, DI # ANL-EBS-MD-000001 (CRWMS M&O 2000a)
Aging and Phase Stability of Waste Package Outer Barrier, DI # ANL-EBS-MD-000002 (CRWMS M&O 2000b)
General Corrosion and Localized Corrosion of Waste Package Outer Barrier, DI # ANL-EBS-MD-000003 (CRWMS M&O 2000c)
General Corrosion and Localized Corrosion of Drip Shield, DI # ANL-EBS-MD-000004 (CRWMS M&O 2000d)
Stress Corrosion Cracking of the Drip Shield, the Waste Package Outer Barrier and the Stainless Steel Structural Material, DI # ANL-EBS-MD-000005 (CRWMS M&O 2000f)
Hydrogen Induced Cracking of Drip Shield, DI # ANL-EBS-MD-000006 (CRWMS M&O 2000h)
Degradation of Stainless Steel Structural Material, DI # ANL-EBS-MD-000007 (CRWMS M&O 2000e)
Abstraction Models and Calculations
WAPDG Analysis of Waste Package and Drip Shield Degradation, DI # ANL-EBS-PA-000001 (CRWMS M&O 2000g)
Abstraction of Models of Stress Corrosion Cracking of Drip Shield and Waste Package Outer Barrier, DI # ANL-EBS-PA-000004 (CRWMS M&O 2000j)
FEPs Screening of Processes and Issues in Drip Shield and Waste Package Degradation, DI # ANL-EBS-PA-000002 (CRWMS M&O 2000l)
Abstraction of Models for Pitting and Crevice Corrosion of Drip Shield and Waste Package Outer Barrier, DI # ANL-EBS-PA-000003 (CRWMS M&O 2000n)
Calculation of Probability and Size of Defect Flaws in Waste Package Closure Welds to Support WAPDEG Analysis, DI # CAL-EBS-PA-000003 (CRWMS M&O 2000k)
Calculation of General Corrosion Rate of Drip Shield and Waste Package Outer Barrier to Support WAPDEG Analysis, DI # CAL-EBS-PA-000002 (CRWMS M&O 2000i)
Abstraction of Models for Stainless Steel Structural Material Degradation, DI #ANL-EBS-PA-000005 (CRWMS M&O 2000o)
Incorporation of Uncertainty and Variability of Drip Shield and Waste Package Degradation in WAPDEG Analysis, DI # ANL-EBS-MD-000036 (CRWMS M&O 2000p)

The results from the last two AMRs (CRWMS M&O 2000o and CRWMS M&O 2000p) are not being used as input to the waste package degradation nominal case analysis. This is because stainless steel inner shell is not being considered a corrosion barrier and therefore not assigning any performance credit to this shell is a conservative approach. The AMR on the uncertainty and variability requires additional data to develop the model further and will be included in the next version of the PMR. For this PMR, the uncertainty and variability are included in the bounding approach used in the process and abstraction models.

Figure 1-4 shows the elements of each process model and interrelationships among the various process models and the AMRs containing them. For example, the process model for general and localized corrosion of the waste package outer barrier includes dry oxidation, humid air corrosion, and expected environment on the surface. A brief overview of each of these models is presented below. Details of the process models and abstraction models are presented in the AMRs and in Chapter 3.

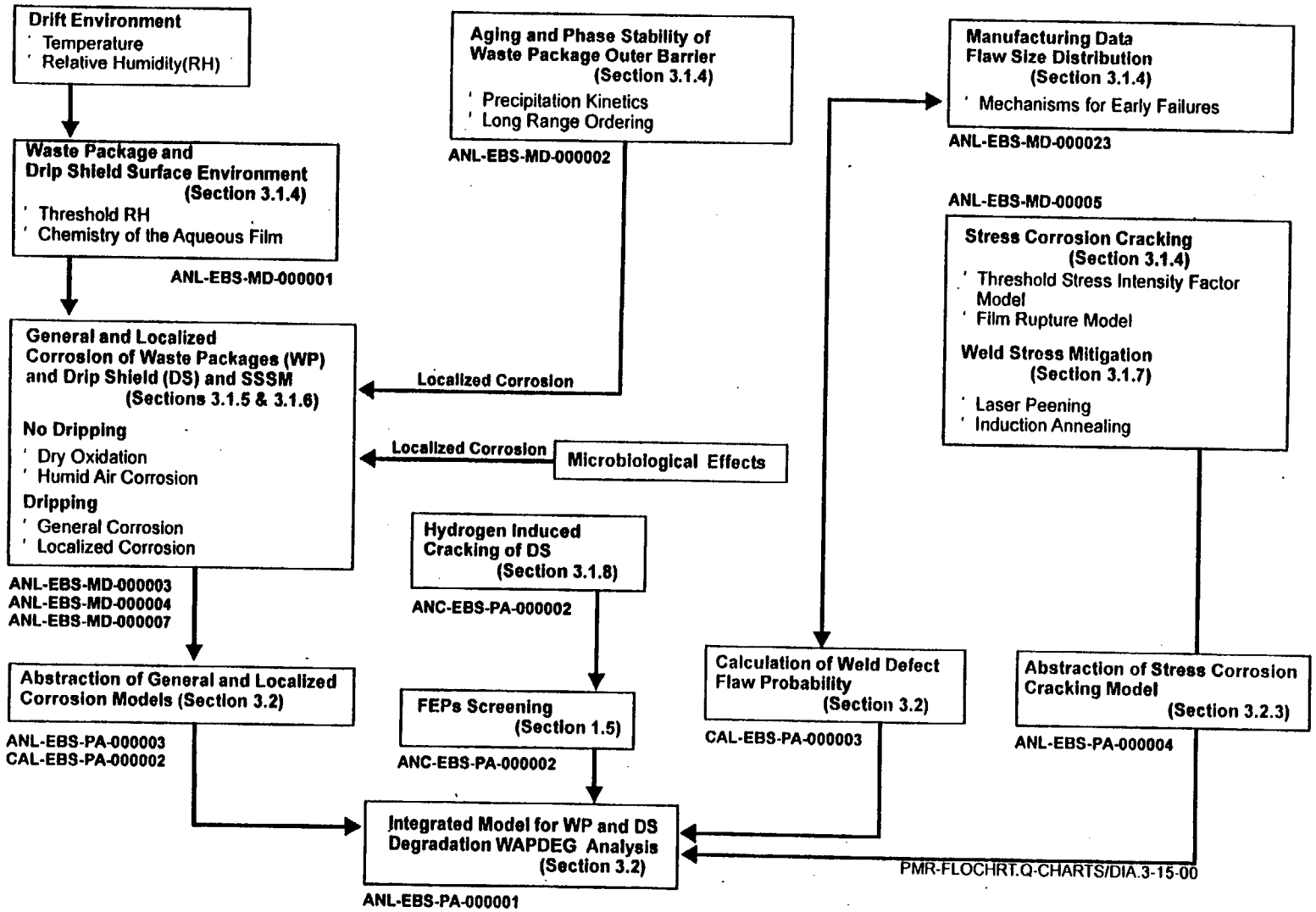

Figure 1-4. Schematic Representation of the Elements of Process Models Interrelationships among the Process Models and the AMRs Containing These Models

1.5.1 Environment on the Surface of Drip Shield and Waste Package Outer Barrier

Information provided below is based on the parent AMR (CRWMS M&O 2000a) and is described in Section 3.1.3. This process model addresses the evolution of the chemistry of the water film on the drip shield and waste package outer barrier (WPOB) as a function of temperature and relative humidity. The concentrations of aqueous salt solutions that can form on the hot waste package surface due to deposited hygroscopic salts are determined experimentally and theoretically (based upon chemical thermodynamics). Hygroscopic salts may be deposited on surfaces by seepage water and episodic water flow, as well as by dust and aerosols entrained in ventilation air.

These concentrations define the medium for testing waste package materials under a worst-case scenario. An example is the development of a simulated saturated water with an elevated boiling point (120-127°C).

Abstracted models are developed for the evolution of environments on the exposed surfaces of the drip shield and WPOB as a function of time and location within the repository. These abstracted models are in forms that are suitable as inputs to the WAPDEG analysis and include the uncertainty and variability of exposure conditions. Additional information on the WAPDEG code is presented in Section 2.2.

1.5.2 Mechanisms for Early Failures

Information provided below is based on the parent AMR (CRWMS M&O 2000m) and is described in greater detail in Section 3.1.2. This analysis addresses the potential for early failures of the waste package due to material defects, as well as defects from waste package fabrication processes. These fabrication processes include welding. The probability of waste package fabrication defects, their uncertainty and variability, and the consequences of the defects on waste package failure times (e.g., number of potential failure sites and flaw size distribution) are discussed.

Abstracted calculations are developed for the occurrence and size distribution of defect flaws from material and manufacturing defects in the waste package. Abstracted calculations include uncertainty and variability of the above properties.

1.5.3 Aging and Phase Stability of Waste Package Outer Barrier

Information provided below is based on the parent AMR (CRWMS M&O 2000m) and is described in greater detail in Section 3.1.4. This process model addresses degradation of the WPOB resulting from exposure to elevated temperatures. In the case of Alloy 22 and related materials, such thermal histories can result in the formation of precipitates (μ, P, σ and other undesirable phases). These precipitates can form within the individual grains, or at grain boundaries. Precipitation can cause embrittlement, thereby increasing susceptibility to damage due to rock fall and impact. Since these precipitates may be rich in molybdenum and chromium, two of the alloying elements responsible for the high degree of passivity of Alloy 22, aging can also result in increased susceptibility to general and localized corrosion, as well as to stress corrosion cracking (SCC). The time-temperature-transformation curve and an expression for

estimating the volume fraction of precipitates in the grain boundary have been developed for Alloy 22. Estimates of uncertainty are made. The effect of aging on corrosion has been addressed, and has been determined to be a corrosion enhancement factor of 2.5 for the fully aged material.

1.5.4 General Corrosion and Localized Corrosion

Information provided below is based on three separate AMRs (CRWMS M&O 2000c, 2000d, and 2000e) and is described in greater detail in Sections 3.1.5 and 3.1.6. Three separate process models were developed and these address both general corrosion and the localized corrosion of the drip shield, waste package outer barrier (WPOB), and the stainless steel structural material. The current design uses Titanium Grade 7 as the drip shield, Alloy 22 as the WPOB, and stainless steel 316NG as the stainless steel structural material. This process model includes several sub-models for dry oxidation, humid air corrosion and vapor phase corrosion, general corrosion in the aqueous phase, and localized corrosion in the aqueous phase. Note that "dry oxidation" and "dry air oxidation" are synonymous terms. While the stainless steel structural material is not specifically intended to be a corrosion barrier, it may affect the chemistry of water entering the waste package and retard the rate of radionuclide release from the breached waste package. Given the limited availability of data for 316NG stainless steel, data for 316L stainless steel are used as representative. This is appropriate since the composition of the two materials are very similar, aqueous corrosion characteristics are expected to be similar. Microbial corrosion is addressed under localized corrosion (Section 3.1.6.8).

1.5.4.1 Dry Oxidation

The process model for corrosion of the drip shield and waste package materials includes a component model (sub-model) for dry oxidation. It is assumed that dry oxidation (or dry air oxidation) can be treated as a single mode of attack, general corrosion. Corrosion rates are estimated as a function of temperature to the extent possible.

1.5.4.2 Humid Air Corrosion & Vapor Phase Corrosion

The process model for corrosion of the drip shield and waste package materials accounts for humid air corrosion and vapor phase corrosion. It is assumed that humid air and vapor phase corrosion are treated as a single mode of attack, general corrosion. To the extent possible, corrosion rates are estimated as a function of temperature.

1.5.4.3 Aqueous Phase Corrosion

The process model for aqueous phase corrosion of the drip shield and waste package accounts for both general corrosion and localized corrosion. In method A, the threshold potential for localized attack of the material is determined from experimentally determined cyclic polarization data obtained with relevant test media. Relevant test environments include simulated dilute water, simulated concentrated water and simulated acidic water at 30, 60, and 90°C, as well as simulated saturated water at 100 and 120°C. The compositions of simulated dilute water and simulated acidic concentrated water are 10X and 1,000X concentrations of J-13 well water, respectively. More recently, basic saturated water has been included in the set of standard test

media. In method A, localized corrosion rates are invoked when the expected open circuit corrosion potential exceeds the threshold potential. If the threshold for localized corrosion is not exceeded, it is assumed that the mode of attack is general corrosion. In method B, the threshold temperature for localized attack at the open circuit corrosion potential is determined from published literature data or from tests at elevated temperature and pressure. General corrosion rates are estimated from various sources of available test data, including weight loss measurements from the Long Term Corrosion Test Facility, as well as measurements of the corrosion current density. If the localized corrosion threshold is exceeded, the rates of penetration and failure mode characteristics (e.g., number failure sites and opening size) are estimated from experimental measurements of crevice corrosion made at Lawrence Livermore National Laboratory. Since pitting has not been observed in laboratory experiments at Lawrence Livermore National Laboratory, the primary mode of localized corrosion is expected to be crevice corrosion. This aqueous phase corrosion model will be applied to each unit area of the waste package exterior surface.

Abstracted models have been developed to account for general corrosion of the drip shield and waste package materials. The abstracted models include thresholds for initiation of various modes of corrosion, as well as the corresponding rates of penetration. The abstracted models are in forms that are suitable for input to the WAPDEG analysis. The relative humidity and temperature thresholds for initiation of humid air corrosion and aqueous phase corrosion are included, as well as the electrochemical potential for initiation of localized corrosion during aqueous phase corrosion. In the case of the drip shield and WPOB, distributions of general corrosion rates are based upon data from the Long Term Corrosion Test Facility, while published data is used as the basis of estimating localized corrosion rates. Both general corrosion and localized corrosion rates of 316NG stainless steel are based upon published data. Estimates of the uncertainty and variability of each quantity are provided. Sufficient information is also provided to enable determination of expected failure mode characteristics (e.g., number failure sites and opening size).

1.5.5 Stress Corrosion Cracking

The process model for the stress corrosion cracking is documented in the AMR (CRWMS M&O 2000f) and is described in Section 3.1.7. Stress corrosion cracking of materials may occur when a combination of material susceptibility, tensile stresses and appropriate environment are present. This process model accounts for the possibility of SCC of the drip shield, the WPOB, and the stainless steel structural material. The model evaluates two alternative methods: method A based on stress intensity threshold factor criterion for initiation of SCC ($K_I > K_{ISCC}$); and method B based upon a finite rate of SCC propagation. The rate of SCC propagation is dependent upon the local environment and the stress intensity factor at the crack tip. The stresses for initiation and propagation of SCC are due to unannealed closure welds, deformation caused by rock fall, and the weight of the waste package. First, appropriate stress analysis models and measurements are used to calculate the through-wall stress distribution for the waste package for representative cross sections, including unwelded base metal, and unannealed welds. This stress distribution is used to calculate a corresponding stress intensity factor distribution for flaws that range in size from zero to the entire thickness of the wall. This stress intensity factor distribution is used as input for both method A and method B. In method A, SCC initiates at pre-existing flaws that develop during fabrication of the waste package, or at flaws that develop

during localized corrosion. Values of K_{ISCC} published in the technical and scientific literature, or determined with the double cantilever beam technique is employed in method A. In method B, the SCC propagation rate is calculated as a function of local environment and stress intensity factor. The time-to-failure is determined by integrating the calculated propagation rate. Relevant test environments include simulated dilute water, simulated concentrated water and simulated acidic concentrated water at 30, 60, and 90°C, as well as simulated saturated water at 100 and 120°C.

Abstracted models have been developed for SCC of the waste package outer barrier (Alloy 22). These abstracted models include: 1) a threshold stress for initiation; 2) a crack growth rate as a function of stress and local exposure conditions, including temperature; 3) crack density; and 4) crack morphology. Crack morphology includes a description of the size of openings. The abstracted models are in a form that is suitable for input to the WAPDEG analysis, and include the uncertainty and variability of the above processes.

1.5.6 Hydrogen Induced Cracking of Drip Shield

This process model establishes the conditions under which the drip shield (Titanium Grade 7) will experience hydrogen uptake, potentially leading to hydrogen embrittlement and hydrogen induced cracking. Hydrogen induced cracking is not a credible degradation model for Alloy 22 and has been excluded as shown in Section 1.6 below.

1.6 SCREENING OF FEATURES, EVENTS, AND PROCESSES

The initial set of features, events and processes (FEPs) have been developed for the Yucca Mountain Project (YMP) TSPA by combining lists of FEPs identified as relevant to the YMP. This combined list consists of 1,261 FEP entries from the Nuclear Energy Agency working group, 292 FEPs from YMP literature and site studies, and 82 FEPs identified during YMP project staff workshops. The FEPs have been identified by a variety of methods including expert judgement, informal elicitation, event tree analysis, stakeholder review, and regulatory stipulation. All potentially relevant FEPs have been included, regardless of origin. The compilation included FEP entries mentioned above and 151 layers, categories and headings. It resulted in a FEP list of 1786. This approach has led to considerable redundancy in the FEP list, because the same FEPs are frequently identified by multiple sources, but it also ensures that a comprehensive review of narrowly defined FEPs will be performed.

Each FEP has been identified as either a Primary or Secondary FEP. The classification resulted in the identification of 310 Primary FEPs. Primary FEPs are those for which detailed screening arguments are developed. The classification and description of Primary FEPs strives to capture the essence of all the Secondary FEPs that map to the primary. Secondary FEPs are either FEPs that are completely redundant or that can be aggregated into a single Primary FEP. The Primary FEPs have been assigned to associated PMRs. The assignments were based on the nature of the FEPs so that the analysis and resolution for screening decisions reside with the subject-matter experts in the relevant disciplines. The resolution of other than system-level FEPs are documented in AMRs prepared by the responsible PMR groups. This section summarizes the screening decisions associated with the FEPs for the waste package and drip shield PMR group.

Details of the screening processes are documented in the associated AMR (CRWMS M&O 2000l).

The scope of the FEPs screening is to identify the treatment of the Primary FEPs affecting waste package and drip shield degradation. The FEPs that are deemed potentially important to repository performance are evaluated, either as components for the TSPA or as separate analyses in the AMR. The scope for this activity involves two tasks, namely:

Task 1: Identify FEPs that are considered explicitly in the TSPA (called included FEPs) and the AMRs in which these FEPs are addressed

Task 2: Identify FEPs not included in TSPA (called excluded FEPs) and provide justification for why these FEPs do not need to be a part of the TSPA model.

Of the original list of FEPs, twenty-eight have been identified as Primary FEPs in relationship to waste package and drip shield degradation. The approach used for this analysis is a combination of qualitative and quantitative screening. The analyses are based on the criteria provided by the Nuclear Regulatory Commission in the proposed 10 CFR Part 63 (Dyer 1999) and by the U.S. Environmental Protection Agency in the proposed 40 CFR Part 197 (64 FR 46976) to determine whether or not each FEP should be included in the TSPA. For FEPs that are excluded from the TSPA based on Nuclear Regulatory Commission or U.S. Environmental Protection Agency criteria, the screening argument includes a summary of the basis and results that indicate either low probability or low consequence. As appropriate, screening arguments cite work performed outside this activity, such as in other AMRs. For FEPs that are included in the TSPA, the TSPA disposition includes a reference to the AMR that describes how the FEP has been incorporated in the process models or the TSPA abstraction models.

The FEPs screening analysis results for the twenty-eight Primary FEPs relevant to waste package and drip shield degradation processes are summarized in Table 1-2. This table shows the FEP number, FEP name, screening decision (include/exclude) and justification for the "Exclude" decision. Details of the screening processes and arguments are given in the accompanying AMR (CRWMS M&O 2000l).

1.7 RELATIONSHIP TO OTHER PROCESS MODEL REPORTS AND DOCUMENTS

This PMR provides information about important environmental factors affecting waste package lifetime such as the thermal, hydrologic, and geochemical processes acting on the waste package surfaces. The PMR uses inputs from other PMRs, such as the EBS PMR and Near Field PMR, and provides outputs to the EBS design and TSPA. The emphasis of the discussion of model inputs and outputs is on information needed for the assessment of postclosure performance. The waste package degradation PMR supports the TSPA and other major Project milestones, such as the Site Recommendation and the License Application.

While the scope of this PMR is to address degradation of the waste package and the drip shield, other PMRs (such as the EBS PMR) address other aspects of drip shield and EBS component performance.

Table 1-2. Primary FEP Summary for Waste Package and Drip Shield Degradation

FEP Number	FEP Name	Screening Decision	Justification
1.1.03.01.00	Error in waste or backfill emplacement	Exclude	Low probability
1.2.02.03.00	Fault movement shears waste container	Exclude	Low probability
1.2.03.02.00	Seismic vibration causes container failure	Exclude	Low consequence; Design requirements
1.2.04.04.00	Magma interacts with waste	Include	
2.1.03.01.00	Corrosion of waste containers	Include	
2.1.03.02.00	Stress corrosion cracking of waste containers	Include	
2.1.03.03.00	Pitting of waste containers	Include	
2.1.03.04.00	Hydride cracking of waste containers	Exclude	Low probability
2.1.03.05.00	Microbially-mediated corrosion of waste container	Include for WP; Exclude for DS	Low consequence
2.1.03.06.00	Internal corrosion of waste container	Exclude	Low consequence
2.1.03.07.00	Mechanical impact of waste container	Exclude	Low consequence; Design requirements
2.1.03.08.00	Juvenile and early failure of waste containers	Include for WP; Exclude for DS	Low probability; Design requirements
2.1.03.09.00	Copper corrosion	Exclude	Low probability; Not applicable to WP design
2.1.03.10.00	Container healing	Exclude	Low consequence; Not applicable to WP corrosion
2.1.03.11.00	Container form	Exclude	Low consequence
2.1.03.12.00	Container failure (long term)	Include	
2.1.06.06.00	Effects and degradation of DS	Include	
2.1.06.07.00	Effects of material interfaces	Include	
2.1.07.01.00	Rockfall (large block)	Exclude	Low consequence
2.1.07.05.00	Creeping of metallic materials in the EBS	Exclude	Low consequence
2.1.09.03.00	Volume increase of corrosion products	Exclude	Low consequence
2.1.09.09.00	Electrochemical effects in waste and EBS	Exclude	Low consequence
2.1.10.01.00	Biological activity in waste and EBS	Include for WP; Exclude for DS	Low consequence
2.1.11.05.00	Differing thermal expansion of repository components	Exclude	Low consequence
2.1.11.06.00	Thermal sensitization of waste containers increases fragility	Include for WP; Exclude for DS	Low probability
2.1.12.13.00	Gas generation (H2) from metal corrosion	Exclude	Low consequence
2.1.13.01.00	Radiolysis	Exclude	Low consequence
2.1.13.02.00	Radiation damage in waste and EBS	Exclude	Low consequence

2. EVOLUTION OF THE PROCESS MODEL

2.1 BACKGROUND

The overall performance of the waste package and drip shield materials has been identified as key factors in the performance of the repository. It is expected that the lifetime goals for the drip shield and waste package may be increased in the future. Therefore, materials and designs that prolong service life are sought.

The reference design used in the viability assessment (VA) has been estimated to experience first through-wall failure by pit penetration in about 2,700 years, with about 1% of the packages failing in approximately 10,000 years. This estimate is based upon models of waste package degradation (WAPDEG) used as input to Total System Performance Assessment (TSPA) (CRWMS M&O 1998, TSPA-VA, Chapter 5). However, the goals of the Yucca Mountain Project have been continuously pushed towards longer waste package lifetimes, thereby requiring that the repository exceed performance requirements of the VA design by a significant margin. Accordingly, a selection process for alternative materials and designs intended to provide higher levels of confidence for an extended waste package lifetime was undertaken. This process resulted in the selection of a double-walled waste package placed under a protective drip shield made of Titanium Grade 7. The outer wall of the waste package is corrosion-resistant Alloy 22, with an inner wall of stainless steel (316NG) that serves as a structural support. This new design is known as Enhanced Design Alternative-II. The selection of this new design configuration, coupled with the selection of new materials, has necessitated the development of new models to predict corrosion rates of waste package degradation. Individual component models (sub-models) are documented in the individual analysis and model reports (AMRs). Each AMR is provided as an input to the Waste Package Degradation Process Model Report (PMR), as well as to the TSPA for Site Recommendation.

2.2 PREVIOUS TREATMENT OF WASTE PACKAGE DEGRADATION MODELING

Modeling of waste package degradation has evolved over the past decade along with changes in materials selected for its containment barriers. Early waste package designs consisted of thin walled stainless steel canister with a heavy walled carbon steel overpacks and were designed for the salt, basalt and tuff repositories. The overpack component design thicknesses were the sum of the structural thickness required, plus the corrosion allowance necessary to assure that the required structural thickness will survive the required containment period. The corrosion allowance was established on the basis of the calculated package surface temperature profile through the containment period, the unexpected presence of an unlimited quantity of anoxic brine, and the resulting corrosion rate.

In late 1987, the U.S. Congress passed the Nuclear Waste Policy Amendments Act (DOE 1995), which reduced the number of potential repository sites to be characterized to one: Yucca Mountain. Prior to this event, work on the waste package design for Yucca Mountain had followed the same rationale as that for salt and basalt repositories. In fact, the initial conceptual design of the waste package developed in early 1983 was the same as that for the other two repositories. However, it was recognized that the expected conditions in Yucca Mountain were quite different from the other two in that the repository was located in the unsaturated zone. The

environment in this zone, although not firmly established, was expected to be oxidizing but dry with low humidity most of the time. The design temperature for the waste package surfaces would not exceed 250°C. Liquid water was expected to be present only under transient conditions, and its composition was not expected to be very aggressive from a corrosion standpoint.

The limitations of 304L stainless steel, from the standpoint of stress corrosion cracking and localized corrosion had been recognized from early on, and alternative materials were being sought. In 1993, the design was changed from thin-walled containers emplaced in bore holes to drift emplaced robust multibarrier waste packages. The proposed materials were Alloy 825 as the inner barrier and a corrosion allowance material "such as weathering steel" as an outer barrier. Degradation modeling of this waste package design included only the aqueous phase corrosion. It was assumed that no corrosion would occur above the temperature at which liquid-phase water could not exist on the waste package surface.

Model enhancements were incorporated in 1995 and were based upon the same double-wall waste package design that was used in 1993. This model attempted to account for humid air corrosion and aqueous phase corrosion. The aqueous phase corrosion model had components that simulated pitting corrosion and galvanic coupling of the corrosion allowance material (CAM) and corrosion resistant materials (CRM). This model included estimates of the variability in waste package corrosion, i.e., waste package-to-waste package and patch-to-patch variability were both accounted for. Estimates of the uncertainty in the threshold relative humidity for initiation of humid air corrosion and aqueous phase corrosion were also made. An empirical model for general corrosion and localized corrosion of the corrosion allowance materials was developed based upon published literature data. Rates of general corrosion and localized corrosion of the corrosion resistant material were based upon the collective opinion of a panel of experts (expert elicitation). The model assumed that galvanic protection would delay localized corrosion (pitting) of the CRM until a specified percentage of the CAM thickness had been consumed by general corrosion.

Exposure conditions included temperature, relative humidity, presence of liquid-phase water (dripping), water chemistry, backfill, and rock fall.

Along with the improvements in the degradation modeling, the evaluation of materials selection for the waste package barriers continued during the following several years. The corrosion resistant material, Alloy 825, was replaced with a more corrosion resistant nickel-based Alloy 625 during this period. The lifetime goals for the waste package was increased further and resulted in the selection of Alloy 22 as the corrosion resistant barrier for the Viability Assessment design.

Additional waste package corrosion model improvements were made for the Viability Assessment design. This model accounted for humid-air general corrosion and localized corrosion of the CAM; aqueous-phase general corrosion and localized corrosion of the CAM; and aqueous-phase general corrosion and localized corrosion of the CRM. Degradation of the waste package was modeled by dividing the surface into patches and populating the corrosion rates stochastically over the patches. The concept of a localization factor was used. Pitting of the CAM was assumed to occur at pH $\geq$ 10.

Microbiologically influenced corrosion (MIC) and stress corrosion cracking (SCC) were not accounted for in the TSPA models used for VA. The effects of salt deposition and evaporative concentration of dripping water on the waste package surface were also neglected. These models were not based upon qualified experimental data from materials testing in repository-relevant environments but relied heavily on the opinion of experts and other published data. For this PMR, a range of laboratory data and associated process models have been developed to more realistically approximate the degradation processes of potential significance to repository performance. Changes to the degradation models have been necessitated by the changes in waste package design and inclusion of the drip shield in the Site Recommendation (SR).

2.3 TOTAL SYSTEM PERFORMANCE ASSESSMENT SITE RECOMMENDATION APPROACH

The approach in the TSPA-SR waste package degradation analysis is an enhanced version of that used in TSPA-VA. (For convenience of discussion in this section, the drip shield is modeled as an integral part of waste package, and no separate discussion is given for drip shield.) The WAPDEG model, which is based on a stochastic approach, is used for the SR waste package degradation analysis. The purposes of the stochastic approach and the WAPDEG model are three-fold:

- provide realistic representation of waste package degradation processes in the repository;
- capture the effects of variation and uncertainty both in exposure conditions and degradation processes over a geologic time scale; and
- perform analysis within a reasonable time and within computational resources.

Abstracted models of the process models for implementation in the WAPDEG model were developed in such a manner that important features of the process models are captured as explicitly as possible and that the degradation processes and their characteristics are properly represented in the waste package degradation analysis. More details of the TSPA-SR approach to waste package and drip shield degradation analysis are given in the supporting AMR (CRWMS M&O 2000g – *WAPDEG Analysis of Waste Package and Drip Shield Degradation*).

As in the TSPA-VA analysis, effects of spatial and temporal variations in the exposure conditions over the repository were modeled by incorporating explicitly relevant exposure condition histories into the waste package degradation analysis. The exposure condition parameters that were considered to be varying over the repository are relative humidity and temperature at the waste package surface, seepage into the emplacement drift, chemistry of seepage water, and rockfall. In addition, potentially variable corrosion processes within a single waste package were represented by dividing the waste package surface into unit areas called "patches" and stochastically populating the corrosion model parameter values and/or corrosion rates over each patch. The model parameter values and corrosion rates were sampled from their distribution over the range of the expected local exposure conditions.

In the nominal case analysis, the waste package outer barrier and drip shield were included in the waste package degradation analysis. The stainless-steel inner container, which is to provide structural support to waste package, is not included in the degradation analysis. Although, in reality, this container would provide some performance for waste containment after the outer barrier breach and also provide a barrier to radionuclide transport after the waste package is breached, the potential performance credit was ignored in the nominal TSPA-SR analysis. This is a conservative approach.

The TSPA-SR waste package degradation analysis included the following potentially important degradation processes:

- general corrosion
- localized (pitting and crevice) corrosion
- stress corrosion cracking (SCC)
- microbiologically influenced corrosion (MIC)
- long-term aging and phase instability of waste package outer barrier (WPOB) and their effect on corrosion, and
- pre-existing manufacturing defects in the waste package closure welds and its effect on stress corrosion cracking.

Significant improvements were made to the general and localized corrosion models that were used in TSPA-VA. In the analysis, the drip shield was considered to be immune to stress corrosion cracking because it will be fully annealed before it is placed in the emplacement drift. Likewise, all the fabrication welds in the waste package, except the welds for the closure lids, will be fully annealed. Therefore they were assumed not subject to SCC. Therefore, only the waste package closure lids were considered in the SCC analysis. In addition, two alternative SCC models, the slip dissolution model and the threshold stress intensity factor model, were considered. The radiolysis effect on corrosion is insignificant under the repository exposure conditions (see Section 3.1.6.6), and thus it was not considered in the nominal case analysis. The drip shield was assumed to be immune to the microbiologically influenced corrosion. The bounding analyses have shown that the hydrogen uptake by the drip shield is much less than the threshold hydrogen concentration required to cause hydrogen induced cracking under the repository exposure condition (CRWMS M&O 2000h), and thus the hydrogen induced cracking is not included in the drip shield degradation model.

The WAPDEG analysis tracks corrosion degradation of waste packages for three penetration modes: stress corrosion cracking (crack penetration), pitting and crevice corrosion (pit and crevice penetration), and general corrosion (patch penetration). The analysis provides, as output, the cumulative probability of waste package failure by one of the three penetration modes as a function of time and also provides the number of penetrations for each of the penetration modes as a function of time. The waste package failure time and penetration number profiles are used

as input to other TSPA analyses, such as the waste form degradation and the radionuclide release rate from waste packages.

The TSPA-SR analysis yields a more explicit representation (than previous TSPA analyses) of the uncertainty and variability in waste package degradation (i.e., waste package failure and penetration number profiles). For the corrosion models and parameters for which data and analyses are available, their uncertainty and variability were quantified and incorporated into the WAPDEG analysis. For other models and parameters for which the uncertainty and variability are not quantifiable, the variance in their value was assumed, and used as uncertainty. In the TSPA-SR analysis, waste package degradation was analyzed with multiple realizations of WAPDEG for the uncertainty analysis of the uncertain corrosion parameters—each WAPDEG realization corresponding to a complete WAPDEG run to account for the waste package degradation variability for a given number of waste packages. Accordingly, each of the WAPDEG analysis outputs (i.e., waste package failure time, crack penetration number, pit penetration number, and patch penetration number) are reported as a group of "curves" that represent the potential range of the output values.

2.4 ISSUES RELATED TO WASTE PACKAGE DEGRADATION

This PMR also addresses related issues identified based on a review of the past two years Advisory Committee on Nuclear Waste (ACNW) and Nuclear Waste Technical Review Board (NWTRB) meeting summaries and correspondences, Viability Assessment (VA) Volume 3, Sections 6.5.2 and 6.5.3 and Volume 4 Section 4.3, TSPA peer review documentation, U.S. Nuclear Regulatory Commission comments on TSPA-VA, expert elicitation recommendations, and licensing correspondence files for the U.S. Nuclear Regulatory Commission, the State of Nevada, and the Nevada counties. Table 2-1 provides a summary of all identified issues and describes how each issue is addressed in this PMR. In addition, acceptance criteria from the Container Life and Source Term Issue Resolution Status Report (NRC 1999) and Total System Performance Assessment (TSPA) and Integration (NRC 1998) are separately addressed in Table 4.2-1 in Chapter 4 of this document.

Table 2-1. Key External Issues for the Waste Package Degradation Process Model Report

Source	Issue	PMR Approach
Viability Assessment, Volume 3, Sec. 6.5.2 (DOE 1998)	Physical events and processes such as degradation of drift with time due to chemical and mechanical effects that have a potential for affecting the WP performance were not considered, or not sufficiently covered, within the TSPA-VA.	Degradation of the drift with time could result in rock fall, which can impact the DS and WP and increase potential for SCC. The incorporation of SCC as a failure mode initiated by rockfall (Section 3.1.7) addresses this issue.
Viability Assessment, Volume 3, Sec. 6.5.2 (DOE 1998)	The panel believes that there is insufficient data to support the selection of the material for use in the final WP design.	Selection process for WP package materials has considered and evaluated all degradation processes. Several materials have been electrochemically tested, with a clear indication that Alloy 22 and Titanium Grade 7 are more corrosion resistant than other candidate materials. Section 3.1.1 provides an overview of the WP materials selected.
Viability Assessment, Volume 3, Sec. 6.5.2 (DOE 1998)	Uncertainties and limitations in WP degradation models (SCC, crevice corrosion, and WP surface chemistry) need to be verified.	In regard to crevice corrosion, experimental studies have been performed to define the crevice chemistry (pH, etc.). In regard to SCC, alternative models are employed. Stress mitigation techniques are being used as a means of eliminating SCC through elimination of the driving force (see Section 3.1.7). Details of these degradation modes are provided in the respective AMRs and PMR sections (Section 3.1.3, 3.1.6, and 3.1.7).
Viability Assessment, Volume 3, Sec. 6.5.2 (DOE 1998)	The issue states the need for additional research on water contact with the WP, critical crevice temperatures, Np solubility and technetium sorption on degraded WP.	Evaporative concentration experiments have been used to determine the concentrations of saturated electrolytes that may form on the surface of the hot WP (see Section 3.1.3). Critical crevice potentials and temperatures for the WP barrier materials have been determined and documented in the various AMRs and PMR Section 3.1.6. Np solubility and technetium sorption are not part of the scope of this PMR but are addressed in waste form degradation PMR.
Viability Assessment, Volume 3, Sec. 6.5.3.2 (DOE 1998)	The rationale for including or excluding any potentially significant feature, event or process needs to be technically justified and clearly articulated.	Identification of features, events, and processes are discussed in Section 1.6.
Viability Assessment, Volume 3, Sec. 6.5.3.3 (DOE 1998)	Modeling assumptions should be consistent across different process models, unless there is a defensible technical rationale.	The AMRs that document assumptions for WP degradation are subject to thorough interdisciplinary reviews to help ensure consistency among assumptions made in more than one document about a given parameter. In addition, the PMR that summarize and integrate the results of the AMRs has been subjected to a review by a single review team, one of whose main objectives is to identify inconsistencies among the PMRs. Finally, assumptions used in the AMRs that feed WP degradation are documented in the WP PMR document. These measures provide confidence that consistent assumptions are used as appropriate among the various models that support the WP PMR.

Table 2-1. Key External Issues for the Waste Package Degradation Process Model Report (Continued)

Source	Issue	PMR Approach
Viability Assessment, Volume 3, Sec. 6.5.3.7 (DOE 1998)	Rockfall effects need to be considered in the design and performance of the Yucca Mountain repository system.	Analyses of seismically induced rockfall damage have been explicitly addressed in TSPA-SR.
NWTRB Letter to DOE (11-10-99) (Cohen 1999a)	The presentation on WP degradation indicated that valuable information is being collected on Alloy 22 at a rapid pace. However, concern still exists about the effects on corrosion of radiolytic species, including species formed in the vapor phase. Resolving that concern may necessitate additional experimental and theoretical work.	Experiments have been performed to determine the maximum increase in corrosion potential that can be caused by hydrogen peroxide, the primary product formed during gamma radiolysis of water. The maximum increase is approximately 200 mV, which is insufficient to cause initiation of LC with materials such as Alloy 22 (Section 3.1.6).
NWTRB Letter to DOE (8-3-99) (Cohen 1999b)	Regarding the engineered repository system, NWTRB highlights four areas: the need to vigorously pursue ongoing studies of degradation associated with stress-corrosion cracking and phase instability of proposed WP materials; the need to determine whether presently unrecognized corrosion mechanisms exist that would be important over the very long term; the need to complete experiments on the formation of radiolysis products in the near field and to model the effects of such radiolysis products on near field component degradation; and the need to intensify investigations into the performance of a titanium DS and the effect this DS and associated backfill would have on other elements of the engineered system.	Ongoing SCC studies are underway at the Corporate Research and Development Center of General Electric Corporation and at Lawrence Livermore National Laboratory. All credible modes of corrosion such as phase stability and SCC are considered in the testing program and the WAPDEG code, so that the unexpected can be accounted for. Experiments have been performed to determine the maximum increase in corrosion potential that can be caused by hydrogen peroxide, the primary product formed during gamma radiolysis of water. The maximum increase is approximately 200 mV, which is insufficient to cause initiation of LC with materials such as Alloy 22. For example, a series of CP of Titanium Grade 7 have been performed in test solutions that are relevant to the repository (Sections 3.1.5 and 3.1.6).
NWTRB Letter to DOE (8-3-99) (Cohen 1999b)	Additional research is needed to determine the likelihood of new mechanisms (beyond typical localized corrosion processes) of deterioration that could affect the very-long-term stability of the passive layer for critical WP and other engineered barrier materials, such as Alloy 22 and titanium. This work could include, for example, examination of fundamental models of passive-regime stability and the factors that may cause deviation from passive-layer dissolution behavior assumed from short-term experiments, prediction of the behavior of the alloy surface under a thick layer of previous passive dissolution products, and a search for relevant natural and archeological analogs.	A variety of cutting edge techniques are now employed to study the long-term degradation of WP materials. For example, TEM is used to quantify the thermal aging of Alloy 22. Such quantification is in the form of TTT diagrams found in this PMR. Thermal aging is important in that it may result in the precipitation of undesirable intermetallic phases. These precipitates can lead to embrittlement and enhanced susceptibility to LC and SCC. Atomic force microscope and X-ray photo electron spectroscopy are being employed to study passive film stability. SIMS is used to quantify the amount of hydrogen in the titanium-based materials that will be used for construction of the DS. All these modes of degradation are addressed in the PMR Sections 3.1.3 through 3.1.9. No appropriate natural or archeological analogs are available for Alloy 22 or titanium

Table 2-1. Key External Issues for the Waste Package Degradation Process Model Report (Continued)

Source	Issue	PMR Approach
NWTRB Letter to DOE (8-3-99) (Cohen 1999b)	The effects of the DS and backfill on the thermal and moisture regime between the DS and the WP and evaluating the corrosion behavior of titanium when it is in contact with backfill or rock fall. The vulnerability of the drip-shield connections to vibratory earthquake motion also needs to be addressed	The testing of material samples have assumed same bounding chemistry for both the DS and the WP outer barrier (Section 3.1.3). The DS is designed to withstand expected earthquake motion and not separate.
TSPA Peer Review, Section II.C (Budnitz et al. 1999)	Experimental data are lacking throughout the treatment of the WP and EBS. In particular, the effect of realistic and extreme environments to come in contact with Alloy 22 and critical temperature for crevice corrosion of Alloy 22.	Electrochemical testing has been done in a wide variety of repository-relevant test solutions, including SDW, SCW, SAW, SCMW, SSW, and BSW. CP tests have been conducted in these media with artificial crevices. Long term exposure testing has been done in SDW, SCW, SAW, and SCMW at temperatures up to 90°C. To determine critical crevice temperatures, SCC testing is underway in similar solutions. Experiments have been performed to quantify the extent that pH can be lowered inside crevices, formed between the Alloy 22 WPOB and the 316NG SSSM (see Sections 3.1.6 and 3.1.7).
TSPA Peer Review, Section IV.D (Budnitz et al. 1999)	The TSPA-VA treatment of crevice corrosion was based on the adaptation of a pitting model. While similar chemical and electrochemical processes occur as part of both modes of corrosion, the TSPA peer review panel has concluded that a direct crevice corrosion model would be more realistic.	In the case of Alloy 22, pitting is not expected. If LC does occur, it is expected to be some form of crevice corrosion. Crevice chemistry determination has been conducted and documented in the supporting AMR and PMR Section 3.1.6.
TSPA Peer Review, Section IV.D (Budnitz et al. 1999)	There is a need both to improve the models and methods for analyzing water chemistries at the metal surfaces of the WPs under realistic conditions, and to collect experimental data to validate and verify these models and the associated analytical methods	From the evaporative concentration experiments, the saturated electrolytes that may form on the WP surface have been defined (Section 3.1.3).
TSPA Peer Review, Section IV.D (Budnitz et al. 1999)	As in the case of analyses of crevice corrosion, additional work will be necessary for SCC prior to the possible LA stage, especially in light of the tentative nature of the SCC model and the fact that failure mode is closely coupled to WP fabrication procedures.	The WAPDEG code now incorporates a wide variety of plausible failure modes, including SCC. The effects of residual weld stress in the final closure weld are now accounted for. The code has developed to a level of sophistication now able to account for stress mitigation techniques such as laser peening and induction annealing (Section 3.1.7).
TSPA Peer Review, Section IV.D (Budnitz et al. 1999)	At the present time, the corrosion behavior of WP with backfill or rock debris covering the WP is not well defined	Electrochemical testing has been done in a wide variety of repository-relevant test solutions, including SDW, SCW, SAW, SCMW, SSW, and BSW. BSW and SSW are determined to be bounding environments and cover the effects of backfill. CP tests are now being conducted in these media with artificial crevices. Experiments have been performed to quantify the extent that pH can be lowered inside crevices, formed between the Alloy 22 WPOB and the 316NG SSSM (Sections 3.1.3 and 3.1.6).

Table 2-1. Key External Issues for the Waste Package Degradation Process Model Report (Continued)

Source	Issue	PMR Approach
TSPA Peer Review, Section IV.D (Budnitz et al. 1999)	The treatment of Alloy-22 corrosion rates and the allocation of total variance to their variability and uncertainty need to be improved prior to the anticipated LA phase.	The large number of samples involved in testing in the LTCTF provide estimates of uncertainty for GC rates (for both HAC and APC). By performing large numbers of CP tests with at least three replicates at each condition, similar estimates of the uncertainty in electrochemical potential measurements are obtained. Separation of uncertainty and variability is difficult with these very corrosion resistant materials. In many cases, the corrosion rates are so low that the measurement limits are exceeded. The treatment of uncertainties and variability in the data is addressed in Section 3.1.9 of the PMR.

AMR	Analysis and Model Report
APC	aqueous phase corrosion
BSW	basic saturated water
CP	cyclic polarization
DS	drip shield
EBS	engineered barrier system
GC	general corrosion
HAC	humid air corrosion
LA	License Application
LC	localized corrosion
LTCTF	Long Term Corrosion Test Facility
Np	Neptunium
PMR	Process Model Report
SAW	simulated acidic concentrated water
SCC	stress corrosion cracking
SCW	simulated concentrated water
SCMW	simulated cement-modified water
SDW	simulated dilute water
SIMS	secondary ion mass spectrometry
SSSM	stainless steel structural material
SSW	simulated saturated water
TEM	transmission electron microscope
TSPA-VA	Total System Performance Assessment Viability Assessment
TTT	time-temperature-transformation
WPOB	waste package outer barrier
WP	waste package

INTENTIONALLY LEFT BLANK

3. MODELS AND ABSTRACTED MODELS

The waste package degradation process model consists of a several different models: dry oxidation, humid air corrosion, aqueous phase corrosion, general corrosion, localized corrosion, microbiologically influenced corrosion (MIC), stress corrosion cracking (SCC), and hydrogen induced cracking. A generic integrated model containing the above component models is illustrated by Figure 1-1. This model can be applied to the drip shield and waste package materials of interest.

3.1 MODEL DESCRIPTIONS

As stated above, the waste package degradation process model includes a number of component models. These component models are discussed in the following sections. Model parameters and definitions for the individual models are provided in the respective Analysis and Model Report (AMR)s.

3.1.1 Overview of Waste Package and Drip Shield Design

As described in the License Application Design Selection report, the recommended waste package design is Enhanced Design Alternative II (EDA-II) (CRWMS M&O 1999a). This design includes a double-wall waste package underneath a protective drip shield. The drip shield is to be fabricated from Titanium Grade 7. The EDA-II corrosion resistant waste package outer barrier (WPOB) is to be fabricated from nickel-based Alloy 22. Stainless steel 316NG is to be used for construction of the structural support container within the WPOB. The 316NG inner cylinder will increase the overall strength of the waste package.

3.1.1.1 Titanium Drip Shield

Titanium alloys have been considered for construction of the drip shield. The current recommendation is to use Titanium Grade 7 [Unified Numbering System for Metals and Alloys (UNS) R52400]. The composition of this alloy is 0.03% N (max), 0.10% C (max), 0.015% H (max), 0.25% O (max), 0.30% Fe (max), 0.12-0.25% Pd (max), and 0.4% Residuals (total), with the balance being Ti (approximately 98.7 to 98.8%). Properties and performance of these materials are reviewed elsewhere and cited in the respective AMRs. The unusual corrosion resistance of titanium alloys is due to the formation of a passive film of TiO_2, which is stable over a relatively wide range of electrochemical potential and pH. A similar material, Titanium Grade 16 with 0.04 to 0.08% Pd, is used as an analog for Titanium Grade 7 in some parts of the testing program. The rates of general corrosion and dry oxidation (or dry air oxidation) of this material have been shown to be very low. Corrosion testing of Titanium Grade 16 has been conducted in the Long Term Corrosion Test Facility (LTCTF) of the YMP (CRWMS M&O 2000d).

3.1.1.2 Nickel-Based Waste Package Outer Barrier

Alloy 22 (UNS N06022) is now being considered for construction of the WPOB. This alloy consists of 20.0-22.5% Cr, 12.5-14.5% Mo, 2.0-6.0% Fe, 2.5-3.5% W, and 2.5% Co (max), with the balance being Ni (approximately 50 to 60%). Other impurity elements include P, Si, S, Mn, Nb, and V. Alloy 22 is less susceptible to localized corrosion in environments that contain Cl^-

than Alloys 825 and 625, materials of choice in earlier waste package designs. Corrosion testing of Alloy 22 has been and continues to be conducted in the Long Term Corrosion Test Facility of the YMP (CRWMS M&O 2000c).

3.1.1.3 Stainless Steel Structural Material

Stainless steel 316NG is to be used for construction of the structural support container inside the WPOB. The 316NG inner cylinder will increase the overall strength of the waste package. Stainless steel 316L is considered to be a good analog for 316NG because the chemical composition of the two alloys are essentially the same, except that 316NG has better mechanical properties than 316L. Stainless steel 316L [UNS S31603] has a composition of 16-18% Cr, 10-14% Ni, 2-3% Mo, 2% Mn (max), 1% Si (max), 0.03% C (max), 0.045% P (max), 0.03% S (max), 0.10% N (max) and the balance being Fe (65-69%). Stainless steel 316L is less susceptible to localized corrosion in environments that contain Cl^- than stainless steel 304, but more susceptible than other corrosion resistant materials (CRMs) such as Alloys 22, 625 and 825 that have been considered in various waste package designs. The superior localized corrosion resistance of stainless steel 316L in comparison to 304 is apparently due to the addition of Mo, which helps to stabilize the passive film at low pH values. Molybdenum oxide is very insoluble at low pH. Consequently, 316L exhibits relatively high thresholds for localized attack (CRWMS M&O 2000e).

3.1.2 Early Failures

Manufacturing defects and failure modes that might lead to early failure of a waste package are accounted for in an AMR (CRWMS M&O 2000m) that supports this Process Model Report (PMR). The AMR on early failure includes a literature review to obtain information on the rate of manufacturing defect-related failures in various types of welded metallic containers, the types of defects that produce these failures, and the mechanisms that cause defects to propagate to failure. Types of defects applicable to the current waste package design are identified. For each applicable type of defect, the probability of its occurrence on a waste package is estimated. Potential consequences to the long-term performance of the waste package if the defect is present are discussed. Specific details on how the defect will affect waste package materials are provided in separate AMR on SCC (CRWMS M&O 2000f).

3.1.2.1 Analysis Assumptions

The following assumptions support the development of probabilities for various size weld flaws in the waste package shell and lid welds. Based on the similarity of the processes for welding of Alloy 22 and stainless steel, they are predicted to have the same weld flaw frequency and size distributions. Information on the reliability of radiographic, ultrasonic and penetrant testing is assumed to be applicable to the materials and inspection methods that will be used for the waste package. This information is based on older reliability studies of these nondestructive examination methods, and that future improvement in the inspection technology will result in increases in the probability of flaw detection. It was assumed that flaws detected by post-weld inspections will be repaired, whenever the flaw size is larger than the flaw size of concern for postclosure performance. Embedded weld flaws are not considered to be a concern for postclosure performance, since the waste package is not a pressure vessel and will not be

subjected to cyclic fatigue (the primary mechanism for causing flaws to grow through-wall in pressure vessels).

The probabilities of human error have not been quantified for the specific actions associated with the fabrication of the waste package, but the information used represents human error probabilities for similar types of actions.

In developing the probability of the use of improper material in the waste package shell or lid welds, it is assumed that a field verification of the chemical composition of weld wire will be performed prior to its use in fabricating any weld and that material controls required in nuclear quality programs will be used. It is further assumed that such field verification will use state-of-the-art instrumentation. This assumption is based on the expected administrative requirements on the process qualification program.

Assumptions are used to support the development of the probability of having corrosion enhancing surface contamination on the waste package or improper heat treatment of the waste package. These assumptions are based on the general descriptions of these activities. The assumptions support the development of event sequence trees for quantifying the probabilities of improper heat treatment or a failure in the cleaning process. The assumptions involve the number of operators involved in each process, the Quality Assurance (QA) procedures and inspections governing the processes, and the reliability of the equipment used.

It is assumed that the probability of damaging a waste package during transport or handling at the repository is equivalent to the probability of damaging spent nuclear fuel assemblies during transport or handling. The basis for this assumption is that a waste package will be subjected to about the same number of handling steps as a spent nuclear fuel assembly. It is assumed that both are handled with about the same amount of care. It is expected that the waste package will be inspected for handling damage upon arrival at the repository and before final emplacement in the drift. It is further expected that the waste package will be completely repaired or scrapped if such handling damage occurs.

3.1.2.2 Analysis Description

The AMR presents the results of a literature review performed to determine the rate of manufacturing defect-related failure for various types of welded metallic containers. In addition to providing examples of the rate at which defective containers occur, this information provides insight into the various types of defects that can occur and the mechanisms that cause defects to propagate to failure. In general, eleven generic types of defects were identified. These are:

- Weld flaws
- Base metal flaws
- Improper weld material
- Improper heat treatment
- Improper weld flux material
- Poor weld joint design
- Contaminants
- Mislocated welds

- Missing welds
- Handling and installation damage
- Administrative and operational error.

For dry storage casks, all of the defects were identified by post-weld inspection prior to commencement of the storage phase, and thus do not represent true instances of early failure as it is defined in the AMR. The eleven types of defects have been reviewed for their applicability to the waste package. The following generic defect types are considered *not applicable* to the waste package: improper weld flux material, poor weld joint design, missing welds, and mislocated welds. This is based on the fact that the welding process for waste package fabrication does not use flux as noted in the AMR. Poor joint design is unlikely because of extensive development and testing. Missing welds and mislocated welds are easily detected and controlled by process qualification. The probability of occurrence and the effect on postclosure performance of the waste package are assessed for the remaining defects.

Using information on linear flaw density, flaw size distribution, inspection reliability and information on various weld lengths, frequencies of various size outer surface breaking weld flaws have been estimated. The procedure is essentially the same for all cases. First, the total flaws per type of waste package weld was calculated by multiplying the weld length by the linear flaw density and by an adjustment factor for the weld thickness. The base flaw linear flaw density with credit for radiographic test and dye-percentage test inspections was used for the shell and bottom lid welds, and the uninspected flaw density was conservatively used for the top lid closure weld. Next, the flaw size distribution for that weld thickness was used to determine the probability that a flaw would have a size within a given range. A range size of 0.5% of the weld thickness was used. This was the largest range size that could be used without introducing any significant (within 2 significant figures) amount numerical error associated with discretizing a continuous size distribution. The probability for each range was then multiplied by the total number of flaws per weld to determine the expected number of flaws within that size range. For welds subjected to a ultrasonic inspection, the expected number of flaws within each range was then reduced by multiplying by the probability of nondetection (PND) for the lower end of the size range (this is conservative because the PND is higher for smaller flaws and ultrasonic inspection identifies small flaws). Since the UT PND is based on a single angle UT examination, and a multi-angle examination is planned for the lid welds (possibly as many as four different angles; see CRWMS M&O (2000m)), the square of the PND was used for the lid welds (this effectively treats a multi-angle exam as two independent examinations). For all cases, each range was then multiplied by 0.34% to yield the expected number of outer surface breaking flaws within that range. Finally, the expected number of outer surface breaking flaws in each size range were summed to determine a new value for total flaws per weld which accounts for the UT inspections. A complementary cumulative distribution of outer surface breaking flaw size was also determined. These results are summarized in Figure 3-1 for the Alloy 22 barrier shell welds, and in Figure 3-2 for the Alloy 22 barrier lid welds.

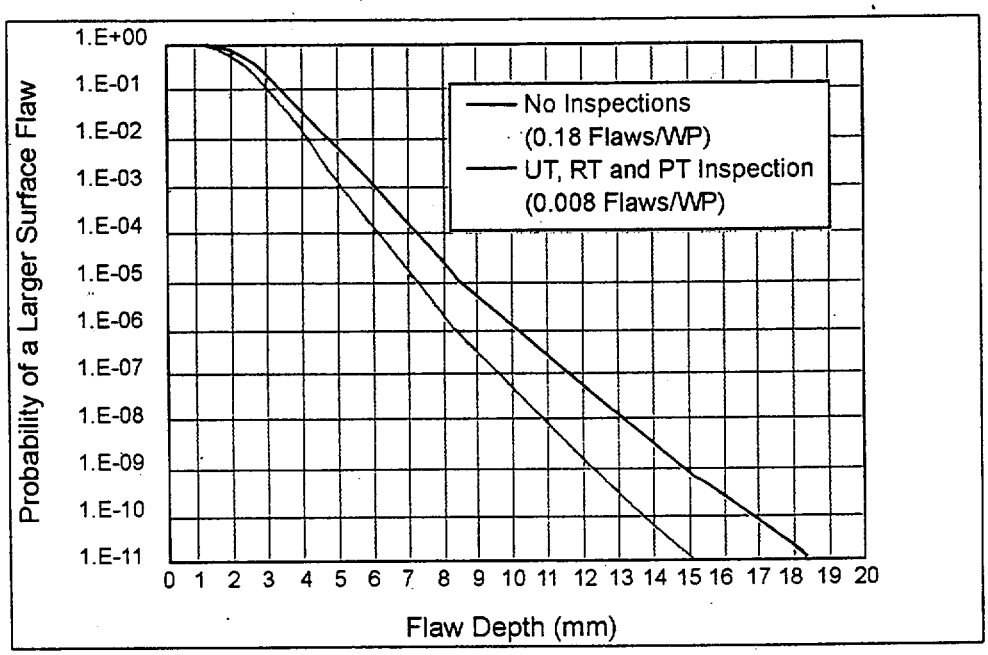

Figure 3-1. Size Distribution for Indicated Frequency of Occurrence for Outer Surface Breaking Flaws in Waste Package Alloy 22 Shell Welds

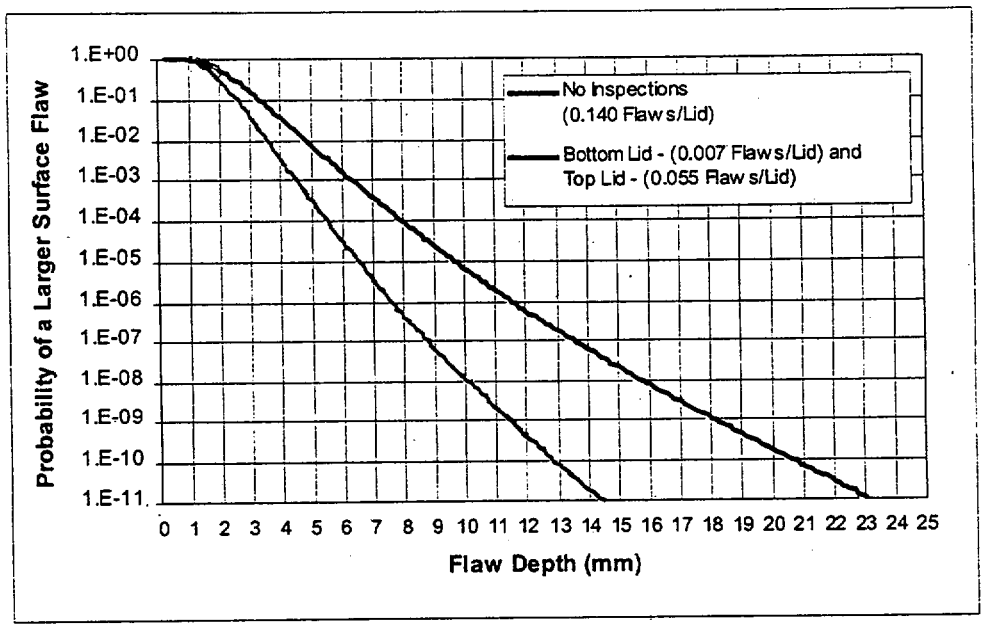

Figure 3-2. Size Distribution for Indicated Frequency of Occurrence of Outer Surface Breaking Flaws in Waste Package Alloy 22 Lid Welds

3.1.2.3 Uncertainties

The inputs used to estimate the probability of various defects (potentially leading to early failures of a waste package) are open to interpretation and uncertainty. An uncertainty analysis was

performed to develop an upper bound for an event sequence probability based on the uncertainty of modeled human actions. The analysis applies to those defects for which probabilities are estimated using event sequence trees, namely: drip shield emplacement error, waste package handling error, waste package surface contamination, thermal misload, and improper heat treatment. The method used to establish an upper bound value for event sequences combines the human error rates probabilistically. Uncertainties are considered only for human error probabilities related to failures. Probability components for success are treated at their nominal level (i.e., without uncertainty), which produces conservative results. No upper bounds were estimated for other failure probabilities related to mechanical failure or based on historical data. Accordingly, the upper bound for an event sequence probability is adjusted for only human error probability uncertainties. (CRWMS M&O 2000m)

3.1.2.4 Analysis Conclusions

The AMR on early failure of the waste package reviewed available literature on defect-related early failures of welded metallic components. Types of components examined include boilers and pressure vessels, nuclear fuel rods, underground storage tanks, radioactive cesium capsules, dry-storage casks for spent nuclear fuel, and tin-plate cans. The fraction of the total population that failed due to defect-related causes during the intended lifetime of the component is generally in the range of 10^{-3} to 10^{-6} per container. In most cases, defects that lead to failure of the component require an additional stimulus to cause failure (i.e., the component was not failed when it was placed into service). In fact, there were several examples that indicate that even commercial standards of quality control could reduce the rate of initially failed components well below 10^{-4} per container. The literature review identified eleven generic types of defects that could cause early failures in the components examined. These are: weld flaws, base metal flaws, improper weld material, improper heat treatment, improper weld flux material, poor weld joint design, contaminants, mislocated welds, missing welds, handling and installation damage, and administrative error resulting in an unanticipated environment. The following defect types are considered *not applicable* to the waste package: improper weld flux material, poor joint design, missing welds, and mislocated welds. The analysis estimates the probability that specific defect types will occur on a given waste package, despite a set of quality controls designed to prevent their occurrence. Results of the analysis for the remaining seven types of defects are shown in Table 3-1.

3.1.3 Environment on the Surface of the Waste Package and Drip Shield

The waste package will experience a wide range of environments during its service life. Initially, the waste package will be hot and dry due to the heat generated by radioactive decay. However, the temperature will eventually drop to levels where both humid air corrosion and aqueous phase corrosion will be possible.

Table 3-1. Summary of Estimated Probabilities and Performance Consequences for Various Types of Waste Package Defects

WP Defect Type		Probability per WP		Possible Consequences for Postclosure Performance				
		Alloy 22 Barrier	SS Structural Barrier	Minimal Effect	Degraded Mechanical Properties	Pitting or Crevice Corrosion	SCC	Early Water Contact
Weld Flaws (Outer Surface Breaking Only)		$< 10^{-4}$ for flaws > 4 mm deep	$< 10^{-4}$ for flaws > 10 mm deep			X	X	
Base Metal Flaws		Factor of 10^{-4} lower than uninspected weld flaw rate				X	X	
Improper Weld Material		1.5×10^{-5}	3.0×10^{-5}		X	X		
Improper Heat Treatment		2.2×10^{-5}			X	X	X	
Surface Contamination		7.3×10^{-5}	4.0×10^{-5}			X		
Handling Damage		5.1×10^{-6}	5.1×10^{-7}			X		
Administrative Error Leading to Unanticipated Environment	Thermal Misload of WP	1.0×10^{-3} to 1.0×10^{-6}		X				
	DS Emplacement Error	1.8×10^{-4}						X

NOTE: SS = stainless steel; WP = waste package

A companion AMR entitled Environment on the Surface of the Drip Shield and Waste Package Outer Barrier (CRWMS M&O 2000a) defines the detailed evolution of the environment on the waste package surface. Input for this AMR includes bounding conditions for the local environment on the waste package surface, which include temperature, relative humidity (RH), presence of liquid-phase water, liquid-phase electrolyte concentration (chloride, buffer, and pH), and oxidant level. This AMR has been used to define the threshold RH for humid air corrosion and aqueous phase corrosion, as well as a medium for testing waste package materials under what is now believed to be a worst-case scenario. These test media are the near neutral pH, simulated saturated water and the high pH, basic saturated water (BSW) with nominal boiling points of 112 and 120°C, respectively.

Crevices will be formed between the waste package and supports, beneath mineral precipitates, corrosion products, dust, rocks, cement, and biofilms. After the waste package is breached, the gap between the WPOB and the stainless steel structural container can form crevices where the environment may be more severe than the near field environment. The hydrolysis of dissolved metal can lead to the accumulation of H^+ and a corresponding decrease in pH. Electromigration of Cl^- (and other anions) into the crevice must occur to balance cationic charge associated with H^+ ions. These conditions can exacerbate subsequent attack of the WPOB and stainless steel structural material by general corrosion, localized corrosion, SCC and other mechanisms. Crevices might also form with the drip shield. These are addressed in the general and localized corrosion discussions in Sections 3.1.5 and 3.1.6.

3.1.3.1 Threshold Relative Humidity

Humid air corrosion can occur at any RH above the threshold, as represented by Equation 3-1 (CRWMS M&O 2000c, 2000d, 2000e):

$$RH \geq RH_{critical} \qquad \text{(Eq. 3-1)}$$

The distribution of humid air corrosion rates is represented by the distribution for aqueous phase corrosion rates during the period when humid air corrosion is operable. Humid air corrosion is assumed to occur uniformly over each waste package degradation code (WAPDEG) patch. Each patch is comparable in size to that of a Long Term Corrosion Test Facility test sample.

As discussed in the AMR entitled *Environment on the Surface of Drip Shield and Waste Package Outer Barrier* (CRWMS M&O 2000a), hygroscopic salts may be deposited on the EBS components by aerosols and dust entrained in ventilation air, backfill, seepage water that enters the drifts and the episodic water that flows through the drifts. Hygroscopic salts enable aqueous solutions to exist at relative humidities below 100%. The threshold RH ($RH_{critical}$) at which an aqueous solution will form for a particular salt is defined as the deliquescence point. This threshold RH defines the condition necessary for aqueous electrochemical corrosion of the metal to occur. The deliquescence point of NaCl is relatively constant with temperature, and is in the range 74-76% RH. In contrast, the deliquescence point of $NaNO_3$ has a strong dependence on temperature, ranging from an RH of 75.36% at 20°C to 65% at 90°C. The equilibrium RH is 50.1% at 120.6°C, which is the boiling point of the saturated solution at 101.32 kPa. The evaporative concentration of well J-13 water which is assumed to be typical of waters contacting the EBS components, results in a solution of Cl, NO_3, CO_3, Na and K ions. Other ions that could

form salts with lower deliquescence points, such as Ca^{2+} and Mg^{2+}, are precipitated. It is therefore conservatively assumed that the deliquescence point of $NaNO_3$ determines the threshold RH. The equilibrium RH for a saturated solution of $NaNO_3$ as a function of temperature is shown in Figure 3-3, and the experimental data fits the following polynomial in temperature:

$$RH_{critical} = -3.5932\times10^{-5}\times T(°C)^3 + 5.9649\times10^{-3}\times T(°C)^2 - 0.45377\times T(°C) + 81.701 \quad \text{(Eq. 3-2)}$$

The goodness of fit is characterized by

$$R^2 = 0.9854$$

where R^2 is the coefficient of determination and where R is the coefficient of correlation. This correlation is shown in Figure 3-3 below.

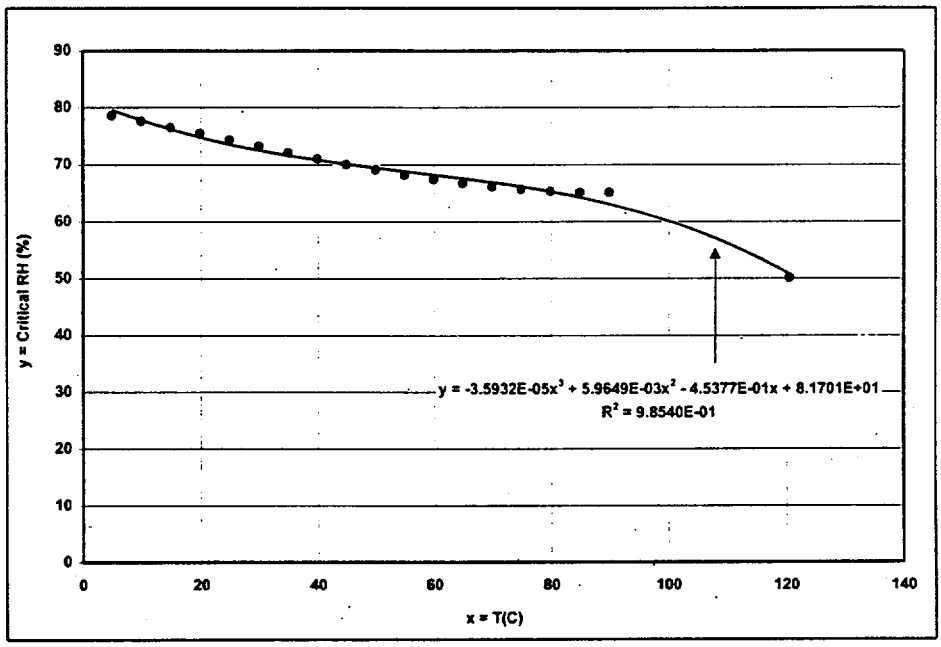

Figure 3-3. Deliquescence Point for Sodium Nitrate Solutions

The evaporation of J-13 type water results in high concentrations of Na^+, K^+, Cl^-, and NO_3^-, and CO_3^-. The concentrations of F^- and SO_4^{2-} initially increase, but eventually fall due to precipitation. The simulated saturated water used for testing is an abstract embodiment of this observation. The simulated saturated water formulation is based upon the assumption that evaporation of J-13 water eventually leads to a sodium-potassium-chloride-nitrate solution. The elimination of carbonate in this test medium is believed to be conservative, in that carbonate would help buffer pH in any occluded geometry such as a crevice.

3.1.3.2 Aqueous Phase Environments

At a given surface temperature, the existence of liquid-phase water on the waste package depends upon the nature of the hygroscopic salt either present on the surface or contained in

water dripping on the surface. Two conditions must exist for aqueous phase corrosion: dripping water, and RH above the deliquescence point of the hygroscopic salts in the dripping water. While dripping can occur without the latter condition being met, both conditions are necessary for aqueous phase corrosion. Without this level of RH, no aqueous phase could be sustained on the surface. This, however, requires that the evaporation rate of water from the surface exceeds the rate of dripping so that equilibrium conditions exist.

This model uses Equation 3-2 to conservatively estimate the threshold RH for aqueous phase corrosion ($RH_{critical}$). The composition of the electrolyte formed on the waste package surface is assumed to be that of concentrated J-13 simulated concentrated water (SCW) below temperatures of 100°C, and that of simulated saturated J-13 water (SSW) above temperatures of 100°C. The composition of these solutions is shown in Table 3-2. General aqueous phase corrosion is assumed to occur uniformly over each WAPDEG patch. Each patch is to be the same size as a standard Long Term Corrosion Test Facility "weight-loss" test sample. Effects of backfill is not considered on the aqueous phase corrosion threshold and rate.

Table 3-2. Composition of Standard Test Media Based upon J-13 Well Water

Ion	J-13 (mg liter^{-1})	SDW (mg liter^{-1})	SCW (mg liter^{-1})	SAW (mg liter^{-1})	SSW (mg liter^{-1})
K^{+1}	535	3.40E+01	3.40E+03	3.40E+03	1.416E+05
Na^{+1}	4360	4.09E+02	4.09E+04	4.09E+04	4.870E+04
Mg^{+2}	0	1.00E+00	1.00E+00	1.00E+03	0.000E+00
Ca^{+2}	6	5.00E-01	1.00E+00	1.00E+03	0.000E+00
F^{-1}	210	1.40E+01	1.40E+03	0.00E+00	0.000E+00
Cl^{-1}	729	6.70E+01	6.70E+03	2.450+04	1.284E+05
NO_3^{-1}	846	6.40E+01	6.40E+03	2.300+04	1.310E+06
SO_4^{-2}	1790	1.67E+02	1.67E+04	3.860+04	0.000E+00
HCO_3^{-1}	4773	9.47E+02	7.00E+04	0.00E+00	0.000E+00
Si	13	27 (60°C), 49 (90°C)	27 (60°C), 49 (90°C)	27 (60°C), 49 (90°C)	0.000E+00
pH	-	8.1	8.1	2.7	7.0

3.1.3.3 Condensation Underneath Drip Shield

Moist air and liquid water flows into and within the drift over time. Although the relative humidity underneath the drip shield increases with time, conditions for condensation on the drip shield can only occur if the drip shield is cooler than the top of the invert and the invert moisture content produces nearly 100% RH. Although this may be conceptually possible, the surfaces of the waste package and drip shield are not likely to experience a condition where the drip shield (above the waste package) is at a lower temperature than the invert.

3.1.3.4 Composition of Water on Exposed Surfaces of Drip Shield and Waste Package

The YMP has used test media relevant to the environment expected in the repository. Relevant test solutions are assumed to include simulated dilute water (SDW), SCW, and simulated acidic

concentrated water (SAW) at 30, 60, and 90°C, as well as simulated saturated water (SSW) at 100 and 120°C. The compositions of all of the environments are given in Table 3-2. The simulated saturated water composition has been recently developed. In general, anions such as chloride promote localized corrosion, whereas other anions such as nitrate tend to act as corrosion inhibitors. Thus, there is a very complex synergism of corrosion effects in the test media.

Basic saturated water (BSW) represents another plausible extreme in water chemistry. The basic saturated water composition was established on the basis of results from a distillation experiment. Tables 3-3 and 3-4, show the corresponding water chemistry. The total concentration of dissolved salts in the starting liquid was approximately five-times (5×) more concentrated than that in the standard SCW solution. It was prepared by using five-times the amount of each chemical that is specified for the preparation of SCW. After evaporation of approximately ninety percent (~90%) of the water from the starting solution, the residual solutions reaches the highest chloride concentration and has a boiling point of ~112°C. The resultant basic saturated water solution contains (sampled at 112°C) 9% chloride, 9% nitrate, 0.6% sulfate, 0.1% fluoride, 0.1% silicate, 1% (total inorganic carbon from carbonate and bicarbonate), 5% potassium ion and 11% sodium ion.

In order to add some soluble silica to the solution, the initial basic saturated water solution recipe was later revised to contain 4.0 g (~1% metasilicate) by adding sodium metasilicate ($Na_2SiO_3 \bullet 9H_2O$). This solution is designated as BSW-SC where SC indicates the presence of silicate and carbonate in the solution.

The pH of aqueous solutions is affected by the partial pressure of CO_2 in the gas phase. The implication of this is that unless an effort is made to control the pH of the basic saturated water solution, the pH may vary with test conditions and time. In order to conduct a long time testing (few months to a year), the testing environments should be stable. It was decided that to make stable testing solutions, carbonate and silicates should not be added to the test solution as both species can affect the solution pH. Gaseous CO_2 must be also removed from the air passing above the solution, because as noted above it will affect the solution pH. With no gaseous CO_2 in contact with the solution and with no carbonate-bicarbonate and no silicates in solution, the test environments will be stable. Sodium hydroxide is used to maintain the higher pH of the solution.

Table 3-3. Initial Basic Saturated Water Solution Recipe

Chemical	Quantity (g)
Na_2CO_3 (anhydrous)	10.6
KCl	9.7
NaCl	8.8
NaF	0.2
$NaNO_3$	13.6
Na_2SO_4 (anhydrous)	1.4
H_2O	55.7

Table 3-4. Modified Basic Saturated Water Solution Recipes

	BSW-13	BSW-12	BSW-11
Chemical	Quantity	Quantity (g)	Quantity (g)
KCl	8.7 g	8.7 g	8.7 g
NaCl	7.9 g	7.9 g	7.9 g
NaF	0.2 g	0.2 g	0.2 g
$NaNO_3$	13.0 g	13.0 g	13.0 g
Na_2SO_4 (anhydrous)	1.4 g	1.4 g	1.4 g
H_2O (deionized)	66 ml	66 ml	66 ml
10N NaOH	2 ml		
1N NaOH		2 ml	
0.1N NaOH			2 ml
CO_2 partial pressure	0	0	0
pH (measured at room temperature)	13.13	12.25	11. 11

NOTE: The CO_2 partial pressure can be minimized by either scrubbing laboratory air or purchasing CO_2 free air.

In order to maintain constant pH conditions, the basic saturated water solution was modified for corrosion tests, yielding basic saturated water-11, basic saturated water-12, and basic saturated water-13. The three solutions have pH values of approximately 11, 12 and 13, respectively. The recipes of these solutions are given in Table 3-4.

3.1.4 Phase Stability and Aging

Exposure of materials like Alloy 22 to elevated temperatures can result in the formation of undesirable phases. The phases which form in Alloy 22 are often rich in molybdenum and chromium which are responsible for the high degree of corrosion resistance of the alloy. Thus the formation of precipitates depletes these alloying elements from the surrounding areas, and this can result in increased susceptibility to general and localized corrosion and stress corrosion cracking. Formation of brittle molybdenum- or chromium-rich intermetallics can also lead to embrittlement of the material and degradation of its mechanical properties. Long-Range Order in alloys similar to Alloy 22 has been linked to an increased susceptibility to SCC and hydrogen embrittlement.

The aging of Alloy 22 is dependent on both time and temperature. While the effects of aging have been observed for exposures to elevated temperatures (>600°C) for short time periods, it is important to know the kinetics of this process to enable prediction of aging effects for lower temperatures (200-300°C) and much longer times (10,000 years).

This section discusses the process model developed for aging and phase stability in Alloy 22. The development of the model is presented in detail in the corresponding AMR (CRWMS M&O 2000b). Only the highlights will be presented here.

3.1.4.1 Phase Identification in Alloy 22

The long-term aging of Alloy 22 at elevated temperature can cause the precipitation of undesirable intermetallic phases, if the temperature is sufficiently high. In order to provide a technical basis for the development of a model for aging effects in Alloy 22, samples were aged for a variety of times at different temperatures: for 40,000 hours at 260, 343, and 427°C; for 30,000 hours at 427°C; for 1000 hours at 482, 538 and 593°C; and for 16,000 hours at 593, 649, 704, and 760°C and then examined in transmission electron microscope (TEM). A weld sample aged at 427°C for 40,000 hours was also examined in the weld metal, in the heat-affected zone, and in the base metal removed from the weld. Several phases were observed to form in Alloy 22: P, μ, σ, carbide, and $Ni_2(Cr, Mo)$ long range ordering (LRO). At 593°C, P phase was observed only on the grain boundary. At the higher aging temperatures (649, 704, and 760°C), both μ and P phases precipitated on grain boundaries. As the aging temperature increased, more μ and P phase precipitation occurred within the grains. Grain boundary carbide precipitation was observed in samples aged at 593 and 704°C. Because of the small amount of carbide present in these samples and the small volume examined in TEM, it is likely that carbides also form at 649°C. A σ phase was observed in the samples aged at 704 and 760°C. The amount of σ phase observed in these samples was small compared to the amount of μ and P phases. Long range order (LRO) was observed in the samples aged at 593°C for 16,000 hours and for 1,000 hours, in the sample aged at 538°C for 1,000 hours, and in the samples aged at 427°C for 40,000 hours and for 30,000 hours. These observations are summarized in Table 3-5.

3.1.4.2 Kinetics of Intermetallic Precipitation in Alloy 22 Base Metal

Table 3-6 shows the aging times for the various stages of intermetallic precipitation in Alloy 22 base metal as a function of temperature. These times were approximated from the examination of aged samples after approximately 1, 10, 100, 1,000, and in some cases 16,000 hours. The errors noted are due to the uncertainty associated with the coarse time intervals of examination and not with any measurement and test equipment uncertainties, which are much smaller. For example, if precipitation was observed on twin boundaries at 100 hours, it could have begun at any time between 10 and 100 hours. In that case, the time noted for the start of precipitation on the twin boundaries would be 55 hours (halfway between 10 and 100), with upper and lower error bars of 45 hours. Because of the coarse examination intervals, there is some judgment involved in choosing the times noted in Table 3-6. These measurements are only intended as an initial estimate of the precipitation kinetics. These observations were also used to generate the isothermal time temperature transformation diagram for Alloy 22 base metal shown in Figure 3-4. Also shown in Figure 3-4 are some of the data presented in Table 3-5. The curve associated with long range order came from TEM observations. Only a limited number of samples were examined in TEM; therefore, it is likely that ordering occurs at shorter times than indicated in Figure 3-4. The precipitation of intermetallic phases at grain boundaries in Alloy 22 is shown in Figure 3-5 by the white phase surrounding the grains of 1,000 hours.

Table 3-5. Intermetallic Phases Observed in Alloy 22 with Transmission Electron Microscopy

Aging Condition	Phases Observed to Form in Alloy 22
260°C for 40,000 hr	No long range order - No signs of grain boundary precipitation in base metal
343°C for 40,000 hr	No long range order - No signs of grain boundary precipitation in base metal
427°C for 30,000 hr	LRO - No signs of grain boundary precipitation in base metal
427°C for 40,000 hr	LRO - No signs of grain boundary precipitation in base metal
482°C for 1000 hr	No long range order - No signs of grain boundary precipitation in base metal
538°C for 1000 hr	LRO - No signs of grain boundary precipitation in base metal
593°C for 1000 hr	LRO - Grain boundary films of P phase
593°C for 16,000 hr	LRO - Grain boundary films of P phase – Carbide precipitates at GB
649°C for 16,000 hr	No long range order– Precipitation of P and μ phase mainly at GB
704°C for 16,000 hr	No long range order – Precipitation of P and μ phase at grain boundary and within the grains - Carbide and σ precipitation at GB
760°C for 16,000 hr	No long range order– Precipitation of P and μ phase at grain boundary and within the grains - σ precipitation at GB

Table 3-6. Time Required for Precipitation of Intermetallic and Carbide Particles on the Grain Boundaries of Alloy 22 Base Metal

Temp	Time to Start on Grain Boundaries			Time to Cover Grain Boundaries		
(°C)	Lower Error	Time (hr)	Upper Error	Lower Error	Time (hr)	Upper Error
593	0	10	90	7500	8500	7500
649	1	1	9	450	550	450
704	0.5	0.5	0.5	90	100	900
760	0.5	0.5	0.5	9	10	109
800	0.5	0.5	0.5	9	10	90
Temp	**Time to Start on Twin Boundaries**			**Time to Start Within Grains**		
(°C)	**Lower Error**	**Time (hr)**	**Upper Error**	**Lower Error**	**Time (hr)**	**Upper Error**
593						
649	450	550	450	7500	8500	7500
704	90	100	900	450	550	450
760	54.5	64.5	54.5	54.5	64.5	54.5
800	45	55	45	45	55	45

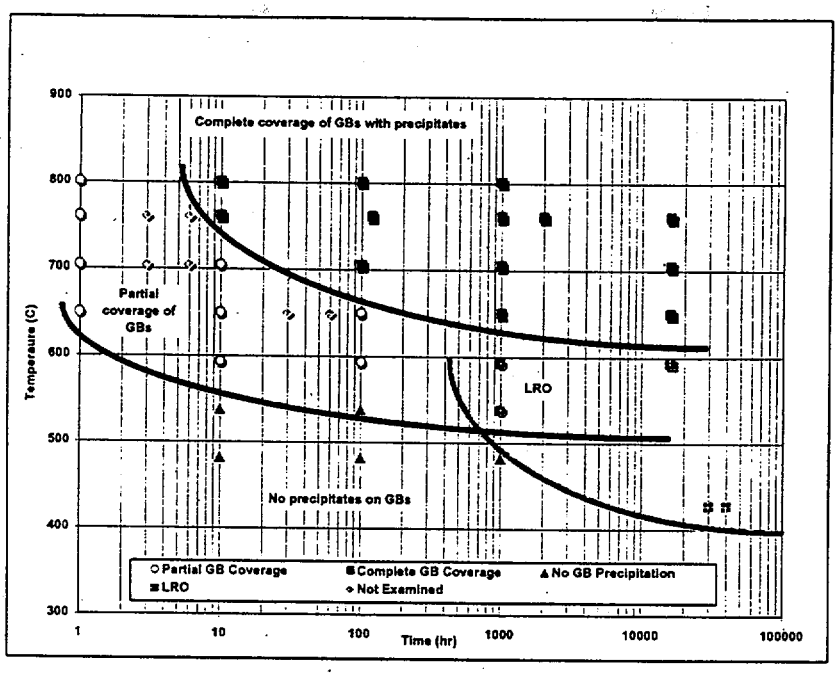

Figure 3-4. Isothermal Time-Temperature-Transformation Diagram for Alloy 22 Base Metal

Nucleation and growth kinetics can often be represented by an equation of the form:

$$f = 1 - \exp(-kt^n) \qquad \text{(Eq. 3-3)}$$

where f is the volume fraction of the precipitating phase, t is time and k and n are constants. The value of k depends on nucleation and growth rates and therefore depends very strongly on temperature, usually of the form:

$$k = C_1 \exp(-C_2 / T) \qquad \text{(Eq. 3-4)}$$

where C_1 and C_2 are constants, and T is the absolute temperature in K. Combining Equation 3-3 and Equation 3-4 at constant volume fraction yields:

$$\ln(t_f) = \frac{C_2}{n} \cdot \frac{1}{T} + C_f \qquad \text{(Eq. 3-5)}$$

where t_f is the time to reach a given volume fraction of grain boundary precipitation. Plots of logarithm of time versus reciprocal temperature for the various precipitation stages in Alloy 22 base metal are given in Figure 3-6. At the higher temperatures, grain boundary precipitation was seen to have already begun after 1 hour, which is the shortest aging time investigated thus far.

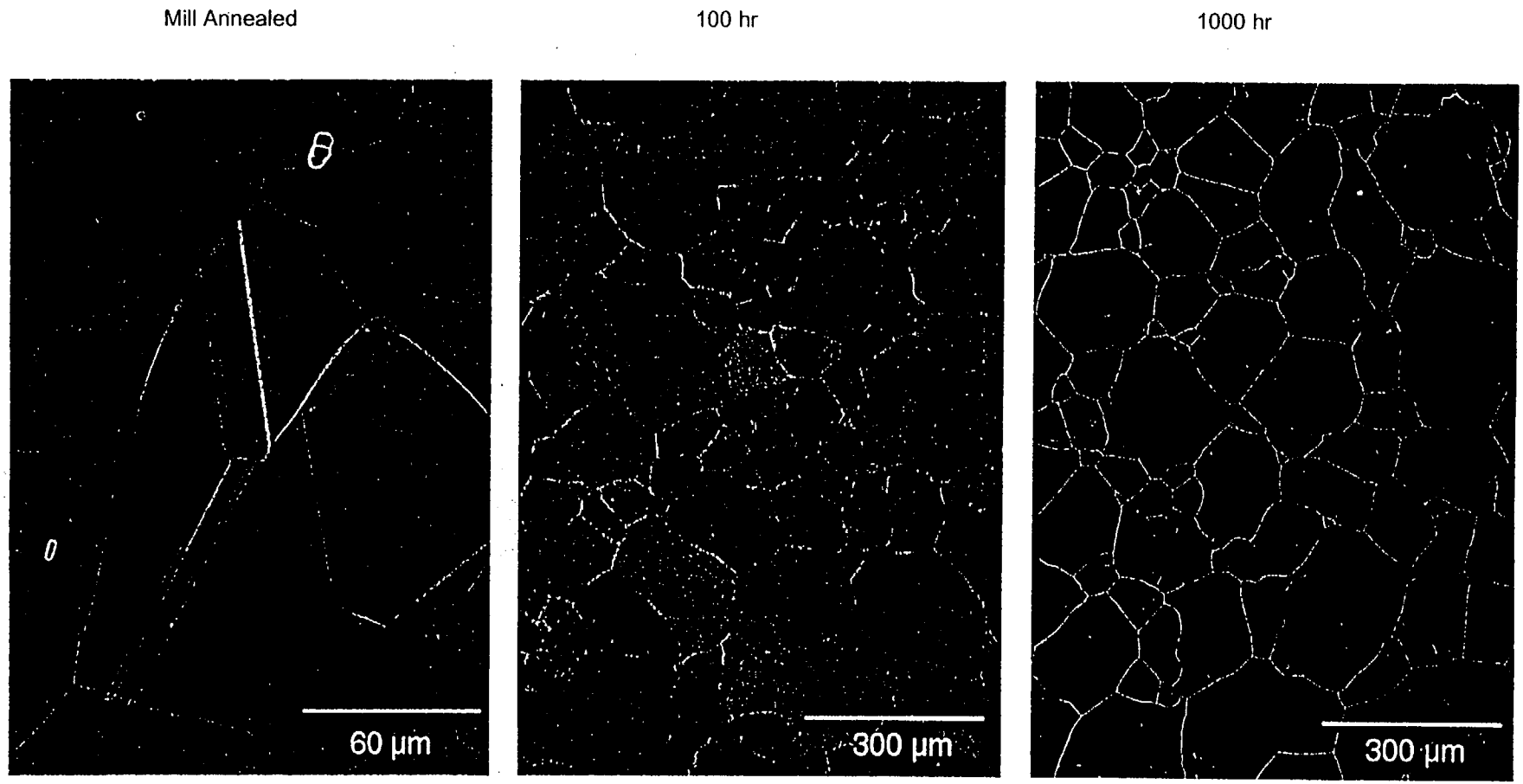

NOTE: Increased precipitation in the grain boundary after 1,000 hr of aging compared to 100 hr.

Figure 3-5. Effect of Thermal Aging at 649°C on the Precipitation of Intermetallic Phases at Grain Boundaries on Alloy 22

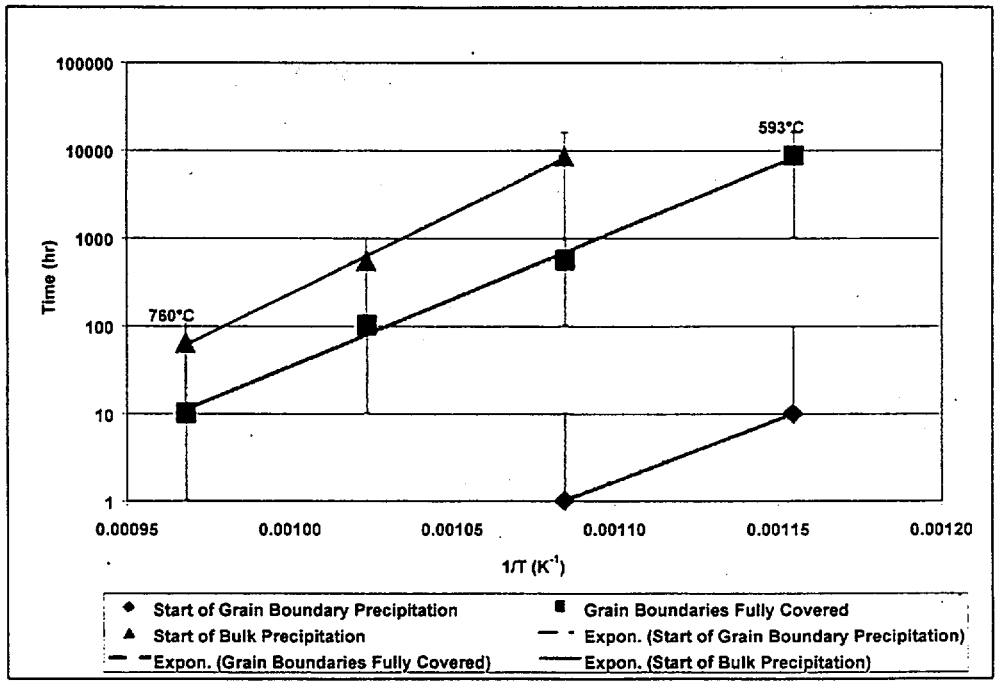

Figure 3-6. Time to Reach Various Stages of Precipitation in Aged Alloy 22 Base Metal Plotted on a Log Scale as a Function of Reciprocal Temperature (see Equation 3-5)

If it can be assumed that the precipitation mechanism does not change, the lines in Figure 3-6 can be extrapolated to give the times that can be expected for the various stages of precipitation at lower temperatures. However, these data are preliminary. The times were estimated from examination of micrographs from samples with widely spaced aging times. Extrapolation to lower temperatures is difficult because the precipitation rate is quite sensitive to temperature; small changes in slope make a very large change in the time obtained from extrapolation to lower temperatures. In order to make a bounding argument, however, the curves associated with grain boundary coverage and bulk precipitation in Figure 3-6 are graphically extrapolated to 10,000 years in Figure 3-7. The start of grain boundary precipitation is not plotted because of the limited amount of available data.

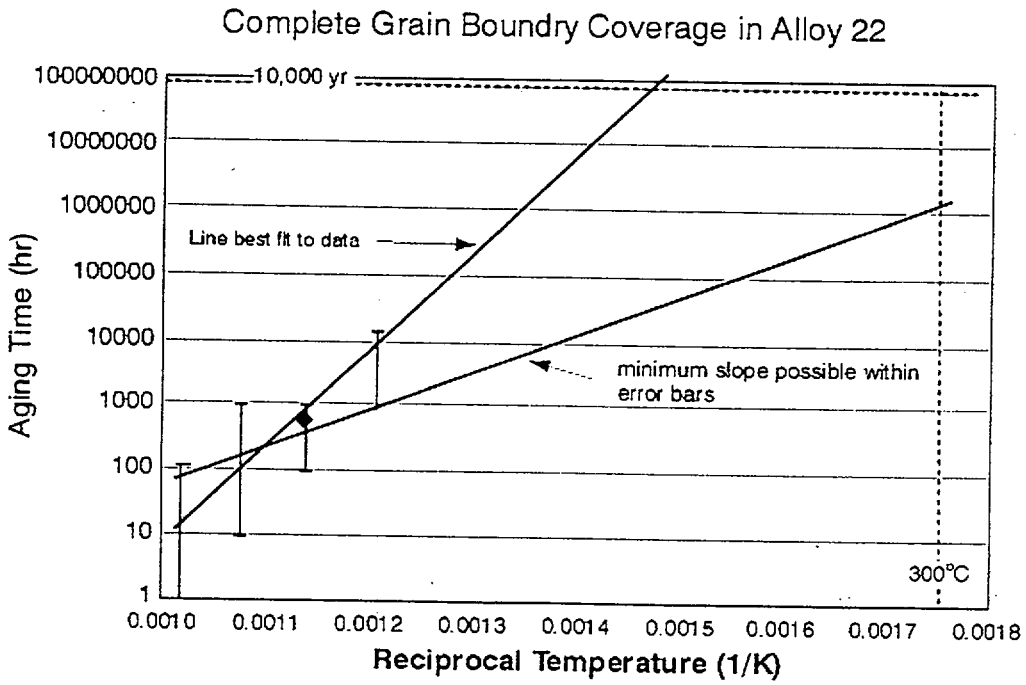

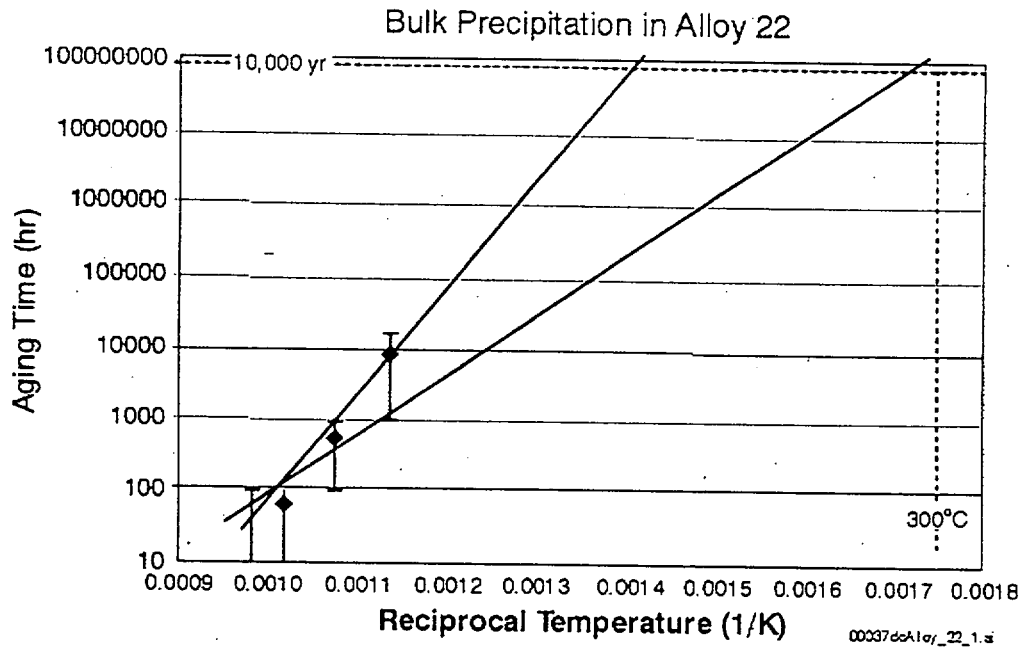

Figure 3-7. Graphical Extrapolation of the Curves to Repository-Relevant Temperatures

The horizontal axes in Figure 3-7 are reciprocal temperature; temperature decreases to the left. If an extrapolation of the data intersects the horizontal line corresponding to 10,000 years to the left of the vertical line corresponding to 300°C, then the temperature must be held higher than 300°C to get bulk precipitation in 10,000 years. In both cases, the data indicate that intermetallic precipitation will not occur in less than 10,000 years even if the temperature is held at 300°C. Also plotted in Figure 3-7 are lines with the minimum possible slope allowed by the error bars on the data. Even accounting for the rather large uncertainty, bulk precipitation does not appear likely in 10,000 years at 300°C. However, grain boundary precipitation might occur if the Alloy 22 stayed at 300°C for 10,000 years. Therefore, a good bounding argument would be to assume that precipitation covers the grain boundary. As can be seen in the time-temperature-transformation diagram of Figure 3-4, samples aged in the laboratory for more than 100 hours at 700°C would produce a microstructure with precipitation covering the grain boundary. Complete grain boundary coverage is taken to represent a fully aged material (worst case). Corrosion data obtained from Alloy 22 base metal samples aged in such a way would represent a worst case condition from a phase stability point of view. Corrosion data on aged samples are presented in Section 3.1.4.5 and presented in greater detail in the AMR on waste package outer barrier (CRWMS M&O 2000c).

As a measure of the reasonableness of the data plotted in Figure 3-7, the activation energy can be calculated. The slopes of the lines in Figure 3-7 (after accounting for the log(e) factor) are equal to C_2/n in Equation 3-5. If these slopes are averaged and n is assumed to be equal to one, then the activation energy is 280 kJ mol^{-1} (68 kcal mol^{-1} using a gas constant R=1.987 cal mol^{-1} K^{-1}). This is close to the value of 62-kcal mol^{-1} obtained for precipitation in Alloy C-276. This value is also typical for diffusion of relevant elements in nickel. For example, the activation energy for diffusion of chromium in nickel is 272.6 kJ mol^{-1}, that of iron is 253-270 kJ mol-1, and that of tungsten in nickel is 300-308 kJ mol^{-1}.

3.1.4.3 Kinetics of Intermetallic Precipitation in Alloy 22 Welds

The heat-affected zone of a weld is the region of the base metal near the weld that is subjected to a significant thermal pulse during the welding process. Intermetallic precipitation processes in the heat-affected zone are expected to be similar to that in the base metal, but actual rates of precipitation (kinetics) may be different. The high temperatures, approaching the melting point, seen in the heat-affected zone of welds might trigger nucleation of intermetallic carbide precipitates. If nuclei are already present, precipitation will proceed much faster than in the base metal where they are not present.

Very few precipitates have been observed in the heat-affected zone of weld samples thus far, but only two weld samples have been examined: one in the as-welded condition and one after aging at 427°C for 40,000 hours. These precipitates may simply be carbides that were present in the mill-annealed (i.e., as-received) condition. Carbides are known to be present in Ni-base alloys similar to Alloy 22, but they are usually within the grains and are generally called primary carbides to distinguish them from other secondary phases that form, often on grain boundary, after an aging treatment.

Welding causes melting of the alloy and the development of an as-cast structure upon cooling. As an Alloy 22 weld solidifies, Mo and Cr are rejected from the solid phase causing their

concentration to increase in the liquid. Therefore, the interdendritic regions, which are the last solid to form in a weld, tend to have high concentrations of these elements relative to typical values for Alloy 22. Because formation of the intermetallic phases, which are also enriched in Mo and/or Cr, are favored by higher Mo and Cr concentrations, these phases are present in the interdendritic regions of Alloy 22 welds.

Because precipitates are present in Alloy 22 welds from the beginning, kinetics of precipitation is not an issue as it is the base metal and the heat affected zone. Corrosion data available from the long-term corrosion test facility shows no measurable difference between welded and base metal samples.

3.1.4.4 Kinetics of Reactions in Alloy 22

Long-range order is treated in a manner similar to that discussed for intermetallic and carbide precipitation. However, very little kinetic data exists for LRO in Alloy 22. Thus far, long-range order has been observed in five samples. A very fine dispersion of ordered domains was seen in Alloy 22 base metal after aging for 30,000 and 40,000 hours at 427°C, and was also seen in a weld similarly aged. The ordering in these cases is so fine that it would be difficult to measure the volume fraction of the ordered domains. Long-range order was also observed in Alloy 22 base metal aged at 593°C for 16,000 hours and at 538 and 593°C for 1,000 hours. The volume fraction of ordered domains has not been measured in these samples. No long-range order was observed in Alloy 22 base metal samples aged for 40,000 hours at 260 and 343°C or for 1,000 hours at 482°C when examined in TEM.

A bounding argument may be made by using the fact that long-range order is just beginning after aging for 30,000 hours at 427°C together with the fact that the long-range order domains are rather small after aging for 1,000 hours at 538°C. These two points are graphed as an Arhenius plot in Figure 3-8. Samples aged for shorter times at 427 and 538°C have not yet been examined in TEM. The curve in Figure 3-8 may shift down (to shorter times) after more data are collected. Because the long-range order domains are very small after aging at 427°C for 30,000 hours, the point corresponding to this aging condition in Figure 3-8 is not likely to change much. In other words, long-range order is not likely to occur in Alloy 22 base metal at 427°C in times significantly less than 30,000 hours. The data point corresponding to aging at 538°C for 1,000 hours will most likely shift down more than that corresponding to aging at 427°C for 30,000 hours after more data are collected. This shift will cause the slope to increase, so the curve in Figure 3-8 represents a bounding case. This graph indicates that long-range order may occur in less than 10,000 years at 300°C. The equation shown in Figure 3-8 was obtained by curve fitting. Taking the natural logarithm of both sides of this equation yields:

$$\ln(t) = \ln\left(5x10^{-7}\right) + \frac{17395}{T} \qquad \text{(Eq. 3-6)}$$

Solving for temperature T:

$$T = \frac{17395}{\ln(t) - \ln(5x10^{-7})} \qquad \text{(Eq. 3-7)}$$

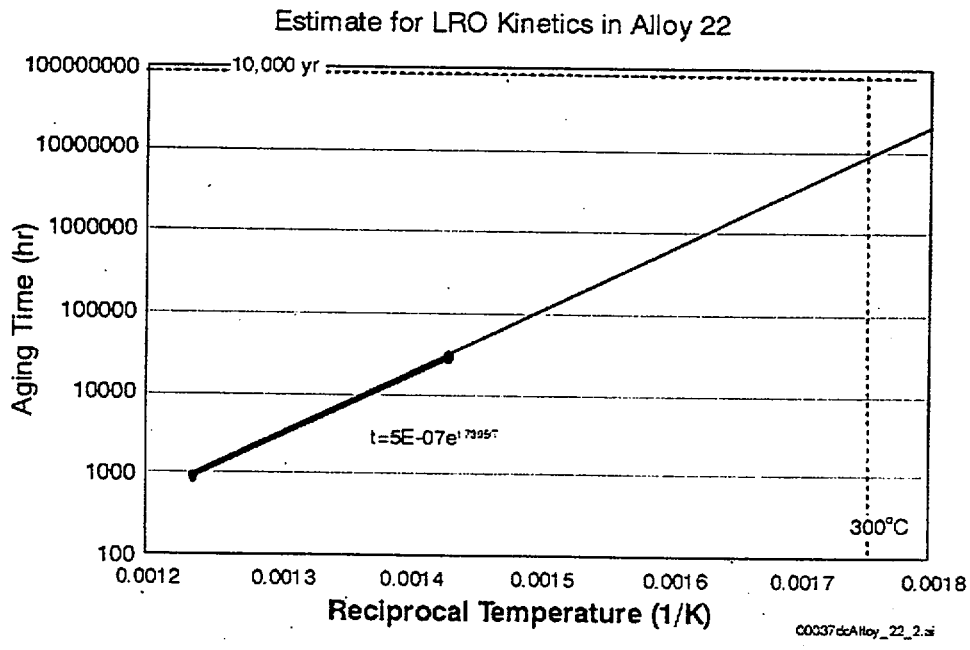

Figure 3-8. Graphical Extrapolation of the Limited Kinetic Data for Long Range Order in Alloy 22 Base Metal

Based upon this analysis, it is concluded that no long-range order will occur after 10,000 years (8.8×10^7 hours), if the temperature remains below approximately 260°C (530 K). More samples are being tested to confirm this conclusion.

3.1.4.5 Effects of Thermal Aging on Corrosion Potential and Rate

The long-term aging of Alloy 22 at elevated temperature can cause the precipitation of undesirable intermetallic phases, if the temperature is sufficiently high. Based upon this analysis, it is recommended that the waste package surface temperature be limited to levels below 300°C. With this constraint, the impact of aging and phase instability on the corrosion of Alloy 22 is not expected to be a problem. An extrapolation of the data shown in Figure 3-6 does not indicate that the phase stability of Alloy 22 base metal will be a problem at less than about 300°C. While this estimate is bounding, it is based on limited data. The significance of the uncertainties in this data is discussed in Section 3.1.9.

Samples of Alloy 22 were aged at 700°C for either 10 or 173 hours. The corrosion resistance of these aged samples is compared to that of base metal in several standardized test media. Figure 3-9 shows a comparison of cyclic polarization curves for base metal and thermally aged material in simulated acidic concentrated water at 90°C. Both curves exhibit generic Type 1 behavior (see Section 3.1.6.3). Type 1 behavior is indicative of passive film stability between the corrosion potential and the thermodynamic limit of the electrolyte (oxygen evolution). In this case, aging shifts the corrosion potential to less noble values, from –176 to –239 mV (versus a standard Ag/AgCl reference electrode). The passive current density is increased slightly, which is indicative of a slight increase in corrosion rate. The highest non-

equilibrium passive current observed for the base metal is approximately 4 μA cm^{-2}, compared to approximately 10 μA cm^{-2} for fully aged material.

Figure 3-10 shows a comparison of cyclic polarization curves for base metal and thermally aged material in SCW at 90°C. In this case, aging also appears to shift the corrosion potential to less noble values, from –237 to somewhere between –328 and –346 mV versus a standard Ag/AgCl reference electrode. In all three cases, the anodic oxidation peak that is characteristic of generic Type 2 behavior is observed. In tests with basic saturated water-13, aging also appears to shift the corrosion potential to less noble values.

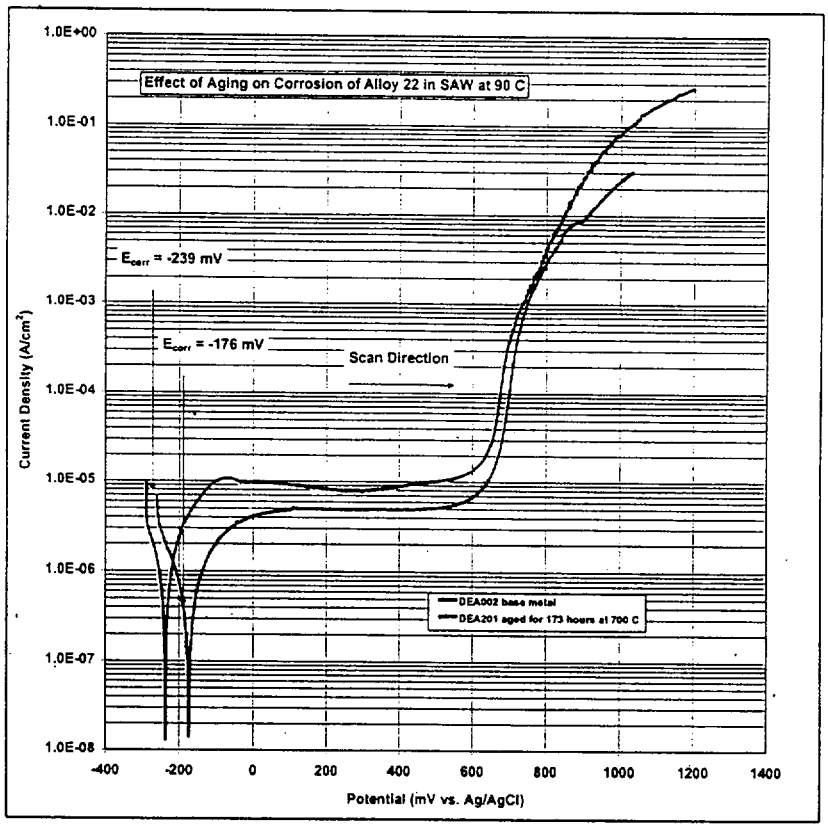

Figure 3-9. Effect of Thermal Aging for 173 Hours at 700°C on the Corrosion Resistance of Alloy 22 in Simulated Acidic Concentrated Water at 90°C (DEA002 and DEA201)

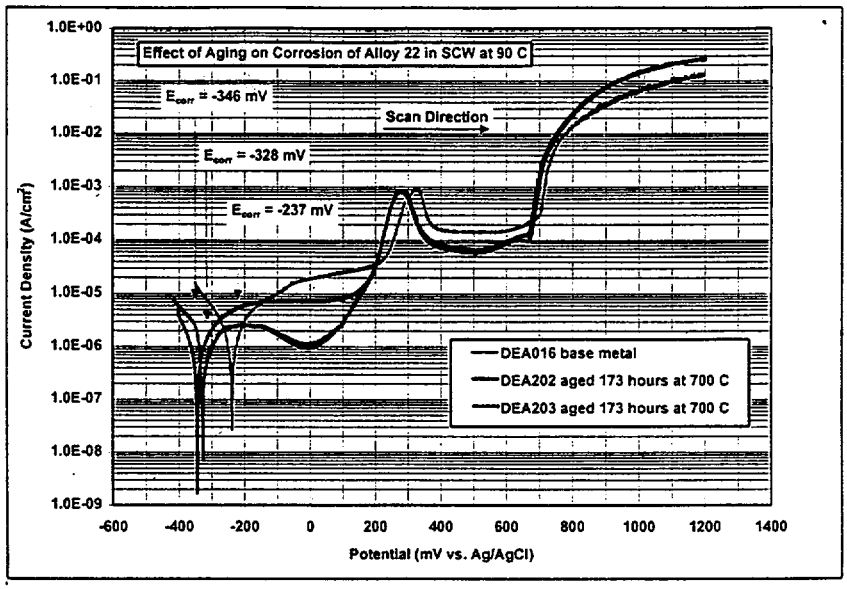

Figure 3-10. Effect of Thermal Aging for 173 Hours at 700°C on the Corrosion Resistance of Alloy 22 in Simulated Concentrated Water at 90°C (DEA016, DEA202 and DEA203)

A fully aged sample of Alloy 22 appears to exhibit a less noble corrosion potential. Typically, the corrosion potential of such a sample is shifted approximately -63 mV in simulated acidic concentrated water at 90°C; -109 mV in SCW at 90°C; and more than -100 mV in basic saturated water at 100°C. Based on this data that E_{corr} can be corrected to account for fully aged material by subtracting approximately 100 mV from values calculated for the base metal. The shift in $E_{critical}$ (threshold potential 1) also appears to be approximately 100 mV in most cases. Thus, the difference $E_{critical}$-E_{corr} is virtually unchanged. This implies that even though the corrosion potential is shifted, the susceptibility to localized corrosion remains unchanged.

The effect of thermal aging on the corrosion rate is accounted for in an enhancement factor, G_{aged}, and is based upon a ratio of the non-equilibrium current densities for base metal and aged material.

$$\left(\left.\frac{dp}{dt}\right|_{effective}\right)_{corrected} = G_{aged} \times \left(\left.\frac{dp}{dt}\right|_{effective}\right)_{original} \qquad \text{(Eq. 3-8)}$$

where $\frac{dp}{dt}$ is the penetration rate for localized corrosion

The value of G_{aged} for Alloy 22 base metal is approximately one ($G_{aged} \sim 1$), whereas the value of G_{aged} for fully aged material is larger ($G_{aged} \sim 2.5$) (CRWMS M&O 2000c). Material with less precipitation than the fully aged material would have an intermediate value of G_{aged} ($1 \leq G_{aged} \leq 2.5$). Therefore, a value to 2.5 for G_{aged} is conservatively used to bound the potential aging effect.

3.1.5 General Corrosion

General Corrosion of the materials of interest includes models for dry oxidation, humid air corrosion and aqueous phase corrosion. Details of these models are provided in the respective AMRs (CRWMS M&O 2000c, 2000d, and 2000e). A schematic representation of a corrosion model for Alloy 22 and an augmentation of this model are shown in Figures 3-11 and 3-12. Only a brief summary of the models is provided in this section.

3.1.5.1 Dry Oxidation

Dry oxidation occurs at any RH below the threshold for humid air corrosion:

$$RH < RH_{critical} \qquad \text{(Eq. 3-9)}$$

This process results in the formation of an adherent, protective oxide film of uniform thickness. The rate of dry oxidation (or dry air oxidation) may be limited by the rate of mass transport through the growing metal oxide film. This scenario is appropriate for Alloy 22 and 316NG due to the availability of data at elevated temperature support such a model. In such cases, the oxide thickness is expected to obey a parabolic growth law (film thickness proportional to the square root of time). Reasonable values of the parabolic rate constant are discussed in a following section of this PMR. However, at lower temperature, a logarithmic law applies. Dry oxidation occurs uniformly over each WAPDEG patch, which is comparable in size to that of a Long Term Corrosion Test Facility sample with generic weight-loss geometry. Backfill effects are not included in dry oxidation threshold and rate.

3.1.5.1.1 Dry Oxidation of Alloy 22 and 316NG

Dry oxidation of Alloy 22 and 316NG stainless steel is expected to occur at any $RH < RH_{critical}$, thereby forming an adherent, protective oxide film of uniform thickness. It is assumed that the protective oxide film is primarily Cr_2O_3. The oxidation reaction is given as

$$4/3\ Cr + O_2 \longrightarrow 2/3\ Cr_2O_3 \qquad \text{(Eq. 3-10)}$$

The rate of dry oxidation is limited by mass transport through this growing metal oxide film with the film thickness being proportional to the square root of time. This is represented by Equation 3-11:

$$x = \sqrt{x_0^2 + k \times t} \qquad \text{(Eq. 3-11)}$$

where x_0 is the initial oxide thickness, x is the oxide thickness at time t, and k is a temperature-dependent parabolic rate constant.

To facilitate an approximate calculation, published values of k can be used (CRWMS M&O 2000c). The highest waste package temperature in the repository is expected to be approximately 350°C (623 K), which corresponds to the limit for the fuel cladding which is much hotter than the WPOB. The value of k corresponding to this upper temperature limit is 2.73×10^{-24} m^2 s^{-1} (8.61×10^{-5} square μm per year). After one year, this corresponds to a growth of

0.0093 μm (about 9.3 nm y^{-1}). This estimated rate is comparable to that expected for aqueous phase corrosion at lower temperatures (based upon data presented in this PMR). The parabolic law is used to represent the dry oxidation Alloy 22 and 316NG. This model is relatively conservative.

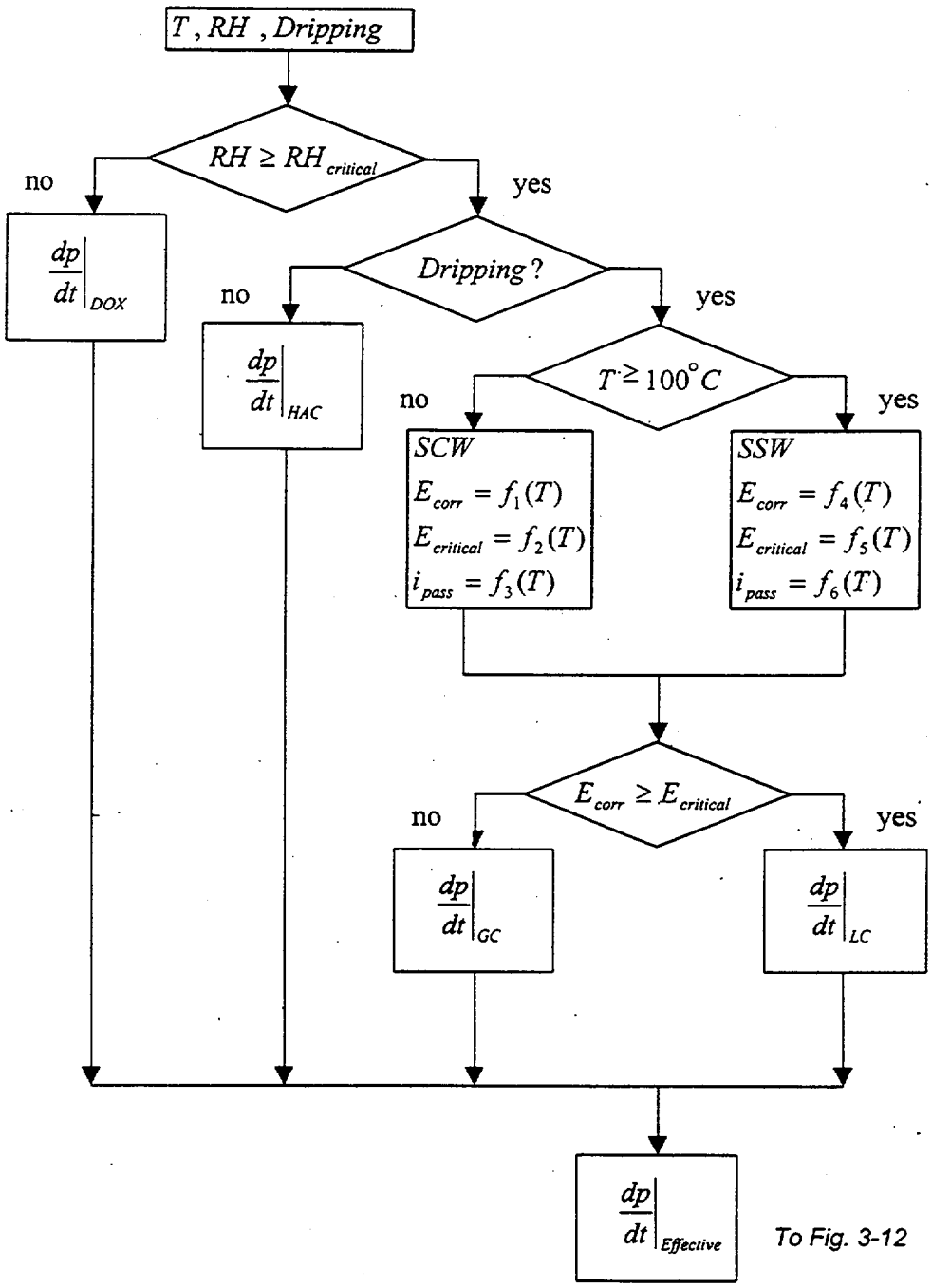

Figure 3-11. Schematic Representation of Model for General Corrosion and Localized Corrosion of Drip Shield and Waste Package Materials

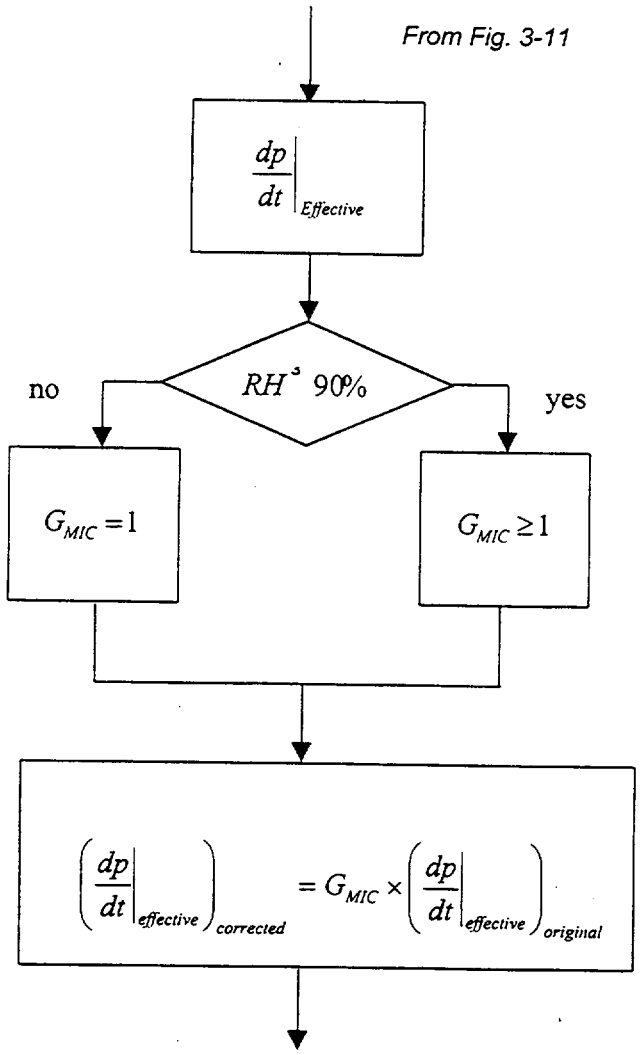

Figure 3-12. Schematic Representation Showing Augmentation of Model for General Corrosion and Localized Corrosion to Account for Microbiologically Influenced Corrosion of Drip Shield and Waste Package Materials

3.1.5.1.2 Dry Oxidation of Titanium Grade 7

As discussed in the AMR for general corrosion and localized corrosion of the drip shield, logarithmic growth laws may be more appropriate at relatively lower temperature than parabolic laws. However, such logarithmic expressions predict that the oxide thickness (penetration) asymptotically approaches a small maximum thickness. In contrast, the parabolic law predicts continuous growth of the oxide, which is much more conservative. Figure 3-13 shows a regression analysis of dry oxidation rate data for titanium. Where X is the oxide thickness X_{max} is the maximum oxide thickness. In $(1-X/X_{max})$ is present the logarithmic growth of oxide film as a function of time. X and X_{max} are in nanometers.

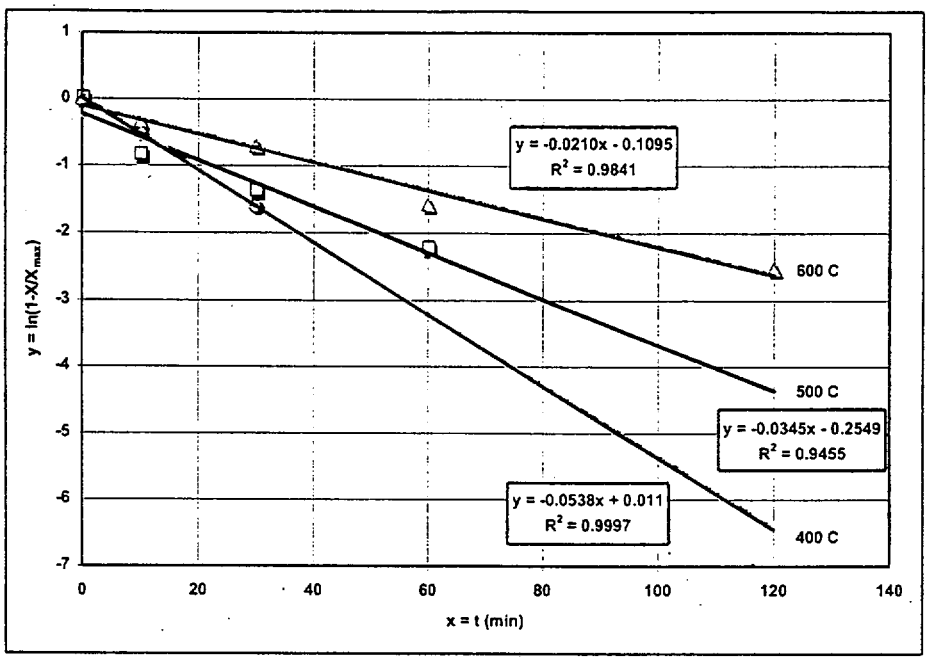

Figure 3-13. Regression Analysis of Dry Oxidation Rate Data for Titanium

3.1.5.2 Humid Air Corrosion

Humid air corrosion is assumed to occur above a threshold RH, provided that there are no impinging drips:

$$RH \geq RH_{critical} \qquad \text{(Eq. 3-12)}$$

The threshold RH for humid air corrosion ($RH_{critical}$) is assumed to obey Equation 3-2. Note that "threshold RH" and "critical RH" are synonymous terms. The existence of this threshold is due to the relationship between water adsorption and RH.

It can be conservatively assumed that the rate of humid air corrosion can be represented by the same corrosion rate distribution used for aqueous phase corrosion during the period where humid air corrosion is operable. It is further predicted that the corrosion rate is constant and does not decrease with time. Less conservative corrosion models assume that the rate decays with time. The rates for aqueous phase corrosion of stainless steel 316NG, Alloy 22, and Titanium Grade 16 (analog of Titanium Grade 7) are described in detail elsewhere in this section.

3.1.5.3 Aqueous Phase Corrosion

At a given surface temperature, the existence of liquid-phase water on the surface of the waste package depends upon the presence of a salt deposit. In the presence of such a deposit, a thin-film liquid phase can be established at a higher temperature than otherwise possible. In the model discussed here, it is assumed that two conditions must be met for aqueous phase corrosion: (1) RH above the deliquescence point of the deposit at the temperature of the waste

package surface; and (2) drips impinging on the waste package surface. The threshold RH for aqueous phase corrosion is identical to that for humid air corrosion:

$$RH \geq RH_{critical} \qquad \text{(Eq. 3-13)}$$

This threshold RH for aqueous phase corrosion ($RH_{critical}$) is assumed to obey Equation 3-2, which is based upon the AMR entitled *Environment on the Surface of Drip Shield and Waste Package Outer Barrier* (CRWMS M&O 2000a). For the time being, the composition of the electrolyte formed on the waste package surface is assumed to be that of SCW below 100°C, and that of simulated saturated water above 100°C. The distributions of general corrosion rates for aqueous phase corrosion of stainless steel 316NG, Alloy 22 and Titanium Grade 16 (analog of Titanium Grade 7) are described in detail in this PMR. It is conservatively assumed that the corrosion rate is constant and that it does not decrease with time.

3.1.5.4 Rates of General and Localized Corrosion

General corrosion rates are utilized in the model if the threshold potential ($E_{critical}$) is not exceeded. General corrosion rates have been estimated from the weight-loss data from the LTCTF. Localized corrosion rates and failure mode characteristics (e.g., number failure sites and opening size) must be estimated from other published data. Only estimates of localized corrosion rates are given in this report. Since pitting of Alloy 22 and Titanium Grade 16 has not been observed in the LTCTF, it is assumed that crevice corrosion is the primary mode of localized corrosion (if localized attack occurs at all). This aqueous phase general corrosion and localized corrosion model will be applied to each element (patch) in the WAPDEG simulation. Uncertainty is accounted for in the WAPDEG stochastic simulation.

3.1.5.4.1 Rates for 316L Stainless Steel – Published Data

The samples under the corrosion testing program do not include stainless steel specimens. Therefore data published in the literature were used to determine the rates of localized corrosion. Rates of general corrosion will be assumed if the threshold potential is not exceeded. The distribution of general corrosion and localized corrosion rates were estimated from the published data for 304 and 316 stainless steel that are summarized in the AMR on stainless steel structural material degradation (CRWMS M&O 2000e). These data are shown in Figures 3-14 through 3-17. Curves are shown for general corrosion in atmospheric environments and aqueous-phase environments, as well as for localized corrosion in aqueous-phase environments. The corresponding distributions can be represented by the following general correlation:

$$y = b_0 + b_1 x \qquad \text{(Eq. 3-14)}$$

where y is the cumulative probability or percentile, and x is the logarithm of the corrosion rate, which is expressed in microns per year. Parameters are given in Figure 3-15. These cumulative distribution functions are truncated for any nonsensical calculated values above one-hundred percent (100%). These distributions do not reflect any environmental dependence, since such a correlation could not be established based upon published data. It is assumed that these distributions are primarily due to variability. In lieu of rigorous estimates of uncertainty, the uncertainty is assumed to be comparable to the variability.

From comparing the data for 304 and 316 stainless steels, the advantages of molybdenum additions are evident. The corrosion rates of 304 are higher than comparable rates of 316. Type 316 stainless steel contains more molybdenum than Type 304 stainless steel. From Figure 3-14, the localized corrosion rates of 316 appear to lie between 10^3 and 10^4 $\mu m\ y^{-1}$. The general corrosion rates for aqueous phase corrosion of 316 appear to lie between 10^{-1} and 10^2 $\mu m\ y^{-1}$. The general corrosion rates for humid air corrosion (atmospheric corrosion) of 316 appear to lie between 10^{-3} and 10^{-1} $\mu m\ y^{-1}$. It is assumed that the published rates for 316 are representative of those for 316NG. The regression line shown in Figure 3-15 is assumed to represent the combined uncertainty and variability. Figures 3-16 and 3-17 show the probability distribution of the corrosion rates and comparison of the observed penetration rates for 304 and 316 stainless steels, respectively.

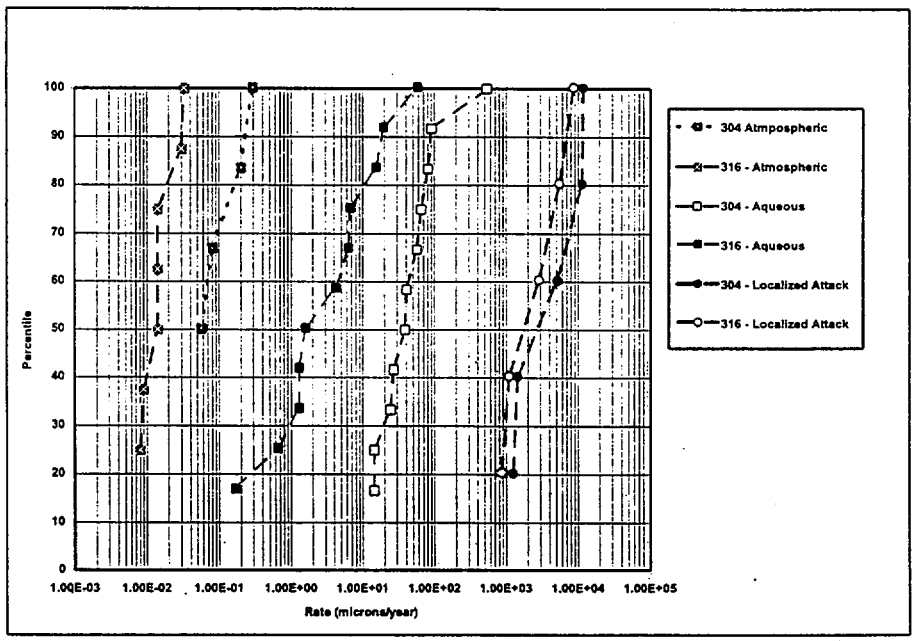

Figure 3-14. Range of Observed Penetration Rates for Stainless Steels 304 and 316 Shown as Cumulative Probability Distributions

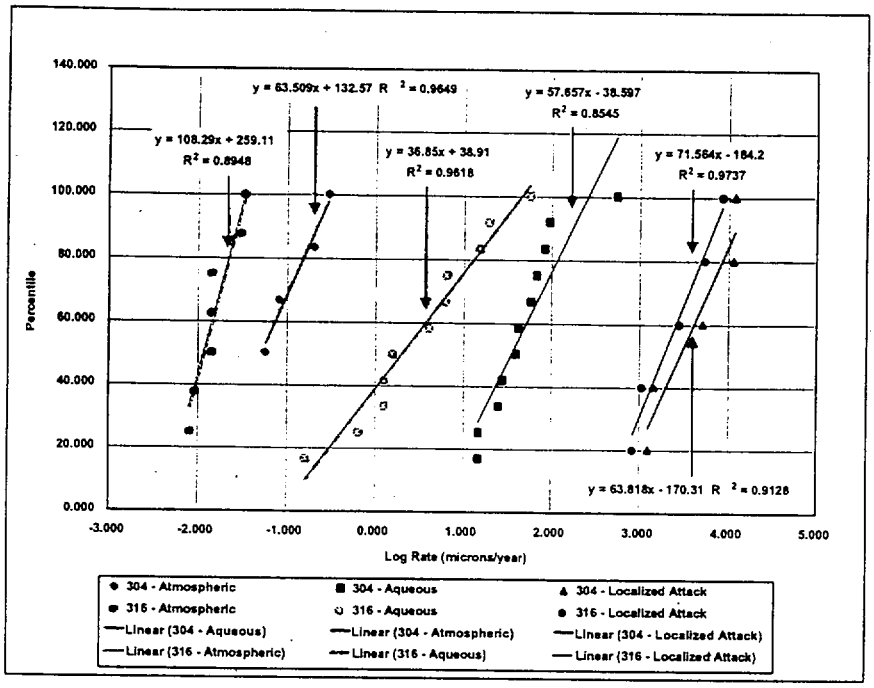

Figure 3-15. Range of Observed Logarithms of Penetration Rates for Stainless Steels 304 and 316 Shown as Cumulative Probability Distributions

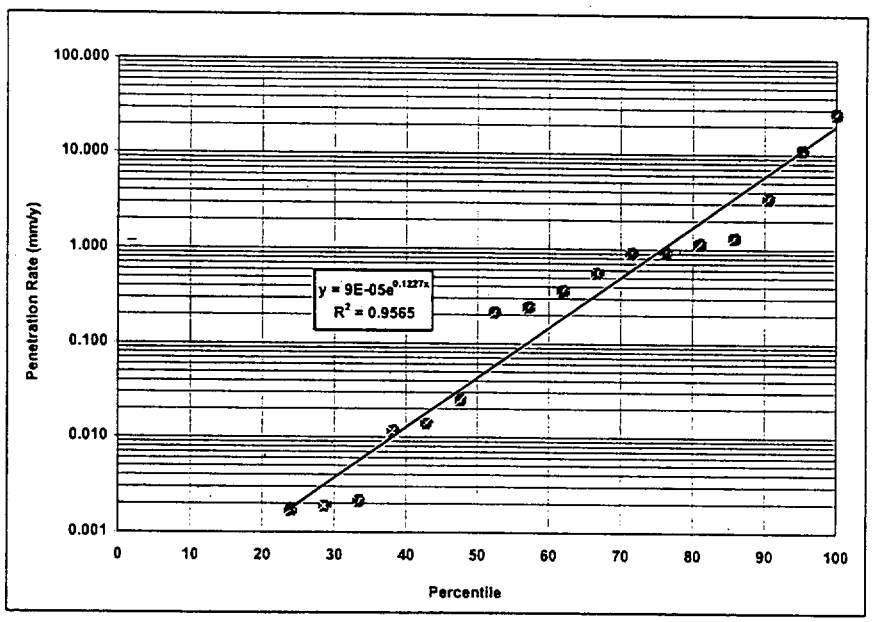

Figure 3-16. Range of Localized Penetration Rates for Stainless Steels 304 and 316

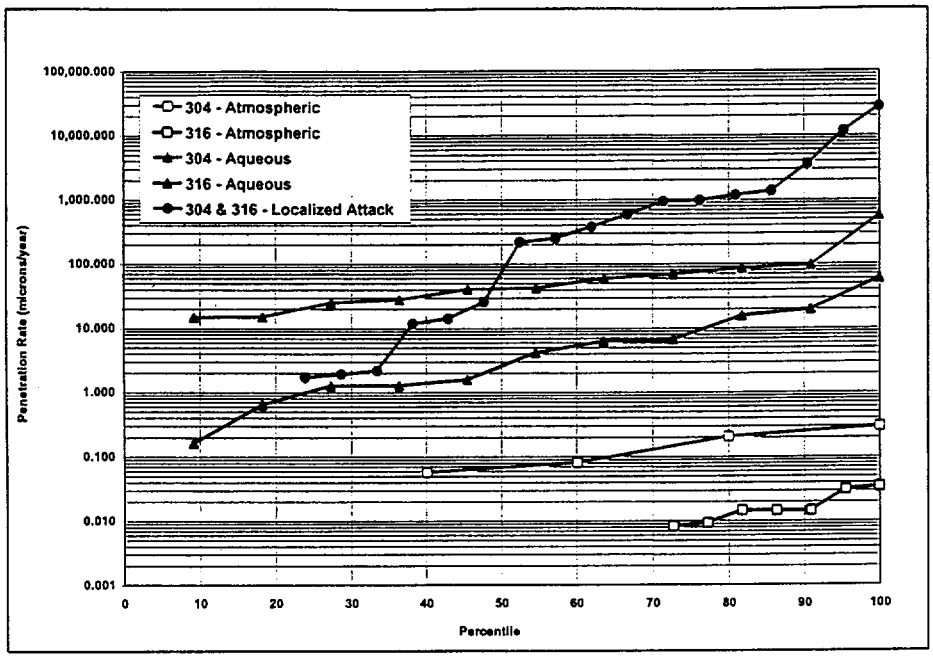

Figure 3-17. Comparison of Observed Penetration Rates for Stainless. Steels 304 and 316

3.1.5.4.2 Rates for Nickel-Based Alloy 22 – Weight Loss Measurements from Long Term Corrosion Test Facility

The Long Term Corrosion Test Facility testing program provides a complete source of corrosion data for Alloy 22 in environments relevant to the potential high-level waste (HLW) repository at Yucca Mountain. The results from that facility are described in detail in the AMR on general corrosion of Alloy 22 (CRWMS M&O 2000c). The general corrosion rates of Alloy 22 measured in the Long Term Corrosion Test Facility should be representative of those expected in the repository. Testing includes a wide range of plausible test media, including simulated dilute water, SCW, simulated acidic concentrated water, and simulated cement-modified water. Simulated dilute water has ten times (10×) the ionic content of J-13 well water, while SCW has 1000× the ionic content. The measured pH levels of the 10× and 1000× J-13 waters are 9.5 to 10. Simulated acidic concentrated water is acidified water that is around 4000× the ionic content of J-13 water with a pH of approximately 2.7. These test solutions mimic the evaporative concentration of electrolytes on the hot waste package surface. Concentrated solutions are intended to mimic the evaporative concentration of the electrolytes on the hot waste package surface. Due to solubility limitations, not all salts in the water concentrate to the nominal levels. However, the more soluble anions such as chloride, sulfate, and nitrate (which have the biggest effects on corrosion) do concentrate to these nominal levels. Two temperature levels (60 and 90°C) are included. The maximum observed rate, which is much less than 1 μm per year, clearly indicates that the life of the Alloy 22 outer barrier will not be limited by general corrosion. It is also assumed that the corrosion rate is constant, and does not decrease with time. Less conservative corrosion models assume that the rate decreases with time.

Specimens are tested at two temperatures (60°C and 90°C) for each of the three water chemistries. Half of the numbers of specimens are fully immersed in the water while the remaining half are exposed to the wet vapor above the water. A few specimens are also placed

right at the water line so that their exposed area is half in the vapor, half in the water. Half of the numbers of test specimens contain welds. All of the specimens were cleaned in accordance with the applicable American Society for Testing and Materials (ASTM) procedure prior to making weight measurements. There were at least 144 test specimens measured during each exposure period. The general corrosion rates are determined from weight loss measurements made at the end of predetermined exposure periods. The uncertainty in these measured rates decreases with increasing exposure time.

Details of the facility and the procedure used for handling the samples are provided in the AMR on general corrosion and localized corrosion of Alloy 22 (CRWMS M&O 2000c). As previously discussed, general corrosion measurements are based upon ASTM G 1-81 (ASTM 1987), or the more recent ASTM G 1-90 (ASTM 1997). The general corrosion (or penetration) rate of an alloy can be calculated from weight loss data as follows with the following general formula:

$$Corrosion\ Rate = \frac{(K \times W)}{(A \times T \times D)} \qquad \text{(Eq. 3-15)}$$

where K is a constant, T is the time of exposure in hours, A is the exposed area of the sample in square centimeters, W is the mass loss in grams, and D is the density of Alloy 22 in grams per cubic centimeter. The value of K used for the Long Term Corrosion Test Facility data was $8.76\times10^{7}\ \mu m\ y^{-1} h\ cm^{-1}$. This formula yields:

$$K = 8.76 \times 10^{7}\ \mu m y^{-1} h cm^{-1}$$
$$W = 0.0001g$$
$$A = 1.0 cm^{2}$$
$$T = 4320h$$
$$D = 8.69 g cm^{-3}$$
$$CorrosionRate = \frac{(8.76 \times 10^{7}\ \mu m y^{-1} h cm^{-1})(0.0001g)}{(1.0\ cm^{2})(4320\ h)(8.69 g cm^{-3})} = 0.23\ \mu m y^{-1}$$

All general corrosion rates for Alloy 22 are based on weight loss measurements. It is observed that these measurements are independent of temperature between 60°C and 90°C. Furthermore, the composition of the test medium (simulated dilute water, SCW or simulated acidic concentrated water) appeared to have little effect on the weight loss measurements. The maximum observed rate based on one year test results is only 160 nm y^{-1}. When all of the measured corrosion rates based upon the weight loss samples are ranked together, regardless of the test medium or temperature, the data is normally distributed around a median value.

All general corrosion rates for Alloy 22 based on Long Term Corrosion Test Facility testing of crevice samples are rates based on areas outside of crevice. In this case, also the measurements are independent of temperature and test medium. When all of the measured corrosion rates based upon the crevice samples from one year tests are ranked together, most of the data points fall below 160 nm y^{-1} and are normally distributed around a median value. However, there are four data points that have abnormally high weight loss that yield rates between 200 and 750 nm, per year. Since no crevice attack of these four samples is evident with microscopic examination,

the high weight loss for these samples is due to the accidental removal of material during mechanical assembly of the crevice sample. The largest measured rate will not lead to failure of the waste package during the first 10,000 years of service. At temperatures less than 90°C, it does not appear that the life of the WPOB will be determined by general corrosion.

The average corrosion rate based upon all weight loss samples is 20 nm y^{-1}, with a standard deviation of 40 nm y^{-1}. The average corrosion rate based upon all crevice samples is 71 nm y^{-1}, with a standard deviation of 89 nm y^{-1}. If the four abnormally high rates are omitted, the average rate is then calculated to be 57 nm y^{-1}, with a standard deviation of 40 nm y^{-1}.

It should be noted that the measured corrosion rates include some negative values. The negative corrosion rates correspond to cases where the samples actually appear to have gained weight during exposure, due to oxide growth or the formation of silicate deposits. To substantiate these interpretations, atomic force microscopy (AFM) has been used to inspect a number of samples removed from the LTCTF. Results of the AFM study are discussed in Attachment I of the AMR on the general corrosion and localized corrosion of Alloy 22 (CRWMS M&O 2000c).

Based upon these data and the associated error analysis, a conservative and defensible representation of the observed corrosion rates is proposed. This approach involves combining the distributions of rates calculated from weight loss and crevice samples. These data are for samples having the generic weight-loss and crevice geometry, respectively. It is conservatively assumed that no scale formation occurs, so all negative rates are eliminated and the entire distribution is assumed to be due to uncertainty. The rate at the 50th percentile is approximately 50 nm y^{-1}, the rate at the 90th percentile is approximately 100 nm y^{-1}, and the maximum rate is 731 nm y^{-1}. Approximately 10 percent of the values fall between 100 and 750 nm y^{-1}.

Figures 3-18 through 3-23 show the data representing 24 months of exposure, which has recently become available. The mean value after 24 months of exposure is 10 nm y^{-1}. The rates of general corrosion do not appear to depend much at all on the temperature and chemical composition of the water tested thus far. Extrapolation of this mean value to 10,000 years would mean an average consumption of only 0.1 mm out of a thickness of 2 cm proposed for the Alloy 22 outer barrier of the waste package. Even at the highest rate measured in this data set, the maximum consumption would be less than 1 mm over the 10,000 year time period. Negative corrosion rates indicate a weight gain by the specimen even after we have thoroughly cleaned off all corrosion products and oxides from the surface.

Cumulative distribution functions generated with 24-month data alone are shown in Figures 3-18 through 3-21. Cumulative distribution functions generated with a combined data set representing 6, 12 and 24-month data are shown in Figures 3-22 and 3-23. The curve shown in Figure 3-22 includes apparent negative rates, while those negative values have been eliminated from the curve shown in Figure 3-23. The curve shown in Figure 3-23 is summarized in Table 3-7. The distributions based upon the 24-month data are more narrow than comparable distributions based upon 6 and 12-month data. Since rates are calculated by dividing exposure time into the weight loss, a doubling of exposure time reduces the estimated error by a factor of two. While outliers were observed in the 6 and 12-month data, none were observed in the 24-month (two-year) data. We believe that these more recent data will greatly extend the range of predicted failure times to

times well beyond the period sought for compliance with the requirement of substantially complete containment.

In observing the surfaces of the exposed specimens for all three time-periods, no evidence of localized corrosion has been observed. Specimens are mounted to the supporting test racks by Teflon coated fasteners and washers. These washers create an intentional crevice to provide a surface area where crevice effects (electrolyte more concentrated than base solution) are developed. In addition, one type of specimen uses a special Teflon crevice former that is spring loaded to ensure that the contact is maintained between washer and specimen (crevice effects are more severe in tight crevices).

Examination of plastically strained U-bend specimens, again for all three time periods, indicates no initiation of SCC in both the base material and in the welded material. Half the number of these U-bend specimens contained welds.

The significance of the observations indicating no localized corrosion (that is no pits, no crevice attack, no intergranular attack) and no stress corrosion crack initiation, as well as a very low general corrosion rate, is reassuring that Alloy 22 will provide an extremely long lived waste package. The longer these corrosion tests operate, the greater will be our assurance of the performance of this material.

In summary, the ranges of general corrosion rates measured at three time intervals (6, 12 and 24 months of exposure) are:

6-month exposure: range –0.06 to +0.73 $\mu m\ y^{-1}$; mean 0.05 $\mu m\ y^{-1}$

12-month exposure: range –0.04 to +0.10 $\mu m\ y^{-1}$; mean 0.03 $\mu m\ y^{-1}$

24-month exposure: range –0.03 to +0.07 $\mu m\ y^{-1}$; mean 0.01 $\mu m\ y^{-1}$

Measurements on the order of 0.01 $\mu m\ y^{-1}$ are around the experimental accuracy of this method. By far, the greatest variation in corrosion rates was measured in the first 6 months of exposure. Thus, the results from the two-year exposure period are very encouraging for Alloy 22. Compared to data generated from earlier exposure time periods, the most recent data set provides greater confidence of the projected corrosion performance of this material.

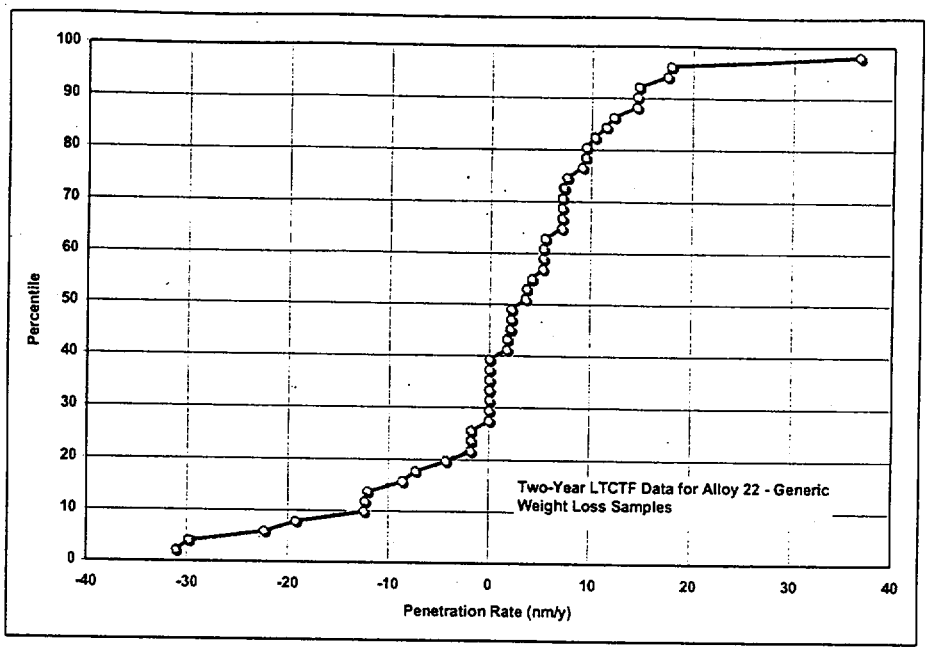

Figure 3-18. Two-Year General Corrosion Rate Data from Long Term Corrosion Test Facility Based Upon Generic Weight Loss Samples

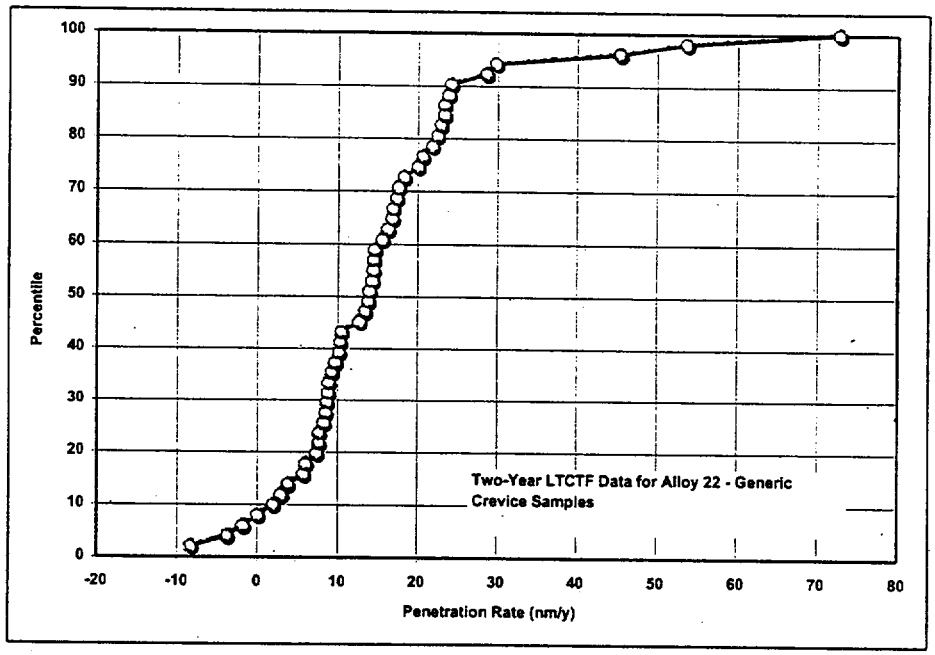

Figure 3-19. Two-Year General Corrosion Rate Data from Long Term Corrosion Test Facility Based Upon Generic Crevice Samples

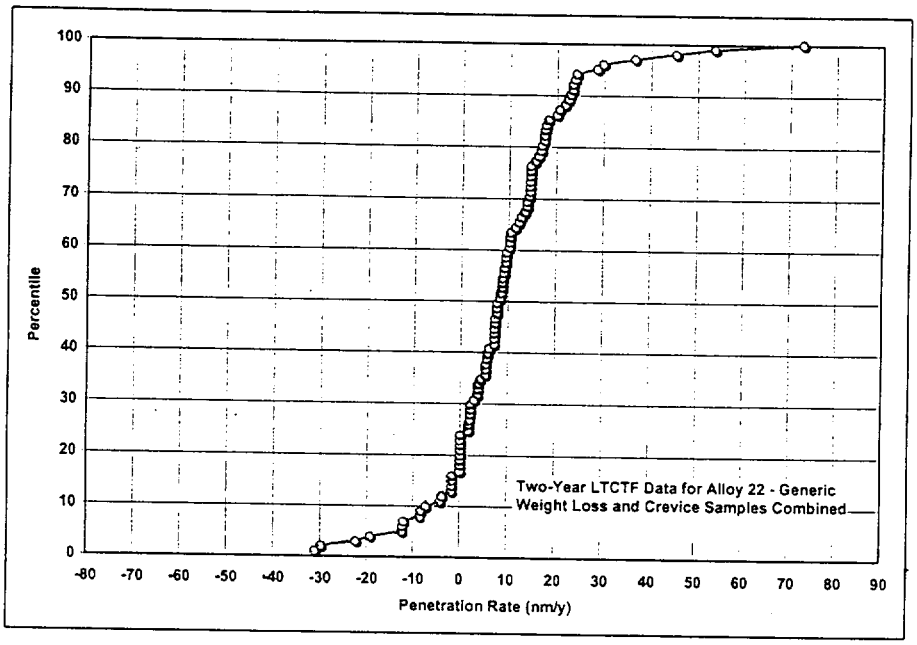

Figure 3-20. Two-Year General Corrosion Rate Data From Long Term Corrosion Test Facility Based Upon Both Generic Weight Loss and Crevice Samples, Including Those with Apparent Negative Rates

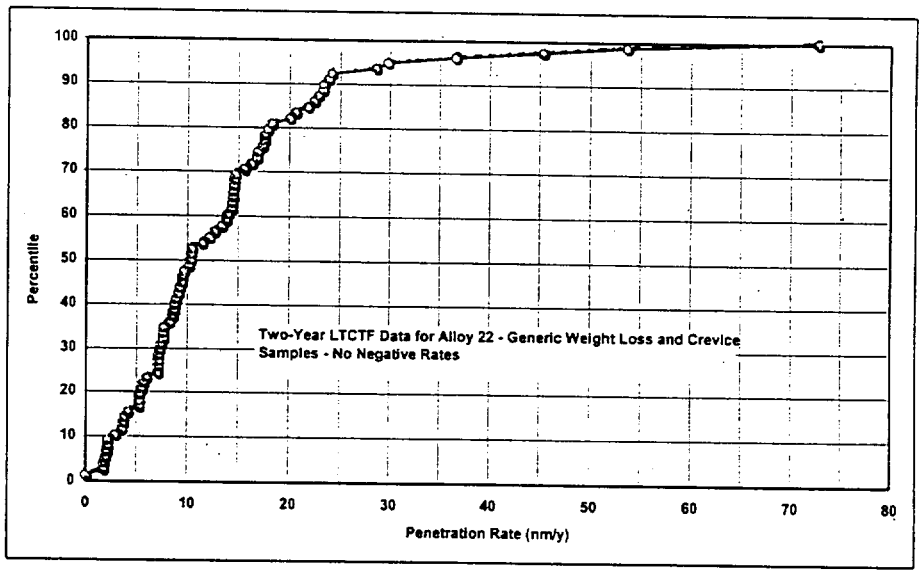

Figure 3-21. Two-Year General Corrosion Rate Data From Long Term Corrosion Test Facility Based Upon Both Generic Weight Loss and Crevice Samples, Excluding Those with Apparent Negative Rates

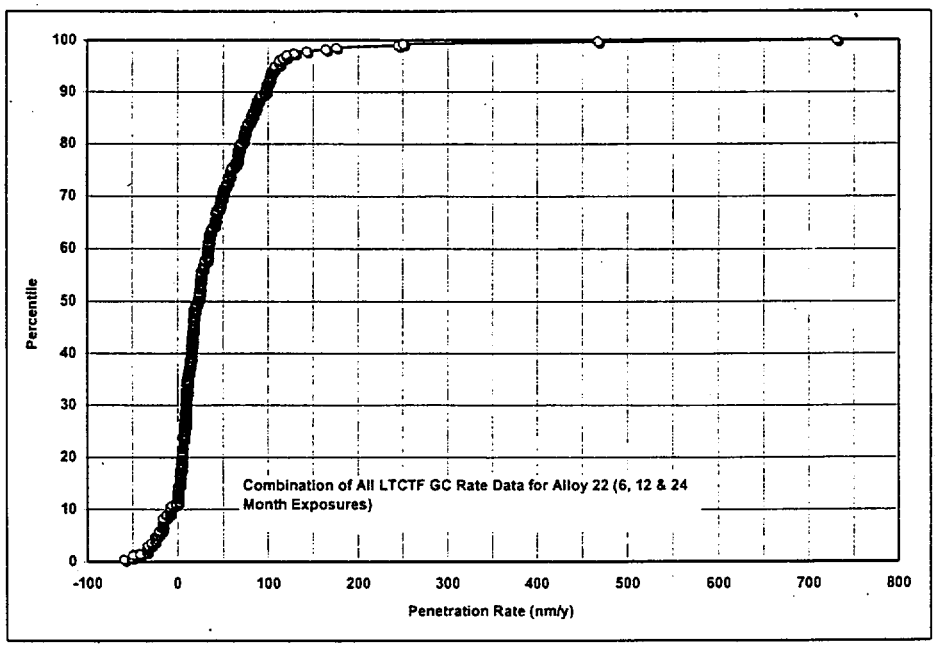

Figure 3-22. Combination of All General Corrosion Rate Data for Alloy 22 from Long Term Corrosion Test Facility, Including 6-, 12-, and 24-Month Exposures

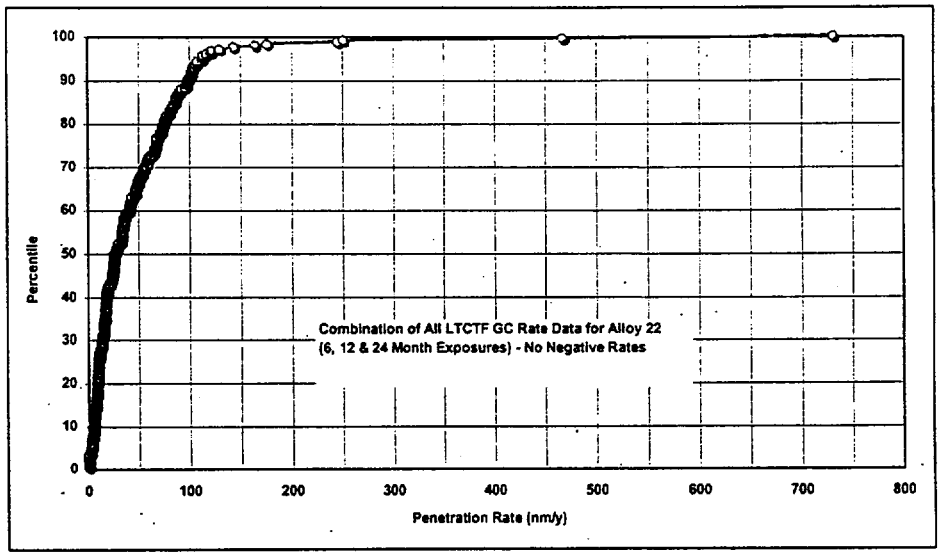

Figure 3-23. Combination of All General Corrosion Rate Data for Alloy 22 from Long Term Corrosion Test Facility, Including 6-, 12-, and 24-Month Exposures with Negative Rates Excluded

Table 3-7. Summary of the Distribution of Rates for General Corrosion of Alloy 22 Samples

Percentile	Penetration Rate (nm y^{-1})
0.00	0
5.20	2.07
10.00	4.21
50.40	26.64
90.00	97.99
95.20	112.54
97.60	143.08
99.20	250.56
99.60	467.28
100.00	730.77

3.1.5.4.3 Rates for Titanium Grade 16 – Weight Loss Measurements from Long Term Corrosion Test Facility

All general corrosion rates for Titanium Grade 16 are based on Long Term Corrosion Test Facility weight loss samples and are shown in Figure 3-24. It appears that these measurements are independent of temperature between 60°C and 90°C. Furthermore, the composition of the test medium (simulated dilute water, SCW, or simulated acidic concentrated water) appeared to have little impact on the measurements. With the exception of four outliers, most of the rates plotted in Figure 3-24 are between -200 and +200 nanometers per year. The median is at approximately zero. The outliers with large negative rates are believed to represent samples where there was significant oxide growth or scale formation (CRWMS M&O 2000c).

This analysis only includes Titanium Grade 16 samples exposed for 12 months in the LTCTF. As discussed by CRWMS M&O (2000d), the cleaning method employed with the 6-month samples resulted in sufficient metal loss to cause the appearance of high corrosion rates that proved to be artifacts. Very little cleaning was used for the 12-month samples, which may account for the large negative values in Figure 3-24 (scale formation).

All general corrosion rates for Titanium Grade 16 based on Long Term Corrosion Test Facility crevice samples are shown in Figure 3-25 (rates based on areas outside of crevice). In this case, it also appears that the measurements are independent of temperature and test medium. Most of the rates plotted in Figure 3-25 are between -350 and +350 nanometers per year. The median is at approximately zero. The largest measured rate shown in Figure 3-25, which is less than +350 microns per year, will not lead to failure of the drip shield during the first 10,000 years of its service life. Based upon these data, it does not appear that the life of the drip shield will be limited by the general corrosion of Titanium Grade 16 (analog of Grade 7) at temperatures less than those involved in the test (90°C).

The crevice samples were configured in such a way as to reveal crevice corrosion if it occurred. Since no obvious crevice attack was observed with the samples represented by these figures, it is assumed that all weight loss in the crevice samples was due to general corrosion outside of the crevice region (area underneath washer). However, higher scatter perhaps indicates more

variability of corrosion inside the crevice. Corrosion inside is more due to differential aeration and/or minor pH changes within the crevice than localized corrosion.

A simple and defensible representation of the observed general corrosion rates is recommended. The distribution of general corrosion rates determined from "weight loss samples" (Figure 3-24) and the distribution of general corrosion rates determined from "crevice samples" (Figure 3-25) are combined into a single distribution. All negative rates are eliminated and the entire distribution is assumed to be due to uncertainty. From Figure 3-26, it can be seen that the rate at the 50th percentile is approximately 25 nanometers per year, the rate at the 90th percentile is approximately 100 nanometers per year, and the maximum rate is less than 350 nanometers per year. About 10 percent of the values fall between 100 and 350 nanometers per year. Figure 3-27 shows that the logarithm of the observed general corrosion rates obeys a rectangular distribution (i.e., a log-uniform Probability Distribution Function).

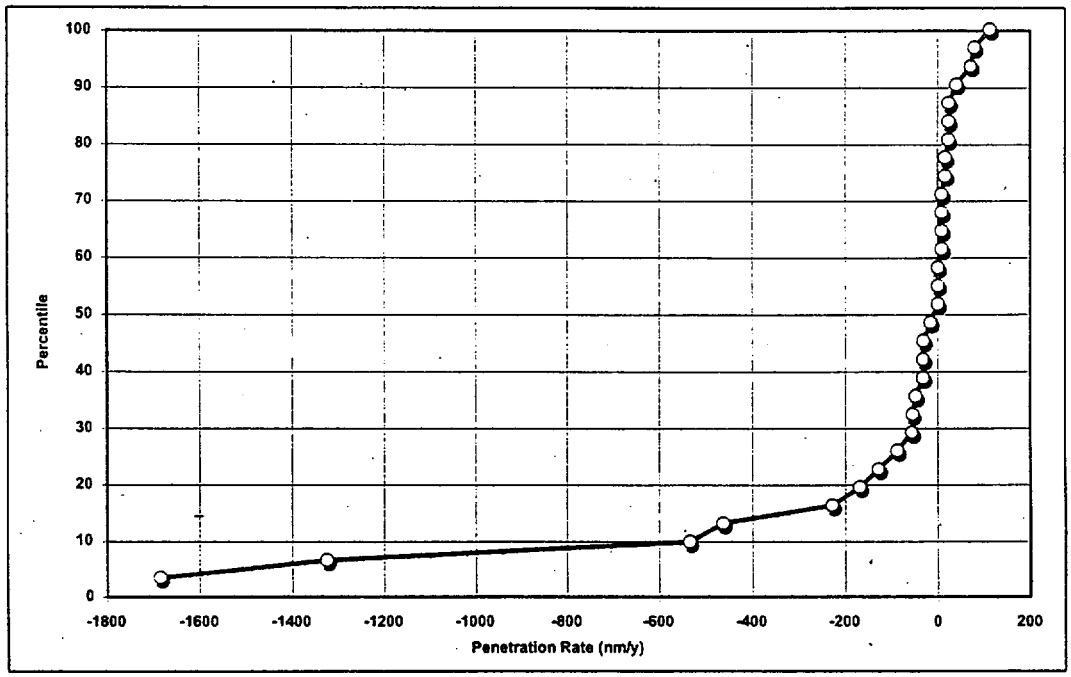

Figure 3-24. General Corrosion of Titanium Grade 16: 12-Month Weight Loss Samples from Long Term Corrosion Test Facility

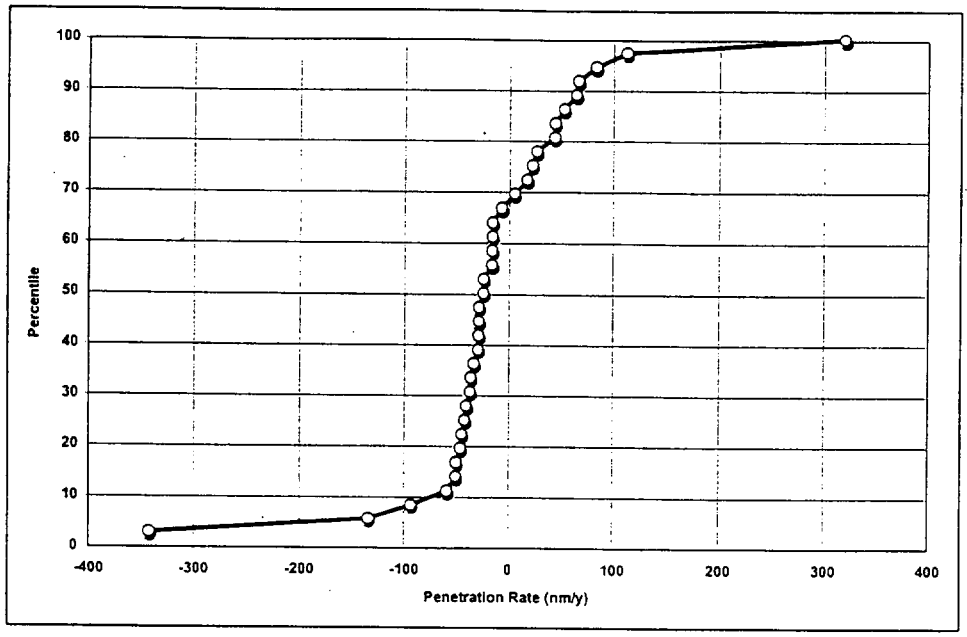

Figure 3-25. General Corrosion of Titanium Grade 16: 12-Month Crevice Samples From Long Term Corrosion Test Facility

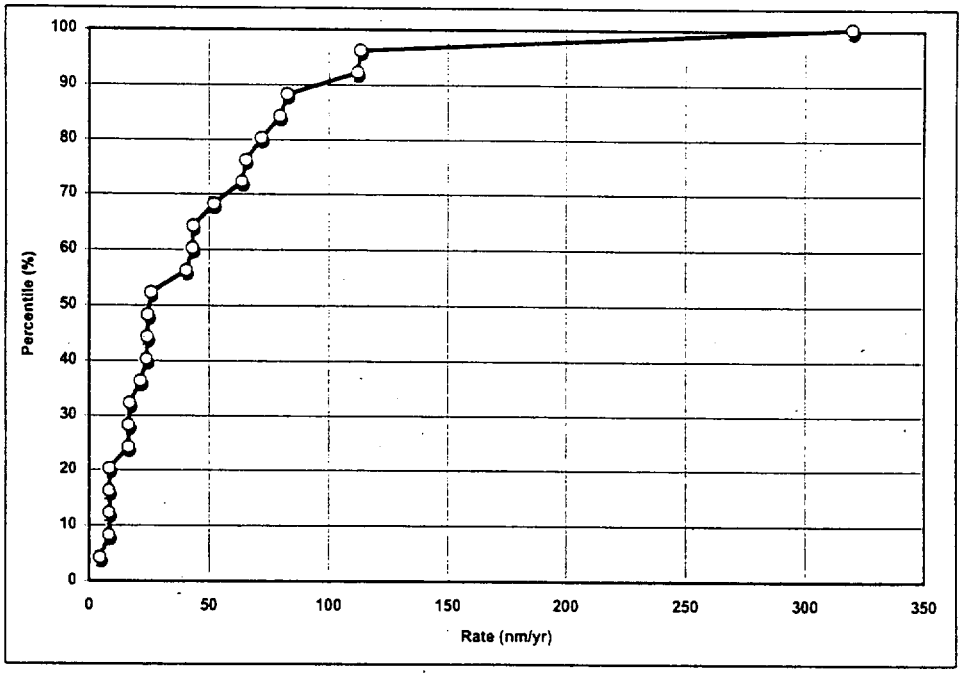

Figure 3-26. Distribution of Positive General Corrosion Rates Based Upon Weight Loss and Crevice Samples

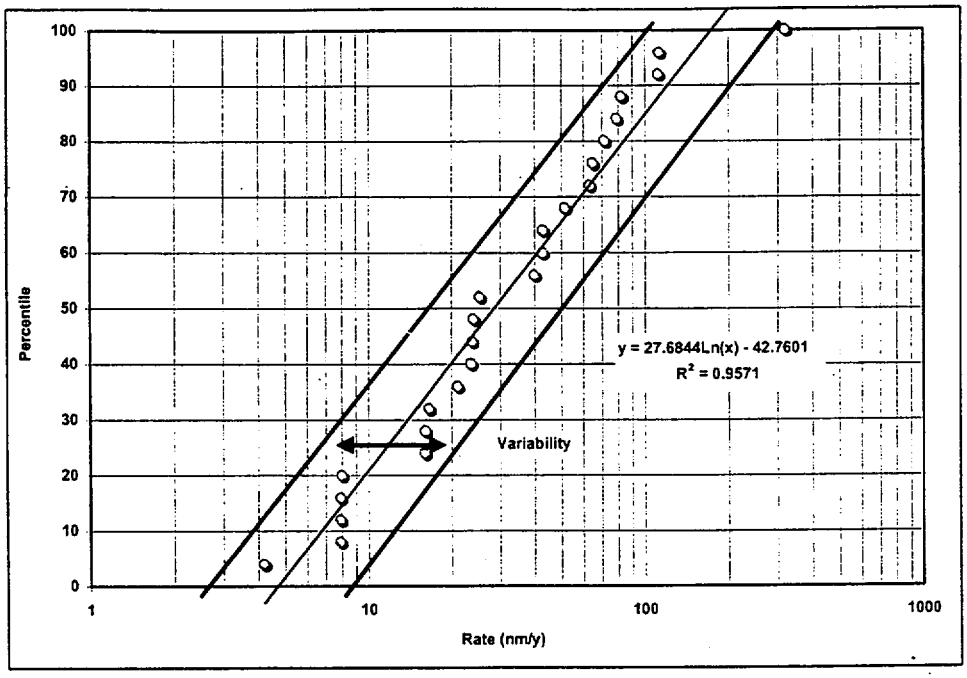

Figure 3-27. Distribution of Positive General Corrosion Rates with Variability Based Upon Weight Loss and Crevice Samples

3.1.5.5 Error Analysis for Corrosion Rates – Weight Loss Measurements from Long Term Corrosion Test Facility

The general method used in the formal error analysis is presented in the AMR on general corrosion and localized corrosion of the WPOB (CRWMS M&O 2000c). The methodology is important since it enables correct interpretation of the data.

The maximum error in the corrosion rate is estimated by calculating numeric values of the partial derivatives from expected values of the independent variables, multiplication of each partial derivative by the corresponding error in the independent variable, and summation of the resulting products. In the case of Alloy 22, the error based upon this method is shown in Table 3-8. The corresponding error for Titanium Grade 16 (Titanium Grade 7 analog) is shown in Table 3-9.

Table 3-8. Summary of Error Analysis for Corrosion Rates Based Upon Weight Loss of Alloy 22

	Assumed Weight Loss		0.0001 g	0.0010 g	0.0100 g
Case	Sample Configuration	Exposure Time	Δy nm y^{-1}	Δy nm y^{-1}	Δy nm y^{-1}
1	Crevice	6 month	12	13	20
2	Weight Loss	6 month	23	25	38
3	Crevice	12 month	6	6	9
4	Weight Loss	12 month	11	12	18

NOTE: Δy = error in general corrosion rate

Table 3-9. Summary of Error Analysis for Corrosion Rates Based Upon Weight Loss of Titanium Grade 16

	Assumed Wt. Loss		0.0001 g	0.0010 g	0.0100 g
Case	Sample Configuration	Exposure Time	Δy nm y^{-1}	Δy nm y^{-1}	Δy nm y^{-1}
1	Crevice	6 month	24	26	47
2	Weight Loss	6 month	45	49	89
3	Crevice	12 month	12	13	22
4	Weight Loss	12 month	22	24	42

NOTE: Δy = error in general corrosion rate

It is concluded that the typical uncertainty observed in weight loss and dimensional measurements prevent determination of corrosion rates for Alloy 22 that are less than approximately 38 nm y^{-1}. The maximum uncertainty is estimated to be approximately 6 to 20 nm y^{-1} in the case of crevice samples, and 11 to 38 nm in the case of weight loss samples. These estimates of probable error are believed to correspond to about one standard deviation (1σ). Therefore, any measured corrosion rate greater than 160 nm y^{-1} (4σ) should be easily distinguishable from measurement error. Any rate less than 160 nm y^{-1} predicts that the WPOB (wall thickness of 2 cm) will not fail by general corrosion. The maximum error in the corrosion rate for Titanium Grade 16 is estimated to be approximately 89 nm y^{-1}, significantly larger than a comparable estimate for Alloy 22. The difference between estimated errors for Alloy 22 and Titanium Grade 16 is attributable to the differences in density.

3.1.6 Localized Corrosion

The difference between E_{corr} and $E_{critical}$ is used to determine whether or not localized corrosion will occur. If $E_{critical}$ is less than or equal to E_{corr}, localized corrosion is likely. These potentials are measured experimentally in electrolyte compositions believed to representative of the repository environment. Such electrolytes are described in a supporting AMR (CRWMS M&O 2000c).

Junction potentials for the reference electrode in all test solutions of interest have been calculated and are discussed in the supporting AMR on general corrosion and localized corrosion of the WPOB (CRWMS M&O 2000c). Since these calculated junction potentials are not very large, it is concluded that no significant error in any potential measurement results by neglecting to correct for the junction potential.

3.1.6.1 Threshold Potentials

The generic localized corrosion model for waste package materials assumes that localized attack occurs if the open circuit corrosion potential (E_{corr}) exceeds the threshold potential for breakdown of the passive film ($E_{critical}$):

$$E_{corr} \geq E_{critical} \qquad \text{(Eq. 3-20)}$$

The repassivation potential is the level at which a failed passive film repassivates, or heals, thereby protecting the surface.

3.1.6.2 Published Repassivation Potentials for Alloy 22

Compared to materials proposed for use in earlier waste package designs, Alloy 22 has superior resistance to localized corrosion. The AMR on general corrosion and localized corrosion of the WPOB includes published repassivation potentials found in the literature (CRWMS M&O 2000c). These data show that the threshold potential for localized corrosion of Alloy 22 is far greater than that of Alloy 625, thereby substantiating the claim that Alloy 22 is superior to the corrosion resistant materials used in earlier waste package designs.

3.1.6.3 Cyclic Polarization in Synthetic Concentrated J-13 Waters

Pitting and crevice corrosion are usually associated with the breakdown of passivity. Tests for evaluating the susceptibility of a material to pitting and crevice corrosion include cyclic potentiodynamic or cyclic polarization test.

ASTM G 61-86 (ASTM 1997) describes a procedure for conducting cyclic potentiodynamic polarization measurements to determine relative susceptibility to localized corrosion. The method is designed for use with iron- or nickel-base alloys in chloride environments. In this test, a cyclic anodic polarization scan is performed at a fixed voltage scan rate.

Particular attention is focused on two features on the cyclic anodic polarization behavior diagram. These are the potential at which the anodic current increases considerably with applied potential or the breakdown potential. In general, the more noble this potential, obtained at a fixed scan rate in this test, the less susceptible the alloy to the initiation of localized attack. The second feature of great interest is the potential at which the hysteresis loop is completed upon reverse polarization scan. In general, once initiated, localized corrosion can propagate at some potential more electropositive than that at which the hysteresis loop is completed (when determined at a fixed scan rate). Therefore, the more electropositive the potential at which the hysteresis loop is completed, the less likely that localized corrosion will occur. This potential is known as the protection potential.

Cyclic Polarization measurements have been based on a procedure similar to ASTM G 5-87 (ASTM 1989), with appropriate and necessary deviations. For example, ASTM G 5-87 calls for an electrolyte of 1N H_2SO_4, whereas simulated dilute water, SCW, simulated acidic concentrated water, and simulated saturated water are used here. Furthermore, aerated solutions were used here, unlike the procedure that calls for de-aerated solutions. A baseline curve with Pt in SCW is shown in Figure 3-28. Representative cyclic polarization curves are shown in Figures 3-29 through 3-37. The shape of these cyclic polarization curves is categorized as type 1, 2, 3, or 4, as will be explained in the following paragraphs.

A generic type 1 curve exhibits complete passivity (no passive film breakdown) between the corrosion potential and the point defined as threshold potential 1. This interpretation was verified by visual inspection of samples after potential scans, and photographic documentation of some of those samples (all samples are held in the archives at Lawrence Livermore National Laboratory (LLNL)). Threshold potential 1 is in the range where the onset of oxygen evolution is expected and is defined by a large excursion in anodic current. This particular definition of threshold potential 1 is specific to type 1 curves. Type 1 behavior has only been observed with

Alloy 22 and is illustrated by Figure 3-29. The interpretation of type 1 curves as exhibiting no passive film breakdown is consistent with Chapter 7 of ASTM G 61-86 (ASTM 1997).

A generic type 2 curve exhibits a well defined oxidation peak at the point defined as threshold potential 1. Threshold potential 2 is in the range where the onset of oxygen evolution is expected, and is defined by a large increase in anodic current. These particular definitions of the threshold potentials are specific to type 2. Repassivation potentials 1 and 2 are defined as the points where the hysteresis loop passes through a current levels of 4.27×10^{-6} and 10^{-5} amps, respectively (not shown). Repassivation potential 3 is determined from the first intersection of the hysteresis loop (reverse scan) with the forward scan. Type 2 is observed with both Alloy 22 and 316L. In the case of Alloy 22, this behavior is illustrated by Figure 3-30. Definitions of the threshold and repassivation potentials are somewhat subjective, and may vary from investigator to investigator. The threshold potential for crevice corrosion of Alloy 22 is defined as the point during the scan of electrochemical potential in the forward direction where the current density increases to a level of 10^{-6} to 10^{-5} A cm^{-2}. The repassivation potential is defined as the point where the current density drops to 10^{-6} to 10^{-7} A cm^{-2}, which is comparable to the definition of repassivation potential 3. The basis for these current densities is discussed in detail in the AMR on general corrosion and localized corrosion of the WPOB (CRWMS M&O 2000c).

As previously discussed, a representative curve for platinum in SCW at 90°C is shown in Figure 3-28. Cyclic polarization measurements of Pt were made to serve as a basis of comparison for similar measurements with Alloy 22 and other materials of interest. From such comparisons, it is concluded that the anodic oxidation peak observed in type 2 curves (between 200 and 600 mV) is due to an anodic reaction of the Alloy 22 passive film. No anodic oxidation peak is observed in the measurement of platinum.

A generic type 3 curve exhibits a complete breakdown of the passive film and active pitting at potentials relatively close to the corrosion potential (E_{corr}). In this case, threshold potential 1 corresponds to the critical pitting potential. Type 3 behavior has only been observed with 316L in simulated saturated water and is illustrated by Figure 3-31. Simulated saturated water is a saturated sodium-potassium-chloride-nitrate electrolyte, formulated to represent the type of concentrated electrolyte that might evolve on a hot waste package surface. This formulation has boiling point of approximately 120°C at ambient pressure. In contrast to the type 3 behavior exhibited by stainless steel 316L in simulated saturated water, Alloy 22 maintains passivity at potentials up to the reversal potential (1200 mV versus Ag/AgCl).

A composite of the cyclic polarization data for Alloy 22 is shown in Figure 3-32. It should be noted that the axes of this figure are changed in comparison to previous figures. The initial portions of these curves show that passivity is maintained at potentials at least as high as 400 mV versus Ag/AgCl in all cases. The lowest potential at which any electrochemical reactivity of the passive film is observed is approximately 200 mV versus Ag/AgCl. Based upon data presented here, it is concluded that pitting attack of Alloy 22 should not occur under conditions expected in the repository. To further substantiate this conclusion, it is noted that no pitting of Alloy 22 has yet been observed in samples removed from the Long Term Corrosion Test Facility after two years of exposure to simulated dilute water, SCW, and simulated acidic concentrated water at 60 and 90°C.

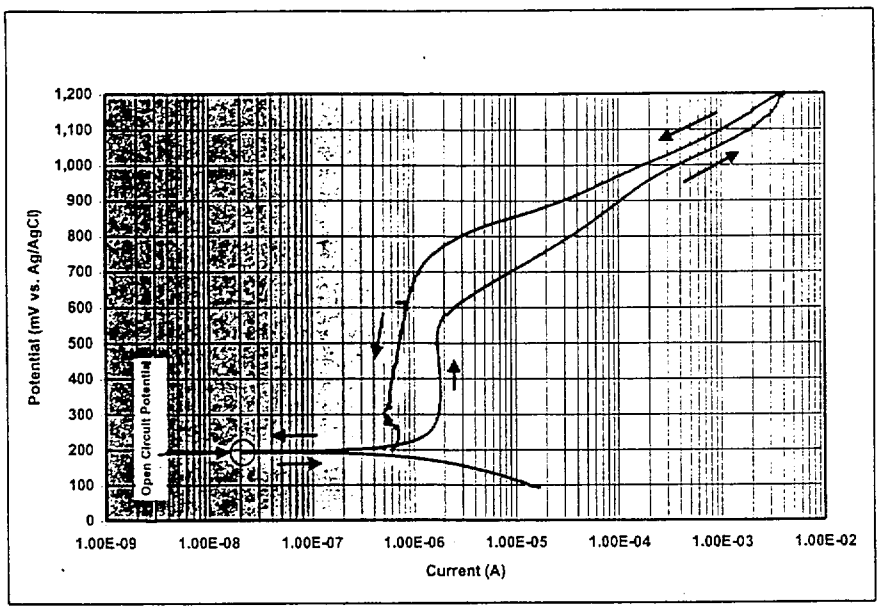

Figure 3-28. Baseline – Platinum in Simulated Concentrated Water at 90°C (PT001)

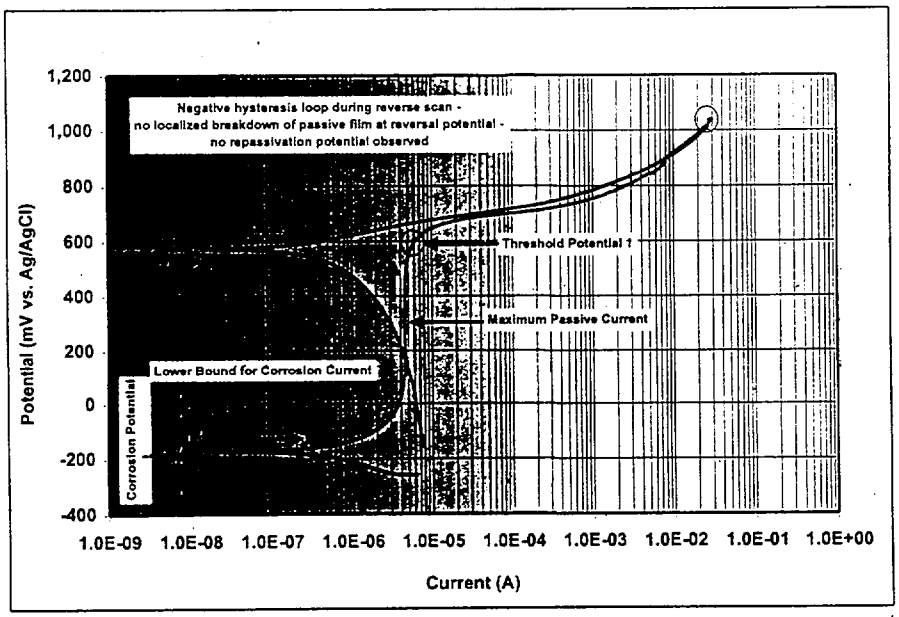

Figure 3-29. Type 1– Alloy 22 in Simulated Acidic Concentrated Water at 90°C (DEA002)

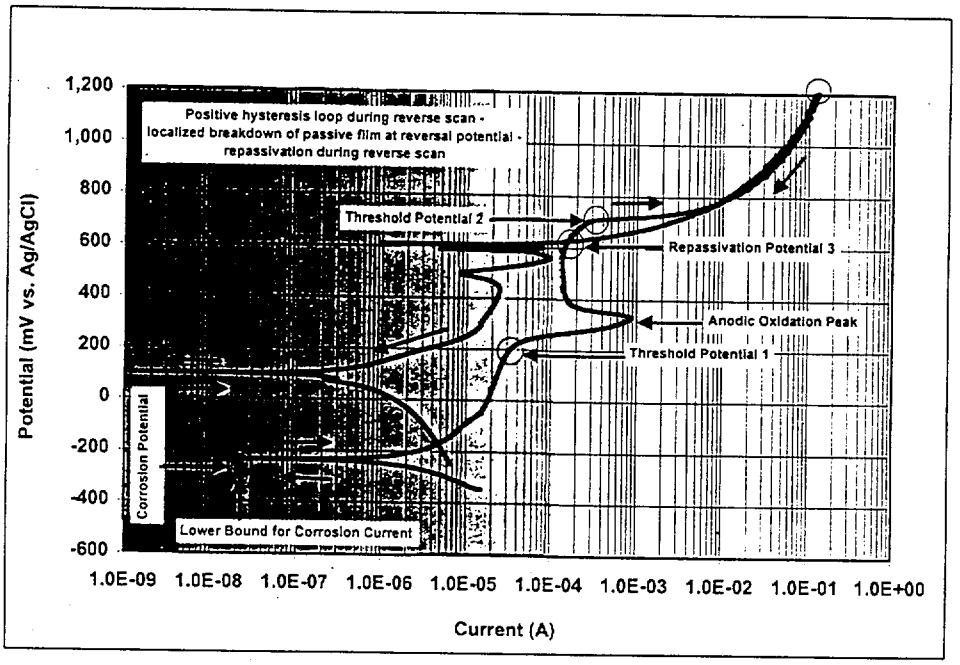

Figure 3-30. Type 2 – Alloy 22 in Simulated Concentrated Water at 90°C (DEA016)

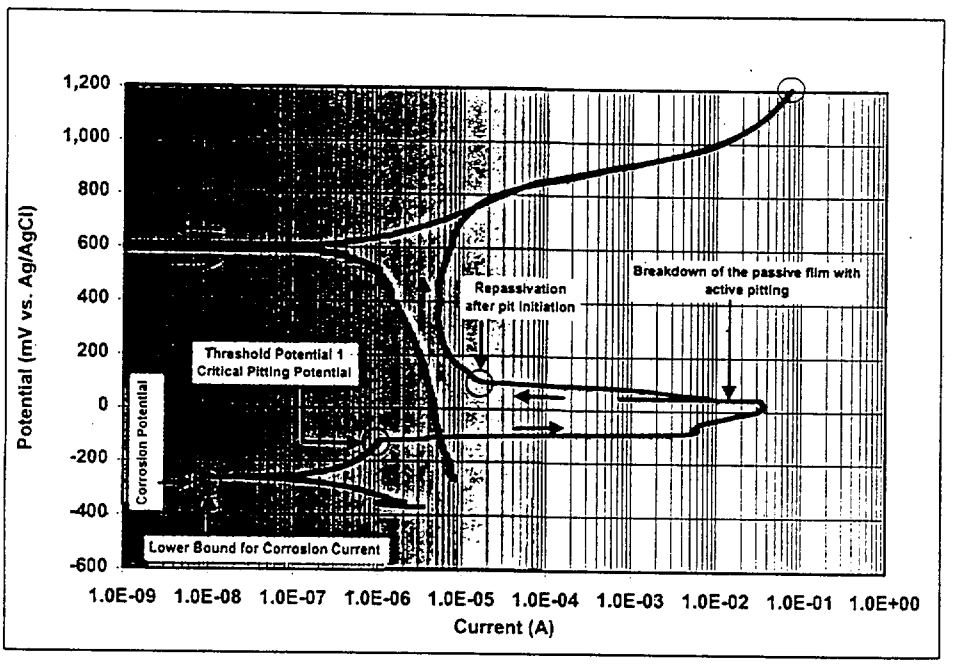

Figure 3-31. Type 3 – 316L in Simulated Saturated Water at 100°C (PEA016)

In regard to type 2 polarization curves for Alloy 22 in SCW, the electrochemical process leading to the anodic oxidation peak (leading edge at approximately 200 mV versus Ag/AgCl) cannot be determined from the cyclic polarization data alone. This peak is probably due to some change in oxidation state of the passive film and probably has very little to do with any loss of passivity. To augment these potentiodynamic measurements, potentiostatic polarization tests have been performed. Figure 3-33 shows the observed transient current when an Alloy 22 sample is polarized at 200 mV versus Ag/AgCl in SCW at 90°C, close to the potential where the leading edge of the anodic oxidation peak is located. The current initially increases to a maximum of approximately 25 microamps per square centimeter (the sample size is approximately 0.96 cm^2) at 9 hours. This corresponds to a typical non-equilibrium passive current density measured for Alloy 22 at this potential in the absence of the anodic oxidation peak. For example, see a type 1 polarization curve for Alloy 22 in simulated acidic concentrated water. Therefore, in regard to type 2 polarization curves, the anodic oxidation peak does not define any localized corrosion or loss in passivity. Furthermore, threshold potential 1 (leading edge of the anodic oxidation peak at approximately 200 mV versus Ag/AgCl) should not be used as the basis for switching on localized corrosion of Alloy 22. Here, it is also assumed that threshold potential 2 represents the lower bound for breakdown of the passive film.

Several cyclic polarization measurements have now been made with basic saturated water electrolytes and are summarized in Table 3-10 and Figures 3-34 and 3-35. As previously discussed, extreme aging of Alloy 22 can shift the corrosion potential in a less noble (cathodic) direction by approximately 100 mV. This is accompanied by a slight increase in non-equilibrium passive current densities. There is some evidence of an anodic oxidation peak, characteristic of type 2 curves. For the present time, we will classify these cyclic polarization curves as intermediate type 1-2.

Examples of cyclic polarization data for Titanium Grade 7 in simulated saturated water and SCW are shown in Figures 3-36 and 3-37, respectively. Both cyclic polarization curves are type 4, showing little evidence of passive film breakdown over a very wide range of potential.

Table 3-10. Electrochemical Potentials Determined from Cyclic Polarization of Alloy 22 in Basic Saturated Water

Sample ID	Aging Time	Aging Temp.	Medium	Temp.	Reversal Potential	Corrosion Potential	Threshold Potential 1	CP Curve Type
	hours	°C		°C	mV	mV	mV	
DEA158	10	700	BSW	110°C	1200	-233	418	Type 1-2
DEA159	10	700	BSW	110°C	1200	-257	419	Type 1-2
DEA208	173	700	BSW	110°C	1200	-345	394	Type 1-2
DEA209	173	700	BSW	110°C	1200	-372	361	Type 1-2

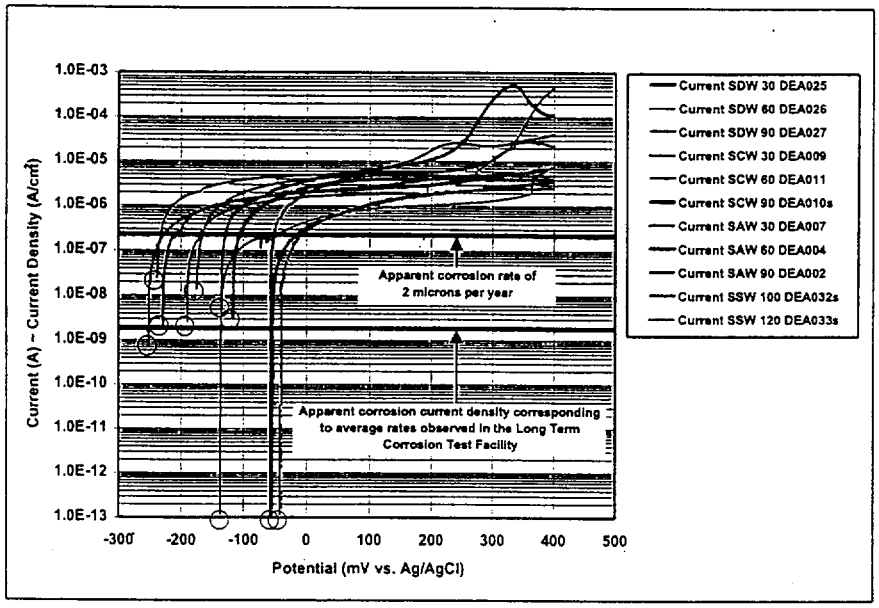

Figure 3-32. Alloy 22 in Various Repository Media – Comparison of Cyclic Polarization Data

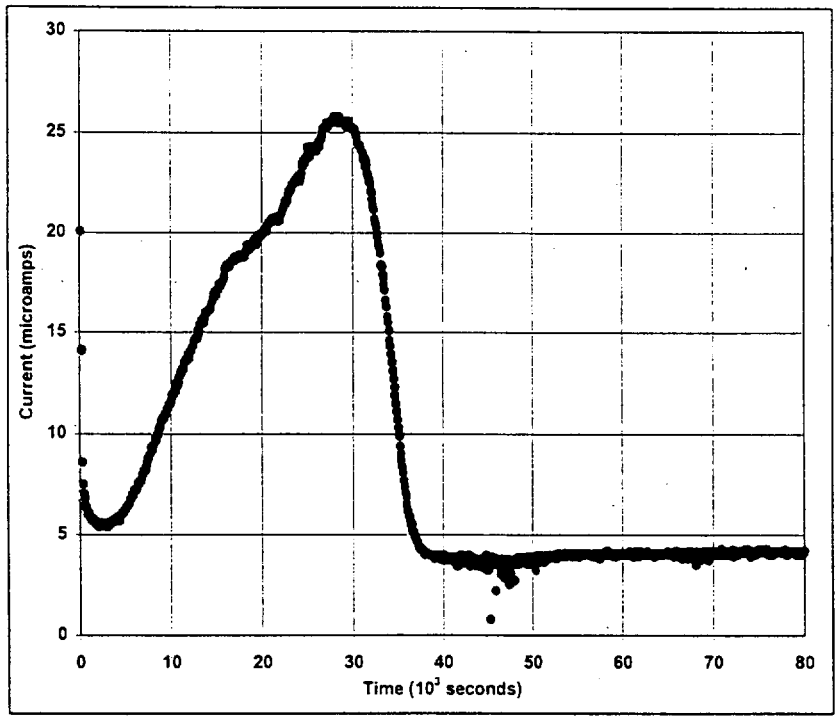

Figure 3-33. Potentiostatic Polarization of Alloy 22 in Simulated Concentrated Water at 90°C and 200mV Versus Ag/AgCl

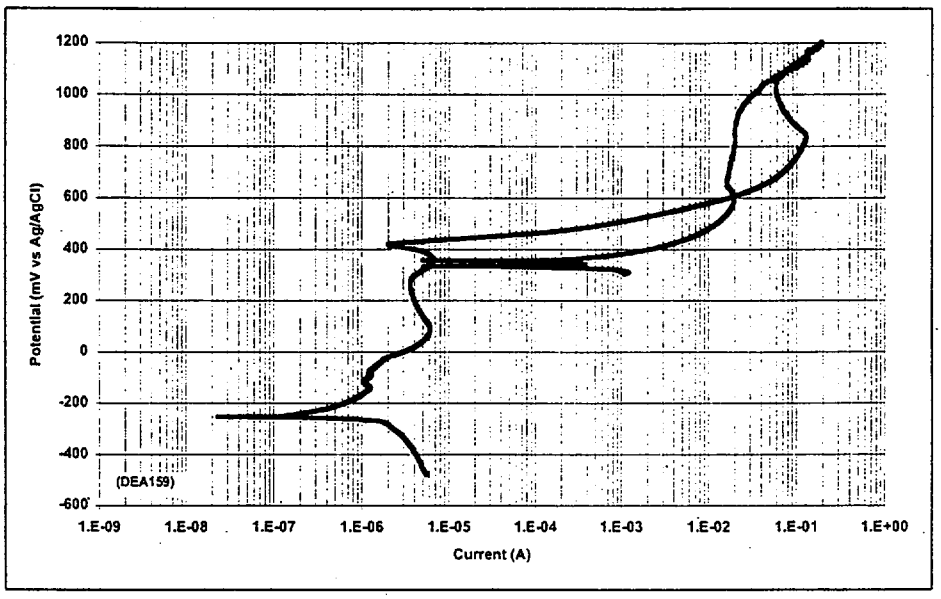

Figure 3-34. Cyclic Polarization Curve for Alloy 22 in 110°C Basic Saturated Water – Thermally Aged at 700°C for 10 Hours (DEA159)

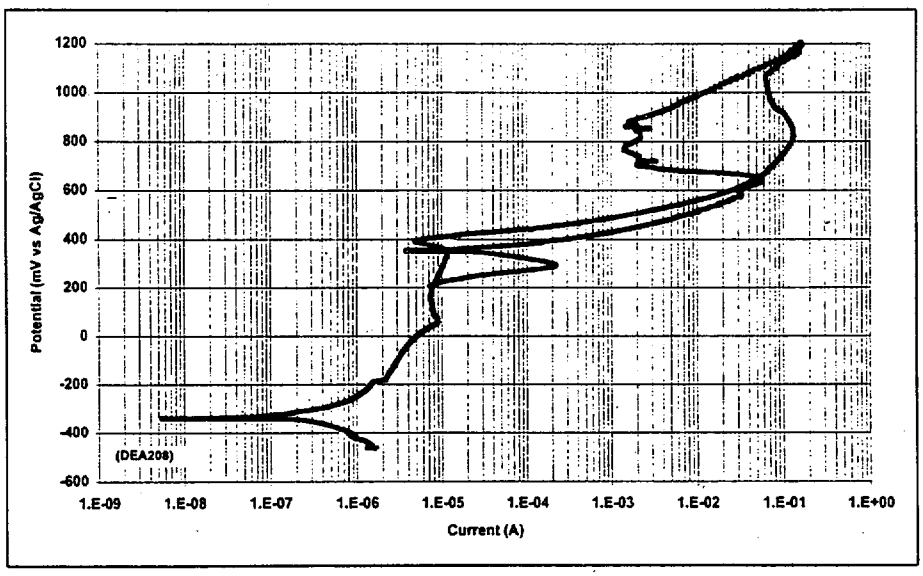

Figure 3-35. Cyclic Polarization Curve for Alloy 22 in 110°C Basic Saturated Water – Thermally Aged at 700°C for 173 Hours (DEA208)

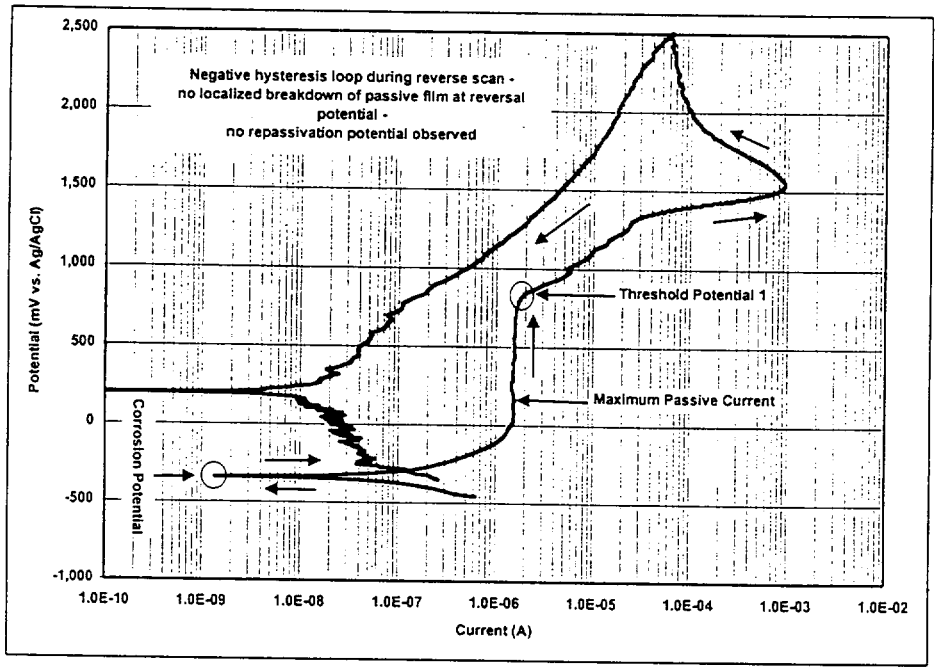

Figure 3-36. Titanium Grade 7 in Simulated Saturated Water at 120°C (NEA031s)

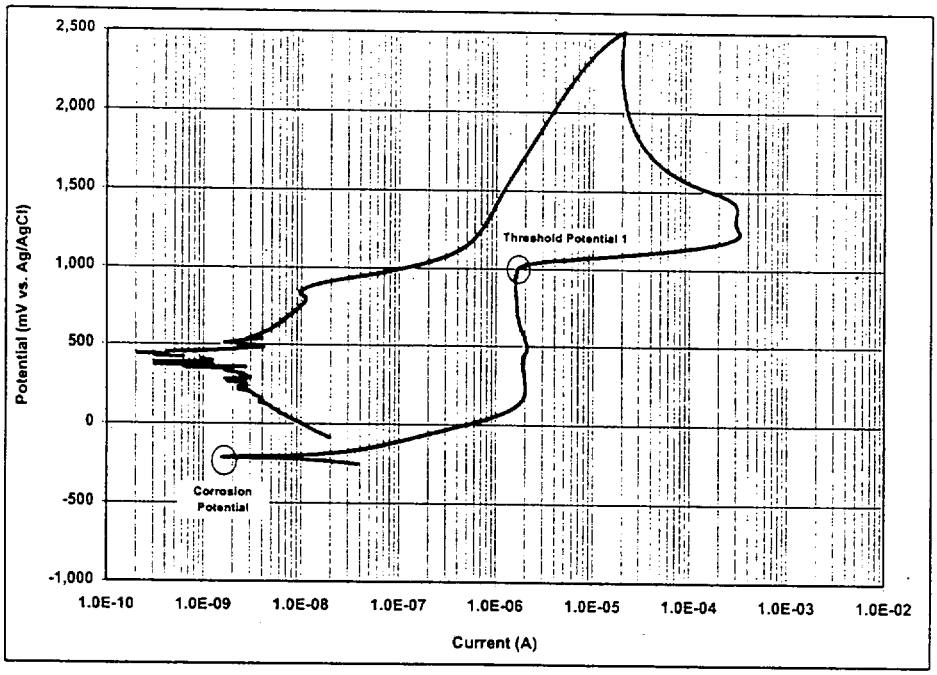

Figure 3-37. Titanium Grade 7 in Simulated Concentrated Water at 90°C (NEA003)

The cyclic polarization data are for test media believed to be representative of the expected repository environment. In such test media and at plausible electrochemical potentials, it does not appear that there will be significant localized breakdown of the passive film. Furthermore,

relatively wide crevices (110 to 540 microns) formed from passive Alloy 22 do not appear to undergo significant increases in hydrogen ion concentration (pH suppression) at reasonable electrochemical potentials. These potentials are generally below the thresholds determined by cyclic polarization. Finally, Alloy 22 and Titanium Grade 16 (Titanium Grade 7 analog) crevices exposed in the Long Term Corrosion Test Facility do not indicate significant crevice corrosion.

However, it should be noted that the University of Virginia has very recently generated some cyclic polarization data with very tight crevices and concentrated electrolytes consisting of 5 M LiCl, 0.24 to 0.024 M $NaNO_3$, 0.026 to 0.26 M Na_2SO_4, and HCl. Testing was conducted at two temperature levels, 80 and 95°C. The crevices were formed with a multiple crevice former, and an applied torque of 70 inch pounds. Under these circumstances, some electrochemical activity indicative of crevice corrosion was observed at potentials ranging from 71 to 397 mV versus Ag/AgCl, depending upon the composition of the electrolyte. Using a current density criterion for repassivation of 10^{-5} A cm^{-2}, repassivation potentials were determined to be slightly above, but relatively close to the open-circuit corrosion potential.

The concentrated lithium-chloride based electrolytes used in the above tests are not relevant to those conditions anticipated in the repository. Unlike compositions based upon J-13 well water, these electrolytes have no buffer ions *per se*. Continued testing is underway with test media relevant to the repository. Tests are being conducted with the tight-crevice geometry used by the University of Virginia and standard electrolytes such as simulated dilute water, SCW, simulated acidic concentrated water and simulated saturated water. In the preliminary test, it has been simulated repository waters (with buffer) appear to inhibit the type of crevice corrosion observed in electrolytes based upon lithium chloride. As more data become available, correlation equations for the corrosion and threshold potentials should be updated, expressing these quantities in terms of temperature, pH, and the concentrations of various ions.

3.1.6.4 Correlation of Potential Versus Temperature Data for Various Test Media

Values of corrosion and threshold potentials for the three waste package materials of interest have been correlated as a function of temperature for the conditions of interest. In general, it has been found that these potential versus temperature data can be represented by the following simple regression equation:

$$y = b_0 + b_1 x + b_2 x^2 \qquad \text{(Eq. 3-21)}$$

where y is either the corrosion or threshold potential (mV vs. Ag/AgCl), and x is the temperature (°C). Parameters for Equation 3-21 are found in Figures 3-38 through 3-48. These parameters were used to calculate values of E_{corr} and $E_{critical}$ for the waste package materials in simulated dilute water, SCW, simulated acidic concentrated water, and simulated saturated water at 10°C intervals. These calculations and tabulations of the parameters are found in the supporting AMR documents (CRWMS M&O 2000c, 2000d, 2000e).

All correlation equations for stainless steel 316NG are found in Figures 3-38 through 3-40. The correlation for E_{corr} and the most conservative correlation for the threshold potential, $E_{critical}$, are labeled. In the case of type 2 cyclic polarization curves, the selected threshold potential is

determined by the position of the observed anodic oxidation peak, and may not result in any actual loss of passivity. In the case of type 3 cyclic polarization curves, the measured threshold potentials are scattered. The transparent square in Figure 3-40 therefore represents the range of potential and temperature where pitting attack is believed to be possible. The lower boundary of the square appears to be very close to the line representing the corrosion potential. Note that these very low threshold potentials are entirely consistent with the published temperature-dependent pitting potentials. These data are represented by Equation 3-21 where $b_0 = 547.76$, $b_1 = -6.617$ and $b_2 = 0$. As this correlation is extrapolated to 100°C, the pitting potential approaches the lower boundary of the transparent box used to bound the threshold potentials.

All correlation equations for Alloy 22 are found in Figures 3-41 through 3-44. The correlation for the corrosion potential (E_{corr}) and the conservative correlation for the threshold potential ($E_{critical}$) are labeled. While calculated values of y are believed to have only three significant figures, coefficients in that regression equation are given with more figures. The correlation equations for Titanium Grade 7 are found in Figures 3-45 through 3-48.

In an ideal case, the crevice corrosion temperature can be estimated from the intersection of the lines representing the corrosion and threshold potentials at elevated temperature. Better correlations of E_{corr} and $E_{critical}$ with material history, water chemistry, and temperature may ultimately allow precise prediction of the crevice corrosion temperature. Improved correlations would provide rigorous statistical estimates of uncertainty and variability in E_{corr} and $E_{critical}$. The precise determination of uncertainty and variability in E_{corr} and $E_{critical}$ would enable designers to determine the impact of accepting 100% of the supplied waste package material on repository performance. In the mean time, crevice corrosion can be forced to occur in the model by equating E_{corr} and $E_{critical}$ over temperature ranges of uncertainty (90-120°C). This assumption would provide a conservative estimate of the crevice corrosion temperature. Improved localized corrosion models with accurate temperature dependence will allow a precise sensitivity study, assessing the impact of various waste package design changes on the radiological dose at the site boundary.

There are precedents for using electrochemical measurements as the basis of water chemistry and materials specifications in the nuclear industry. For example, measurements of corrosion potential are indicative of dissolved oxygen and can be used to assure adequate deaeration in various regions of the steam cycle. The role of electrochemical potential on SCC has been well documented (CRWMS M&O 2000c).

3.1.6.5 Prediction of Critical Temperatures for Pitting and Crevice Corrosion

As previously discussed, a threshold temperature (critical temperature) can be used as an alternative to a threshold potential for the initiation of localized corrosion. In an ideal case, the critical temperatures for pitting and crevice corrosion can be estimated from the intersection of the lines representing the corrosion and threshold potentials as functions of temperature. This intersection occurs at elevated temperature. The critical temperature for pitting of stainless steel 316L is illustrated by Figures 3-49 and 3-50. To force crevice corrosion to occur in the model, E_{corr} and $E_{critical}$ can simply be equated above the critical temperature.

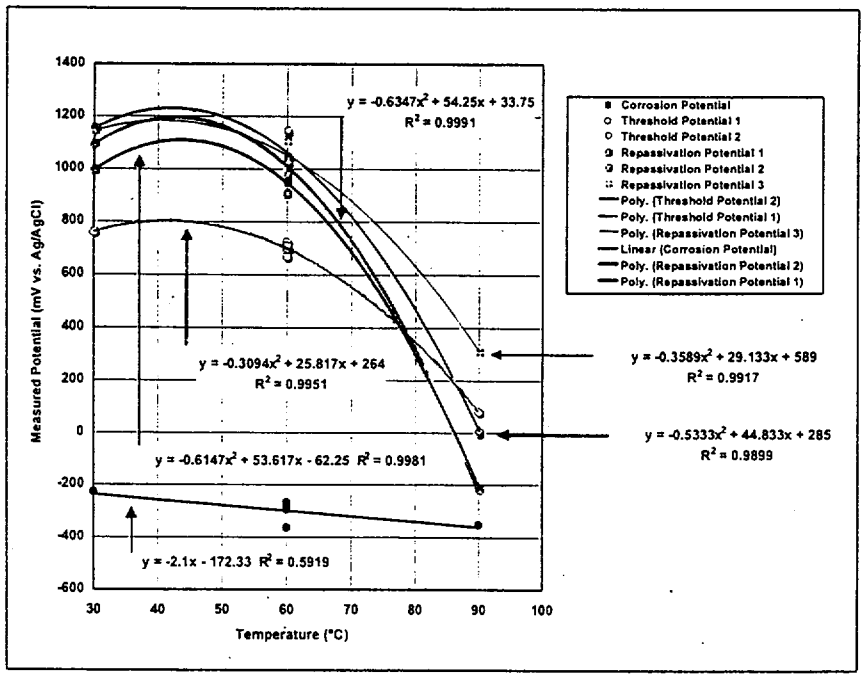

Figure 3-38. Potentials versus Temperature – Stainless Steel 316L in Simulated Acidic Concentrated Water

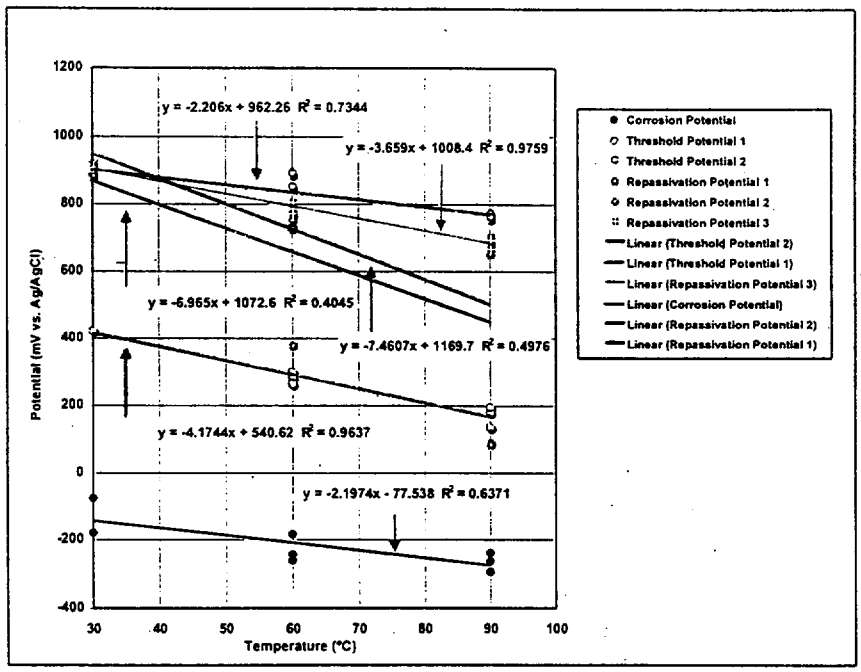

Figure 3-39. Potentials versus Temperature – Stainless Steel 316L in Simulated Concentrated Water

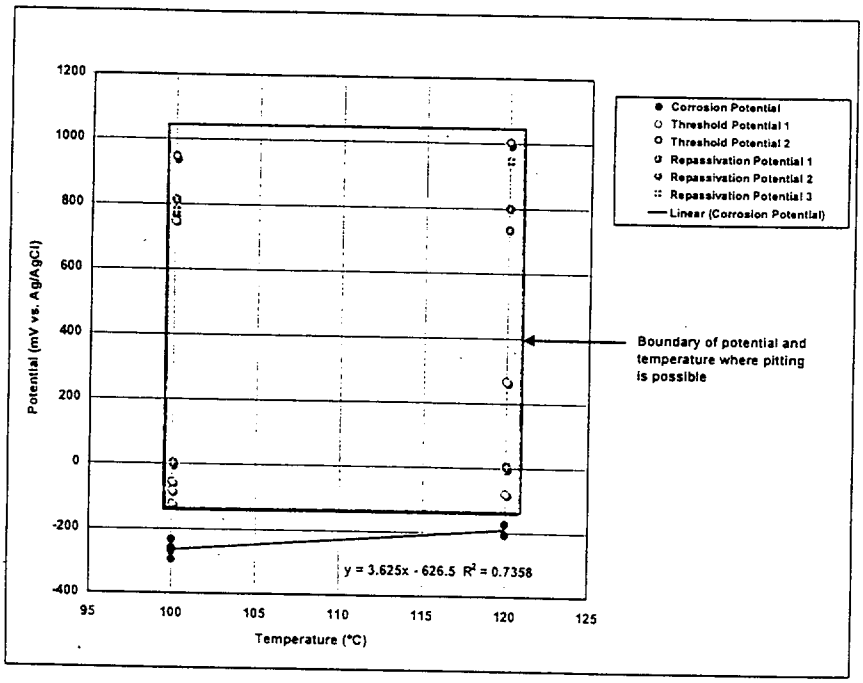

Figure 3-40. Potentials versus Temperature – Stainless Steel 316L in Simulated Saturated Water

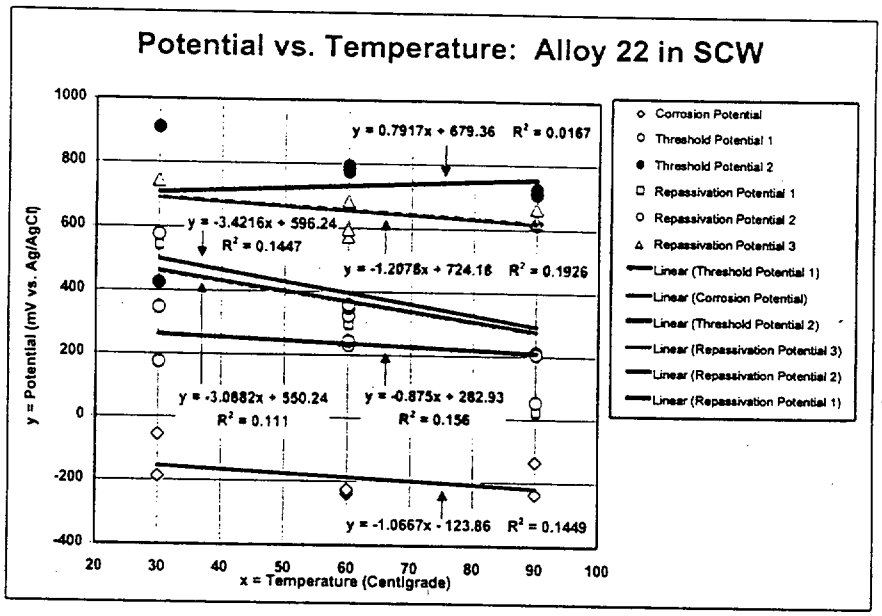

Figure 3-41. Potentials versus Temperature – Alloy 22 in Simulated Dilute Water

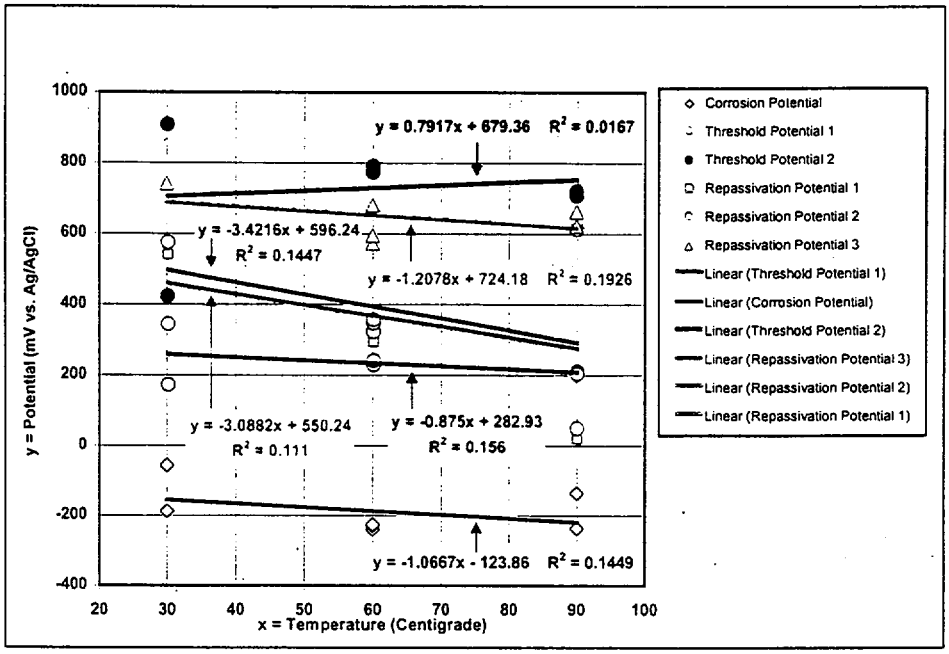

Figure 3-42. Potentials versus Temperature – Alloy 22 in Simulated Concentrated Water

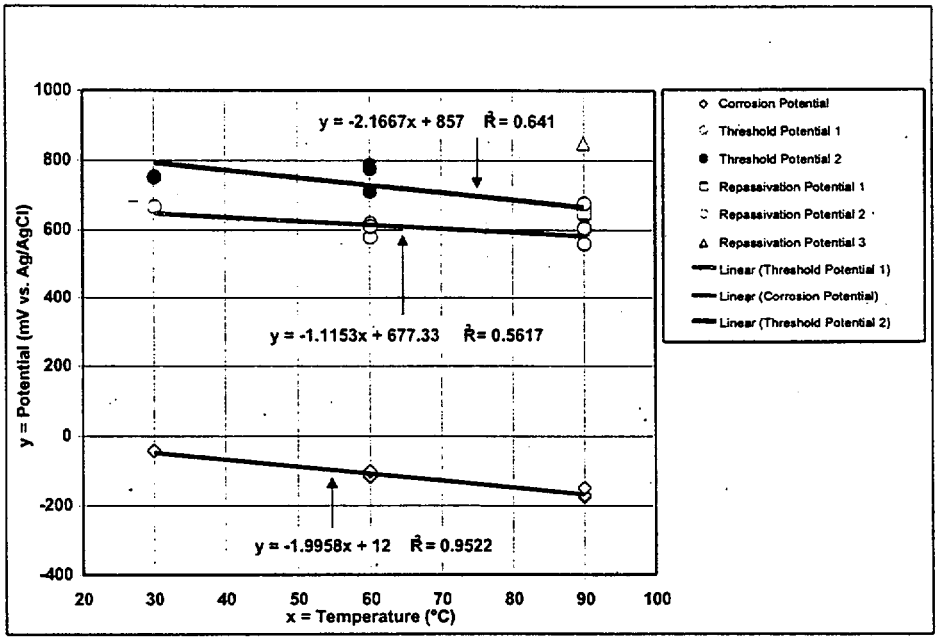

Figure 3-43. Potentials versus Temperature – Alloy 22 in Simulated Acidic Concentrated Water

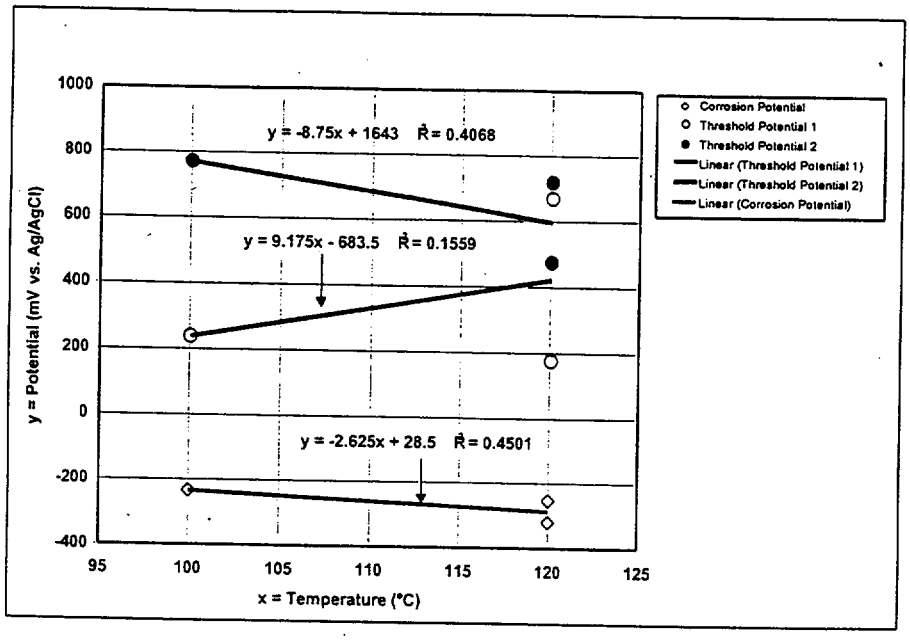

Figure 3-44. Potentials versus Temperature – Alloy 22 in Simulated Saturated Water

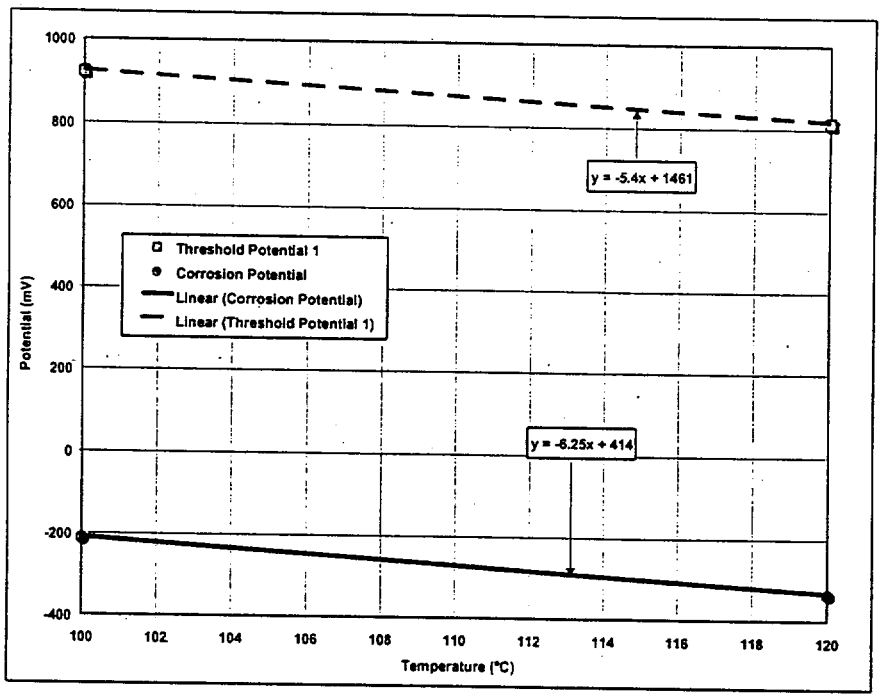

Figure 3-45. Corrosion and Threshold Potentials of Titanium Grade 7 in Simulated Saturated Water (NEA031s)

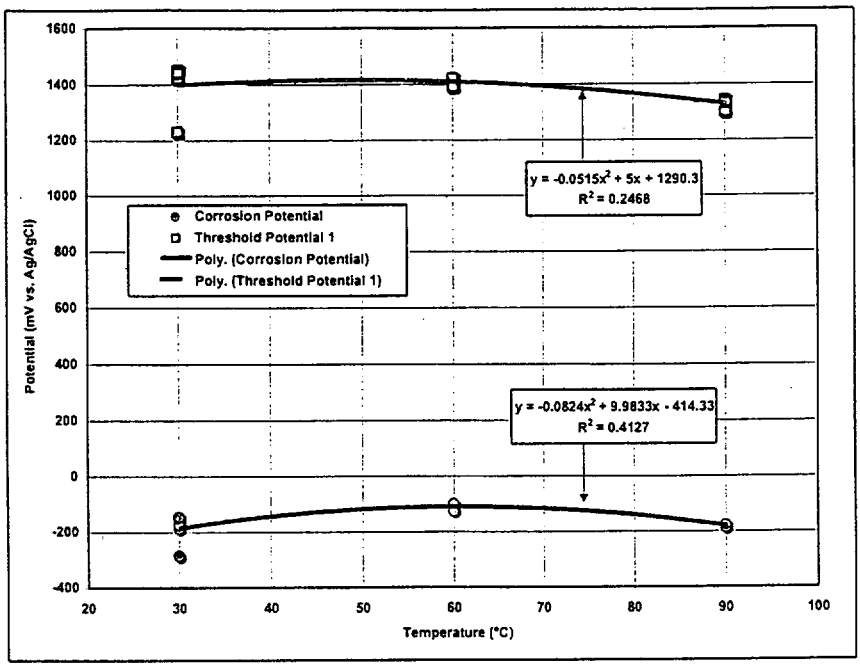

Figure 3-46. Corrosion and Threshold Potentials for Titanium Grade 7 in Simulated Acidic Concentrated Water

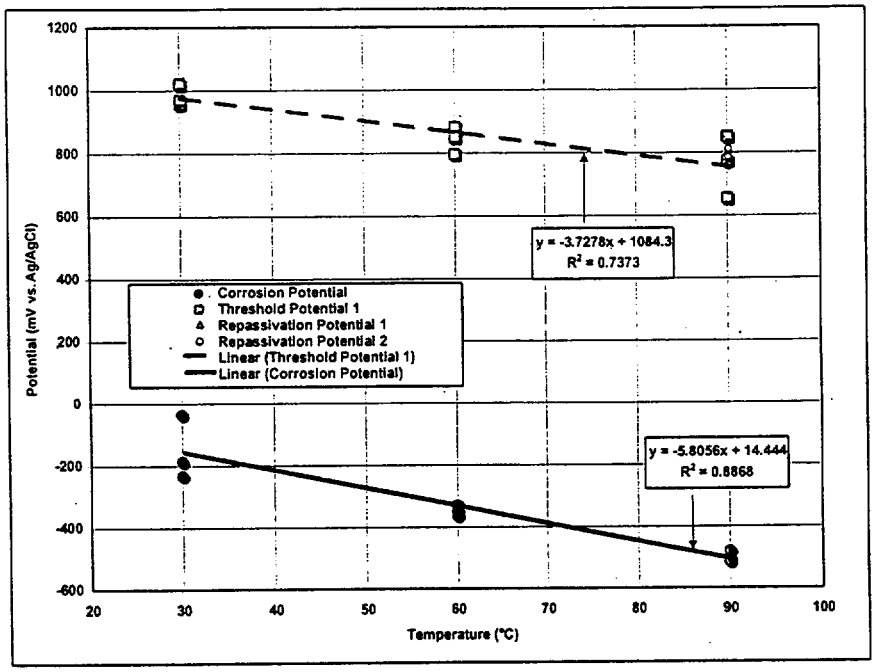

Figure 3-47. Corrosion and Threshold Potentials for Titanium Grade 7 in Simulated Concentrated Water

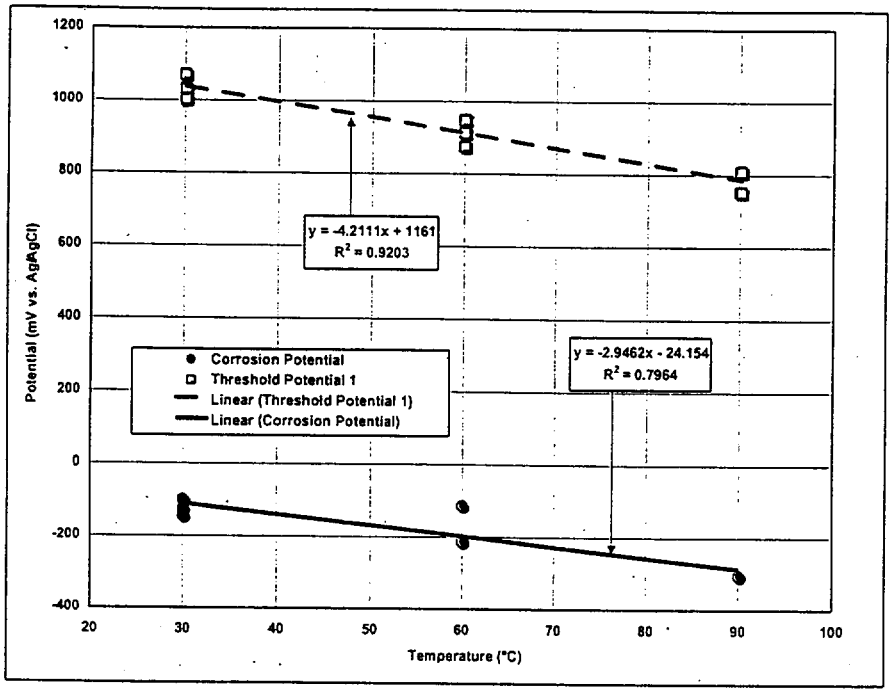

Figure 3-48. Corrosion and Threshold Potentials for Titanium Grade 7 in Simulated Dilute Water

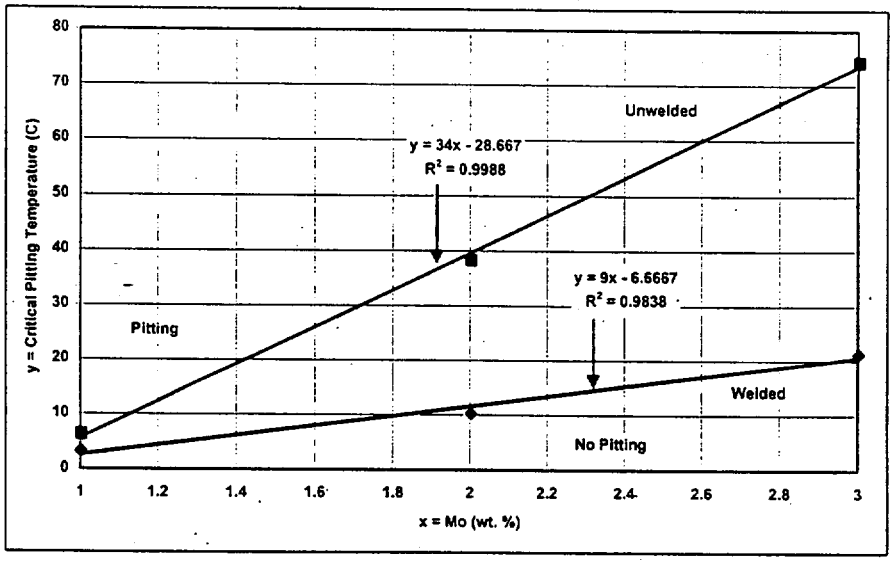

Figure 3-49. Effect of Molybdenum on the Critical Pitting Temperature of Stainless Steels in Ferric Chloride Solution

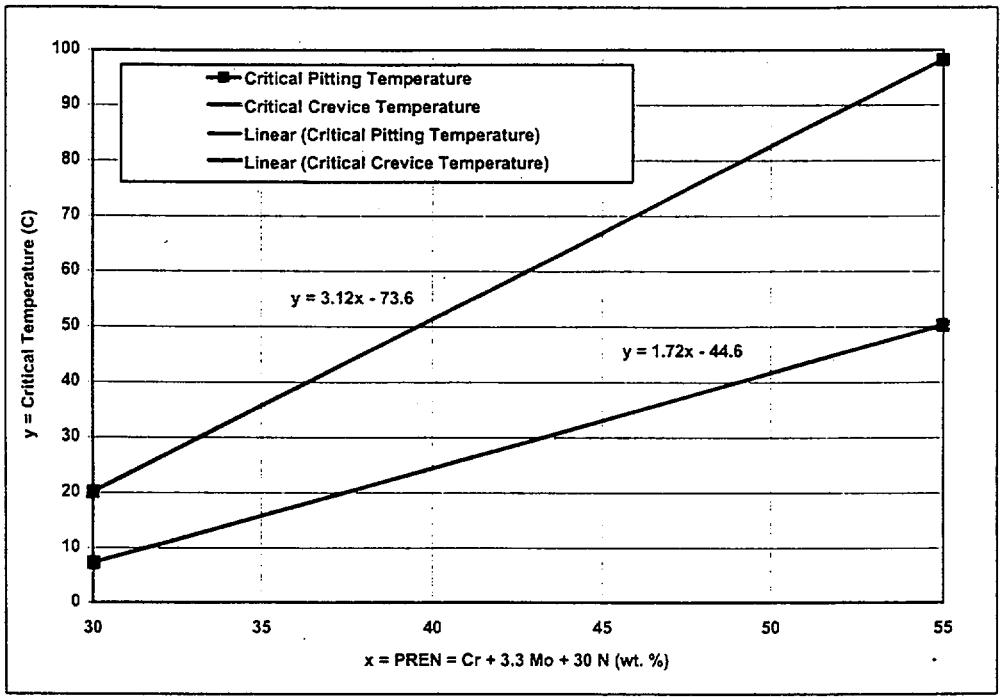

Figure 3-50. Effect of Pit Resistance Equivalence Number on the Critical Pitting and Crevice Corrosion Temperature of Stainless Steels in Ferric Chloride Solution

3.1.6.6 Effect of Gamma Radiolysis on Corrosion Potential

Anodic shifts in the open circuit corrosion potential of stainless steel in irradiated aqueous environments have been experimentally observed (CRWMS M&O 2000c). It is now accepted as fact by much of the engineering community that this observation is due to the generation of hydrogen peroxide by the radiation. Experiments performed at ambient-temperature cyclic polarization of 316L samples in 0.018 M NaCl solution during exposure to 3.5 Mrad hr^{-1} gamma radiation showed that the corrosion potential shifted in the anodic direction by approximately 200 mV. It was concluded that there is very little increase in the corresponding corrosion current density. However, the separation between the corrosion potential and the threshold for localized attack decreased slightly. This shift in corrosion potential was shown to be due to the formation of hydrogen peroxide. This finding was subsequently confirmed by another cyclic polarization experiment at ambient-temperature with 316 stainless steel in acidic (pH~2) 1.5 M NaCl during exposure to 0.15 Mrad hr^{-1} gamma radiation which showed a 100 mV anodic shift in the corrosion potential, with very little effect on the corrosion current. Note that these experiments were performed on stainless steels; not Alloy 22.

To determine the maximum impact that gamma radiolysis could have on the corrosion potential, hydrogen peroxide was added to electrolytes used for testing Alloy 22. Experiments at 25°C are illustrated by Figures 3-51 and 3-52. As the concentration of hydrogen peroxide in simulated acidic concentrated water approaches 72 ppm (calculated from number of added drops of H_2O_2), the corrosion potential asymptotically approaches 150 mV versus Ag/AgCl, well below any threshold where localized attack would be expected in simulated acidic concentrated water. Similarly, as the concentration of hydrogen peroxide in SCW approaches 72 ppm, the corrosion potential asymptotically approaches –25 mV versus Ag/AgCl, well below any threshold where

localized attach would be expected in SCW. This change in corrosion potential is also below any level where a change in oxidation state would be expected. Gamma radiolysis is not expected to exacerbate the localized corrosion of Alloy 22 since the maximum shift in corrosion potential induced by hydrogen peroxide additions is less than that required for breakdown of the passive film.

3.1.6.7 Crevice Corrosion

3.1.6.7.1 Local Chemistry in the Crevice

Crevices can form at points of contact between the waste package and other solid objects. These occluded geometries can lead to differential aeration of the crevice solution (electrolyte). Dissolved oxygen can become depleted deep within the crevice, while the concentration near the crevice mouth remains relatively high. Cathodic reduction of dissolved oxygen at the crevice mouth may create a sufficiently high electrochemical potential to drive anodic processes inside the crevice, thereby causing an anodic current to flow along the crevice towards the crevice mouth. Anodic processes inside the crevice are therefore expected to occur at a rate that corresponds to the local passive current density. Two primary electrochemical processes can lead to acidification of the solution in a crevice: (1) the preferential transport of anions into the crevice from the mouth, driven by the electric field that accompanies the crevice current; and (2) hydrolysis reactions of dissolved metal cations.

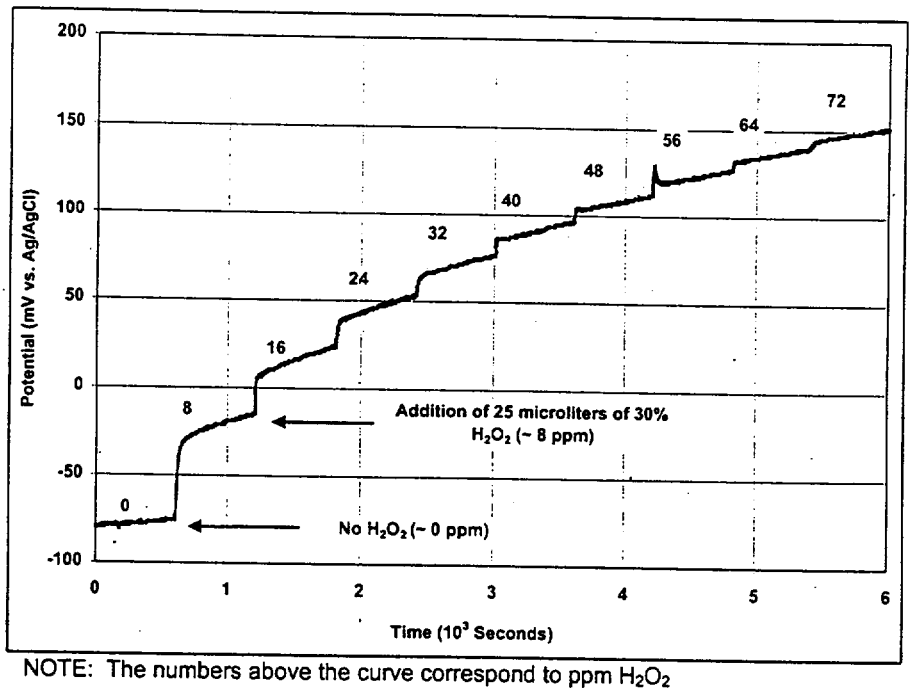

NOTE: The numbers above the curve correspond to ppm H_2O_2

Figure 3-51. Effect of Hydrogen Peroxide on Corrosion Potential of Alloy 22 in Simulated Acidic Concentrated Water at 25°C

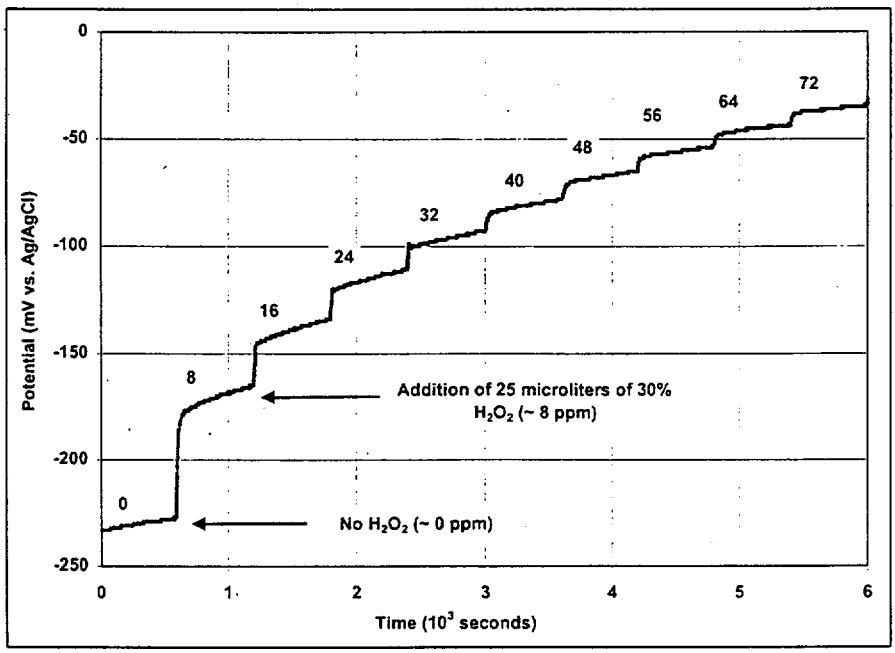

NOTE: The numbers above the curve correspond to ppm H_2O_2

Figure 3-52. Effect of Hydrogen Peroxide on Corrosion Potential of Alloy 22 in Simulated Concentrated Water at 25°C

Chloride anion will be driven into the crevice by the potential gradient, as discussed in the literature and summarized in the AMR. The corresponding concentration in the crevice is:

$$[Cl^-] = [Cl^-]_0 \exp\left[-\frac{F}{RT}\Phi(x)\right] \qquad \text{(Eq. 3-22)}$$

where $[Cl^-]_0$ is the concentration at the crevice mouth, $\Phi(x)$ is the potential in the crevice relative to that at the mouth, and (x) is the distance from the crevice mouth. Field-driven electromigration of Cl^- (and other anions) into crevice must occur to balance cationic charge associated with H^+ ions, as well as the charge associated with Fe^{2+}, Ni^{2+}, Cr^{3+}, and other cations. If such conditions do develop inside Alloy 22 crevices, accelerated attack of this material by localized corrosion or SCC may be possible.

In crevices made of steels containing more than 20 weight percent chromium, very acidic pH levels have been observed (pH < 2). The effect of chromium content on the ultimate crevice pH in a number of commercial and binary Fe-Cr alloys is illustrated by Figure 3-53, while the increase in concentration of dissolved metals in such crevices is illustrated by Figure 3-54 (CRWMS M&O 2000e). Based upon experimental work with passive crevices without buffer, it is believed that the applied potentials required for significant acidification (pH <5) are not plausible (CRWMS M&O 2000c). A minimum crevice pH of approximately 5 is assumed.

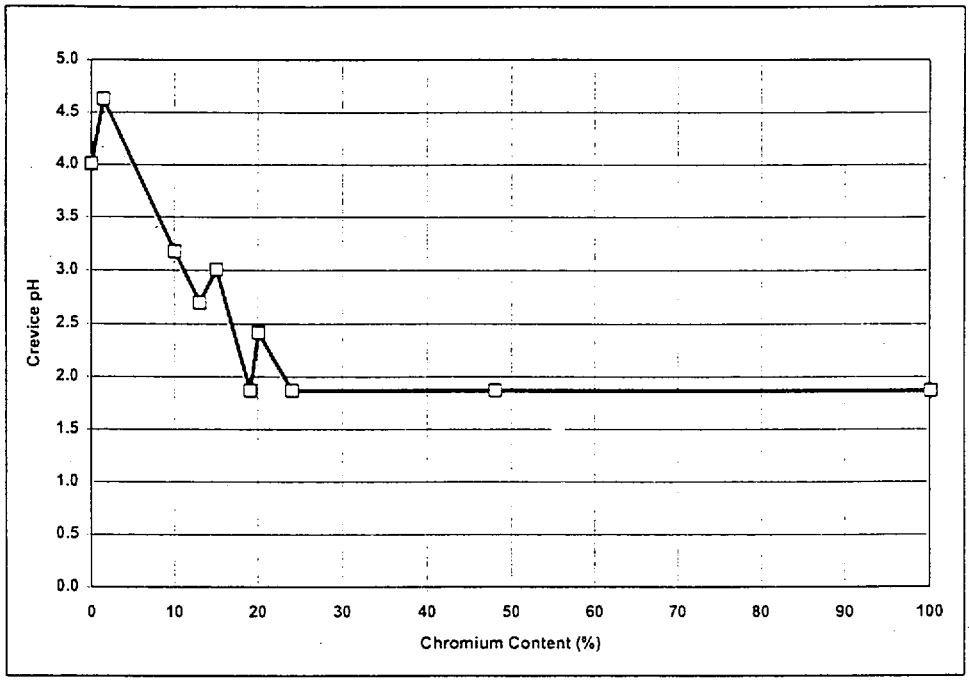

Figure 3-53. Effect of Chromium Content in Ni-Cr Alloys on Ultimate Crevice pH

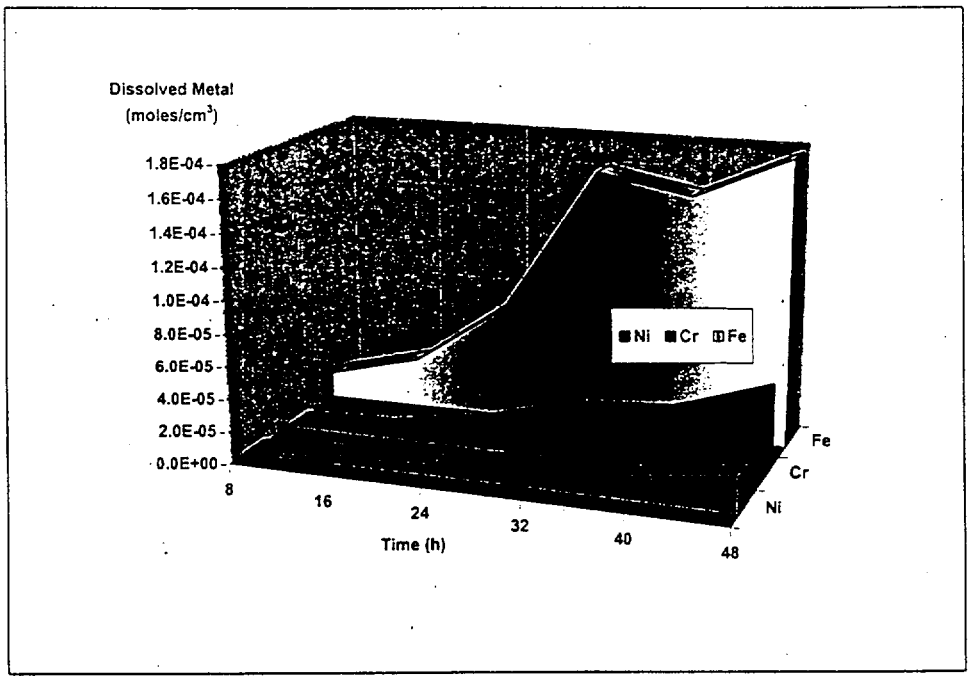

Figure 3-54. Concentrations of Dissolved Metals in Stainless Steel 304 Crevice Exposed to 0.1 N NaCl

3.1.6.7.2 Deterministic Models of the Crevice

A detailed deterministic model has been developed to calculate the spatial distributions of electrochemical potential and current density in waste package crevices, as well as transient concentration profiles of dissolved metals and ions. These quantities are calculated with the transport equations, which govern electromigration, diffusion, and convective transport. First, the axial current density along the length of the crevice is calculated by integrating the wall current density. The electrode potential along the length of the crevice can then be calculated from the axial current density. The partial differential equations that define transient concentrations in the crevice require determination of the potential gradient, as well as the local generation rates for dissolved species. The concentrations of dissolved metals at the crevice mouth are assumed to be zero. Computations are facilitated by assuming that the crevices are symmetric about a mirror plane where the flux is zero. This model has been used to estimate the extent of pH depression in waste package crevices due to the simultaneous hydrolysis and transport of dissolved Fe, Ni, Cr, Mo and W. The experimental measurements discussed below were used for validation.

3.1.6.7.3 Experimental Determinations of Crevice pH and Current

The local crevice environments for Alloy 22 and other relevant materials have been determined experimentally. Crevices have been constructed from square metallic samples, 2 inches on each side and 1/8 inch thick (same size as crevice samples used in the LTCTF). The samples are masked with plastic tape, thereby forming an exposed square area, 1.7 inches on each side. The exposed area is placed underneath a clear plastic window with an access port for a pH sensor in the center. In this case, the sensor is a miniature reference electrode separated from the crevice solution with a thin glass membrane. A second pH sensor is located at the mouth of the crevice, in close proximity to a Saturated Calomel Electrode. In parallel experiments, paper strips with a pH-sensitive dye (pH paper) have been sandwiched between the clear plastic window and photographed with a digital electronic camera in a time-lapse mode to add confidence to the measurements made with pH sensors. Spectroscopic-grade graphite counter electrodes are also placed in the electrolyte lying outside the mouth of the crevice. A potentiostat is then used to control the electrochemical potential at the mouth of the crevice. Temperature, potential, current, and pH is then recorded electronically during the course of the experiment.

An example of the pH measurements inside a crevice formed from 316L stainless steel is shown in Figure 3-55. The electrolyte was 4M NaCl and was maintained at ambient temperature. Since this electrolyte contains no buffer ions, it is considered to be a far more severe medium than media representative of various concentrations of J-13 well water. The electrochemical potential at the mouth was maintained at 200 mV vs. Ag/AgCl. Crevice corrosion could be seen initiating near the crevice mouth and propagating towards the pH sensor, which was located about 0.5 cm inside the crevice mouth. When the corrosion front reaches the pH sensor, the pH dropped from the initial value (pH~7) to a very low value (pH~1). The fixed one-liter volume of electrolyte outside of the crevice became slightly alkaline. In similar experiments with 316L exposed to SCW, no significant lowering of the pH was observed.

Measurements of pH inside crevices formed with Alloy 22 surfaces are shown in Figure 3-56 for a 4 M NaCl electrolyte. The data illustrate the effect of increasing the applied potential above

the threshold required for localized breakdown of the passive film. The figure shows the effect of incremental changes in applied potential on crevice pH. The corresponding measurements of crevice current can be found in the supporting AMR (CRWMS M&O 2000c). At an applied potential of 400 mV, the steady-state crevice pH remained close to neutrality (pH~6.1). As the potential was stepped to 1000 mV, the crevice current increased dramatically and the pH dropped below one. At an applied potential of 1100 mV, extreme localized attack of the Alloy 22 was observed at the crevice mouth, with a crevice pH measurement near zero.

Figure 3-57 is a summary of several experiments where crevice pH was determined in situ as a function of applied potential. These data are represented by the following polynomial:

$$y = b_0 + b_1 x + b_2 x^2 \qquad \text{(Eq. 3-23)}$$

where x is the potential applied at the crevice mouth (mV versus Ag/AgCl) and y is the steady-state pH inside the crevice. Coefficients for the above equation are shown in the figure for both Alloy 22 and 316L, under a broad range of conditions. The correlations for 4M NaCl and SCW could be used to bound the crevice pH, using interpolation based upon the concentration of buffer ion between the two limits. Similar behavior is expected in titanium alloys. Additional testing with titanium alloys are planned to confirm this.

In summary, there was no visible evidence of localized corrosion of the metal inside the crevice at applied potentials less than the threshold. However, even though the crevice remained passive, the passive current density and imposed electric field within the crevice was sufficient to cause significant acidification. In many of the experiments described here, both the applied potential and the test medium are more severe than those expected in the repository.

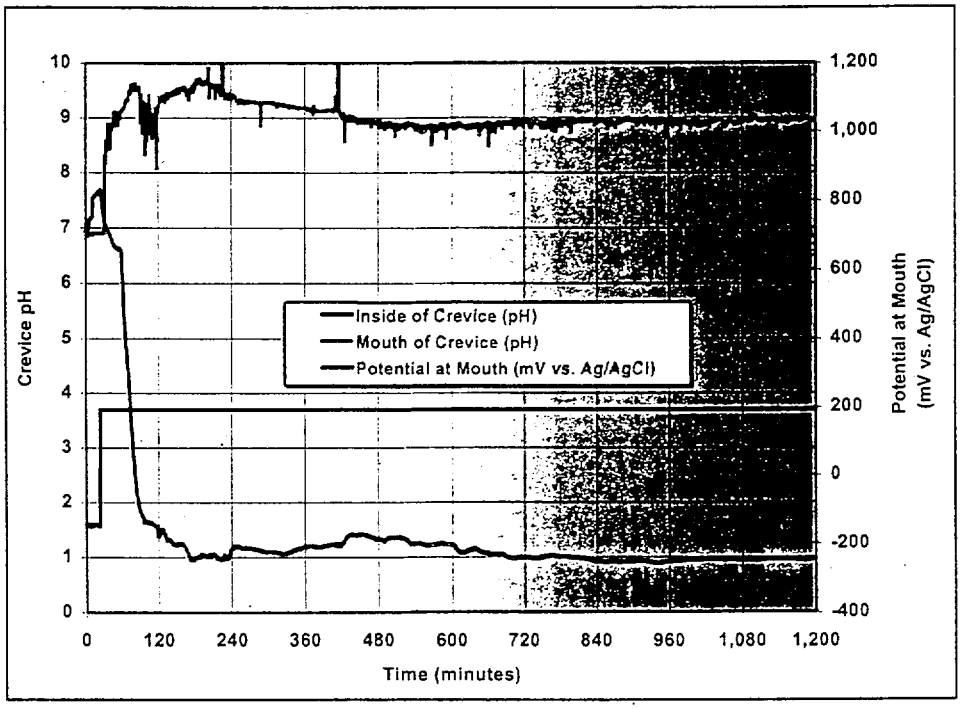

Figure 3-55. Stainless Steel 316L, 4M NaCl, 200 mV & 23°C – Crevice pH versus Time

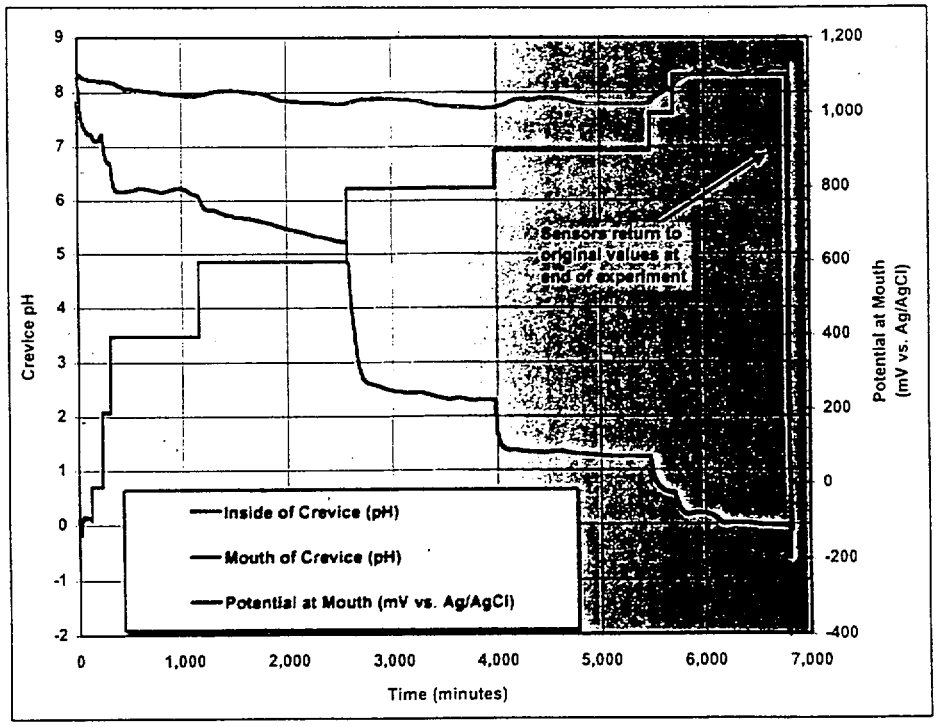

Figure 3-56. Alloy 22, 4M NaCl at 23°C – Crevice pH versus Time

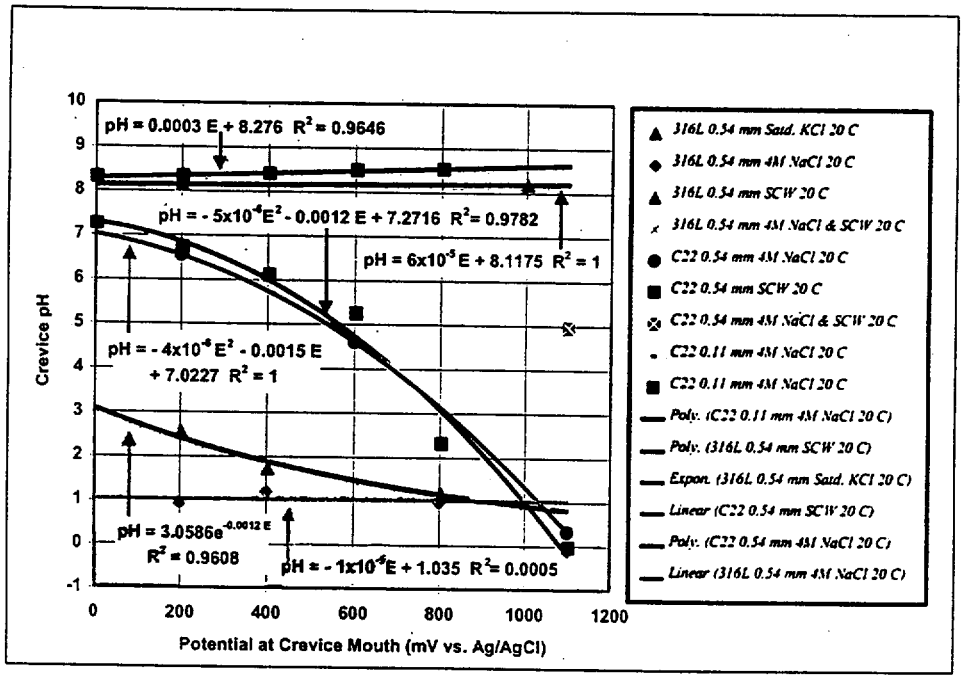

Figure 3-57. Determination of Crevice pH for Waste Package Materials

3.1.6.7.4 Estimated Localized Corrosion Rate of Alloy 22 and Titanium Grade 7

If the threshold potential for localized attack is exceeded, a corrosion rate representative of localized corrosion must be assumed. Due to the outstanding corrosion resistance of Alloy 22, very little data exists for such localized corrosion under plausible conditions. Work summarized in the AMR indicates that the corrosion rate of Alloy 22 in 10 wt. % $FeCl_3$ at 75°C might be as high as 12.7 μm per year. This rate is significantly higher than those measured in the LTCTF, and may be representative of the types of rates expected for localized corrosion, including crevice corrosion. In a solution composed of 7 vol. % H_2SO_4, 3 vol. % HCl, 1 wt. % $FeCl_3$, and 1 wt. % $CuCl_2$, a penetration rate of 610 μm per year was observed at 102°C. In other work, the corrosion rate of Alloy C-276 in dilute HCl at the boiling point is somewhere between 5 and 50 mils per year (127 and 1270 μm per year). Comparable rates would be expected for Alloy 22. The highest passive current density found is approximately 10 μA cm^{-2}, which corresponds to a corrosion rate of approximately 100 μm per year. Based on the above data, it is expected that the logarithm of the localized corrosion rate of Alloy 22 is normally distributed, as shown in Table 3-11. This distribution reasonably bounds those extreme penetration rates found in the literature, and is centered about the rate corresponding to the passive current density.

Similar to Alloy 22, due to the outstanding corrosion resistance of Titanium Grade 7, relatively little data exists for localized corrosion under plausible conditions. From the reviewed literature discussed in the AMR (CRWMS M&O 2000d), a crevice corrosion depth of 250 microns was observed in a crevice formed from Ti-0.2%Pd and teflon after a 582 day exposure in deaerated brine at 90°C (157 microns per year). In a metal-metal crevice, a crevice corrosion depth of 70 microns was observed in a crevice formed from Ti-0.2%Pd after 489 days (52 microns per year). Other more severe values are shown in Table 3-12 below. A rectangular distribution based on this table should be assumed for the localized corrosion of Titanium Grade 7.

Table 3-11. Distribution of Localized Corrosion Rates for Alloy 22

Percentile	LC Rate (μm per year)
0th	12.7
50th	127
100th	1270

Table 3-12. Distribution of Localized Corrosion Rates for Titanium Grade 7

Percentile	LC Rate (μm per year)	Conditions
0th	490	19% HCl + 4% $FeCl_3$ + 4% $MgCl_2$ at 82°C
100th	1120	Boiling 3:1 Aqua Regia

3.1.6.7.5 Surface Topography of Materials Explored with Atomic Force Microscopy and X-Ray Diffraction

The AFM has been used to characterize the surface topographies of five weight-loss coupons of Alloy 22, which had been exposed to various environments in the Long Term Corrosion Test Facility for one year. Having sub-nanometer vertical resolution, the AFM is an ideal tool for detecting extremely small penetrations in corrosion-resistant materials such as Alloy 22. These samples include an unexposed control sample (DWA163), a sample exposed to aqueous phase simulated acidic concentrated water (DWA051), a sample exposed to vapor-phase simulated acidic concentrated water (DWA048), a sample exposed to aqueous-phase SCW (DWA120), and a sample exposed to vapor-phase SCW (DWA117). The sample numbers are designations of the YMP. After the samples were removed from the LTCTF, they were ultrasonically agitated in deionized water, acetone, and methanol for ten minutes each. The Digital Instruments DM3100 AFM was then used for imaging. Each set of data consists of a large-area scan (25 μm × 25 μm), followed by smaller-area details of the region displayed in the large-area scan.

The gross surface topography is dominated by the machining grooves, with typical heights of several hundred nm and typical lateral periodicities of several μm, features plainly visible on images of the control sample (DWA163). Samples removed from the Long Term Corrosion Test Facility exhibit varying degrees of coverage by a deposit on top of this gross topography. The AFM images show that the most extensive deposit formation occurred on the sample exposed to aqueous-phase simulated acidic concentrated water (DWA051). The next most extensive deposit formation occurred on the sample exposed to vapor-phase simulated acidic concentrated water (DWA048). X-ray diffraction scans of all five coupons show that the deposit is predominantly a silicate or SiO_2, with some NaCl appearing on the two samples which were in the simulated acidic concentrated water tank. Based upon both AFM and X-ray diffraction data, the two samples exposed to SCW showed lesser degrees of coverage by the silicate deposit. In some cases, depressions can be seen in the silicate deposit. However, it is not believed that any of these penetrate to the underlying metal.

At the present time, there is insufficient data to determine the amount of silicate removed from exposed Alloy 22 samples by the standard cleaning method (CRWMS M&O 2000c). Accordingly, a worst-case estimate of the impact of SiO_2 on measured general corrosion rates will be used.

The formation of SiO_2 deposits on the surface of the Alloy 22 could bias the distributions of general corrosion rate shown in earlier sections of this Waste package degradation PMR. From various AFM images of Alloy 22 samples removed from the LTCTF, it appears that a typical deposit can have a thickness as great as 0.25 microns after 12 months of exposure. It is assumed that the deposit has the density of lechatelierite (amorphous SiO_2), which is approximately 2.19 g cm^{-3}. It is further assumed that the surface is completely and uniformly covered by this deposit. The estimated surface areas of the weight-loss and crevice samples are 30.65 and 57.08 cm^2, respectively (4.75 and 8.85 in^2, respectively). Consequently, the deposit thickness translates into a mass change of 1.678 and 3.125 mg for the weight-loss samples and the crevice samples, respectively, after 12 months of exposure. The formula used to calculate corrosion rate from weight loss and dimensional change is then applied to determine the impact of such a positive mass change on the calculated rate. The estimated bias is 0.063 microns per year (63 nm y^{-1}) for all weight loss samples.

The distributions of general corrosion rate shown in previous sections can be corrected for the maximum bias due to SiO_2 deposit formation by adding a constant value of 63 nm y^{-1} to each estimated value of the general corrosion rate. This is equivalent to shifting the curves shown in figures to the right by 63 nm y^{-1}. Similar corrections could be applied to the Titanium Grade 7 data.

The AFM has been used to examine areas inside and outside of Alloy 22 crevices exposed to SCW at 90°C for 12 months. Though the images were obtained with a welded sample (DCB100), the unwelded area was imaged with the AFM. There appears to be no significant difference between the roughness of the four areas that were examined. Since it has been observed that corrosion tends to roughen the surface, it is concluded that there is no more attack inside the crevice than outside.

3.1.6.8 Microbial Influenced Corrosion

It has been observed that nickel-based materials such as Alloy 22 are relatively resistant to MIC (CRWMS M&O 2000c). Furthermore, it is believed that microbial growth in the repository will be limited by the availability of nutrients. For example, H^+ is known to be generated by bacterial isolates from Yucca Mountain. Furthermore, thiobacillus ferrooxidans oxidize Fe^{2+}, while geobacter metallireducens reduce Fe^{3+}. Other microbes can reduce SO_4^{2-} and produce S^{2-}. Ultimately, the impact of MIC will be accounted for by adjusting E_{corr}, $E_{critical}$, pH, and the sulfide concentration. The possible acceleration of abiotic corrosion processes by microbial growth is addressed here. (CRWMS M&O 2000c) has shown that MIC can enhance corrosion rates of Alloy 22 by a factor of two (2×). Figure 3-11 is a schematic representation of the corrosion model for the Alloy 22 outer barrier. The augmentation of corrosion rates due to MIC is accounted for in the model as shown in Figure 3-12; here, G_{MIC} is the enhancement factor.

$$\left(\left.\frac{dp}{dt}\right|_{effective}\right)_{corrected} = G_{MIC} \times \left(\left.\frac{dp}{dt}\right|_{effective}\right)_{original} \qquad \text{(Eq. 3-24)}$$

This factor is calculated as the ratio of corrosion rates (microbes to sterile). (CRWMS M&O 2000e) have shown that MIC can enhance corrosion rates of 304 stainless steel by a factor

of approximately ten (×10). The value of G_{MIC} for 304 stainless steel in sterile media is approximately one ($G_{MIC} \sim 1$), whereas the value of G_{MIC} for 304 stainless steel in inoculated media is larger ($G_{MIC} \sim 10$). It is assumed that MIC will have the same effect on 316NG stainless steel. The value of G_{MIC} for Alloy 22 in sterile media is approximately one ($G_{MIC} \sim 1$), whereas the value of G_{MIC} for Alloy 22 in inoculated media is larger ($G_{MIC} \sim 2$).

The principal nutrient-limiting factor to microbial growth *in situ* at Yucca Mountain, has been determined to be low levels of phosphate. There is virtually no phosphate contained in J-13 groundwater. Yucca Mountain bacteria grown in the presence of Yucca Mountain tuff are apparently able to dissolve phosphate contained in the tuff to support growth to levels of 10^6 cells ml^{-1} of groundwater. When exogenous phosphate is added (10 mM), then levels of bacterial growth increase to 10^7 to10^8 cells ml^{-1}. The difference of one to two orders-of-magnitude in bacterial growth with and without the presence of exogenous phosphate is almost certainly not significant with respect to effects on corrosion rates. Therefore, nutrient limitation at least at a first approximation, was not factored into the overall MIC model. It may be noted, however, that the 2-fold G_{MIC} included in the model was in the presence of sufficient phosphate to sustain higher levels of bacterial growth (in an effort to achieve accelerated Alloy 22 attack).

Other environmental factors that could effect levels of bacterial growth include temperature and radiation. However, these factors are closely coupled to RH. As temperature and radiation decrease in the repository, RH is predicted to increase. There are some types of micro-organisms that can survive elevated temperatures (≤ 120°C) and high radiation doses, if there is no available water then bacterial activity is completely prevented. Thus, because water availability is the primary limiting factor, and this factor is coupled to other less critical limiting factors, water availability (as expressed by RH) was used as the primary gauge of microbial activity.

A conservative approach is to assume that a critical mass of bacteria exists for MIC. Bacterial densities in Yucca Mountain rock have been determined to be on the order of 10^4 to 10^5 cells g^{-1} of rock. In absolute terms, this is almost certainly above the threshold required to cause MIC. Further, bacterial densities were shown above to increase 1 to 2 orders-of-magnitude when water is available. More germane concerns are the types of bacteria present, their abundance, and how their relative numbers are affected when water is available for growth. Corrosion rates will be affected (at least on some waste package materials), for example, if organic acid producers out compete sulfate reducers or inorganic acid producers for available nutrients when water is sufficient to support growth. No data is currently available regarding the composition of the bacterial community over the changing environmental conditions anticipated during repository evolution. Instead, this issue has been addressed in the current model by determining overall corrosion rates under a standardized set of conditions, in the presence and absence of a defined set of characterized Yucca Mountain bacteria.

3.1.7 Stress Corrosion Cracking

3.1.7.1 Background

One of the potential failure modes of the drip shield, the WPOB, and the stainless steel structural container is the initiation and propagation of SCC. Such environmental cracking may be induced by the combination of waste package environment and various sustained tensile stresses that can

develop in the waste package materials. For the current design of the drip shield and WP, however, the drip shield and the stainless steel structural material will be excluded from the SCC evaluation. The drip shield is excluded because stresses that are relevant to SCC are insignificant in the drip shield. The major sources of stresses in the drip shield are loadings due to backfill and earthquakes. These stresses will not induce SCC because the stress caused by backfill is generally compressive stress and the stress caused by earthquakes is temporary in nature. The stainless steel structural material of the WP will be excluded from the SCC evaluation because the performance assessment will not treat this material as a corrosion barrier. The purpose of this section of the PMR is to provide a detailed description of the process models that can be used to predict the performance of the WPOB in repository-relevant environments that may be capable of causing SCC.

There are several corrosion modes that could lead to premature breach of the WPOB. One of the most threatening modes is SCC, which can cause the initiation and propagation of through-wall cracks at relatively low stress intensity factors. The three driving forces for SCC are metallurgical susceptibility, a corrosive environment, and static (or sustained) tensile stresses.

Environments that cause SCC are usually aqueous and can be condensed layers of moisture or bulk solutions. The SCC of a particular alloy is usually caused by the presence of a specific chemical species in the environment. For example, the SCC of copper alloys is virtually always due to the presence of ammonia in the environment. Chloride ions cause SCC in stainless steels and aluminum-based alloys. Changes in the environmental conditions, which include temperature, dissolved oxygen, and ionic concentrations, will normally influence the SCC process.

The effects of stress on the propagation of SCC can be characterized by the stress intensity factor, K_I. The definition and detailed calculations of the stress intensity factor are described in the AMR on SCC (CRWMS M&O 2000f).

The SCC evaluation is focused on the WPOB lid welds because welds are more susceptible to SCC due to (1) welding processes can produce very high tensile residual stresses in the weld; and (2) pre-existing flaws due to fabrication and welding have much higher distribution in the weld than in the base material.

Two alternative models that deal with SCC are described and evaluated in the AMR. The first model, the Threshold Model, is based on the theory that there exists a threshold value (K_{ISCC}) for the stress intensity factor such that no growth occurs in a crack having a stress intensity factor less than the threshold value. This model is described in a subsequent section.

The second model, the Slip Dissolution or Film Rupture Model, relates crack advance to the metal oxidation that occurs when the protective film at the crack tip is ruptured. The Slip Dissolution or Film Rupture SCC model is described in a subsequent section.

Leakage can occur if SCC propagates to the point where a crack penetrates the container wall. The model predictions indicate that SCC can lead to WPOB breach, it has been concluded that it is necessary to mitigate stress and other driving forces, thereby lowering the probability of cracking.

3.1.7.2 Overview of Two Alternative Models for Stress Corrosion Cracking

3.1.7.2.1 Model A – Stress Corrosion Cracking Threshold Model

The concept of threshold stress intensity factor (K_{ISCC} or K_{th}) has been commonly used to assess the susceptibility of material to SCC as described in the SCC AMR (CRWMS M&O 2000f). The applicability of this model to Alloy 22 (the material to be used for the WPOB) was experimentally evaluated at LLNL.

3.1.7.2.2 Model B – Stress Corrosion Cracking Slip Dissolution or Film Rupture Model

The theory of slip dissolution and film rupture was successfully applied to assess the SCC crack propagation for light water reactors at high temperature (approximately 288°C). The detailed description of the SCC model based on the theory of slip dissolution and film rupture can be found in the SCC AMR (CRWMS M&O 2000f). This model was adopted to assess the SCC capability of the material to be used for the WPOB.

3.1.7.3 Computer Software for Stress Analysis

The computer program ANSYS, Version 5.3 was used to calculate weld-induced residual stress profiles which were converted to stress intensity factor profiles in the WPOB lid welds using the pc-CRACK, Version 3.1 computer code.

3.1.7.4 Parameters and Inputs for Stress Corrosion Cracking Models

3.1.7.4.1 Material Properties

The material properties are important in the determination of the final weld residual stress. The material properties used in this evaluation are documented in the SCC AMR (CRWMS M&O 2000f).

3.1.7.4.2 Welding Parameters

In evaluating weld-induced stress, the effect of each weld pass was determined by simulating the heat being deposited by the welding process through heat generation rate that is deposited over a prescribed time interval. The typical parameters for a weld application are the electrical energy input rate, weld speed, and heat efficiency. This information presented in the SCC AMR was used to determine the heat generation rate for the elements that represent each weld bead pass.

3.1.7.4.3 Threshold Stress Intensity Factor

According to the current design, the material to be used for the WPOB is Alloy 22. K_{ISCC} values for Alloy 22 were evaluated by using wedge-loaded precracked double cantilever beam specimens in deaerated acidic brine (pH 2.7) at 90°C. Duplicate samples of each material were loaded at four different initial stress intensity factor (K_I) values ranging between 20 and 39 ksi in$^{1/2}$. (or 18 and 35 Mpa m$^{1/2}$). Both metallography and compliance methods were used to determine the final crack length. The final stress intensity factor for SCC (K_f) was computed

from the measured final wedge load on the double cantilever beam specimens and the average crack length. The final stress intensity factor K_f is taken to be the SCC threshold value K_{ISCC}.

3.1.7.4.4 Input for Slip Dissolution Model

The parameter "n" in the crack growth equation for the slip dissolution model was obtained from SCC crack growth tests for Alloy 22 at 110°C and a stress intensity factor of 30 MPa(m)$^{1/2}$. The input source resulted in a value of 0.84 for "n," which is considered an upper bound value. A lower bound value of 0.75 was derived from engineering judgement based on comparison of available data for Alloy 22 and more SCC resistant stainless steels.

3.1.7.4.5 Laser Peening Data

Residual stress in WPOB can be mitigated by the laser peening technique. Measured data indicated that laser peening is capable of producing a compression surface layer of about 1.5 mm with compressive stress in the range of 20 to 60 ksi for a one inch thick Alloy 22 plate.

3.1.7.5 Assumptions in Stress Corrosion Cracking Models

The following assumptions were made to develop the models for SCC:

Only the WPOB will be subjected to SCC susceptibility evaluation. The drip shield and the stainless steel structural container will be excluded from the evaluation for reasons discussed in Section 3.1.7.1. For the WPOB, only the closure welds will be considered for performance assessment. It is recognized that the closure weld is the most susceptible to SCC because welding procedure can produce very high tensile stress in the weld and pre-existing flaws due to fabrication and welding have much higher distribution in the weld.

It is assumed that embedded flaws will not grow by fatigue propagation due to lack of cyclic stress, and thus, only outer surface-breaking flaws are of concern for performance.

The SCC models will be applied to a latest WPOB dual-lid design. For the WPOB design, the only stress that is significant to the SCC is the weld-induced residual stress. Dead load stress is insignificant. Seismic stress is temporary in nature. Shrink-fit stress will be eliminated by fabrication process. To remove deleterions residual tensile stresses, the closure weld in the outer lid will be treated by induction heat annealing and the inner lid weld will be treated by laser peening to mitigate the tensile weld residual stresses. The dual-lid concept has been adopted for the WPOB to prolong the design life based on experience learned from previous waste package closure weld designs, where both calculated and measured weld residual stresses were found to be high.

For the waste package closure welds, the flaw orientation most likely susceptible to crack propagation is assumed to be that of either a circumferential flaw (parallel to weld) or a radially oriented flaw (perpendicular to weld). A radially oriented flaw would be potentially driven by the resulting hoop stress. A circumferentially oriented flaw would be driven by the radial stress.

In the Performance Assessment, only radial cracks will be considered because the driving stress (hence stress intensity factor) for a radial crack is much higher than the driving stress for a

circumferential crack. Only one crack per closure weld patch was considered (AMR). The patch size used in the Performance Assessment will be twice the lid thickness (~ 2 inches).

The slip dissolution mechanism (Equation 3-28) fundamentally relies on two parameters, the crack tip strain rate (which encompasses the effects of mechanics parameters) and the repassivation slope *n* (which encompasses the effects of material characteristics and water chemistry). Because of the expected similarity in SCC behavior and in the absence of other data or guidance, the same crack tip strain rate formulations that were employed for quantitative prediction of SCC in austenitic 304 or 316 stainless steels in 288°C high-purity boiling water reactor (BWR) water can be used for this analysis.

The characterization of the slip dissolution model is that SCC susceptibility decreases with increased repassivation slope "n". For stainless steels more susceptible to SCC than Alloy 22, test data indicated that n = 0.54 gives a good prediction. Recent SCC crack growth test results for Alloy 22 indicated that n = 0.84 or higher. For conservative purpose, n = 0.84 is considered to be the upper bound value for n. Based on published literature values for SCC resistant stainless steels, a lower bound value of n = 0.75 for a highly SCC resistant Alloy 22 is judged to be appropriate (see Section 3.1.7.4.4).

Although the SCC Film Rupture Model assumes crack growth can initiate at any surface defect that can generate a stress intensity (K_I) regardless of size and surface tensile stress level, examination of the relevant SCC literature indicates that there is a threshold stress below which SCC will not initiate on a "smooth" surface. In the case of the waste package closure weld, a "smooth" surface is defined as an as-machined surface with a maximum roughness of 250 rms. This threshold stress is conservatively estimated at 20-30% of the material yield stress, based on literature SCC initiation test results for susceptible stainless steels and nickel alloys with comparable surfaces exposed to very aggressive environments such as boiling magnesium chloride at ~ 155°C. Thus, the Film Rupture Model is not invoked, i.e., V_t of Equation 3-28 is equal to zero when the surface stress is less than 20% of yield stress.

3.1.7.6 Stress Analysis and Stress Intensity Factor Calculations

3.1.7.6.1 Calculation of Stress Intensity from Weld Residual Stress

Determining the weld residual stress is a problem that can best be solved using finite element analysis methods. The ANSYS Version 5.3 finite element program was used for this evaluation. The finite element model mesh arrangement for the initial WPOB design and the various waste package cross sections evaluated are shown in Figure 3-58. Results of the analysis for the Alloy 22 closure weld region are shown in Figures 3-59 and 3-60 for the radial and hoop stresses, respectively (CRWMS M&O 2000f).

For the WPOB closure welds, the flaw orientation most likely susceptible to crack propagation is that of a circumferential flaw (parallel to weld) and radially oriented flaw (perpendicular to weld). Figure 3-61 shows the flaw orientations with respect to the weld. A radially oriented flaw would be potentially driven by the resulting hoop stress. A circumferentially oriented flaw would be driven by the radial stress.

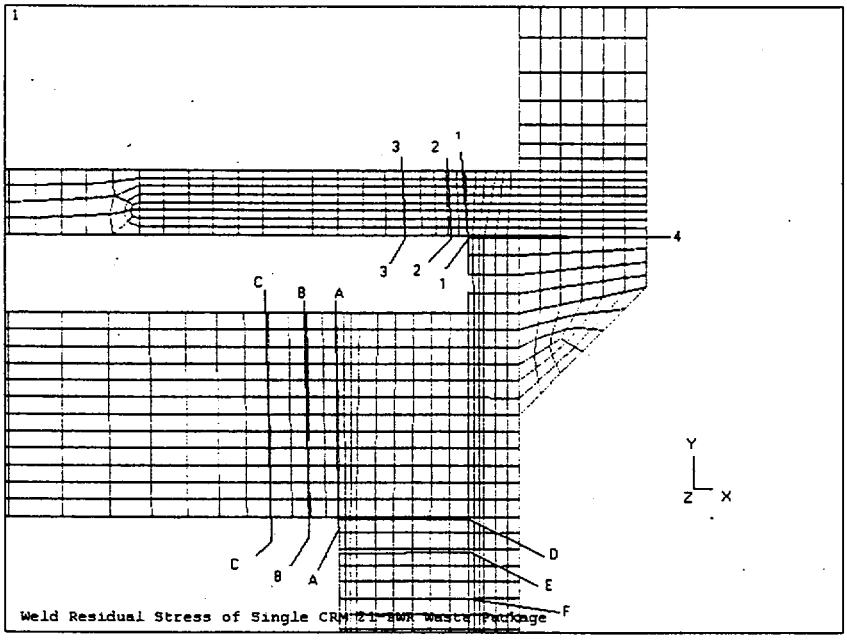

Figure 3-58. Finite Element Model for the Initial WPOB Design and Selected Cross-Sections for Stress Plots

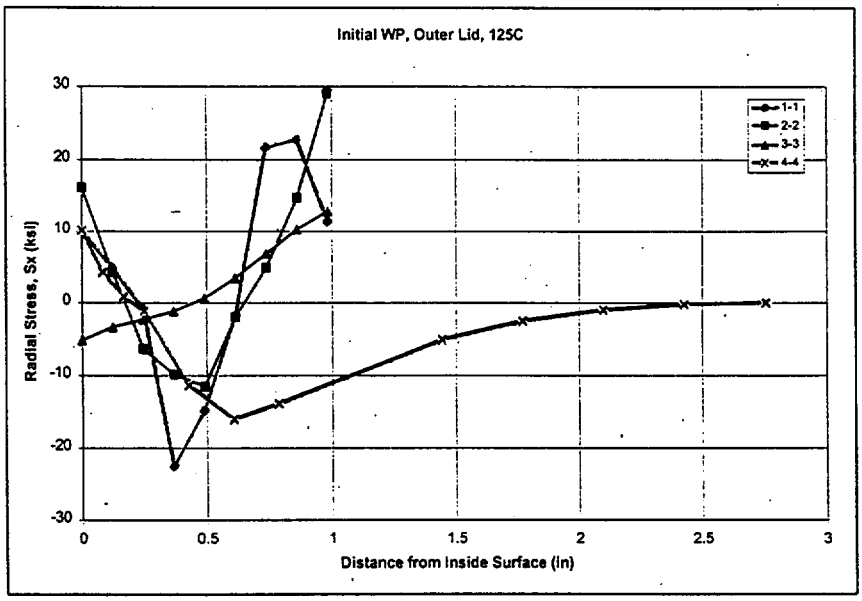

Figure 3-59. Radial Stress - Initial WPOB Outer Lid at 125C

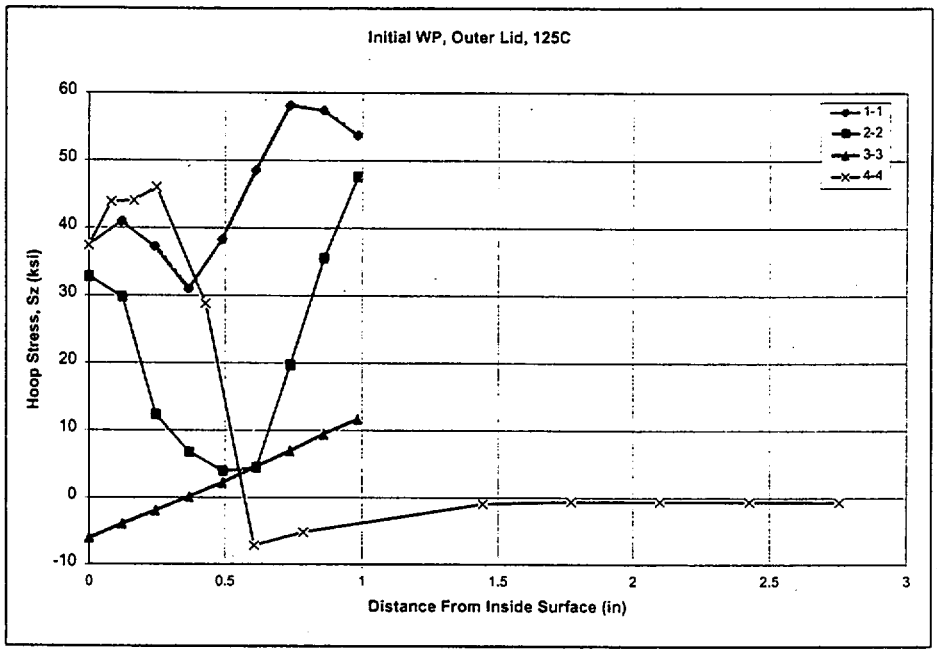

Figure 3-60. Hoop Stress - Initial WPOB Outer Lid at 125C

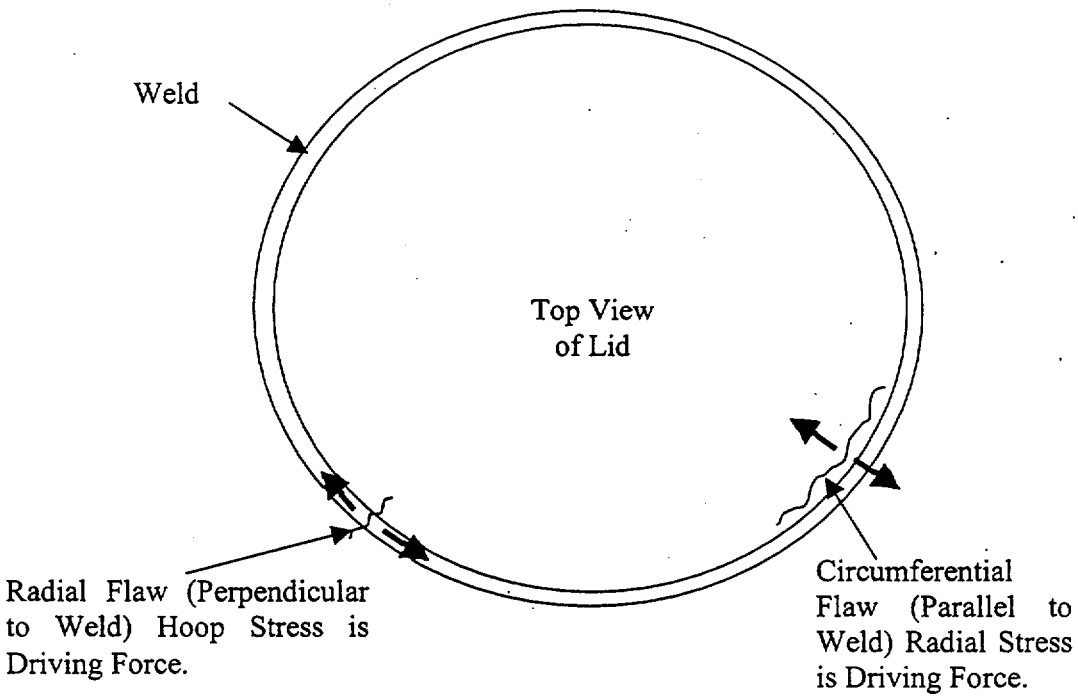

Figure 3-61. Flaw Orientations for Lid Welds

The stress intensity factor K_I is usually defined as a function of stress (σ) and crack depth (a):

$$K_I(a,\sigma) = \beta\sigma\sqrt{\pi a} \qquad \text{(Eq. 3-25)}$$

where β is a geometry factor dependent on the shape of the crack and the configuration of the structural component, and σ is the tensile stress.

3.1.7.6.2 Impact of Corrosion

The results presented for the initial WPOB in the SCC AMR (CRWMS M&O 2000f) were performed for the as-built condition. Thus, the full thickness for all the waste package components was used. In order to simulate the effect of wall thinning caused by general corrosion, a layer of elements from the outside surface of the outer lid was removed. The thickness of this layer is 0.125 inch, which is equivalent to the removal of 12.7% of the wall of the outer lid. The general corrosion rates are very low for the Alloy 22 material, ranging from 0.05 microns per year (50th percentile) to 0.731 microns per year (maximum). The 0.125-inch removal is the amount of material subject to general corrosion in 4,300 to 63,500 years, depending on the general corrosion rate.

This can be simulated using the ANSYS computer program by assigning a death status to the elements; which comprise the outer row. Since these elements contributed to the equilibrium state, removal of these elements causes a redistribution of the stress pattern. ANSYS performs this redistribution to the new equilibrium condition.

Figure 3-62 shows the stress intensity factor distributions for the circumferential crack. This figure shows the stress intensity factor as a function of distance from the outside surface and normalized distance from the outside surface. This figure demonstrates that the overall effect of general corrosion is small, but, in general, makes the stress intensity factor slightly higher.

3.1.7.6.3 Mitigation of Weld Residual Stress

Examination of the through-wall residual stress profiles for the initial WPOB design (Figures 3-59 to 3-60) reveals that tensile stresses exceeding 20% of Alloy 22 yield stress, i.e., ~ 10 ksi exist in the vicinity of the closure weld surface in both the radial and circumferential directions. This indicates SCC initiation in unacceptably short times cannot be precluded with this as-welded design. Further, examination of the stress intensity plot in Figure 3-62 indicates that, at least for radially oriented SCC cracks, through-wall crack propagation is possible once a crack initiates. Since relatively high as-welded tensile residual stresses are generated with the initial waste package unmitigated as-welded closure weld, it is necessary to implement a tensile residual stress reduction process either during or following closure welding to extend waste package lifetime.

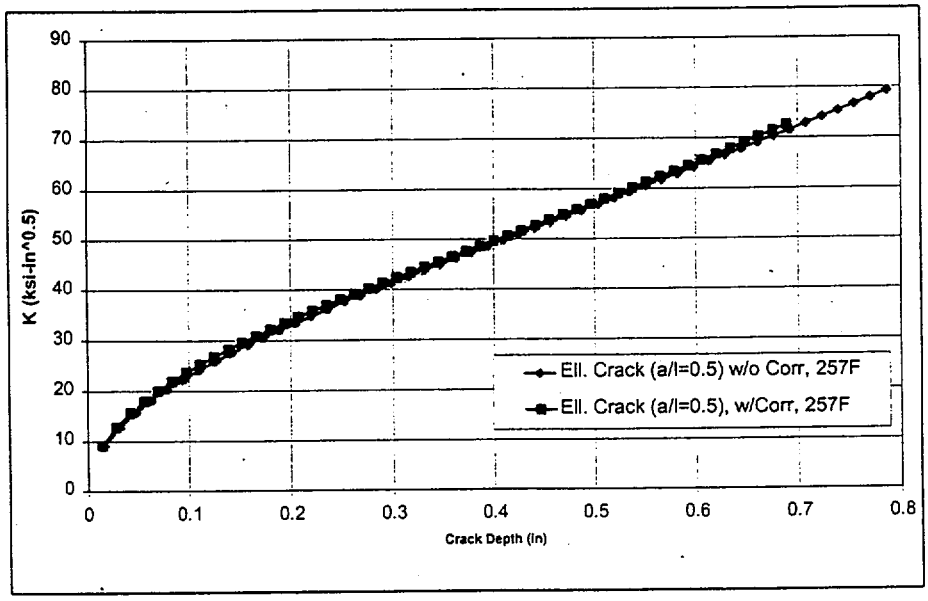

Figure 3-62. Stress Intensity Factor for Radial Crack in Initial WPOB Outer Lid

To reduce weld residual tensile stresses below the SCC initiation threshold level, the waste package program has been evaluating improved WPOB design (such as the new dual-lid concept, Figure 3-63) and low-residual-stress welding techniques and other post-weld techniques such as induction annealing and laser peening that can mitigate tensile residual stresses. Based on evaluations to date and a review of the relevant literature, the latter two processes, post-weld induction annealing and laser peening were selected as tensile stress reduction processes to be implemented on a modified waste package closure design. To optimize this design, experimental measurements were made to quantify the expected stress reduction benefit resulting from laser peening. In addition, extensive ANSYS Finite Element Model calculations were performed to determined the expected stress and stress intensity reduction benefits resulting from the application of both processes. The results of these calculations are presented in Attachment I of the AMR on SCC (CRWMS M&O 2000f). Figures 3-64 and 3-65 show, respectively, the effects of laser peening on the hoop stress and the associated stress intensity factor profiles in the WPOB closure weld. The annealing thermal cycle consists of rapidly increasing the closure weld region temperature to a maximum of 1,120°C in 35 seconds while maintaining a gradual temperature gradient between the immediate induction heated weld region and the remainder of the waste package outer shell. The temperature distribution is held constant for 10 seconds. Then the temperature at the surface is brought down to near room temperature in 30 seconds to simulate the effect of quenching. The heat is dissipated by conduction within the waste package. A steady state is reached after three minutes from the beginning of the simulation.

As can be seen by examination of the post-process through wall stress distributions (Attachment I, AMR), both processes reduce the surface residual stresses below the 20% of yield stress (the SCC initiation threshold value) to depths of about 2 to 3 mm for laser peening and at least 6.5 mm for post-weld induction annealing (see Figure 3-64 for the effect of laser peening). However, because general corrosion of the waste package outer surface may eventually corrode away the beneficial low tensile stress surface layers resulting from either process, it was deemed

prudent to conservatively further modify the waste package closure weld design to encompass two separate Alloy 22 lids, the outer lid being post-weld induction annealed and the inner lid being post-weld laser peened (Figure 3-63).

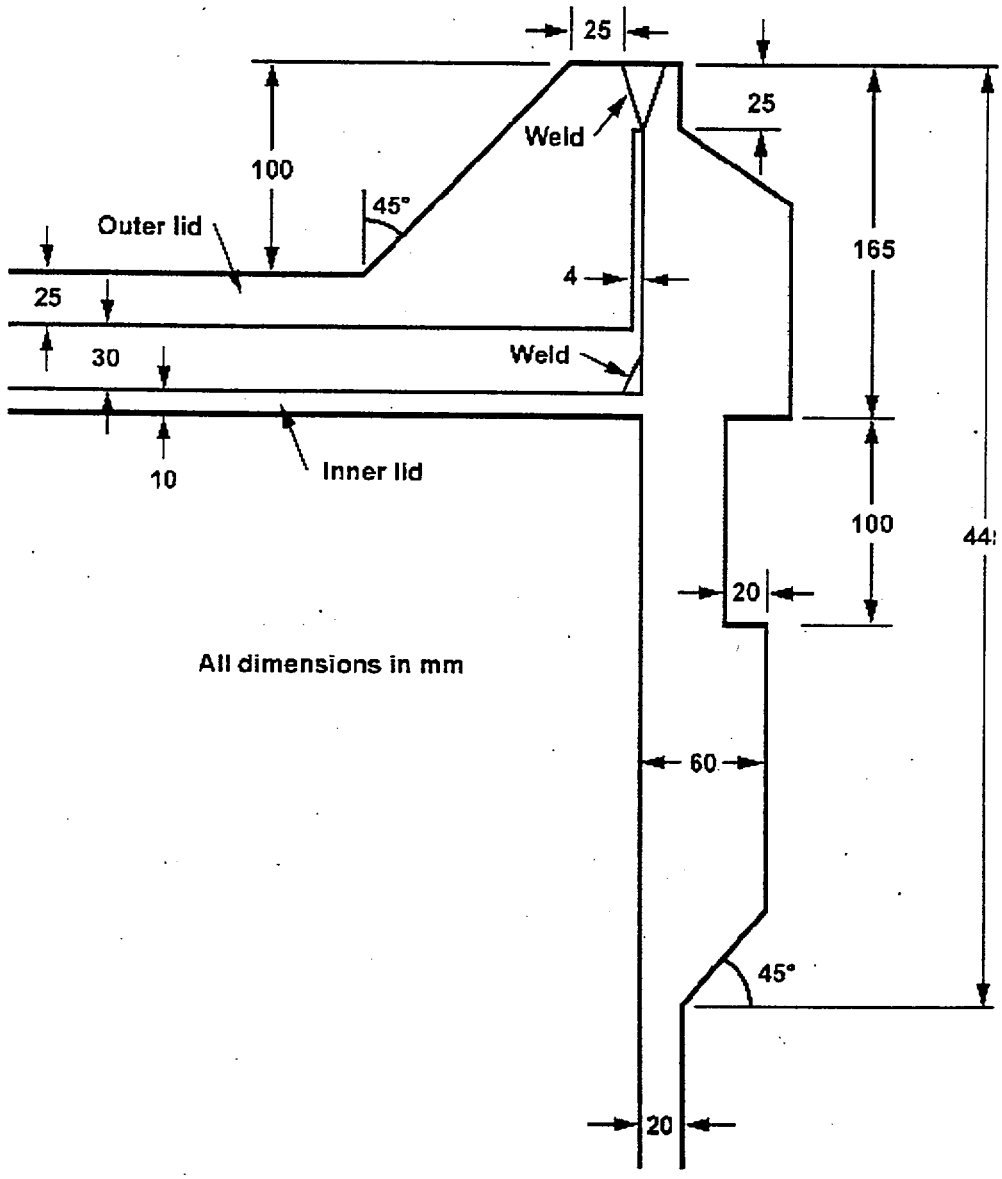

Figure 3-63. Schematic and Dimensions for Dual-Lid WPOB Design

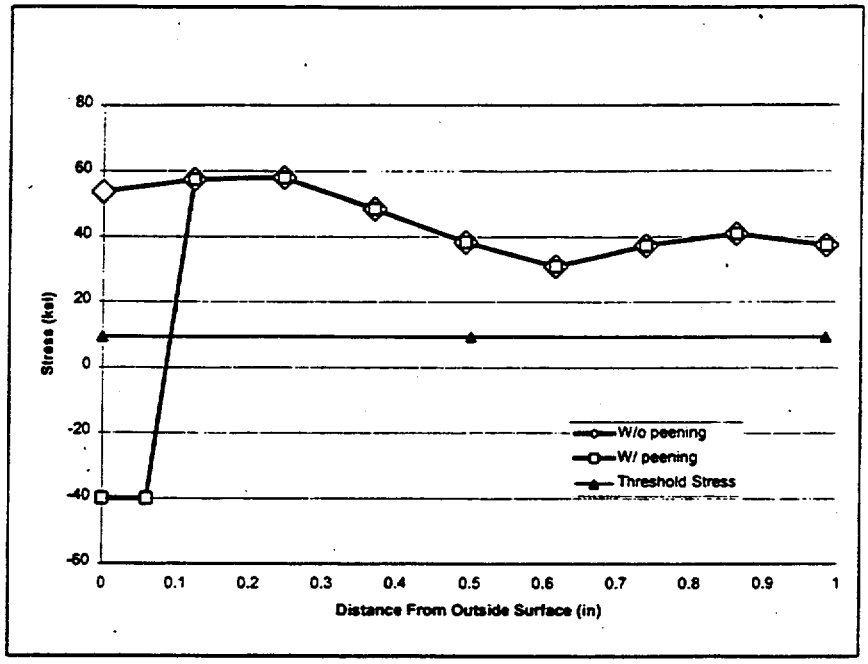

Figure 3-64. Measured Hoop Stress with and without Laser Peening Showing Stress Threshold for SCC. (Figure modified from that in the AMR)

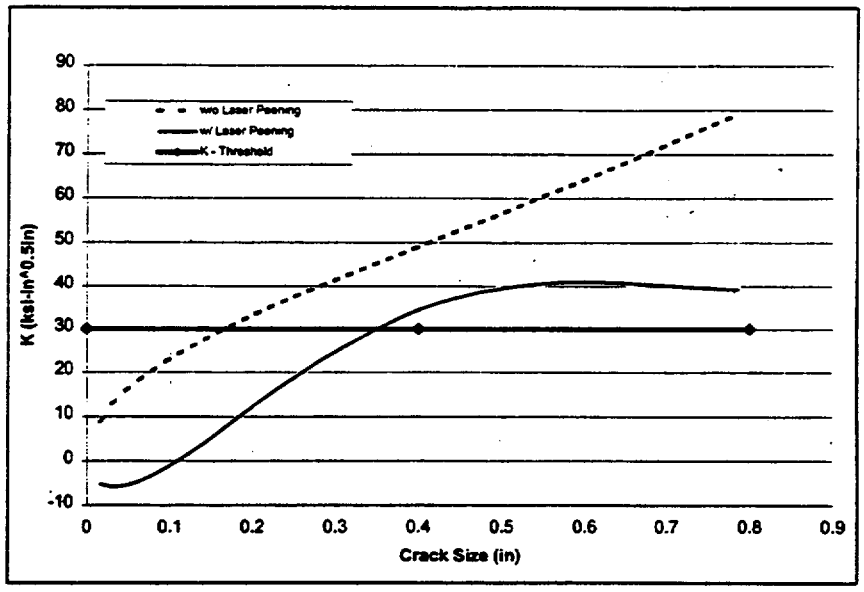

Figure 3-65. Calculated Stress Intensity Factor for Hoop Stress with and without Laser Peening. Threshold Stress Intensity Factor for SCC is also Shown. (Figure modified from that in the AMR)

3.1.7.7 Stress Corrosion Cracking Model A – The Threshold Stress Intensity Factor

For SCC to occur three factors have to exist: stress; a flaw (crack initiation site); a susceptible microstructure and a material-specific corrosive environment. Flaws can either pre-exist due to poor manufacturing practices, or be initiated at locations where high stress concentration exists, such as grooves and corrosion pits. Stress can exist due to welding process among other sources. Once a crack is initiated, the crack will grow by SCC when the applied stress intensity factor, K, is equal to or larger than SCC resistance parameter, K_{ISCC}.

$$K_I \geq K_{ISCC} \qquad \text{(Eq. 3-26)}$$

K_{ISCC} is a material and environment dependent property; which can be obtained through fracture mechanics testing of the materials in the specified environment.

According to the current design, the material to be used for the WPOB is Alloy 22. Currently, the only existing source related to K_{ISCC} for Alloy 22 and Titanium is the experimental work performed at LLNL as described in the SCC AMR.

The final stress intensity factor K_f, obtained by examining the specimen at the end of the test period, is taken to be the SCC threshold value K_{ISCC}, although it may only represent an upper bound of K_{ISCC}, and this may not be conservative. In accordance with the SCC AMR, the K_f values for the eight Alloy 22 specimens are 27.96, 28.73, 28.78, 29.58, 29.66, 30.94, 31.98, and 32.39 ksi in$^{1/2}$. If a normal distribution is assumed, the mean value, $(K_{ISCC}|_{MEAN})$ and the standard deviation, $(K_{ISCC}|_{SIGMA})$, can be calculated:

$$(K_{ISCC}|_{MEAN}) = 30 \pm 1.6 \text{ ksi in}^{1/2} \text{ or } 33 \pm 1.8 \text{ Mpa m}^{1/2} \qquad \text{(Eq. 3-27)}$$

The K_{ISCC} value can vary in accordance with different environmental conditions. In the absence of more data needed for the assessment of the variability of K_{ISCC}, the values derived are used. These values are conservative because of low pH (2.7) of the test environment.

The mean value of the threshold stress intensity factor is 33.00 Mpa m$^{1/2}$ for the outer Alloy 22 lids. The maximum stress intensity factors calculated for a circumferential flaw initiated at the outer surface of the WPOB is 22 Mpa m$^{1/2}$ for the outer lid and 13 Mpa m$^{1/2}$ for the inner lid. Since the mean values of the threshold stress intensity factors are less than the stress intensity factors associated with circumferential flaws, SCC initiation at these flaws is not a significant concern. However, the maximum stress intensity factor for the hoop stress in either the inner lid or the outer lid may exceed the threshold value. This is illustrated for the outer lid in Figure 3-62 were stress intensity factor for the hoop stress can exceed 80 Mpa m$^{1/2}$.

3.1.7.8 Stress Corrosion Cracking Model B–The Slip Dissolution Model

3.1.7.8.1 Background on Slip Dissolution Model

As stated previously, environmental cracking has historically been separated into "initiation" and "propagation" phases. This distinction is almost always arbitrary, for initiation is invariably defined as the time at which a crack is detected, or when the load has relaxed a specific amount

(in a strain-controlled test); in these cases, initiation generally corresponds to a crack depth of significant metallurgical dimensions (e.g., 2 mm).

A lifetime prediction model can be via a fundamental understanding of the cracking mechanism. The formulation of such a model of crack propagation requires the choice of a working hypothesis for the cracking mechanism and the evaluation of the parameters of importance in the mechanism. For the systems of interest, the slip dissolution or film rupture mechanism has been chosen. This cracking mechanism has been successfully applied to model the SCC for stainless steel, low-alloy steel, and nickel-based alloys in light water reactor environments as described in the SCC AMR (CRWMS M&O 2000f). The model is described in detail in the SCC AMR.

3.1.7.8.2 Application to Cracking Prediction of 304 Stainless Steel in Boiling Water Reactor

The slip dissolution is represented by Equation 3-28, which shows the dependence of crack propagation rate (V_t) on the crack tip strain rate (ε_{ct}) (CRWMS M&O 2000f):

$$V_t = A\left(\dot{\varepsilon}_{ct}\right)^n \qquad \text{(Eq. 3-28)}$$

The parameters A and n depend upon the material and environment at the crack tip. These two parameters can be determined from the measured rate of repassivation. Such measurements are made by rapidly straining wires that are fabricated from the material of interest.

The initial application of the slip dissolution or film rupture model was on the quantitative prediction of cracking in type 304 or 316 stainless steels in 288°C high-purity BWR water. These extensive investigations led to a quantification of the parameters:

$$A = 7.8\times10^{-3}(n)^{3.6} \qquad \text{(Eq. 3-29)}$$

Equations 37 and 38 have been combined to yield:

$$V_t = 7.8\times10^{-3}(n)^{3.6}\left(\dot{\varepsilon}_{ct}\right)^n \qquad \text{(Eq. 3-30)}$$

where V_t has the unit of cm s^{-1} and ε_{ct} has the units of s^{-1}. The crack tip strain rate in Equation 3-31 is related to the engineering stress (or stress intensity) parameters via the formulations in the given in the SCC AMR (CRWMS M&O 2000f). The relationship for constant load is:

$$\dot{\varepsilon}_{ct} = 4.1\times10^{-14}\,K_I^4 \qquad \text{(Eq. 3-31)}$$

where K_I is the stress intensity factor in the units of Mpa $m^{1/2}$. Since the waste package closure weld loads are constant with time substitution of Equation 3-31 for constant load into Equation 3-30 yields the following relevant alternative expression for the SCC propagation rate:

$$V_t = \bar{A}(K_I)^{\bar{n}} \qquad \text{(Eq. 3-32)}$$

where

$$\bar{A} = A\left(4.1\times10^{-14}\right)^{n} \qquad \text{(Eq. 3-33)}$$

and

$$\bar{n} = 4n \qquad \text{(Eq. 3-34)}$$

3.1.7.8.3 Application To WPOB Material

There is ample reason to hypothesize that SCC of nickel-based Alloy 22 occurs by the same fundamental mechanism characterized by the slip dissolution SCC model as described in Section 3.1.7.8.2, (i.e., Equations 3-28 through 3-34). The only remaining question is that associated with the quantification of "n".

The characterization of the slip dissolution model is that SCC susceptibility decreases with increased repassivation slope "n". For stainless steels, test data indicated that n = 0.54 gives a good prediction. Recent SCC crack growth test results for Alloy 22 indicated that n = 0.84. For conservative purposes, n = 0.84 is considered to be the upper bound value for n. A lower bound value of n = 0.75 for a highly SCC resistant Alloy 22 is judged to be appropriate.

In the smooth metal components dealt with in this PMR, the size of an incipient crack is expected to be exponentially distributed with a maximum possible size of 50 μm and a median size of 20 μm . A crack will be either circumferential or radial. In either case, only one crack per weld patch will be considered. Based on the relatively high stress intensity factors for radial cracking in the outer Alloy 22 lid of the initial waste package design, it is evident as discussed earlier that the slip dissolution/film rupture model also predicts eventual through-wall radial cracking. This prediction led to the development of the longer life, stress mitigated Dual Alloy 22 Lid Design.

It is generally assumed that crack initiation will not occur if the stress is below a threshold value. Available data suggested a lower bound of 20% of yield strength and an upper bound of 30% of yield for the threshold stress.

3.1.7.9 Estimate of Crack Opening

Leaking through a crack can occur if the crack grows into a through-thickness crack. A comprehensive finite element analysis may be attempted in order to estimate the crack opening. A simplified approach, however, is described. The following assumptions are made for the simplified approach:

1. A crack is either circumferential (perpendicular to the radial stress) or radial (perpendicular to the hoop stress) in the WPOB closure weld. A circumferential crack has a semi elliptical shape with depth "a" and length "2c". A radial crack has a semi-circular shape (a = c).

2. The crack length "2c" of a circumferential crack remains unchanged, but the final length of a through-wall crack is at least twice the wall thickness. Under this assumption, most cracks will grow in both directions of the minor (depth "a") and major (length "2c") axes and assume the semi-circular shape (i.e., a = c) when they become through-wall cracks. According to fracture mechanics, "a" tends to grow faster than "c" because the stress intensity factor tends to have a maximum value at the end of the minor axis and a minimum value at the end of the major axis. So, eventually, a semi-elliptical crack will become a semi-circular crack. The crack length "2c" will remain unchanged only for very long cracks, with initial crack length greater than twice the wall thickness. For such long cracks, the occurrence rate is usually very low. The length of a semi-circular crack will always be equal to twice the crack depth.

3. The crack opening has an elliptical shape with length $2c$ and a gap δ.

SCC AMR (CRWMS M&O 2000f) showed that the opening of a crack, δ, with length $2c$ in an infinite sheet is given for plane stress condition as:

$$\delta = \frac{(4c)\sigma}{E} \qquad \text{(Eq. 3-35)}$$

where σ is the stress and E is Young's modulus. The opening area, A_{cr}, for an elliptical crack, therefore, can be estimated by:

$$A_{cr} = \tfrac{\pi}{4}\delta(2c) = \frac{(2\pi c^2)\sigma}{E} \qquad \text{(Eq. 3-36)}$$

When Equations 3-35 and 3-36 are used to estimate the crack opening and opening area, σ is the maximum stress across the thickness of either the radial stress (for a circumferential crack) or the hoop stress (for a radial crack).

3.1.7.10 Summary of Stress Corrosion Cracking Model

Two alternative models that deal with SCC have been developed for the performance assessment of the materials to be used for the WPOB of the Yucca Mountain Program.

The first model (threshold stress intensity factor model) is based on the theory that there exists a threshold value (K_{ISCC}) for the stress intensity factor such that there is no growth of a crack having a stress intensity factor less than the threshold value (CRWMS M&O 2000f). The concept of threshold stress intensity factor (K_{ISCC} or K_{th}) has been commonly used to assess the susceptibility of materials to SCC. The applicability of this model to Alloy 22 (the material to be used for the outer shell of the waste package) was tentatively verified experimentally.

Preliminary results show that the initial design waste package is able to arrest circumferential SCC but not radial SCC based on the threshold stress intensity factor model. For a circumferential flaw initiated at the outer surface, the mean values of the assumed threshold stress intensity are greater than the maximum stress intensity factors estimated for a circumferential flaw initiated at the outer surface (CRWMS M&O 2000f). The mean values of the threshold stress intensity are 33.00 Mpa $m^{1/2}$ for the outer lid and 20.54 Mpa $m^{1/2}$ for the inner lid. The maximum stress intensity factors estimated for a circumferential flaw initiated at the outer surface are 22 Mpa m1/2 for the outer Alloy 22 lid. However, based on the threshold value, through-wall, radial cracking can occur.

The second model (slip dissolution or film rupture model) relates crack advance to the metal oxidation that occurs when the protective film at the crack tip is ruptured. The theory of slip dissolution and film rupture was successfully applied to assess the SCC crack propagation for light water reactors at high temperature. This model was adopted to assess the SCC capability of the materials to be used for the WPOB (Alloy 22). Based on the high calculated radial stress intensity factor for the outer Alloy 22 weld of the initial waste package design, the model also predicts eventual through-wall radial cracking.

3.1.7.10.1 Waste Package Potential Failures Due to Stress Corrosion Cracking – Mitigation or Elimination

Since the crack growth analyses produced by either SCC model indicate that through-wall radial cracking is a potential issue to the initial waste package design, it is necessary to implement SCC mitigating processes to eliminate potential for SCC.

3.1.7.10.2 Mitigation or Elimination of Closure Lid Weld Stresses

As mentioned previously, two methods have been identified for localized treatment of the closure weld region. One of these involves use of induction heating coils to effect a localized annealing of the weld region. This process has been used successfully in the annealing of weld stresses in large components such as girth welds in large diameter solid fuel rocket casings. This process is expected to remove all of the initially present weld residual tensile stresses through the thickness of the material. There are, however, several concerns associated with this approach. Calculations indicate that temperature gradients resulting during cool down due to this process tend to shift the location of the tensile stresses to another adjacent region of the waste package making that region potentially vulnerable to SCC. A second concern is that the process may heat the waste to unacceptably high temperatures. As discussed earlier, both these possibilities were analyzed using the finite element code ANSYS. The results of this analysis show that the localized annealing by induction heating is a viable approach for producing low tensile stresses (< 20% yield stress to depth ≥ 7 mm).

The second method involves the use of the laser peening process, where a high powered laser beam is used to introduce shock pulses onto the material surface. These pulses introduce compressive stresses on the surface. Multiple passes of laser peening are used to increase the depths of the compressive stress layer. This process has been successfully demonstrated at LLNL on sample weldments (Figure 3-64). It has been shown that compressive stress can be introduced to depths of 2 to 3 mm using multiple passes. Additional depth may be possible but has not been demonstrated. A shortcoming of this approach is that this process only delays the potential start of SCC. Below the layer of compressive stresses, the weld region is still under tensile stresses and when the treated layer of material is lost due to corrosion, the remaining material is still vulnerable to SCC.

An optimized low tensile stress induction annealing closure weld design was developed based on ANSYS stress analysis. Also, post-process through-wall residual stresses have been calculated for both mitigation processes using the ANSYS program (see the SCC AMR for results, CRWMS M&O 2000f). As a result, a dual Alloy 22 lid waste package design employing both stress mitigation process was developed to maximize expected waste package lifetime with respect to potential SCC.

3.1.8 Hydrogen Induced Cracking

As discussed in Sections 3.1.5 and 3.1.6, titanium drip shield is highly resistant to general and localized corrosion. Other degradation mechanisms are not life-limiting. The material has been shown to be susceptible to SCC under certain conditions. As discussed in Section 3.1.7, mitigation of weld residual stresses makes this an unlikely mechanism when backfill is present to preclude rockfall generated stresses. Another likely failure mechanism for titanium and its alloys under waste disposal conditions is via the process of hydrogen absorption leading to hydrogen induced cracking. Hydrogen induced cracking is also called hydrogen embrittlement, which is a process resulting in a decrease of fracture toughness or ductility of a metal due to the presence of atomic hydrogen. The usual failure mode for a ductile material is the ductile tearing observed during slow crack growth. The decrease of fracture toughness can also cause fast crack growth (brittle fracture) of a normally ductile material under sustained load. During slow crack growth, material will fail as the stress intensity factor K reaches a value K_S. During fast crack growth, the same material will fail as the stress intensity factor K reaches a value K_H, which is less than K_S.

Generally, the passive oxide film on titanium acts as an excellent barrier to the transport of hydrogen through the oxide, and hydrogen absorption under open-circuit (i.e., natural corrosion) conditions would not be expected and is generally not observed. The concern remains, however, that over normal operating periods (up to tens of years), the process of hydrogen absorption may have been too slow to be observed analytically, and that over the course of many years (10^3 to 10^5), this absorption could lead to a significant accumulation of hydrogen and the danger of hydrogen induced cracking.

Under Canadian waste repository conditions a very simple approach was adopted to predict when hydrogen induced cracking might become a potential failure process in a waste container. In essence, this model is a susceptibility model or the equivalent of an initiation model for localized corrosion processes such as pitting and crevice corrosion. The basic premise of the

model is that failure will occur when the hydrogen content exceeds a certain limit or critical value (H_c). Combinations of stress intensity factor and hydrogen concentration that lead to fast crack growth due to brittle fracture (K_H), slow crack growth due to either sustained load cracking or ductile rupture (K_S), or no failure are discussed in AMR on hydrogen induced cracking (CRWMS M&O 2000h).

This model presented in the AMR is very conservative because it assumes that, when the environmental and material conditions can support the particular corrosion process, failure will be effectively instantaneous.

Clearly, the propagation of a localized corrosion process, whether it be a pit, a crevice, a stress corrosion crack, or a hydrogen-induced crack, does not proceed instantaneously to failure. However, if the rate of propagation is fast on the geologic time scales being considered, then the process can be thought of as instantaneous, e.g., 30 years of "slow" crack growth is irrelevant on a time scale of 10^3 to 10^5 years. Another factor ignored in this analysis is the impact of propagation-limiting processes. For example, with a pit or crevice, repassivation may occur; or with a stress corrosion crack, crack blunting could occur. In the hydrogen induced cracking model described below, no crack initiation or crack blunting processes are considered.

3.1.8.1 Model Description

The model can best be summarized as follows:

1. The passive oxide is assumed to be permeable to atomic hydrogen.

2. Atomic hydrogen is generated at the surface of the Ti alloy. This is described by a hydrogen generation rate, which is taken to be proportional to the general passive corrosion rate.

3. A fraction of the hydrogen is absorbed into the oxide and assumed to directly enter the alloy. The remainder combines to yield hydrogen gas, which is lost to the surroundings. The rate of absorption is taken to be directly proportional to the hydrogen generation rate multiplied by an absorption efficiency coefficient.

4. Once in the alloy, the hydrogen is transported throughout the entire thickness of the material to yield a uniform distribution of hydrogen. In other words, transport processes within the alloy are rapid compared to the rate of absorption.

5. The hydrogen content of the alloy is allowed to increase until a critical level is reached. The material then fails immediately. The model allows for the calculation of hydrogen content and for comparison with the critical concentration.

3.1.8.2 Elements of the Model Assumptions

3.1.8.2.1 The Oxide is Assumed to be Permeable to Hydrogen

The potential Yucca Mountain repository will not achieve anoxic conditions. In the early stages of repository lifetime, when temperatures are high, the oxygen content of the repository will be

low, but so will the water content, which is the only significant potential source of hydrogen (due to reaction with the titanium). Eventually, oxidizing conditions will be established and an open-circuit corrosion potential, too positive to allow the redox transformations in the oxide, will be established. Also, for oxidizing conditions, any exposed noble metal intermetallic particles (e.g., Ti_2Ni in Titanium Grade 12, Ti and Pd in Titanium Grades 16 and 7) will be passivated by a surface oxide film, and their catalytic properties for hydrogen production and absorption may be lost.

The oxide film remains impermeable to hydrogen until the electrical potential becomes sufficiently negative that the oxide becomes chemically unstable. When this occurs, Ti (IV) within the TiO_2 oxide is reduced to Ti (III) and hydrogen can be incorporated as a doping defect. When this process becomes possible, it is conservatively assumed that the oxide becomes permeable to hydrogen, which then has free access to the alloy, i.e., any hydrogen entering the oxide can be rapidly transported to the metal (CRWMS M&O 2000h).

Several mitigating factors indicate that this is a very conservative scenario. First, experimental evidence suggests that total permeability is not established as soon as this oxide transformation begins. Second, it is unlikely that, in the absence of specific unexpected reducing reagents, such redox transformations could be induced in the passive film.

Assuming that the maximum temperature at which an aqueous condition can be sustained on the titanium is 125°C, a pH > 13 would be required for significant hydrogen absorption (CRWMS M&O 2000g). It would be judicious to assume, therefore, that hydrogen absorption is possible within the temperature range of approximately 100 to 125°C. This range effectively defines a window of susceptibility for hydrogen absorption.

The probability of hydrogen absorption by titanium alloys at Yucca Mountain is low but cannot be ruled out within the window of susceptibility defined by the temperature range of 100 to 125°C.

3.1.8.2.2 Hydrogen is Generated at the Surface of the Titanium Alloy

The only feasible source of absorbable hydrogen appears to be the reaction of Ti with water. The direct absorption of radiolytically produced hydrogen requires a combination of high dose rate (> 10^4 R h^{-1}) and high temperature (> 200°C) and a steam or aqueous environment. This combination of conditions seems extremely unlikely at Yucca Mountain. Under open-circuit conditions, the rate of hydrogen production will be directly related to the general corrosion rate. In the presence of dissolved oxygen, this rate has been shown to be extremely low and effectively immeasurable by standard procedures such as weight change measurements. Consequently, the rate of hydrogen production (the essential model boundary condition) will also be extremely low.

Further, oxidizing conditions expected in the repository will not lead to a significant enhancement of general corrosion; the process will be blocked by the excellent protective properties of the passive TiO_2 film. Under these oxidizing conditions, the intermetallic precipitates should be covered by a passive oxide film and their catalytic properties severely degraded.

Thus under Yucca Mountain repository conditions, the corrosion rate of titanium alloys (with the possible exception of Titanium Grade 12), and, hence, the rate of hydrogen production, will most likely be slow and transitory. Evidence suggests that even when corrosion, in the form of film growth, is initially accelerated under oxidizing conditions, the accumulation of mineral precipitates leads to the eventual blocking of corrosion processes.

3.1.8.2.3 A Fraction of the Hydrogen is Absorbed into the Metal

Even if the oxide film present on the titanium surface provides just a semi-impermeable barrier to hydrogen absorption into the metal, only a fraction of the hydrogen produced will actually be absorbed into the metal, and, hence, contribute to the eventual embrittlement of the alloy. This critical fraction must be known. A consistent single value may not represent the real absorption efficiency of the alloy because this efficiency would be expected to change as the condition of the surface changed. The initial surface could be relatively free of absorbed hydrogen, and the initial absorption efficiency could be high. Subsequently, it would be expected to decrease as the number of available surface sites for absorption become saturated. These absorption sites could be the usual defects and dislocations known to trap hydrogen and, in addition, noble metal intermetallic particles, which would have a high solubility for hydrogen. Alternatively, the formation of surface hydrides could lead to a change in the mechanism of proton reduction and a decrease in the rate of hydrogen absorption into the alloy.

However, the concern remains that, in the temperature range 100°C to 125°C, in the presence of an aggressive saline solution, the passive oxide film will be degraded and the hydrogen absorption efficiency increased. The rate of passive film growth (rate of hydrogen production), as well as the hydrogen absorption rate for Titanium Grade 12 in extremely saline solutions at 25 and 100°C are discussed in the AMR on hydrogen induced cracking (CRWMS M&O 2000h). These values 0.03 μ/y and 10% respectively for passive film growth and hydrogen absorption would be conservatively appropriate for Titanium grade 7 under degraded passive conditions, because they closely resemble those anticipated at Yucca Mountain.

3.1.8.2.4 Hydrogen is Uniformly Distributed in Titanium Alloy

Once hydrogen is in the metal, its fate becomes dependent on the diffusion rate and how that rate is affected by the microstructure of the material and the strength and distribution of stresses within the material.

It was assumed that, because the rate of absorption of hydrogen into the metal would be very slow, its transport throughout the bulk of the material would be comparatively rapid. Hence, the hydrogen would be uniformly distributed throughout the alloy. At much higher absorption rates generally found during electrochemical experiments, absorbed hydrogen leads to the formation of a surface hydride layer. Such a layer is innocuous, not leading to failure by cracking. The presence of such a layer appears to impede the absorption of further hydrogen, i.e., its presence reduces the absorption efficiency of the alloy.

However, hydrogen accumulates at the titanium surface. A conservative assumption is that it remains available for transport into the alloy. When the temperature is low enough so that the transport rate can be assumed to exceed the absorption rate (below 100°C), the thickness of the

hydride layer will decrease as the hydride is redissolved in the alloy. The layer of hydride on the surface serves as a source of hydrogen for infusion into the bulk material. The hydride continues to redissolve until the surface layer is depleted.

3.1.8.2.5 Hydrogen Concentration Increases to Critical Level where Failure Occurs

The slow strain rate tests (CRWMS M&O 2000h) show that titanium can tolerate substantial amounts of hydrogen before it becomes susceptible to cracking. This critical hydrogen concentration is not related to the solubility of hydrogen in the alpha matrix of the alloy but to the number density of precipitates, which must be capable of supporting a crack propagation process through the material. Values for critical hydrogen concentration (H_c) were obtained from published literature for Titanium Grades 2, 12 and 16 (CRWMS M&O 2000h). The high value for Titanium Grade 16 (greater than 1000 μg per gram) appears to be due to the ability of the intermetallics to soak up hydrogen, thereby preventing them from forming hydride precipitates in the alloy.

Whichever process is assumed for the dispersion of hydrogen throughout the titanium alloy, failure is assumed to occur once this critical value is achieved. However, this remains a very conservative approach because slow strain rate tests have determined the point at which the necessary stress level will inevitably be achieved. Also, the critical value is a threshold value, representing the lowest concentration at which influence of hydrogen is observed. It is feasible that much higher concentrations of hydrogen could be tolerated before failure actually occurs.

3.1.8.3 Determination of the Critical Hydrogen Concentration

Using the slow strain rate technique on precracked compact tension specimens precharged with known amounts of hydrogen, it has been shown that fracture toughness of Titanium Grade 2 and that of Titanium Grade 12 is not significantly affected until their hydrogen content exceeds a critical value, H_c. The as-received materials, containing 20 to 50 μg per gram of hydrogen, are very tough and fail by ductile overload under high stress. This ductile tearing is also observed during slow-crack growth for both materials. The hydrogen concentration above which slow-crack growth is no longer observed and only fast-crack growth occurs is defined as H_c.

Critical hydrogen concentrations (H_c) of 400 to 2,000 μg per gram were reported for Titanium Grade 2, 400 to 1,000 μg per gram for Titanium Grade 12, and 1,000 to 2,000 μg per gram for Titanium Grade 16 (CRWMS M&O 2000h). Critical hydrogen concentrations are not available for Titanium Grade 7. The value of H_c for Titanium Grade 7 is conservatively assumed to be at least 400 μg per gram, which is the lower bound value observed for Titanium Grade 2, Titanium Grade 12, and Titanium Grade 16, as indicated previously.

3.1.8.4 Determination of Hydrogen Concentration

Analytical formulas can be derived to represent the hydrogen concentration in the metal as a function of time of emplacement of the container. There are two processes by which hydrogen could be produced, and possibly absorbed, under passive conditions: (1) direct absorption of hydrogen produced by water radiolysis and (2) absorption of atomic hydrogen produced by the corrosion process to produce oxide. The direct absorption of radiolytically produced hydrogen

does not appear to be significant except at high dose rate (>102 Gy/h) and high temperature (>150°C). This condition is clearly unattainable under Yucca Mountain conditions, and will not be considered, leaving the corrosion process as the only feasible source of hydrogen for absorption.

The rate of hydrogen absorption will be controlled by the rate of the corrosion reaction, which dictates the rate of production of absorbable hydrogen. Since titanium oxide, TiO_2 is extremely stable and protective in the repository environment, the corrosion reaction will be effectively limited to an oxide film growth reaction.

While the rate of hydrogen production and absorption is directly proportional to the rate of film growth, the fraction of hydrogen absorption needs to be determined. Available test data suggest 0.1 and 0.02 for fractional efficiency for absorption values, f_h to represent high and low hydrogen absorption efficiencies for titanium alloys. The low value would appear most appropriate for Ti-2 since the passive film is a good transport barrier to hydrogen absorption. For Ti-16 and Ti-7 in which intermetallic formation is very limited or avoided, the lower value is appropriate.

Based on a constant film growth rate, and hence the corrosion rate, the concentration of hydrogen in the metal, H_A, can be calculated as a function of time of emplacement (t in years) from the expression,

$$H_A = 4(\rho_{Ti}/10^3) f_h R_{uc} t [M_{Ti}(d_o - R_{uc} t)]^{-1} \qquad \text{(Eq. 3-37)}$$

where

H_A = hydrogen content (g/mm^3)

ρ_{Ti} = density of Ti (g/cm^3)

f_h = fractional efficiency for absorption

R_{uc} = rate of general passive corrosion (mm/y)

t = time of emplacement in years (y)

M_{Ti} = atomic mass of Ti = 47.9

d_o = original corrosion allowance (mm) = container wall thickness

The units of atomic mass are grams per gram-atom which for hydrogen is 1.0 grams per gram-atom and for titanium is 47.9 grams per gram-atom. Since there is one gram of hydrogen per gram-atom, the values of H_A in (g/mm^3) and in (g-atoms/mm^3) are equal (to within less than 1 percent).

Considering a Ti-7 plate with 1 mm^2 surface area, it is noted in Equation 3-37 that hydrogen in grams produced by the general corrosion after t years of emplacement is based on the reaction:

$$Ti + 2H_2O \rightarrow TiO_2 + 2H_2;$$

The derivation of Equation 3-37 is based on a constant general corrosion rate. It was noted that the assumption of constant corrosion rate is conservative and less conservative corrosion models assume that the rate decays with time. (CRWMS M&O 2000d)

The rate of general passive corrosion, R_{uc} can be calculated from the rate of oxide film thickness, R_{ox} by the following formula:

$$R_{uc} = R_{ox}(\rho_{ox} / M_{ox})(\rho_{Ti} / M_{Ti})^{-1} \qquad \text{(Eq. 3-38)}$$

where

ρ_{ox} = density of the oxide in g/cm^3
M_{ox} = molecular mass of the oxide

Since the value of $(\rho_{ox}/M_{ox})(\rho_{Ti}/M_{Ti})^{-1}$ is always greater than unity, it is conservative to assume that $R_{uc} = R_{ox}$.

The general corrosion rates reported for Ti-7, at the 50th percentile is approximately 25nm/a, the rate at the 90th percentile is approximately 100 nm/y, and the maximum rate is less than 350 nm/a. (CRWMS M&O 2000d).

3.1.8.5 Critical Hydrogen Concentration

The H_C value for Ti-7 is assumed to be at least 400 μg/g, which is the lower bound value observed for Ti-2 and Ti-12 as indicated previously. This assumption appears to be extremely conservative based on data reported for Ti-16. As noted Ti-7 and Ti-16 are similar alloys because of their similar chemical compositions.

The fractional efficiency for absorption, based on previous discussion, is $f_h = 0.02$ for Ti-7. The rate of general passive corrosion is R_{uc}= 100x10^{-6} mm/a (90th percentile value) or 25x10^{-6} mm/a (50th percentile value). The time of employment is t = 10,000 years. A minimum wall thickness of 15 mm is assumed for d_o.

Case 1: Conservative Estimate

R_{ox}=100x10^{-6}mm/y (90th percentile value)
f_h=0.02
d_o=15mm
t=10000y
H_A=119 μg/g < Hc = 400 μg.g.

Case 2: Best Estimate

R_{ox}=25x10^{-6}mm/y (50th percentile value)
f_h=0.02
d_o=15mm
t=10000y
H_A=28 μg/g < Hc = 400 μg.g.

The hydrogen concentration in the drip shield at 10,000 years after emplacement is 119 μg/g resulting from a conservative estimate and 28 μg/g from a best estimate. The estimated hydrogen concentration in either case is significantly less than the conservatively selected critical hydrogen concentration of 400 μg/g for Ti-7. These results indicate that there exists a big margin of safety for the drip shield against the effects of hydrogen induced cracking and this degradation mechanism is not credible under repository conditions.

3.1.8.6 Model Results

In the description of the hydrogen induced cracking model presented in the corresponding AMR (CRWMS M&O 2000h), extensive evidence has been provided to support a qualitative assessment of Titanium Grade 7 as an excellent choice of material for the drip shield with regard to degradation caused by hydrogen-induced cracking. Quantitative evaluation based on this model indicates that the drip shield material (Titanium Grade 7) is able to sustain the effects of hydrogen-induced cracking. Available corrosion test data show that the hydrogen concentration is below 120 μg per gram, which is less than the critical hydrogen concentration of 400 μg per gram for Titanium Grade 7.

3.1.9 Model Uncertainties

Uncertainties in each of the process models were identified in the discussion of the models in the previous sections and in the individual AMRs. The approach used in dealing with these uncertainties is to be conservative and bound the uncertainties. A review of the uncertainties in the various models is presented below.

3.1.9.1 Thermal Aging

A graphical approach to bounding the uncertainty in the aging model is illustrated in Figure 3-7. The line representing a "best fit" to the data for "complete grain boundary coverage" predicts that more than 10,000 years at 300°C will be required to completely cover the grain boundaries of Alloy 22 with intermetallic precipitates. However, the line with the "minimum slope possible within the error bars" shows that complete grain boundary coverage might occur in as little as 100 years (very unlikely bounding case). The "best fit" line is the most likely scenario. In the case of bulk precipitation, none is predicted with the line representing the minimum possible slope. Thus, we conclude with reasonable certainty that no bulk precipitation will occur after 10,000 years at 300°C.

From Figures 3-9 and 3-10, it appears that a fully aged sample of Alloy 22 could change the observed corrosion potential. For example, corrosion potential was shifted in a less noble (negative) direction by 63 mV in simulated acidic concentrated water at 90°C. This potential

was shifted in a less noble (negative) direction by 99 mV in SCW at 90°C. Full aging of Alloy 22 (complete coverage of the grain boundaries) does not appear to significantly alter passive film stability.

Thermal aging of Titanium Grade 7 at 300°C is expected to have little impact on the corrosion resistance of this material. Since no credit is claimed for the corrosion resistance of 316NG, the TSPA calculation is insensitive to the uncertainty associated with the corrosion of 316NG.

3.1.9.2 Dry Oxidation

In the case of Alloy 22 and 316NG, the rates of dry oxidation are very small. Therefore, uncertainty in the dry oxidation rate is not expected to have any significant impact on the performance of these materials. The current model is based upon published data, and does not include estimates of uncertainty.

3.1.9.3 Humid Air and Aqueous Phase Corrosion

The threshold relative humidity is represented by Equation 3-2. This correlation represents the deliquescence point of $NaNO_3$ and has an excellent fit of the data (correlation coefficient of 0.9854). Uncertainty in this threshold is primarily due to the composition of the salt film. The waste package and drip shield would always experience some combination of humid air and aqueous phase corrosion. The uncertainty in this parameter is discussed in more detail in the associated AMRs.

The distribution of general corrosion rates for either humid air corrosion or aqueous phase corrosion represented by the curves given in Section 3.1.5.4. Distributions for 316NG are represented by Figure 3-15, which shows distributions formed from published data. Figure 3-23 shows the distribution of rates for Alloy 22, based upon data taken from the LTCTF. Figures 3-26 and 3-27 shows the distribution for Titanium Grade 7 rates, also based upon data from the LTCTF. The dispersion in these curves is assumed to be entirely due to uncertainty.

The variability is assumed to be comparable in magnitude and is represented by a triangular distribution.

A detailed analysis of the error in general corrosion rate is given in each supporting AMR, with the results summarized in Tables 3-8 and 3-9.

Determinations of corrosion and threshold potential are based upon three replicate cyclic polarization measurements at each combination of environment and temperature. The results are tabulated in the supporting AMR, as summarized in Figures 3-38 through 3-48. The uncertainty in the corrosion potential due to gamma radiolysis is addressed by Figures 3-51 and 3-52 (maximum positive shift in error of about 250 mV). Some uncertainty in the selection of corrosion and threshold potential is shown in the figures as Threshold Potential 1, through 3. The bounds of the threshold potential are shown graphically in the figures. Numerical representations of this uncertainty have been made and are embedded in WAPDEG.

The rates of localized corrosion have been bounded with the range of values found in the published literature, and are summarized in Tables 3-11 and 3-12.

3.1.9.4 Stress Corrosion Cracking

For the first time, stress corrosion cracking has been included in the performance assessment calculation done with WAPDEG. Two alternative SCC models have been considered, one based upon a threshold stress intensity factor (Method A), and another based upon a threshold stress for a smooth surface (Method B). In the second approach, cracks are assumed to propagate by the slip-dissolution mechanism after initiation. Method B is used as the basis of the performance assessment. The slip-dissolution model (Method B) predicts that crack propagation is a function of the local stress intensity at the crack tip. Thus, the uncertainty in this driving force must be estimated.

The local stress intensity is calculated from the local stress and the crack penetration. The uncertainties in the stress distribution (stress vs. depth) are based upon analyses of measured residual stresses in welds, before and after mitigation, as well as finite element modeling with the ANSYS code. These uncertainties are abstracted for WAPDEG and shown quantitatively in Figures 3-73 through 3-80.

Aside from the stress intensity, K_I, the parameters in the slip-dissolution model for SCC propagation are based upon measurements for stainless steel from the BWR industry. Since stainless steels are much more prone to SCC than Alloy 22, these parameter estimates are projected to be conservative.

The threshold stress for initiation of SCC on a smooth surface is very conservatively estimated to be approximately 20 to 30% of the yield stress, based upon the determination of such thresholds for related but more susceptible alloy systems exposed to very aggressive environments such as boiling $MgCl_2$. The uncertainty is assumed to be within ± 5% of the median value.

3.1.10 Model Validation

According to ASTM C1174, (*Standard Practice for Prediction of the Long-Term Behavior of Materials, Including Waste Forms, Used in Engineering Barrier Systems (EBS) for Geologic Disposal of High-Level Radioactive Waste*) model validation is the process through which independent measurements are used to ensure that a model accurately predicts an alteration behavior of waste package materials under a given set of environmental conditions (e.g., under repository environment over the time periods required). Obviously, no model can be validated over the 10,000 year service life (time period) of the repository. The only means of validating models must involve accelerated testing. According to the same ASTM procedure, an accelerated test is a test that results in an increase in the rate of an alteration mode, when compared with the rates for service condition. Changes in alteration mechanism, if any, must be accounted for in the use of the accelerated test data.

The thermal aging model is represented by equations 3-5 and 3-6, both of which assume Arhenius-type kinetics. Precipitation and long-range ordering can be accelerated by increasing the temperature above those levels expected in the repository. If the model can accurately predict the kinetics of these phenomena at combinations of time and elevated temperature, it will be considered valid for making predictions at lower temperature and longer time.

Since all available data has been used to establish these correlations the correlations are considered valid for their intended use. Additional data that are being collected will help to reduce uncertainties and improve the level of confidence in the model.

The effects of precipitation and long-range ordering on corrosion are determined with electrochemical techniques. Through application of electrochemical potentials more anodic than the open circuit corrosion potential, corrosion phenomena can be accelerated. Variations in corrosion and threshold potential can be correlated with the extent of thermal aging. Similarly, variations in rates of dissolution through the stable passive film can also be correlated with the extent of thermal aging. These rates of dissolution are accelerated by application of a potential between the corrosion and threshold potentials, and are proportional to the passive current density. The corrosion rate enhancement factor is determined by calculating the ratio of measured passive current densities for aged and unaged samples. Since all available electrochemical data has been used to establish the corrosion model for thermally-aged samples, this model is considered valid for its intended use.

The models for dry oxidation of Alloy 22, Titanium Grade 7, and 316NG stainless steel are based upon published data found in the scientific literature. More specifically the model for dry oxidation of Alloy 22 is based upon the parabolic growth of the oxide film at elevated temperature. However, in the absence of any such low-temperature data, the parabolic rate constant for high temperature is applied at low temperature. Given the extremely small magnitudes of these rates, dry oxidation is expected to have no significant impact on waste package performance.

The threshold relative humidity for humid air corrosion is based on the deliquescence point of sodium nitrate. The threshold for salt films deposited in the repository may be slightly different. However, salt deposits produced by evaporating simulated J-13 water to dryness, support this basis.

Rates of humid air corrosion are expected to follow general distributions based upon weight-loss data from the LTCTF. The distributions for Alloy 22 data for 6, 12, and 24 months of exposure to a variety of test media. Corroborative measurements made with the atomic force microscope and other surface analytical techniques have also been used as further means of model validation. The test program will continue; ultimately providing data for 60-months of exposure. Future data will be considered independent and corroborative, and will be used to reduce uncertainties and conservatism in the model.

The threshold relative humidity for aqueous phase corrosion is the same as that used for humid air corrosion. The same approach has been used for validation. Rates of general corrosion in the aqueous phase also obey the general distributions based upon weight-loss data from the LTCTF. The same approach described for validation of the rate model for humid air corrosion has been employed for validation of the rate model for general corrosion in the aqueous phase.

Comparisons of corrosion and threshold potentials are used to determine whether rates for general or localized corrosion are applicable. The initial correlations given in this PMR are based upon standard cyclic polarization measurements in simulated dilute water, SCW,

simulated acidic concentrated water and simulated saturated water, covering a broad range of temperature.

The stress corrosion model is primarily based on published data. Very limited data have been obtained under repository relevant conditions. The data obtained under the Yucca Mountain project include pre-cracked specimens tested under very aggressive environments. Thus the model uses a very conservative approach. Future data obtained by the Project will serve to reduce the level of conservatism and improve the confidence in the model.

3.1.11 Alternative Approaches or Models

Alternative models have been considered for rates of dry oxidation, localized corrosion thresholds, stress corrosion thresholds, stress corrosion cracking, stress mitigation, & hydrogen induced cracking. These alternatives are summarized below.

3.1.11.1 Dry Oxidation

Method A – Parabolic Growth Law
Method B – Logarithmic Growth Law

In the case of dry oxidation, Method A is used for Alloy 22 and 316 NG, while Method B is used for Titanium Grade 7. These model selections were based upon the availability of published data to support the corresponding models.

3.1.11.2 Localized Corrosion Threshold

Method A – Threshold Electrochemical Potential
Method B – Threshold Temperature

In the case of localized corrosion, Method A is used because the threshold potential model is more solidly rooted in the theoretical concepts underlying passive film stability. Furthermore, it is expected that good correlations of threshold and corrosion potential can be used to deduce a threshold temperature. The threshold temperature would be the temperature at which the corrosion and threshold potentials are equivalent.

3.1.11.3 Stress Corrosion Cracking

Method A – Threshold Stress Intensity Factor at Pre-Existing Flaw
Method B – Threshold Stress In Initiation on Smooth Surface/Propagation by Slip – Dissolution Mechanism

Method B is preferred for stress corrosion cracking since it is believed to be the more conservative model, and since it has been used for predicting the performance of TSWRs, and since a wealth of data exists for stainless steel, a material more prone to SCC than Alloy 22. In prediction based upon a correlation for stainless steel would yield a conservative prediction for Alloy 22.

Weld Stress Mitigation

Method A – Induction Annealing
Method B – Laser Peening

In regard to stress mitigation, Method A is preferred for any external lid on the Alloy 22 WPOB. This selection is based upon the ability of the induction annealing process to place compressive stress deeper into the weld. Method B, laser peening will be used on any internal lid weld, due to the occluded nature of such a weld.

3.1.11.4 Hydrogen Induced Cracking – Titanium

Method A – Threshold Electrochemical Potential
Method B – Threshold Hydrogen Concentration

Hydrogen induced cracking evaluation is based upon a threshold hydrogen concentration. Since such concentrations are possible to measure with secondary iron mass spectrometry, method B is therefore preferred. Further, the drip shield design avoids any galvanic couple that would lead to the possibility of hydrogen induced cracking via Method A, the threshold electrochemical potential method.

A simple and conservative model has been developed to evaluate the effects of hydrogen-induced cracking on the drip shield. The basic premise of the model is that failure will occur once the hydrogen content exceeds a certain limit or critical value (H_c). This model is very conservative because it assumes that, once the environmental and material conditions can support that particular corrosion process, failure will be effectively instantaneous. Extensive evidence has been provided to support a qualitative assessment of Titanium Grade 7 as an excellent choice of material for the drip shield with regard to degradation caused by hydrogen-induced cracking (CRWMS M&O 2000h).

Quantitative evaluation based on the hydrogen induced cracking model described in the corresponding AMR indicates that the drip shield material (Titanium Grade 7) is able to sustain the effects of hydrogen-induced cracking. Available test data show that the hydrogen concentration is below 180 μg per gram, which is less than the critical hydrogen concentration of 400 μg per gram for Titanium Grade 7.

3.2 INTEGRATED MODEL

The WAPDEG software was used to develop and implement the integrated model for waste package and drip shield degradation analysis and to perform the degradation simulations. WAPDEG version 4.0 is an appropriate tool for this application, because it was specifically designed to analyze drip shield and waste package degradation profiles in a manner consistent with the information requirements for implementation in the total system performance assessment (TSPA) model. WAPDEG version 4.0 was used within the range of values for which it is being validated (CRWMS M&O 2000g).

3.2.1 Conceptual Model for the Integrated Model

This section discusses the conceptual model for the integrated model for waste package and drip shield degradation analysis in TSPA-SR. More detailed descriptions of the conceptual model are given in the companion AMR (CRWMS M&O 2000g – *WAPDEG Analysis of Waste Package and Drip Shield Degradation*). In the TSPA-SR analysis, WAPDEG models various types of corrosion mechanisms that may occur on a waste package and drip shield as a function of the exposure time and conditions. [For a convenience of discussion in this section, drip shield is considered as an integral part of waste package. Except where it is necessary, no separate discussion is given for drip shield.] In the nominal case analysis of TSPA-SR, the waste package outer barrier (WPOB) and drip shield (DS) were included in the waste package degradation analysis. Because the stainless-steel inner container, which is to provide structural support to waste package, is not expected to provide any substantial time-period for the waste containment performance after an initial breach (or failure) of the outer barrier, it was not included in the degradation analysis. Although, in reality, it would provide some performance for waste containment after the outer barrier breach and also as a barrier to radionuclide transport after the waste package breach, the potential performance credit was ignored in the nominal TSPA-SR analysis. This is a conservative approach.

In the analysis the humid-air corrosion condition is defined as an exposure condition for which the RH at the waste package surface is equal to or greater than the threshold RH in the absence of drips. The aqueous corrosion condition requires the presence of drips. The corrosion and other degradation processes and their models and parameters that have been incorporated into the TSPA-SR waste package degradation analysis are described below.

- Threshold relative humidity (RH) for corrosion initiation. The threshold RH is based on the deliquescence point of $NaNO_3$ salt and a function of temperature (see Section 3.1.3). The same threshold RH is used for both the dripping and non-dripping cases. It is assumed that stable water that can support electrochemical reactions of corrosion forms if RH is equal to or greater than the threshold RH.

- Humid-air and aqueous general corrosion rate of waste package outer barrier. The same general corrosion rate is used both for humid-air general corrosion and aqueous general corrosion (i.e., in the presence of drips).

- Humid-air and aqueous general corrosion rate of drip shield. The same general corrosion rate is used both for humid-air general corrosion and aqueous general corrosion (i.e., in the presence of drips).

- Localized corrosion (pitting and crevice corrosion) initiation threshold for waste package outer barrier. The initiation threshold is based on the corrosion potential (E_{corr}) and threshold corrosion potential (E_{th}) as a function of the contacting solution pH. If $E_{corr} \geq E_{th}$, localized corrosion initiates. Localized corrosion also requires the presence of drips. Localized corrosion ceases when the exposure condition changes to such a way that E_{corr} becomes less than E_{th}.

- Localized corrosion (pitting and crevice corrosion) penetration rate for waste package outer barrier.

- Localized corrosion (pitting and crevice corrosion) initiation threshold for drip shield. The initiation threshold is based on the corrosion potential (E_{corr}) and threshold corrosion potential (E_{th}) as a function of the contacting solution pH. If $E_{corr} \geq E_{th}$, localized corrosion initiates. Localized corrosion also requires the presence of drips. Localized corrosion ceases when the exposure condition changes to such a way that E_{corr} becomes less than E_{th}.

- Localized corrosion (pitting and crevice corrosion) penetration rate for drip shield.

- The hoop stress and corresponding radial-crack stress intensity factor versus depth in the outer and middle closure-lid welds of waste package outer barrier, incorporating their uncertainty and variability (see Section 3.2.2.3).

- Two alternative models for SCC: the Slip Dissolution Model and Threshold Stress Intensity Factor (K_{ISCC}) Model.

- Probability of occurrence and size of manufacturing defects in waste package outer barrier closure-lid welds and its effect on SCC.

- Threshold RH for the initiation of microbiologically influenced corrosion (MIC) of waste package outer barrier and the enhancement factor (uniform distribution between 1 and 2) to the general corrosion rate due to MIC. The drip shield is assumed not subject to MIC.

- The enhancement factor (uniform distribution between 1 and 2.5) to the general corrosion rate for long-term aging and phase instability of waste package outer barrier. The drip shield is assumed not subject to the thermal aging.

- Radiolysis enhanced corrosion of waste package outer barrier and drip shield. It was concluded that waste package and drip shield are not subject to radiolysis enhanced corrosion under the repository conditions.

- Rockfall induced mechanical damage to drip shield and its effect on the corrosion. The rockfall effect is assumed insignificant because of the presence of backfill over the drip shield.

- Both the upper and under sides of drip shield were assumed subject to corrosion if the initiation threshold is met, that is, the RH on the drip shield being equal to or greater than the threshold RH. This is because the both sides are exposed to the exposure conditions in the emplacement drift.

- Inside-out corrosion of waste package after breach. When waste package fails, the waste package degradation analysis also considers corrosion degradation of the waste package from the inside-out corrosion. The inside-out corrosion analysis includes general

corrosion and localized corrosion of the waste-package outer barrier. The inside-out corrosion would cause penetrations by general and localized corrosion in addition to those by the outside-in corrosion only. The inside-out general corrosion is assumed to initiate at the time of the waste package failure. Like the outside-in localized corrosion, initiation of the inside-out localized corrosion is based on the corrosion potential and threshold corrosion potential, which are a function of the pH of water inside the breached waste package. The in-package water chemistry results from degradation of the waste form and other internal materials (such as basket materials).

The drip shield was assumed not subject to SCC because it will be fully annealed before it is placed in the emplacement drift. Likewise, all the fabrication welds in the waste container, except the welds for the closure lids, were assumed fully annealed and thus not subject to SCC. Therefore, only the closure-lid welds were considered in the SCC analysis. It was assumed that SCC is operative on the closure-lid welds if the RH of the waste package surface is greater than the threshold RH. The bounding analyses have shown that the hydrogen uptake by the drip shield is much less than the threshold hydrogen concentration to cause hydrogen induced cracking (HIC) under the repository exposure condition (CRWMS M&O 2000h), and thus the HIC was not included in the drip shield degradation analysis. The drip shield was assumed not subject to microbiologically influenced corrosion (MIC) under the repository exposure condition (CRWMS M&O 2000d).

As discussed in detail in Section 3.1.7, a dual closure-lid design has been proposed for the closure-end of waste package outer barrier—one Alloy 22 lid on one end of the outer barrier and two Alloy 22 lids on the closure end of the outer barrier. This dual-lid design is to mitigate potential premature failure of waste packages by SCC. A schematic in Figure 3-66 illustrates the dual closure-lid design. The dual closure-lids are referred to as the outer-lid and inner-lid, respectively, in this section. The outer lid is 25-mm thick and the inner lid is 10-mm thick. There is a physical gap between the two lids. Thus, any SCC cracks penetrating the outer closure-lid stop at the gap between the closure lids. Then the inner closure-lid welds are considered for the SCC crack initiation and growth.

The exposure conditions that were included in the TSPA-SR waste-package degradation analyses are temperature and relative humidity at the waste package and drip shield surface, in-drift water dripping, and pH of the water contacting waste package and drip shield. The temperature and relative humidity histories at the waste package and drip shield surface are provided from the thermal-hydrologic model abstraction. The evolution of the geochemical conditions inside the emplacement drift is provided from the near-field geochemical environment model abstraction.

In the analysis, the waste package surface RH is tested against the threshold RH (RH_{th}) for corrosion initiation of the drip shield (DS) and waste package outer barrier (WPOB). When the surface RH becomes greater than the threshold RH, the waste package and drip shield could undergo different corrosion degradation modes depending on whether it is dripped on or not.

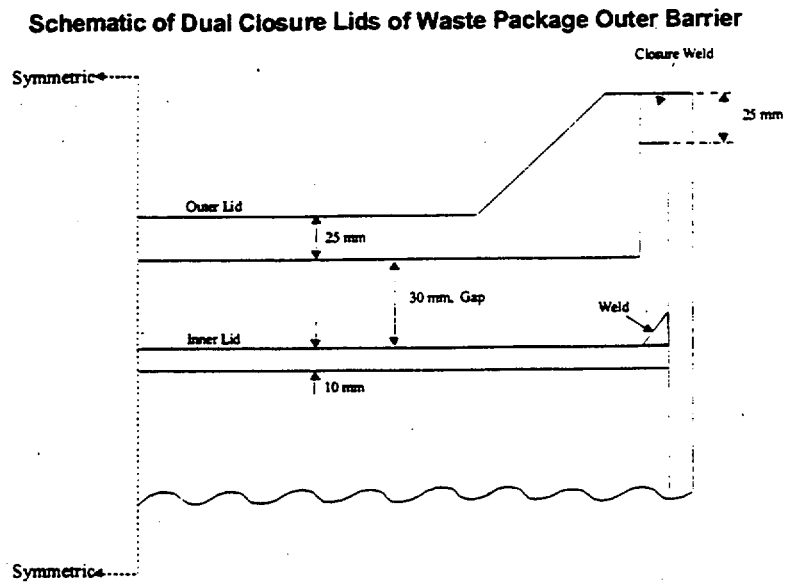

Figure 3-66. A Schematic of the Dual Closure-Lid Design of Waste Package Outer Barrier

For waste packages that are not dripped on, the waste package outer barrier (and drip shield) undergoes humid-air corrosion. Under humid-air conditions, the waste package outer barrier (and drip shield) undergoes general corrosion all the time and fails eventually by gradual thinning. The general corrosion rates of the waste package outer barrier (and drip shield) are very low.

For waste package and drip shield that are dripped on, the wetted area of the drip shield and waste package by drips was assumed to undergo aqueous corrosion if the RH at the surface is greater than the threshold RH. For the dripping conditions the waste package was assumed to undergo humid-air conditions while the drip shield was functioning. General corrosion occurs all the time under aqueous corrosion condition. Initiation of localized (pitting and crevice corrosion) corrosion is dependent on the local exposure environment on the wetted patches. In the current analysis, localized corrosion of the drip shield and waste package outer barrier is assumed to initiate only under dripping conditions. This is because of the necessary presence of aggressive ions (such as chloride) in order to initiate and sustain pit and crevice growth and because the only mechanism for these ions to gain ingress to the drift is through drips. Localized corrosion for a drip shield patch is assumed to initiate if the corrosion potential (E_{corr}) is greater than or equal to the threshold corrosion potential (E_{th}). After initiated, localized corrosion continues while $E_{corr} \geq E_{th}$. When E_{corr} becomes less than E_{th}, localized corrosion stops.

After failure of the drip shield, the waste package was assumed to be subject to dripping. The area of the waste package surface wetted by drips would depend on the penetration opening location, size and number in the drip shield. Thus, only the waste package surface that is directly underneath the failed patches in the drip shield would get wetted by drips. As additional patches fail in the drip shield, more water could potentially contact the waste package. As with the drip shield, localized corrosion for a waste-package outer-barrier patch was assumed to initiate if the

corrosion potential (E_{corr}) is greater than or equal to the threshold corrosion potential (E_{th}). After initiated, localized corrosion continues while $E_{corr} \geq E_{th}$. If E_{corr} becomes less than E_{th}, localized corrosion stops. Note that, as discussed previously, SCC of the waste package closure-lid welds was assumed operative as long as the RH is greater than the threshold RH regardless of whether it is dripped on or not.

The WAPDEG analysis tracks down corrosion degradation of waste packages for three types of penetration modes: crack penetration by SCC, pit and crevice penetration by localized corrosion, and patch penetration by general corrosion. The analysis provides, as output, the cumulative probability of waste package failure by one of the three penetration modes as a function of time, and the number of penetrations for each of the penetration modes as a function of time. The waste package failure time and penetration number profiles are used as input to other TSPA analyses such as waste form degradation and radionuclide release rate from waste packages.

3.2.2 Abstraction of General Corrosion Models for Waste Package Outer Barrier and Drip Shield

This section discusses the approaches and assumptions used in the abstraction of general corrosion models for waste package outer barrier (WPOB) and drip shield (DS), and the abstraction results.

3.2.2.1 Approaches and Assumptions

The model abstractions are to develop two cumulative distribution functions (CDFs) each one representing the GC rate distribution for the WPOB (Alloy 22) and the other for the DS (Titanium Grade 7). For each alloy, the weight loss and crevice sample penetration rate data were combined to yield one GC rate data set for each alloy. The GC rate data were then sorted in ascending order. Any negative GC rates were then deleted from the data set as suggested in Section 3.1.5. Cumulative probabilities were assigned to each GC data point based on its rank (position) in the sorted data set yielding a CDF. The units of the GC rates were converted from nm per year (reported in Section 3.1.5) to mm per year. For the waste package outer barrier, as the variance in the data is reduced with the exposure time (see Section 3.1.5), only the 2-year data were used in the model abstraction (i.e., the 6-month and 12-month data were not included). For the drip shield a combined set of the 6-month and 12-month data were used in the model abstraction. An upper bound (corresponding to the 100th percentile cumulative probability) was also applied to the resulting GC rate CDFs. The upper bound was 7.30E-5 mm/year for Alloy 22 (see the assumption below) and 3.25E-4 mm/year for Titanium Grade 7 (see the assumption below). Details of the abstraction approaches are described in CRWMS M&O (2000i).

A set of assumptions were employed in the model abstraction. Key assumptions are described below.

- For both alloys considered (Alloy 22 and Titanium Grade 7), corrosion penetration rate data from the weight loss of both plain and creviced geometry test coupons were considered to represent GC penetration rates.

- The maximum GC rate for Alloy 22 was set to 7.30E-5 mm/year. This assumed upper bound is greater than the maximum penetration rate of 7.25E-5 mm/year observed in the LTCTF (Section 3.1.5).

- The maximum GC rate of Titanium Grade 7 was set to 3.25E-4 mm/year. This assumed upper bound is greater than the maximum penetration rate of 3.19E-4 mm/year observed in the LTCTF (Section 3.1.5).

- The Gaussian Variance Partitioning (CRWMS M&O 1998, TSPA-VA Technical Basis Document Chapter 5, Section 5.7.2) is an adequate method to separate uncertainty and variability from a distribution that represents the combination of the both.

Detailed discussion of the assumptions employed in the model abstraction is given in CRWMS M&O (2000i).

3.2.2.2 General Corrosion Model for Waste Package Outer Barrier

The original CDF for the GC rate for WPOB is shown in Figure 3-67. The CDF is considered a mix of uncertainty and variability of the GC rate. However, quantification of uncertainty and variability in the corrosion rate measurements is very limited because the corrosion rates are extremely low and considered to be within the measurement noise. Because of this, it is highly uncertain what the fraction of the total variance in the parent CDF represents the uncertainty and what fraction represents the variability. In the waste package degradation analysis the fraction for the split of the uncertainty and variability from the parent CDF is treated as an uncertain parameter (CRWMS M&O 2000g). Figure 3-67 also shows, along with the original CDF, the resulting variability CDFs for GC rates using 25%-75%, 50%-50% and 75%-25% uncertainty and variability partitioning ratios, and 50th uncertainty percentile. Figures 3-68 and 3–69 show the resulting variability CDFs using 25th and 75th uncertainty percentile, respectively.

3.2.2.3 General Corrosion Model for Drip Shield

The resulting original CDF for the GC rate for DS is shown in Figure 3-70. As with the CDF for the WPOB GC rate, the CDF is considered a mix of uncertainty and variability of the GC rate. However, quantification of uncertainty and variability in the corrosion rate measurements is very limited because the corrosion rates are extremely low and considered within the measurement noise. Because of those it is highly uncertain what the fraction of the total variance in the parent CDF represents the uncertainty and what fraction represents the variability. In the waste package degradation analysis the fraction for the split of the uncertainty and variability from the parent CDF is treated as an uncertain parameter (CRWMS M&O 2000g). Figure 3-70 also shows, along with the original CDF, the resulting variability CDFs for GC rate using 25%-75%, 50%-50% and 75%-25% uncertainty and variability partitioning ratios, and the 50th uncertainty percentile. Figures 3-71 and 3-72 show the resulting variability CDFs using 25th and 75th uncertainty percentile respectively.

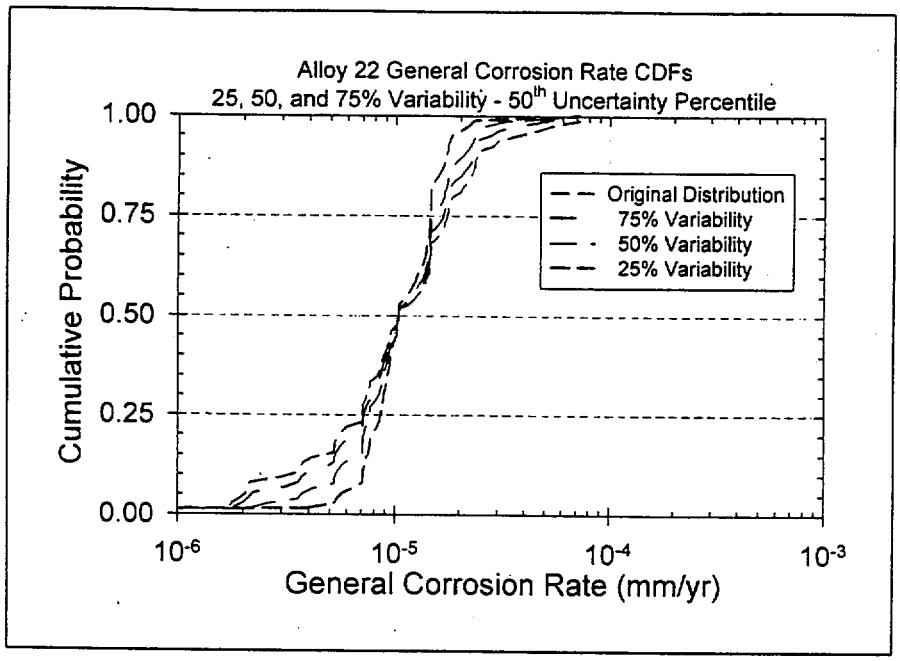

Figure 3-67. The Variability Cumulative Distribution Functions for the General Corrosion Rate of Waste Package Outer Barrier Using 25%-75%, 50%-50%, and 75%-25% Uncertainty and Variability Partitioning Ratios and 50th Uncertainty Percentile

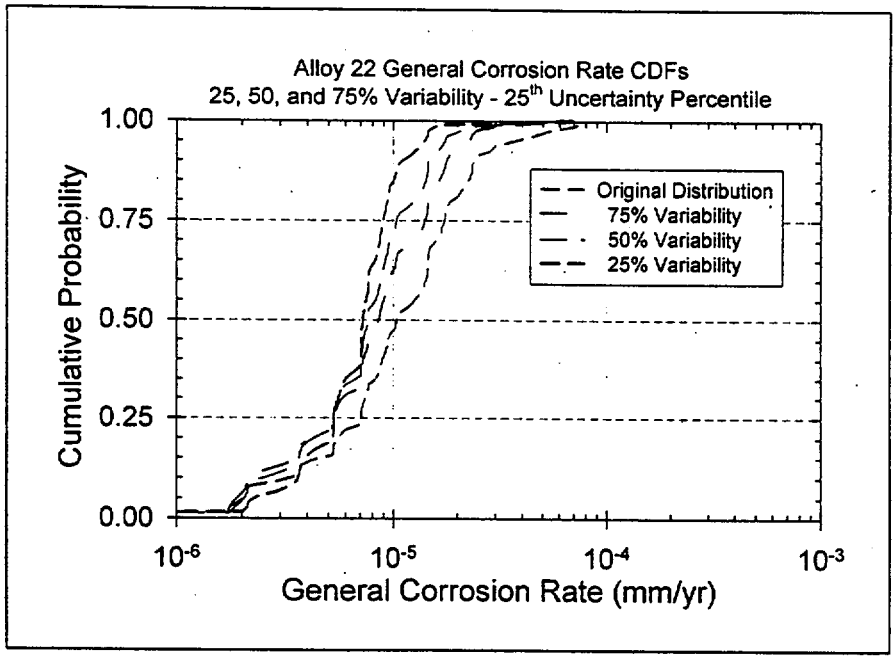

Figure 3-68. The Variability Cumulative Distribution Functions for the General Corrosion Rate of the Alloy 22 Waste Package Outer Barrier Using 25%-75%, 50%-50%, and 75%-25% Uncertainty and Variability Partitioning Ratios and 25th Uncertainty Percentile

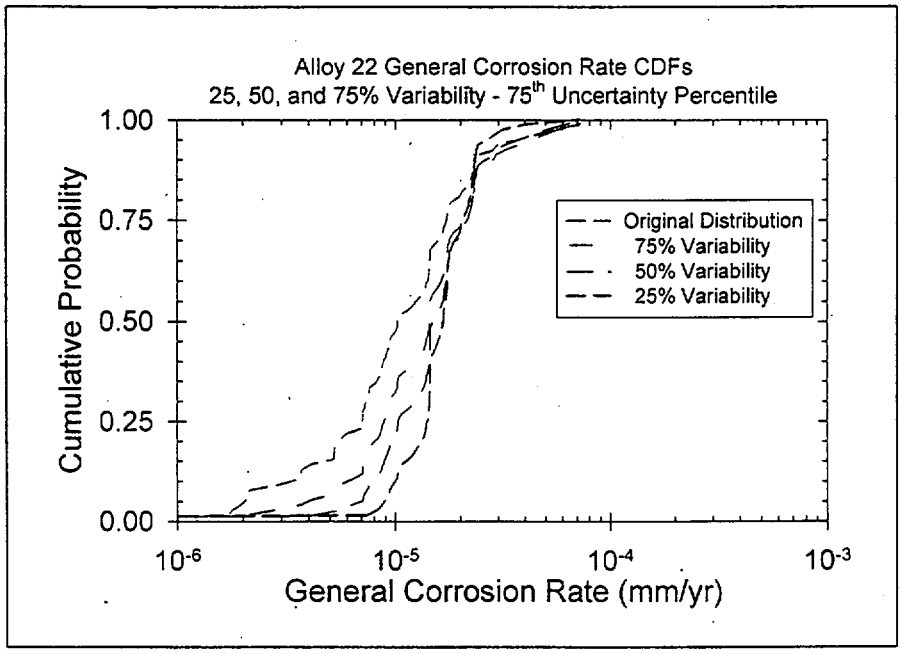

Figure 3-69. The Variability Cumulative Distribution Functions for the General Corrosion Rate of the Alloy 22 Waste Package Outer Barrier Using 25%-75%, 50%-50%, and 75%-25% Uncertainty and Variability Partitioning Ratios and 75th Uncertainty Percentile

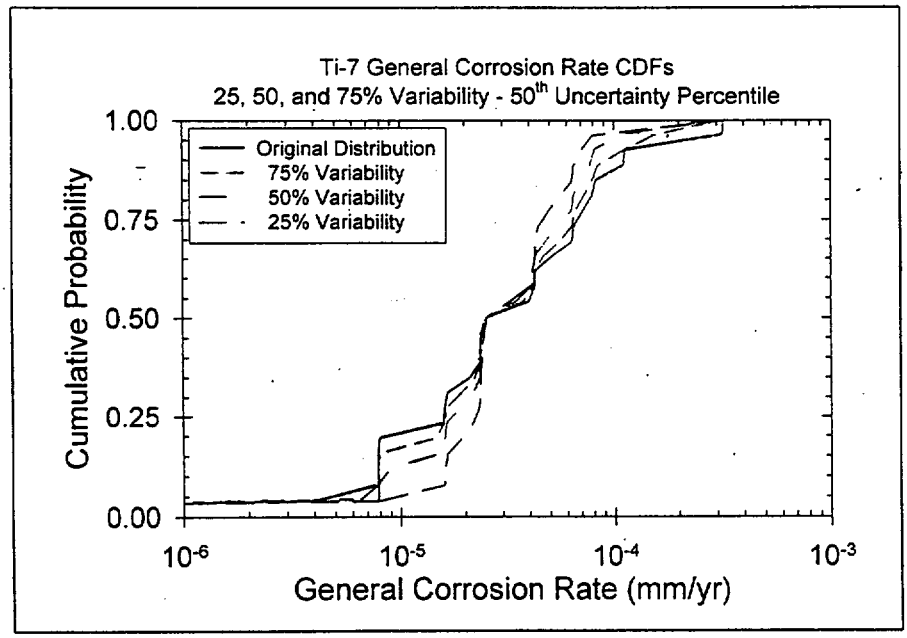

Figure 3-70. The Variability Cumulative Distribution Functions for the General Corrosion Rate of the Ti-7 Drip Shield Using 25%-75%, 50%-50%, and 75%-25% Uncertainty and Variability Partitioning Ratios and 50th Uncertainty Percentile

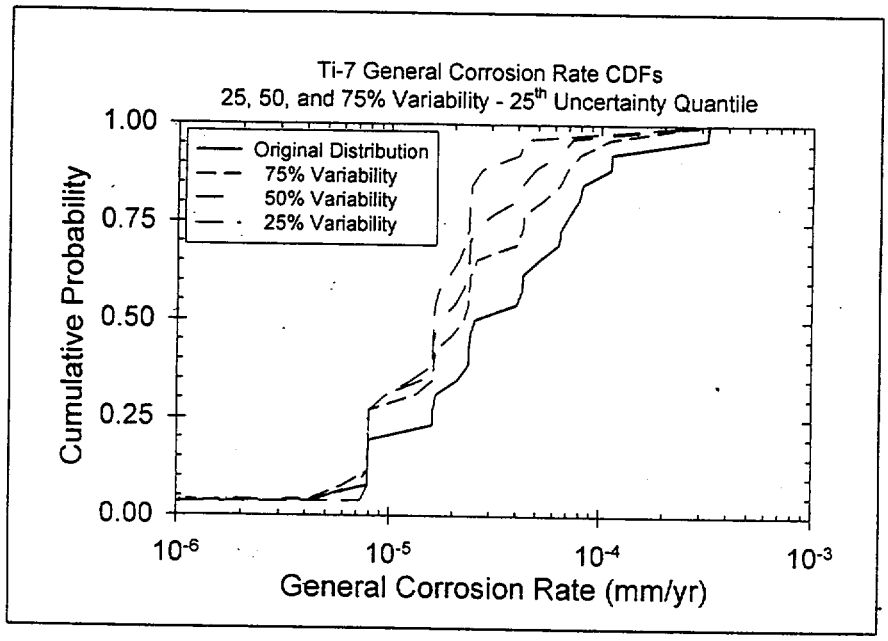

Figure 3-71. The Variability Cumulative Distribution Functions for the General Corrosion Rate of Ti-7 Drip Shield Using 25%-75%, 50%-50%, and 75%-25% Uncertainty and Variability Partitioning Ratios and 25th Uncertainty Percentile

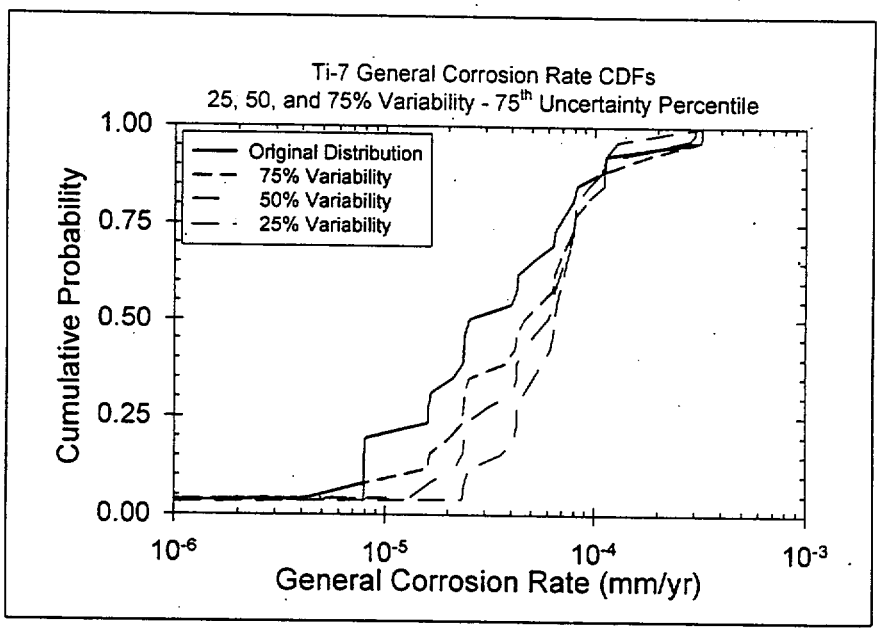

Figure 3-72. The Variability Cumulative Probability Distribution Functions for the General Corrosion Rate of Ti-7 Drip Shield Using 25%-75%, 50%-50%, and 75%-25% Uncertainty and Variability Partitioning Ratios and 75th Uncertainty Percentile

3.2.3 Abstraction for Manufacturing Defects in Waste Package Closure Welds

This section describes the approaches and assumptions employed in developing abstracted models for the probability and size of manufacturing defects in the waste package closure-lid welds. The abstraction results and their implementation in the waste package degradation (SCC) analysis are discussed in this section.

3.2.3.1 Approaches and Assumptions

The analyses are to develop abstracted models representing the frequency of occurrence and size of defects potentially found in waste package closure-lid welds. Flaw density and flaw size distributions are obtained from other analyses (see Section 3.1.2; CRWMS M&O 2000m). The flaw density is used as the parameter for a Poisson distribution used to represent the frequency of occurrence of flaws in a given length of closure weld. The flaw sizes are given as a probability density function on each closure-lid weld.

Major assumptions employed in the abstraction are described below. Further details of the assumptions used in the abstraction analyses are discussed in CRWMS M&O 2000k.

- Only surface breaking flaws are considered, since these are the types of flaws that may potentially lead to SCC.
- Flaws occur randomly as represented by a Poisson distribution.
- The mean flaw density (Poisson distribution parameter) of the closure weld is from CRWMS M&O 2000m (0.6839 flaws/meter of one-inch thick weld).
- The fraction of surface breaking flaws is uniformly distributed between the minimum (0.13%) and maximum (0.49%) fractions used to determine the average fraction quoted in CRWMS M&O 2000m. The use of the uniform distribution is a reasonable representation of the uncertainty in expressing this value.
- Pre-inspection flaw sizes are log-normally distributed, with distribution parameters (dependent on the weld thickness) as given in CRWMS M&O 2000m.
- The probability of non-detection is given as a function of flaw size as provided in CRWMS M&O 2000m. The model is dependent on the detection threshold (p), the location parameter (b), and the scale parameter (υ). The location parameter (b) and the scale parameter (υ) are taken to be uncertain with a uniform distribution. The ranges for these distributions are determined from the values identified in the literature as quoted in CRWMS M&O 2000m. This is reasonable, as the manufacturing and detection processes for welds on the waste container are not specified to date. The best that may be modeled at this time are values based on similar industrial manufacturing practices as reported in CRWMS M&O 2000m.
- Results of the residual stress analyses for the closure-lid welds have indicated that the hoop stress (and the radial crack driven by the hoop stress) is the dominant stress that

could lead to SCC through-wall cracks in the closure-lid weld (CRWMS M&O 2000f). As a conservative approach, all the surface-breaking manufacturing defects are considered radial cracks and assumed to have a semi-circular shape.

3.2.3.2 Abstraction Results for the Probability and Size of Defect Flaws

Initial (pre-inspection) mean flaw densities and flaw sizes used in the analyses for this calculation were from CRWMS M&O 2000m. Calculation of the outer surface-breaking mean flaw density begins with the base mean flaw density of 0.6839 flaws/meter of weld for a one inch thick stainless steel Tungsten Inert Gas weld (this density was measured from an actual weld performed under shop conditions) subject to radiographic (RT) and dye-penetrant (PT) tests (CRWMS M&O 2000m). To convert this value to a flaw density for an uninspected weld, the base flaw density is increased by the sum of the flaw reduction factors provided for the RT and PT tests. The adjustment for the RT exam increases the total flaw density by a factor of 12.8 while the PT exam, which detects only surface-breaking flaws, increases the density of only the surface-breaking flaws by a factor of 31.4 (CRWMS M&O 2000m). Next the effect of weld thickness on flaw density is used to adjust for the actual weld thickness on the closure weld. For the 25-mm thick closure weld, the flaw reduction factor (R) is 97.3% (865 divided by 889) (CRWMS M&O 2000m). Multiplying this result by this circumference of the closure-lid weld results in the flaw density per closure weld (or per waste package). A final multiplication by the fraction of surface breaking flaws results in the final mean flaw density of surface breaking flaws per waste-package closure weld.

The resulting cumulative probability for defect flaws for the outer (25-mm thick) and inner (10-mm thick) closure-lid welds are shown in Figure 3-73. Each of the cumulative probabilities in the figure is from 100 realizations with random sampling of the location parameter (b) and the scale parameter (υ)and represent the actual defect probability used in the waste package SCC analysis (CRWMS M&O 2000g). Figure 3-74 shows several probability density functions for defect sizes in the closure lid welds for various combinations of values for the location parameter (b) and the scale parameter (υ). The same probability density functions are used for both the outer and inner lid welds.

3.2.3.3 Implementation of Closure Weld Flaw Abstraction Results in Waste Package Degradation Analysis

The number of flaws that appear on a patch is sampled stochastically as a Poisson random variable. For each flaw that occurs, a flaw size is randomly assigned to it by sampling from the calculated flaw size cumulative distribution function. This flaw's location and size are then used in the SCC analysis. The abstracted results are then input to the waste package degradation model (WAPDEG) to analyze its effect on waste package performance (CRWMS M&O 2000g).

The approach used in this abstraction is that, as these distributions accommodate the variability observed in the occurrence, frequency and size of flaws, some of the parameters that determine these distributions need to be treated as uncertain. The instances of where uncertainty is included are for: 1) the flaw detection distributions (parameters b and ν) and 2) the fraction of surface breaking flaws. The parameters are treated as follows. The b and ν parameters of the detection distribution are allowed to uniformly range between 1.6 to 5 mm and 1 to 3,

respectively. The fraction of surface breaking flaws in CRWMS M&O 2000m is the average of three observations (0.13%, 0.40%, and 0.49%) and is 0.34%. Instead of using the average value of 0.34%, the parameter should be allowed to uniformly range from 0.13 to 0.49%. The model parameters are varied independently. Sensitivity analyses with the proposed distributions of the model parameters are needed to analyze the affect of not knowing the correct (deterministic) value of the parameters.

3.2.4 Abstraction of Stress and Stress Intensity Factor Profile in Waste Package Closure Welds

This section discusses the approaches and assumptions used to develop abstracted models for stress and stress intensity factor profiles as a function of depth in the closure-lid welds of waste package outer barrier (WPOB). The resulting abstracted models represent uncertainty and variability of the profiles and used as input to the SCC analysis in the closure lid welds using the integrated waste package degradation model (WAPDEG).

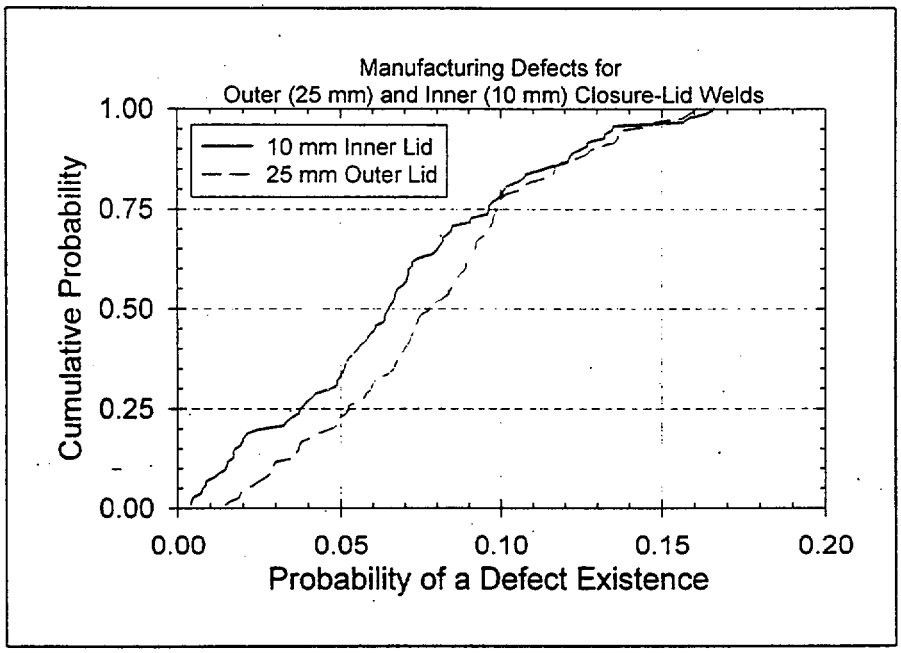

Figure 3-73. Cumulative Probability for the Occurrence of Defects in the Welds of the Outer (25-mm thick) and Inner (10-mm thick) Lids of Waste Package Outer Barrier

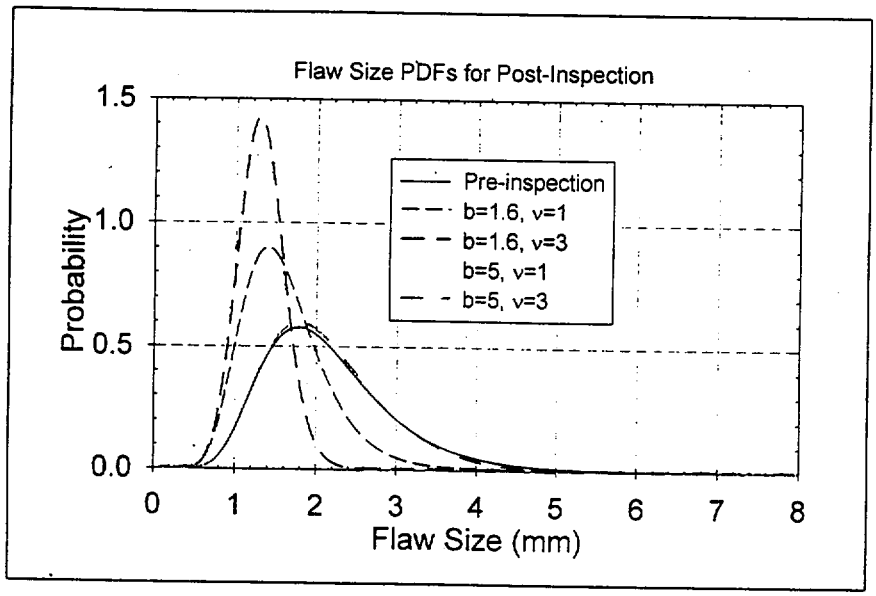

Figure 3-74. Conditional Probability Density Functions of Defect Sizes in the Closure Lid Welds for Various Combinations of Values for the Location and Scale Parameters (*b* & *v*)

3.2.4.1 Approaches and Assumptions used in Abstraction

The WPOB has dual closure lids (referred to as outer (25-mm thick) and inner lid (10-mm thick) respectively). The process model analyses calculated the stress and stress intensity factor profiles along the circumference of the welds for each of the closure lids (CRWMS M&O 2000f). The results were analyzed to develop abstracted models to represent uncertainty and variability of the profiles in the closure-lid welds. In addition, the abstraction was to present the profiles in a format that is suitable for implementation in the integrated waste package degradation model (WAPDEG). Details of the abstraction approaches are discussed elsewhere (CRWMS M&O 2000j).

Major assumptions employed in the abstraction development are described below.

- The hoop stress (and the corresponding stress intensity factor for radial crack) is the prevailing stress in the closure-lid welds that could lead to SCC through-wall cracks in the closure-lid weld of waste packages. Thus, the current abstraction is limited to the profiles for the hoop stress and corresponding stress intensity factor for radial crack.

- The hoop stress (and corresponding stress intensity factor profiles for radial crack) in the inner lid welds are for a plane that is inclined at about 37 degrees from a plane normal to the outer surface of the inner lid. Because the SCC analysis in the integrated waste package degradation (WAPDEG) model assumes that cracks propagate normal to the lid surface, the profiles were projected to a plane normal to the outer surface of the lid. The crack orientation used in the abstraction is in the radial direction, which is normal to the hoop stress. As discussed above, the radial crack is considered in the abstraction because the hoop stress was found to be the dominant stress in the closure-lid welds. The hoop

stress is likely to be close to the first principal (or maximum) stress. It is assumed the SCC analysis with the projected profiles properly represents the hoop stress and stress intensity factor profiles for the inclined plane.

- The hoop stress and corresponding stress intensity factor profiles as a function of depth in the closure lid welds from the process model analyses (CRWMS M&O 2000f) represent the mean profiles.

- The uncertainties in the hoop stress and corresponding stress intensity factor profiles are represented with normal distribution, and the uncertainty range is bounded within three standard deviations (± 3 s.d.'s) around the mean profiles.

- The hoop stress and stress intensity factor profiles vary along the circumference of the closure lid welds, and those represent the variability in the profiles on a given waste package. It is assumed that the same degree of the profile variability is applied equally to all the waste packages in the repository, and there is no variability in the profiles among waste packages.

- As a crack propagates in the closure lid welds or the weld is thinned by general corrosion, the residual stresses in the welds may re-distribute in such a way that the SCC initiation and crack growth are mitigated (CRWMS M&O 2000f). Such stress re-distribution or relaxation is not considered in the current abstraction. This is a conservative approach.

3.2.4.2 Abstraction Results for Stress and Stress Intensity Factor Profiles

The abstraction results for the uncertainty range of the hoop stress as a function of depth in the outer closure lid welds (25-mm thick) are given in Figure 3-75. The stress profiles are at a reference location (0° angle) on the circumference of the lid welds. As will be shown later in Figure 3-77, the reference location on the lid weld circumference was selected in such a way that it has the highest hoop stress. The figure shows that the hoop stress in the outer lid welds is compressive at the surface and becomes tensile at a depth of about 8 mm. The uncertainty becomes larger with the weld depth. The corresponding stress intensity factor profiles as a function of radial crack depth are shown in Figure 3-76. The stress intensity factor is negative at the surface and becomes positive at a depth of about 12 mm, thus no SCC crack will initiate until the 12-mm thick layer is removed. As with the hoop stress, the uncertainty of the stress intensity factor increases with the weld depth. Figures 3-77 and 3-78 show respectively the hoop stress as a function of depth and the corresponding stress intensity factor as a function of radial crack depth, both at 0°, 90°, and 180° angle along the circumference of the outer-lid welds for a given waste package. The reference location designated at 0° angle has the largest hoop stress, and the location at 180° angle has the least hoop stress. As shown in the figures, the variability of the both profiles along the weld circumference in a waste package is minor.

The abstraction results for the uncertainty range of the hoop stress as a function of the projected depth in the inner closure lid welds (10-mm thick) are given in Figure 3-79. The stress profiles are at a reference location (0° angle) on the circumference of the lid welds. The hoop stress in the inner lid welds is compressive at the surface, transits to tensile state at a projected depth of

about 2 mm, and then back to compressive state at a projected depth of about 8.5-mm. The uncertainty in the profiles is larger for the tensile region in the weld depth. The corresponding stress intensity factor profiles as a function of the projected radial crack depth are shown in Figure 3-80. The stress intensity factor is negative at the surface and becomes positive at a projected depth of about 5 mm, thus no SCC crack will initiate until the (projected) 5-mm thick layer is removed. The uncertainty of the stress intensity factor increases slightly with the weld depth beyond the depth it becomes positive. Figures 3-81 and 3-82 show respectively the hoop stress as a function of the projected depth and the corresponding stress intensity factor as a function of the projected radial crack depth, both at 0°, 90°, and 180° angle along the circumference of the inner-lid welds for a given waste package. As shown in the figures, the variability of the both profiles along the weld circumference in a waste package is minor.

3.2.5 Nominal Case Analysis of Drip Shield and Waste Package Degradation

This section reports the nominal-case WAPDEG analysis results for the waste package and drip shield degradation. The WAPDEG model, an integrated model used for waste package and DS degradation analysis, is based on a stochastic simulation approach and provides a description of waste package degradation, which occurs as a function of time and repository location for specific design and thermal-hydrologic modeling assumptions. The corrosion modes that were included in the nominal case analysis are:

- Humid-air phase general corrosion of drip shield
- Aqueous phase general corrosion of drip shield
- Localized (pitting and crevice) corrosion of drip shield
- Humid-air phase general corrosion of waste package outer barrier
- Aqueous phase general corrosion of waste package outer barrier
- Localized (pitting and crevice) corrosion of waste package outer barrier
- Stress corrosion cracking of closure-lid welds of waste package outer barrier.

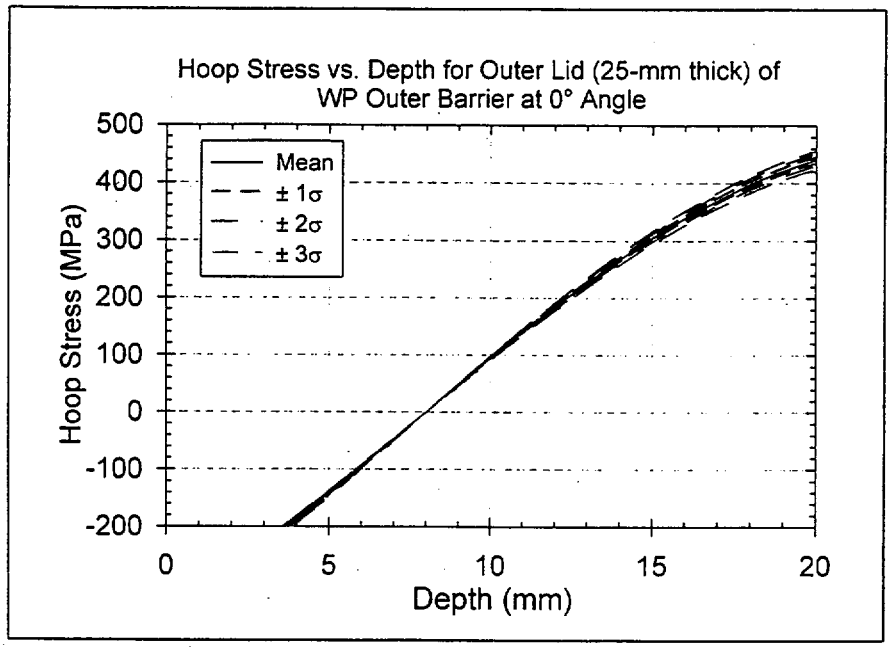

Figure 3-75. Hoop Stress as a Function of Depth in the Alloy 22 Outer-Lid Welds (25-mm thick) at the Reference Location on the Outer-Lid Weld Circumference and the Uncertainty Range

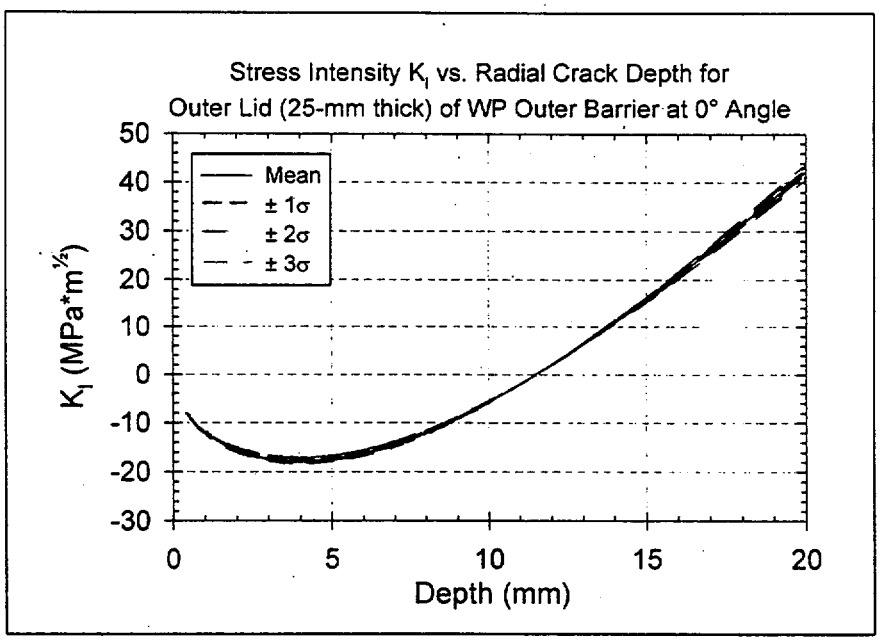

Figure 3-76. Stress Intensity Factor as a Function of Radial Crack in the Alloy 22 Outer-Lid Welds (25-mm thick) at the Reference Location on the Outer-Lid Weld Circumference and the Uncertainty Range

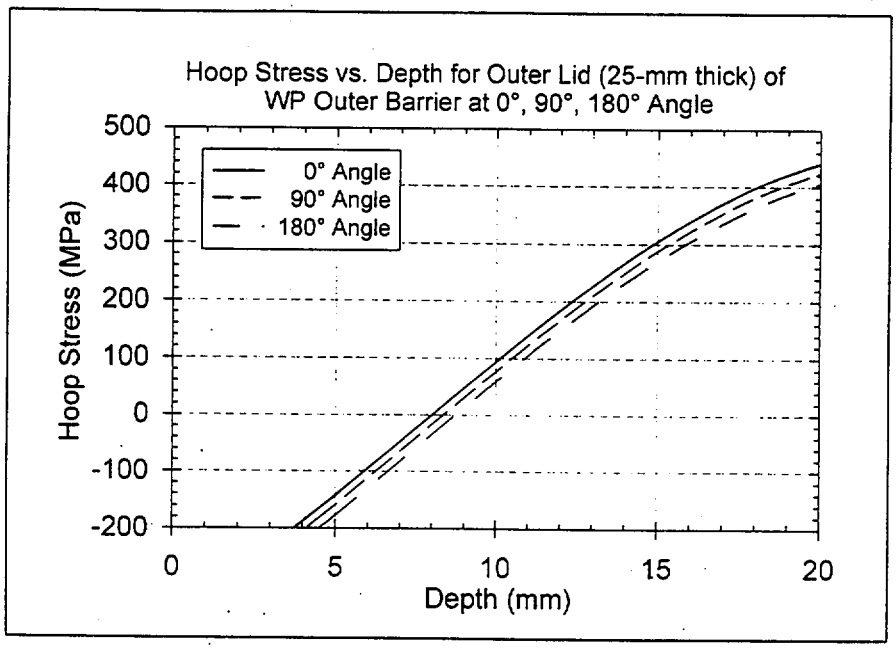

Figure 3-77. Hoop Stress as a Function of Depth in the Alloy 22 Outer-Lid Welds (25-mm thick) at 0°, 90° and 180° Angles Along the Circumference of the Outer-Lid Weld

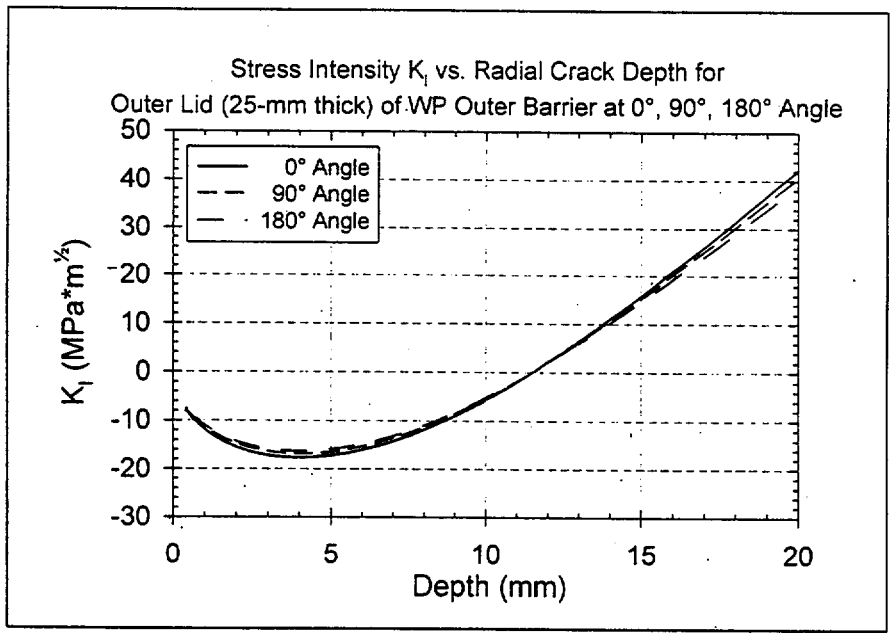

Figure 3-78. Stress Intensity Factor as a Function of Radial Crack in the Alloy 22 Outer-Lid Welds (25-mm thick) at 0°, 90° and 180° Angles Along the Outer-Lid Weld Circumference

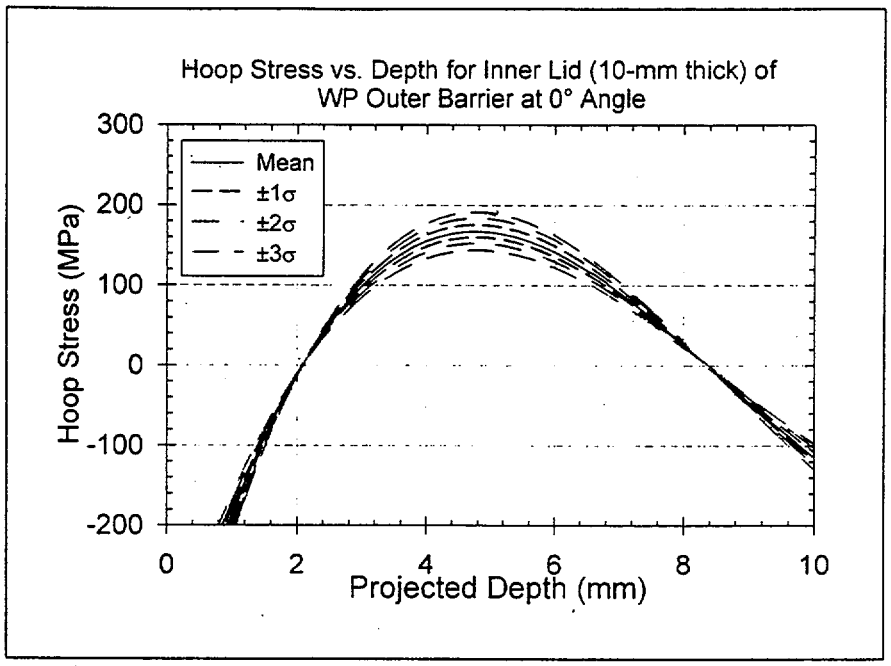

Figure 3-79. Hoop Stress as a Function of the Projected Depth in the Alloy 22 Inner-Lid Welds (10-mm thick) at the Reference Location on the Inner-Lid Weld Circumference and the Uncertainty Range

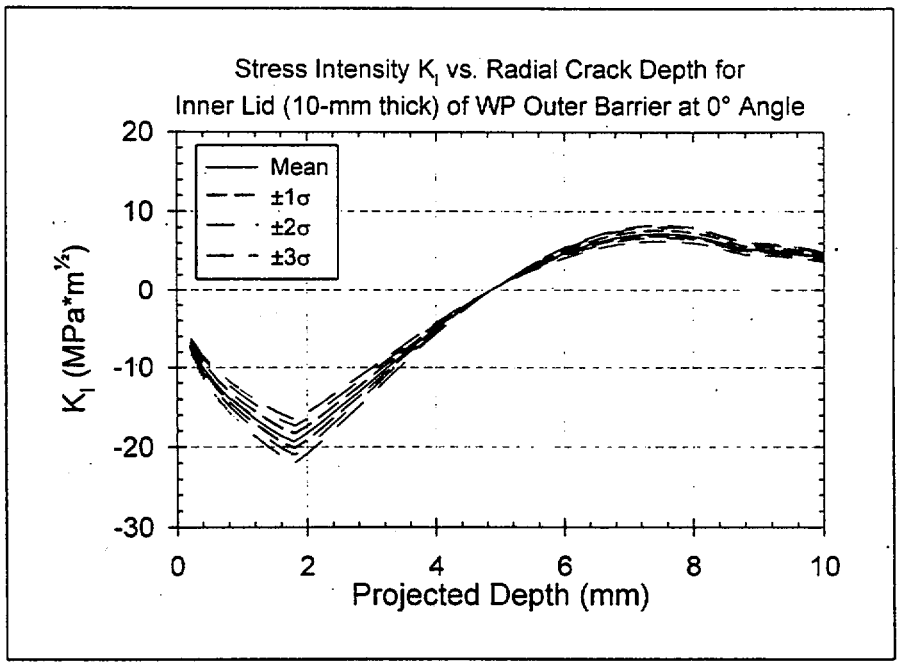

Figure 3-80. Stress Intensity Factor as a Function of the Projected Radial Crack Depth in the Alloy 22 Inner-Lid Welds (10-mm thick) at the Reference Location on the Inner-Lid Weld Circumference and the Uncertainty Range

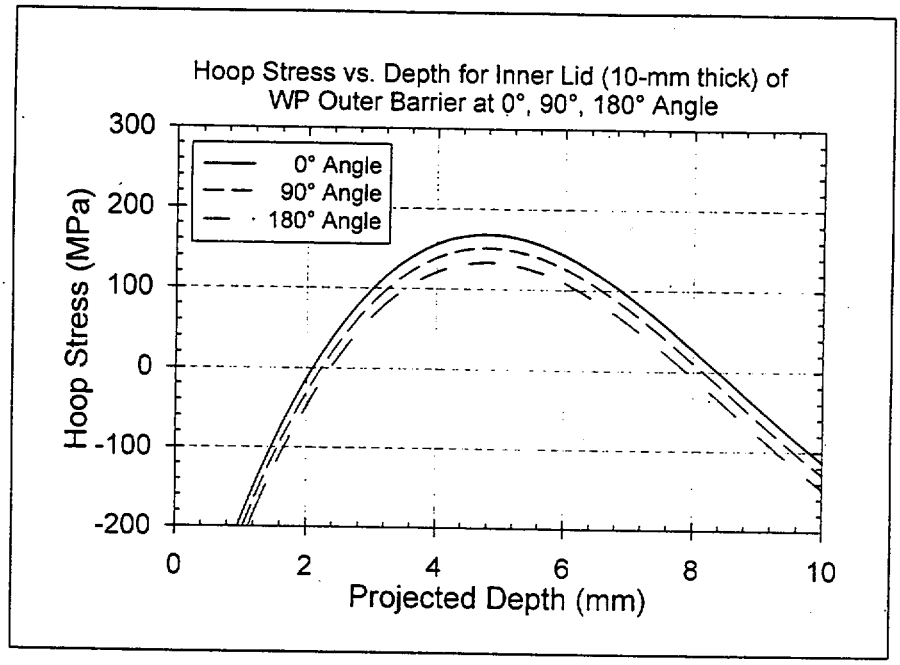

Figure 3-81. Hoop Stress as a Function of the Projected Depth in the Alloy 22 Inner-Lid Welds (10-mm thick) at 0°, 90° and 180° Angles Along the Circumference of the Inner-Lid Weld

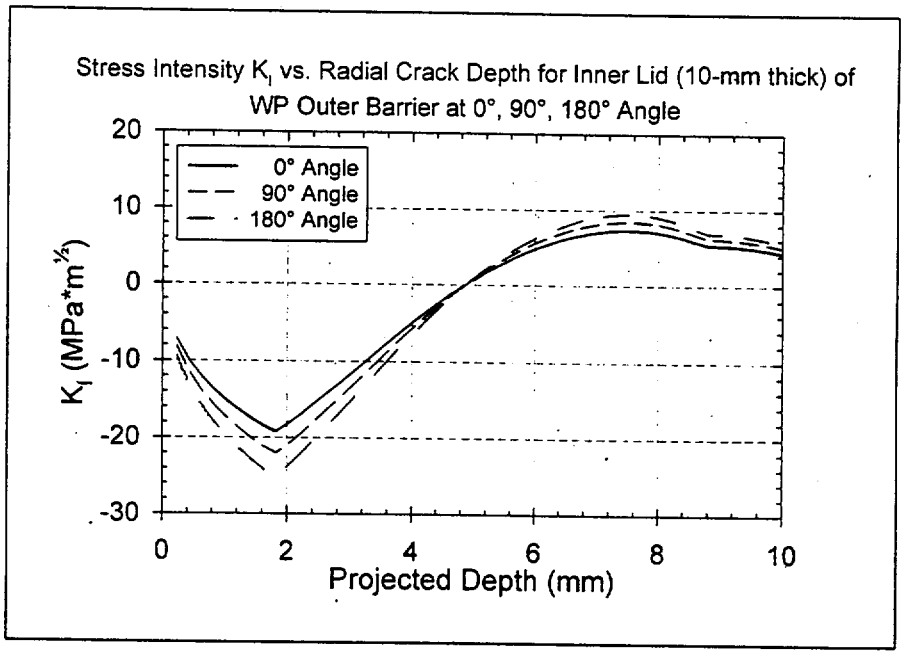

Figure 3-82. Stress Intensity Factor as a Function of the Projected Radial Crack Depth in the Alloy 22 Inner-Lid Welds (10-mm thick) at 0°, 90° and 180° Angles Along the Inner-Lid Weld Circumference

In addition, the following corrosion parameters were abstracted and included in the nominal case analysis:

- Relative humidity threshold for corrosion initiation of drip shield and waste package outer barrier
- Corrosion potential-based threshold for localized corrosion initiation of drip shield and waste package outer barrier
- Probability of the occurrence and size of manufacturing defects in closure-lid welds of waste package outer barrier
- Stress and stress intensity factor profiles in the closure-lid welds of waste package outer barrier incorporating stress mitigation techniques
- Threshold stress intensity factor (KISCC) for waste package outer barrier used with the threshold stress intensity factor model
- Threshold stress for the initiation of SCC crack growth for waste package outer barrier used with the slip dissolution model
- Corrosion enhancement factor for aging and phase instability of waste package outer barrier
- Corrosion enhancement factor for MIC of waste package outer barrier.

For the corrosion models and parameters for which data and analyses are available to quantify their uncertainty and variability, they were represented explicitly in the WAPDEG analysis. Variability in the degradation of the waste packages to be modeled is represented by allocating the total variances of the individual corrosion models and their parameters to waste package-to-waste package variability and to patch-to-patch variability within a single waste package. For other corrosion models and parameters that their uncertainty and variability are not quantifiable and that the variance in their value is considered representing a mix of the uncertainty and variability, the fraction of the total variance to separate each other was treated as an uncertain parameter and sampled randomly for each realization.

Because, except the RH threshold for corrosion initiation, temperature and RH do not affect waste package and DS degradation, a representative set of T and RH histories were used in the current analysis. Also, no separate analysis was conducted for different waste-type waste packages (i.e., commercial spent nuclear fuel waste packages, high-level waste waste-packages, etc.), which could give rise to varying thermo-hydrologic conditions to the DS and waste packages. In addition, the threshold for localized corrosion initiation of DS and waste package outer barrier that requires the presence of drips is much higher than the conditions expected in the repository. Other corrosion models are not dependent on dripping conditions (i.e., drip vs. no-drip). Therefore, no separate analyses were conducted for different dripping conditions. The stainless steel inner layer of waste package was not considered in the analysis. Details of the

approaches and assumptions associated with the analyses are described in the supporting report (CRWMS M&O 2000g).

In the Total System Performance Assessment-Site Recommendation analysis, waste package degradation was analyzed with multiple realizations of WAPDEG for the uncertainty analysis of the uncertain corrosion parameters—each WAPDEG realization corresponding to a complete WAPDEG run to represent the degradation variability for a given number of waste package and drip shield pairs. Accordingly, the WAPDEG analysis outputs are reported as a group of "curves" that represent the potential range of the output parameters. The nominal case analysis for waste package and DS degradation constitutes 100 realizations of WAPDEG simulation (or 100 WAPDEG runs) that uses 100 input vectors for uncertain corrosion model parameters and the simulation parameters that were sampled from their respective range. The major simulation parameters used in the analysis are summarized below:

- Temperature, relative humidity, and contacting solution pH histories in the presence of backfill
- 400 waste package and drip shield pairs
- 20-mm thick waste package outer barrier (Alloy 22)
- 15-mm thick drip shield (Titanium Grade 12)
- 1000 patches per waste package
- 500 patches per drip shield.

The WAPDEG analysis results (i.e., waste package and drip shield failure time and number of crack, pit and patch penetrations) are reported as a group of "degradation profile curves" that represent the potential range of the output parameters. The analysis results will be presented for the upper and lower bounds, median, and 95th, 75th, 25th and 5th percentiles as a function of time for the following output parameters:

- Waste package first breach (or failure)
- Drip shield first breach (or failure)
- Waste package first crack penetration
- Waste package first patch penetration.

Note that localized corrosion does not initiate for both the waste package (Alloy 22 outer barrier) and drip shield because the exposure conditions on the drip shield and waste package surface are not severe enough to initiate localized corrosion (i.e., the corrosion potential is less than the threshold corrosion potential) (see Section 3.1.6). Therefore no pit or crevice penetration is reported. Also note that the drip shield is assumed not subject to stress corrosion cracking, thus there is no crack penetration failure of drip shield. Thus, for drip shield, the first patch breach time profile is the same as the failure time profile.

Figure 3-83 shows the upper and lower bounds, median, and 95th, 75th, 25th and 5th percentile confidence intervals of the first breach profile of waste packages with time. The upper bound profile, which is the upper extreme of the probable range of the first breach time, indicates that the earliest possible first breach time of waste package is about 51,000 years. Note that the estimated earliest possible first breach time has a very low probability. It can be shown by comparing with the upper bound profile in Figure 3-85 (showing the first crack breach profiles of waste packages with time) that the first breach is by a SCC crack penetration. The median estimate of the first breach time of the upper bound profile is about 120,000 years. The first breach time of the median profile is about 80,000 years. The second waste package breach time of the upper bound and median profiles is about 59,000 and 86,000 years respectively. The time to fail 10 percent of waste packages for the two profiles is about 80,000 and 97,000 years respectively.

Figure 3-84 shows the first breach profiles of drip shields with time. Because the drip shields are not subject to stress corrosion cracking and localized corrosion, the first breach profiles shown in the figure are all by general corrosion only. Both the upper and under sides of drip shield are exposed to the exposure conditions in the emplacement drift and are subject to corrosion. In addition, the both sides experience the same exposure conditions regardless of whether the drip shields are dripped on or not. Thus, in the analysis, the general corrosion rate for the drip shields is sampled twice independently, one for the patches on the upper side and the other for the patches on the under side. This results in reduced variability in the degradation profiles and thus fast failure rate (i.e., many drip shields failing over a short time period). This is shown in the upper bound profile, in which the drip shield first breach starts at about 24,000 years and 50 percent of the drip shields fail within a couple of thousand years after the initial failure. Similar trends are also seen with the 95th, 75th and median profiles. In terms of the number of patch penetration openings per failed drip shield with time (not shown here; see CRWMS M&O 2000g, Figure 19), the upper bound profile shows that as the drip shields fail, a large number of patches are perforated over a relatively short time period (a few thousand years). A similar trend is seen for the 95th percentile profile. However, a lot more spread of the profile is shown for the other profiles.

Figures 3-85 and 3-86 show respectively the first crack penetration and patch penetration profiles of waste packages with time. The first crack breach time of the upper and 95th percentile profiles is about 51,000 and 61,000 years respectively (Figure 3-85), and the first patch breach time of the upper and 95th percentile profiles is about 62,000 and 64,000 years respectively (Figure 3-85). Comparison of the first crack and patch breach profiles with the first breach profiles indicates that the initial breach (or failure) of the waste packages is likely by a SCC crack penetration in the waste package closure lid welds. For the 75th percentile profiles in the figures, the first crack and patch penetration times are about the same (about 72,000 years). For the remaining profiles, the first crack and patch penetration times are reversed.

The waste package and drip shield degradation analyses have shown that based on the current corrosion model abstractions and assumptions, both the drip shields and waste packages do not fail within the regulatory time period (10,000 years). In particular, the waste package service lifetime is predicted to extend far beyond the regulatory time period (failure beginning at about 50,000 years). The candidate materials for the drip shield (Titanium Grade 7) and the waste package outer barrier (Alloy 22) are highly corrosion resistant and, under the repository exposure

conditions, expected not subject to the degradation processes that, if initiated, could lead to failure in a short time period. Those degradation modes are localized corrosion (pitting and crevice corrosion), stress corrosion cracking (SCC), and hydrogen induced cracking (HIC) (applicable to drip shield only). Both the drip shield and waste package degrade by general corrosion at very low passive dissolution rate. The current experimental data and detailed process-level analyses, upon which the model abstractions incorporated in the WAPDEG analysis are based, have also indicated that the candidate materials would not be subject to those rapidly penetrating corrosion modes under the expected repository conditions, except the closure-lid welds of the waste package, for which complete stress mitigation may not be possible. Because of the potential residual stresses, the closure-lid welds would be subject to SCC. Once a SCC crack initiates, it penetrates the closure-lid thickness in a very short time. Thus stress mitigation in the closure-lid welds is a key design element to avoid premature failures of waste packages by SCC.

The estimated long life-time of the waste packages in the current analysis is attributed mostly to 1) the stress mitigation to the substantial depths in the dual closure-lid welds and 2) the very low general-corrosion rate applied to the closure-lid welds to remove the compressive stress zones, providing a long delay time before initiating SCC crack growth. Major uncertainties are associated with the current analyses. The uncertainties associated with the hoop stress and stress intensity factor used in the current analyses need to be closely re-evaluated to reduce uncertainties and improve conditions in the models. Another major uncertainty in the current analysis is the general corrosion rate used for the closure-lid welds. Additional testing and analyses are needed to reduce these uncertainties.

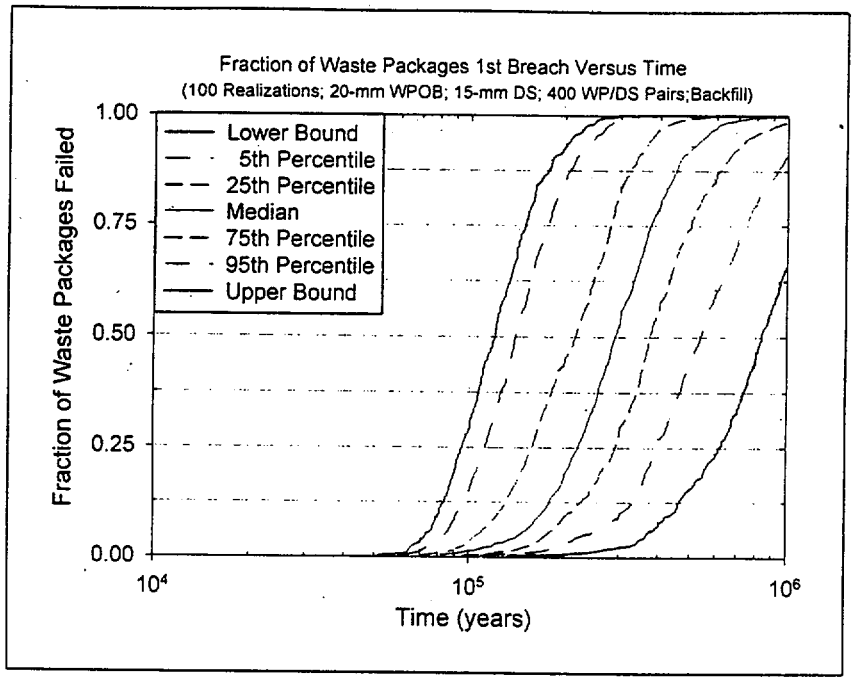

Figure 3-83. The Upper and Lower Bounds, Median, and 95th, 75th, 25th and 5th Percentile Confidence Intervals of the First Breach Profile of Waste Packages with Time

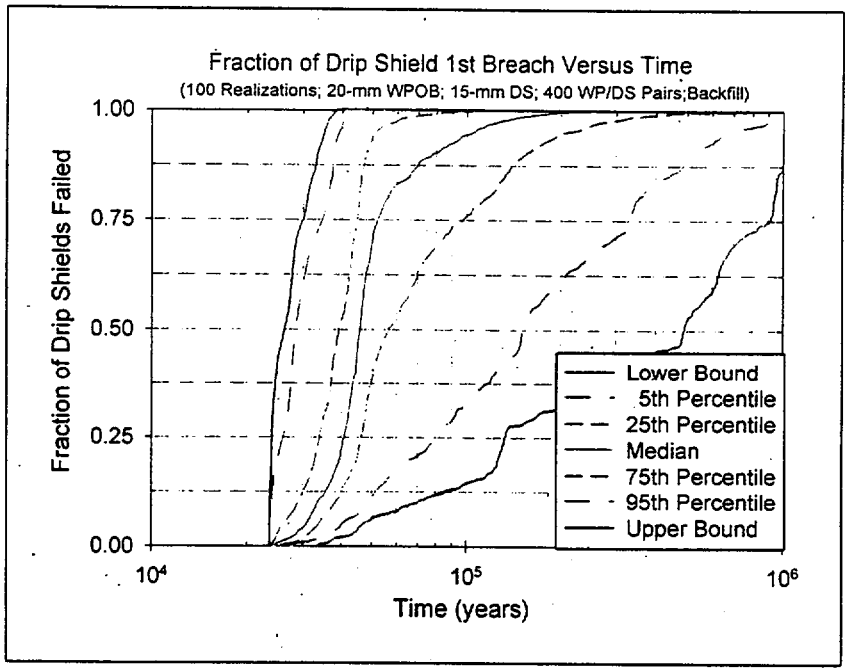

Figure 3-84. The Upper and Lower Bounds, Median, and 95th, 75th, 25th and 5th Percentile Confidence Intervals of the First Breach Profile of Drip Shield with Time

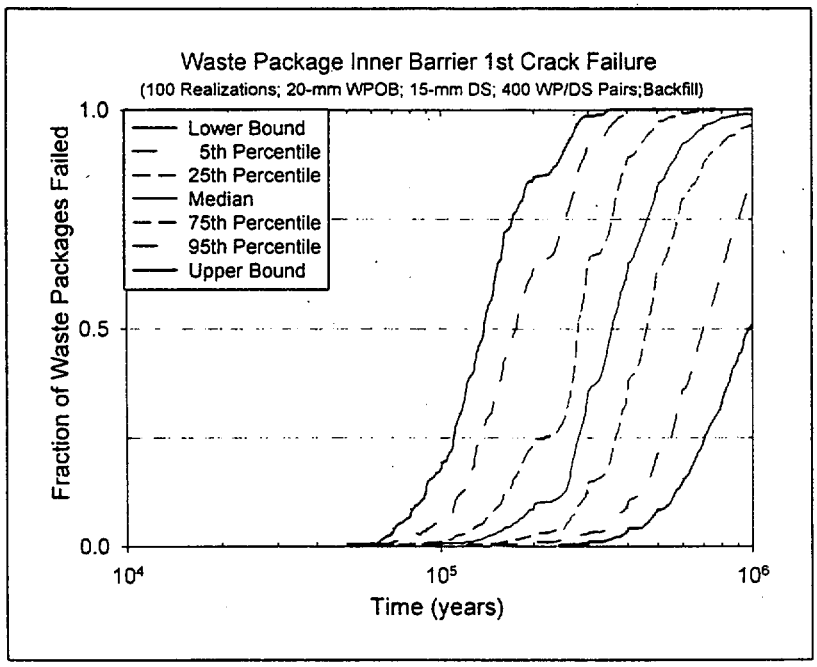

Figure 3-85. The Upper and Lower Bounds, Median, and 95th, 75th, 25th and 5th Percentile Confidence Intervals of the First Crack Breach Profile of Waste Packages with Time

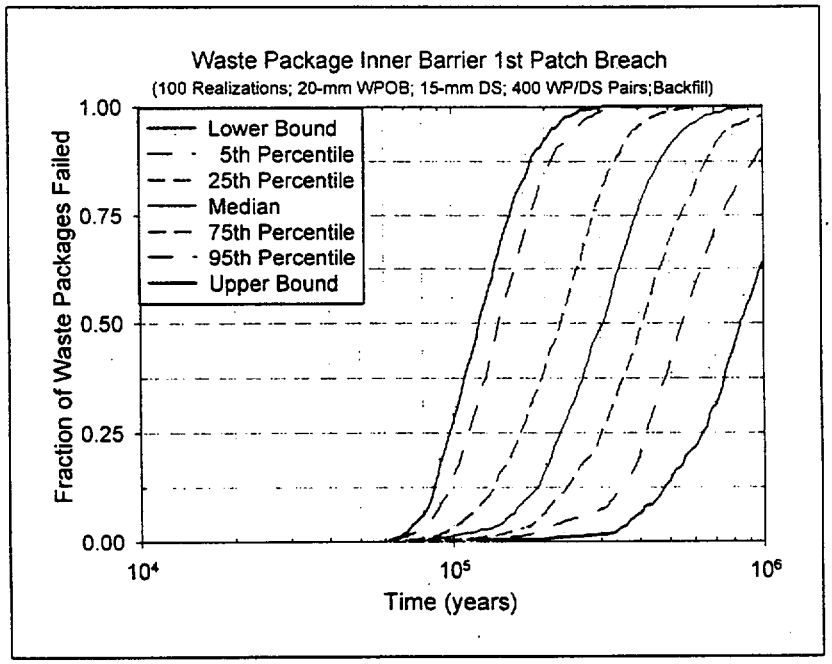

Figure 3-86. The Upper and Lower Bounds, Median, and 95th, 75th, 25th and 5th Percentile Confidence Intervals of the First Patch Breach Profile of Waste Packages with Time

4. RELATIONSHIP TO NRC ISSUE RESOLUTION STATUS REPORTS

4.1 SUMMARY OF THE KEY TECHNICAL ISSUES

As part of the review of site characterization activities, the Nuclear Regulatory Commission (NRC) has undertaken an ongoing review of information on Yucca Mountain site characterization activities to allow early identification and resolution of potential licensing issues. The principal means of achieving this goal is through informal, pre-licensing consultation with the DOE. This approach attempts to reduce the number of, and to better define, issues that may be in dispute during the NRC licensing review, by obtaining input and striving for consensus from the technical community, interested parties, and other groups on such issues.

The NRC has focused pre-licensing issue resolution on those topics most critical to the post-closure performance of the potential geologic repository. These topics are called Key Technical Issues (KTIs). Each KTI is subdivided into a number of subissues. The KTIs are:

- Activities Related to Development of the EPA Standard
- Container Lifetime and Source Term
- Evolution of the Near-field Environment
- Igneous Activity
- Radionuclide Transport
- Repository Design and Thermal Mechanical Effects
- Structural Deformation and Seismicity
- Thermal Effects on Flow (TEF)
- Total System Performance Assessment (TSPA) and Integration
- Unsaturated Zone (UZ) and Saturated Zone (SZ) Flow Under Isothermal Conditions.

Identifying KTIs, integrating their activities into a risk informed approach, and evaluating their significance for post-closure performance helps ensure that NRC's attention is focused on technical uncertainties that will have the greatest affect on the assessment of repository safety.

Early feedback among all parties is essential to define what is known, what is not known and where additional information is likely to make a significant difference in the understanding of future repository safety. The Issue Resolution Status Reports (IRSRs) are the primary mechanism that the NRC staff uses to provide feedback to the DOE on the status of the KTI subissues. IRSRs focus on NRC acceptance criteria for issue resolution and the status of issue resolution, including areas of agreement or when the staff has comment or questions. Open meetings and technical exchanges between NRC and DOE provide additional opportunities to discuss issue resolution, identify areas of agreement and disagreement and plans to resolve any disagreements.

Each KTI is subdivided into a number of subissues. For most subissues, the NRC staff has identified technical acceptance criteria that the NRC may use to evaluate the adequacy of information related to the KTIs. The NRC has also identified two cross cutting programmatic criteria that apply to all IRSRs related to the implementation of the Quality Assurance Program and the use of expert elicitation.

Chapter 4 documents DOE's approach to addressing the acceptance criteria and work performed that is related to the criteria. The following sections provide a summary level discussion of the related KTIs by subissues and specific NRC acceptance criteria.

4.2 RELATION OF THE WASTE PACKAGE PMR TO THE KEY TECHNICAL ISSUES

The WP PMR provides technical information and analyses that relate to two of the KTIs and their associated IRSRs. These include the Container Life and Source Term (CLST) IRSR (NRC 1999a) and the Total System Performance Assessment (TSPA) and Integration (NRC 1999b). Several subissues of these KTIs that relate directly to the WP PMR are discussed in the following sections. Table 4-1 summarizes these KTIs and their subissues that relate directly to this PMR, the related acceptance criteria and PMR approach. In addressing each acceptance criteria, it is assumed that the criteria apply to the DS performance as well.

4.2.1 Container Life and Source Term

The primary issue of the KTI on Container Life and Source Term (CLST) IRSR (NRC 1999) is adequacy of the engineered barrier system (EBS) design to provide reasonable assurance that containers will be adequately long-lived, and radionuclide releases from the EBS will be sufficiently controlled, and that the container design and packaging of spent nuclear fuel and HLW glass will make a significant contribution to the overall repository performance. The site-specific proposed 10 CFR 63 (Dyer 1999) regulation, currently in the public commenting period, is a performance-based regulation. The current CLST IRSR is mainly focused on the containers and waste forms as the primary engineered barriers, but it also considers other engineered sub-system enhancements (i.e., DS, backfill) incorporated as options in the EBS design. For the purpose of this IRSR, the NRC defines the physical boundary of the EBS by the walls of the waste package emplacement drifts. The CLST IRSR identifies six subissues and associated general and specific acceptance criteria deemed important to the resolution of this KTI:

1. The effects of corrosion processes on the lifetime of the containers
2. The effects of phase instability of materials and initial defects on the mechanical failure and lifetime of the containers
3. The rate at which radionuclides in spent nuclear fuel are released from the EBS through the oxidation and dissolution of spent fuel
4. The rate at which radionuclides in HLW glass are leached and released from the EBS
5. The effect of in-package criticality on waste package and EBS performance
6. The effects of alternate EBS design features on container lifetime and radionuclide release from the EBS.

The IRSR provides acceptance criteria for resolution of each of these subissues from the standpoint of performance of the container materials. Subissues 1, 2, and 5, 6 are related to the WP PMR. The following paragraphs address each of the subissues. Also, specific acceptance

criteria related to each of these subissues are discussed in Table 4-1, along with the approach to addressing the criteria and sections of the PMR that describe these approaches. In addressing each acceptance criterion, it is assumed that the criterion applies to DS performance as well.

4.2.1.1 Container Life and Source Term Issue Resolution Status Report General Criteria

In addition to the specific acceptance criteria addressed in Table 4-1, the CLST IRSR includes a set of generic acceptance criteria dealing with expert elicitation and all aspects of data collection, qualification, verification, documentation of uncertainties and limitations in both data and process models. All these general acceptance criteria fall into two NRC's programmatic criteria for quality assurance and the use of expert elicitation. These programmatic criteria apply to all subissues, thus, they are addressed generically for all subissues.

The acceptance criteria for quality assurance addresses DOE's implementation of an adequate quality assurance program. The WP PMR and supporting AMRs were developed in accordance with project procedures for documenting data, analyses, models, and/or computer codes and preparing and reviewing technical reports (see Section 1.4). The programmatic criterion for expert elicitation specifies that DOE conduct expert elicitation in accordance with NUREG-1563 (Kotra et al. 1996) or other acceptable approaches. The WP PMR addresses the NRC's programmatic criteria for quality assurance. No expert elicitation results or data have been used in preparation of this PMR.

4.2.1.2 Container Life and Source Term Issue Resolution Status Report Subissue 1

Subissue 1 considers failure of outer and inner overpacks as a result of various corrosion processes affecting both waste package materials, such as dry-air oxidation, humid-air and uniform aqueous corrosion, LC, microbiologically influenced corrosion (MIC), SCC and HIC. Models for these corrosion processes have been developed and incorporated into the waste package degradation model and are discussed in various parts of the WP PMR. Acceptance criteria related to this subissue and the PMR approach that address the acceptance criteria are provided in Table 4-1.

4.2.1.3 Container Life and Source Term Issue Resolution Status Report Subissue 2

Subissue 2 (NRC 1999, Sections 4.2 and 5.2) examines long-term degradation of mechanical properties of container materials as a result of prolonged exposures of the waste packages (thousands of years) at elevated temperatures. Mechanical failure due to phase instability of waste package materials is highly dependent on material chemical composition and processing history. Examples of material instability that can degrade mechanical properties include segregation of metalloid elements such as phosphorus and sulfur, precipitation of carbides of intermetallic phases, and long-range ordering. Fabrication defects that may lead to early failure of container materials are also the subject of this subissue, as well as the effects of damage due to disruptive events, such as seismicity, faulting, and igneous activity.

Acceptance criteria related to this subissue and the PMR approach that addresses the acceptance criteria are provided in Table 4-1.

4.2.1.4 Container Life and Source Term Subissue 5

Subissue 5 addresses the effects of in-package criticality on waste package and engineered barrier subsystem performance. In-package criticality is not addressed in this PMR. However, the related acceptance criteria are addressed in DOE's *Disposal Criticality Analysis Methodology Topical Report* (YMP 1998) and its supporting references.

4.2.1.5 Container Life and Source Term Issue Resolution Status Report Subissue 6

Subissue 6 addresses performance of the alternative EBS design features such as the DS and backfill. The concerns addressed by the NRC in the IRSR relate to the DS design to be fabricated from titanium alloys. These materials can suffer from thermal embrittlement. Both temper embrittlement of steels and thermal embrittlement of titanium alloys occur as a result of a thermally activated redistribution of barely soluble impurities from grain interiors to grain boundary. Titanium alloys have been long recognized for being highly resistant to corrosion as a result of their ability to form a protective oxide film when in contact. The pH and chloride concentrations have been found to have a relatively minor influence on the passive dissolution rate of some titanium alloys, although data are limited in this area. A review of the literature indicates that some of titanium alloys are susceptible to crevice corrosion. Insufficient experimental data are available for titanium-palladium alloys such as Titanium Grade 7 in relevant environments to state with absolute certainty whether or not these materials will undergo crevice corrosion over a period of 10,000 years. It is generally accepted in the material science community that the addition of palladium to titanium does improve the crevice corrosion resistance of such materials. However, given the lack of data for titanium-palladium alloys, further investigation of crevice corrosion is warranted (NRC 1999).

Environmentally assisted cracking (EAC) of titanium-palladium alloys has not been extensively investigated. Many titanium alloys are susceptible to EAC due to hydrogen embrittlement associated with the precipitation of hydrides ahead of the crack tip. However, the titanium-palladium alloys may be highly resistant to EAC, especially those that have low equivalent oxygen content. The addition of palladium to titanium has also been thought to enhance EAC resistance because hydrogen evolution as H_2 would preferentially take place at Pd-rich sites, thereby decreasing the available atomic hydrogen that could be absorbed into the titanium lattice. It is unclear if this mechanism is operable. Thus, the NRC notes in the CLST IRSR that further DOE investigation of the EAC behavior of titanium-palladium alloys is needed, with particular emphasis on methodologies that would enable monitoring and measurement of slow crack propagation rates (NRC 1999).

The performance modeling of the DS is addressed in this PMR and the effects and performance of the backfill are addressed in the PMR on EBS. Acceptance criteria related to this subissue and the PMR approach that addresses the acceptance criteria are provided in Table 4-1.

4.2.2 Total System Performance Assessment and Integration

The overall goal of the TSPA Integration key technical issue (NRC 1998) is to delineate staff's systematic approach for determining compliance with an overall system performance objective. The objective of this KTI is to describe an acceptable methodology for conducting performance

assessments of repository performance and using these assessments to demonstrate compliance with the overall performance objective and requirements for multiple barriers. The acceptance criteria for each subissue address fundamental elements of the DOE's TSPA model for the Yucca Mountain site. Two of the subissues and some of the elements of these subissues relate to the WP PMR are discussed below.

4.2.2.1 Subissue 3, Model Abstraction

This subissue focuses on the information and technical approaches needed to develop defensible model abstractions and their integration into TSPA. The following aspects of model abstraction are addressed under this subissue: data used in the development of conceptual approaches or process models, the abstracted models, and estimates of system performance. Specifically, this subissue requires documentation of data used to develop conceptual or process models for model abstractions, verification of the consistency of the abstractions, and explanation of their integration (such as coupling and dependencies) into the TSPA. The WP degradation model addresses Elements 1, 2, and 3 related to the waste package corrosion, mechanical disruption, water contacting waste package and waste forms, respectively. Acceptance criteria for elements listed above and the PMR approach in addressing the acceptance criteria are provided in Table 4-1.

4.2.2.2 Subissue 4, Scenario Analysis

This subissue focuses on the attributes of an acceptable methodology for identifying, screening, and selecting Features, Events, and Processes (FEPs) for inclusion in the TSPA. FEPs that could affect future system performance are used to formulate scenarios. This includes construction of scenario classes, assignment of probabilities to scenario classes, and their incorporation into the TSPA. This is a key factor in ensuring the completeness of the TSPA. A systematic method was applied to identify and screen FEPs for WP degradation. A description of this method is provided under Section 1.6. The results of the FEPs screening analyses are also summarized in Table 1-2.

This subissue includes five elements related to the identification of initial FEPs, classification of FEPs, screening, formation of scenarios, and screening of scenario classes. Acceptance criteria for these elements and the PMR approach in addressing the acceptance criteria are provided in Table 4-1.

Table 4-1. Issue Resolution Status Reports, Subissues, Technical Acceptance Criteria, and PMR Approach

NRC Technical Acceptance Criteria	PMR Approach
IRSR: Container Life and Source Term	
SUBISSUE 1 – The Effect of Corrosion Processes on the Lifetime of the Containers	
1. DOE has identified and considered likely modes of corrosion for container materials, including dry-air oxidation, humid-air corrosion, and aqueous corrosion processes, such as GC, LC, MIC, SCC and HIC, as well as the effect of galvanic coupling.	All likely modes of corrosion have been considered and modeled in this PMR (See Section 1.5). The constituent models of this PMR include process models for dry-air oxidation, humid-air corrosion, stress corrosion cracking, hydrogen induced cracking, and aqueous corrosion processes, such as general corrosion, localized corrosion, and microbial influenced corrosion. Galvanic coupling effects have been minimized.
2. DOE has identified the broad range of environmental conditions within the waste package emplacement drifts that may promote the corrosion processes listed previously, taking into account the possibility of irregular wet and dry cycles that may enhance the rate of container degradation.	The corrosion models in this PMR include environmental thresholds that can be used to switch between dominant modes of corrosion. For example, as the waste package temperature drops and the RH increases, the mode of attack changes from dry-air oxidation to humid-air or aqueous-phase corrosion. A comparison of the corrosion and threshold potentials is used to determine whether or not LC will occur. WAPDEG uses bounding conditions that envelop wet and dry cycles (see Section 3.2.3) depending upon the condition at a given time step.
3. DOE has demonstrated that the numerical corrosion models used are adequate representations, taking into consideration associated uncertainties, of the expected long-term behaviors and are not likely to underestimate the actual degradation of the containers as a result of corrosion in the repository environment.	Uncertainties are accounted for in corrosion rates. The rate at the 50th percentile is approximately 50 nm y^{-1}, the rate at the 90th percentile is approximately 100 nm y^{-1}, and the maximum rate is 731 nm y^{-1}. About 10 percent of the values fall between 100 and 750 nm y^{-1}. The effects of thermal aging over extended periods of time (10,000 years) is being accounted for in the overall corrosion model for the WPOB (Section 3.1.4).
4. DOE has considered the compatibility of container materials, the range of material conditions, and the variability in container fabrication processes, including welding, in assessing the performance expected in the containers intended waste isolation.	The effects of welding and thermal aging on the corrosion resistance of the waste package materials have been accounted for. A fully aged sample of Alloy 22 exhibits a less noble corrosion potential, shifted in the cathodic direction by approximately: 63 mV in the case of SAW at 90°C; 109 mV in the case of Simulated Concentrated Water (SCW) at 90°C; and by more than 100 mV in the case of BSW at 100°C. It is assumed that E_{corr} is corrected to account for fully aged material by subtracting approximately 100 mV from values calculated for the base metal. The shift in $E_{critical}$ (threshold potential 1) is approximately 100 mV in most cases. Thus, the difference $E_{critical}$-E_{corr} is virtually unchanged. The effect of thermal aging on the corrosion rate is accounted for in an enhancement factor, G_{aged}, and is based upon a ratio of the non-equilibrium current densities for base metal and aged material. The value of G_{aged} for base metal is approximately one ($G_{aged} \sim 1$), whereas the value of G_{aged} for fully aged material is larger ($G_{aged} \sim 2.5$). Material with less precipitation than the fully aged material would have an intermediate value of G_{aged} ($1 \leq G_{aged} \leq 2.5$) (Section 3.1.4).

Table 4-1. Issue Resolution Status Reports, Subissues, Technical Acceptance Criteria, and PMR Approach (Continued)

NRC Technical Acceptance Criteria	PMR Approach
IRSR: Container Life and Source Term	
SUBISSUE 1 – The Effect of Corrosion Processes on the Lifetime of the Containers	
5. DOE has justified the use of data collected in corrosion tests not specifically designed or performed for the Yucca Mountain repository program for the environmental conditions expected to prevail at the Yucca Mountain site.	The Waste package degradation process models are based on bounding environmental conditions (temperature, humidity, chemistry, etc.) expected in the proposed repository (See Section 3.1.3). The threshold RH used to determine whether vapor phase attack is by DOX or HAC is based upon the deliquescence point of salt deposits that could form on the waste package surface due to aerosol transport. Measurements of GC rates in the vapor and aqueous phases, electrochemical potentials, and other relevant performance data were in test media that can be directly related to water chemistry expected on the waste package surface during the service life of Alloy 22. These water chemistries are based upon evaporative concentrations of the standard J-13 well water chemistry. Crevice chemistry is being measured in situ, with and without the presence of buffer ions. In the aqueous phase, a range of temperature extending from room temperature to 120°C is being investigated. The high-temperature limit is based upon the boiling point of a near-saturation water chemistry without buffer. The expected boiling point of the aqueous phase on the waste package surface is expected to be lower. In addition to the data generated from long-term and short-term corrosion tests, the process model development also includes data generated outside the Yucca Mountain project. These data in general include testing in environments not directly applicable to the YMP and therefore are used as corroborative information.
6. DOE has conducted a consistent, sufficient, and suitable corrosion testing program at the time of the LA submittal. In addition, DOE has identified specific plans for further testing to reduce any significant area(s) of uncertainty as part of the performance confirmation program.	The DOE has established a corrosion test program that addresses all anticipated modes of corrosive attack of the waste package. There is a clear linkage between the experimental data being collected and modules in the predictive WAPDEG code that serves as the heart of the Total System Performance Assessment (TSPA). Data and modules have been developed for each key element of the EDA II design: the WPOB (Alloy 22); the inner structural support (stainless steel 316NG); and the protective DS (Titanium Grade 7). Companion AMRs provide data and modules for the stainless steel 316NG and the Titanium Grade 7 alloy. Studies include exposure of over 18,000 samples of candidate waste package material in the Long Term Corrosion Test Facility (LTCTF). A large number of pre- and post-exposure measurements of dimension and weight allow establishment of distribution functions for representation of the GC rate. Microscopic examination of samples from the LTCTF and other corrosion tests is done with Scanning Electron Microscopy (SEM), Atomic Force Microscopy (AFM), X-Ray Diffraction (XRD), X-Ray Photoelectron Spectroscopy, Secondary Ion Mass Spectrometry (SIMS), and other state-of-the-art surface analytical techniques. Potentiodynamic and potentiostatic electrochemical tests are conducted with base metal, thermally aged material and simulated welds. Thermally aged material is fully characterized with the transmission electron microscope as discussed by Summers and Turchi (CRWMS M&O 2000b). The present test results provide sufficient confidence for the current design. In addition, the Project will continue testing of materials both in the laboratory and in the field. This part of the testing program is covered in the Performance Confirmation Plan (CRWMS M&O 2000q).

Table 4-1. Issue Resolution Status Reports, Subissues, Technical Acceptance Criteria, and PMR Approach (Continued)

NRC Technical Acceptance Criteria	PMR Approach
7. DOE has established a defensible program of corrosion monitoring and testing of the engineered sub-system components during the performance confirmation period to assure they are functioning as intended and anticipated.	Testing activities during performance confirmation period are not covered in this PMR. This acceptance criterion will be addressed as part of the Performance Confirmation Program currently under development.
SUBISSUE 2 - The effects of phase instability of materials and initial defects on the mechanical failure and lifetime of the containers	
1. DOE has identified and considered the relevant mechanical failure processes that may affect the performance of the proposed container materials.	As described in this report, all likely degradation modes, including HIC and SCC as two possible mechanical failure modes have been considered. Both modes have been included in WAPDEG, and are described in the report (Sections 3.1.7 and 3.1.8, respectively).
2. DOE has identified and considered the effect of material stability on mechanical failure processes for the various container materials as a result of prolonged exposure to the expected range of temperatures and stresses, including the effects of chemical composition, microstructure, thermal treatments, and fabrication processes.	This PMR presents data showing that Alloy 22 has adequate phase stability to serve as a waste package material, provided that the temperature is not allowed to exceed 260°C. Expected range of temperature and stresses, chemical composition, microstructure, thermal treatments, and fabrication processes are all related to the material stability and have been considered in modeling in Section 3.1.4 of the PMR.
3. DOE has demonstrated that the numerical models used for container materials stability and mechanical failures are effective representations, taking into consideration associated uncertainties, of the expected materials behavior and are not likely to underestimate the actual rate of failure in the repository environment.	Uncertainties, assumptions, and limitations of the specific models are addressed in the related AMRs. As indicated in Section 3.2.1, the WAPDEG analysis also takes into account quantifiable uncertainties and variability of the degradation model for the possible ranges of corrosion parameters and exposure conditions. The WAPDEG model includes modules for DOX, HAC, APC, SCC and HIC. Also, both GC and LC are considered. The possibility of using either localized thermal annealing or laser peening is considered as a means of mitigating SCC in the waste package closure weld.
4. DOE has considered the compatibility of container materials and the variability in container manufacturing processes, including welding, in its waste package failure analyses and in the evaluation of radionuclide release.	The design now used prevents galvanic coupling of Titanium Grade 7 with carbon steel, thereby preventing any hydrogen charging of the DS due to the cathodic reduction of hydrogen ions on the titanium surface. Variabilities in processes used for weld stress mitigation are accounted for in the SCC models for both laser peening and induction annealing techniques (See Section 3.1.7).
5. DOE has identified the most appropriate methods for nondestructive examination of fabricated containers to detect and evaluate fabrication defects in general and, particularly, in seam and closure welds.	An NDE protocol is under development and will be used for DS and waste package inspection. Such inspection will limit the size of manufacturing defects as a means of helping prevent SCC and HIC. Materials used in waste package construction will be tested electrochemically, to assure that those materials being used are not unexpectedly susceptible to LC.
6. DOE has justified the use of material test results not specifically designed or performed for the Yucca Mountain repository program for environmental conditions (i.e., temperature, stress, and time) expected to prevail at the proposed Yucca Mountain repository.	Various AMRs supporting this report, such as the AMR on degradation of stainless steel (CRWMS M&O 2000e), provide discussion for the use of material test results from published data not specifically designed or performed for the Yucca Mountain repository program for environmental conditions expected to prevail at the proposed Yucca Mountain repository.
7. DOE has conducted a consistent, sufficient, and suitable material testing program at the time of the LA submittal. In addition, DOE has identified specific plans for further testing to reduce any significant area(s) of uncertainty as part of the performance confirmation program.	Testing activities during performance confirmation period are not covered in this PMR. This acceptance criterion will be addressed as part of the Performance Confirmation Program currently under development.

Table 4-1. Issue Resolution Status Reports, Subissues, Technical Acceptance Criteria, and PMR Approach (Continued)

NRC Technical Acceptance Criteria	PMR Approach
8. DOE has established a defensible program of monitoring and mechanical testing of the engineered sub-systems components, during the performance confirmation period, to assure they are functioning as intended and anticipated, in the presence of thermal and stress perturbations.	Testing activities during performance confirmation period are not covered in this PMR. This acceptance criterion will be addressed as part of the Performance Confirmation Program currently under development.
SUBISSUE 5 - The effect of in-package criticality on waste package and EBS performance	
Subissue 5 addresses the effects of in-package criticality on waste package and engineered barrier subsystem performance. In-package criticality is not addressed in this PMR. However, the related acceptance criteria are addressed in DOE's *Disposal Criticality Analysis Methodology Topical Report* (YMP 1998) and its supporting references.	
SUBISSUE 6 - The effects of alternate EBS design features on container lifetime and radionuclide release from the EBS	
1. DOE has identified and considered the effects of backfill, and the timing of its emplacement, on the thermal loading of the repository, waste package lifetime (including container corrosion and mechanical failure), and the release of radionuclides from the EBS.	The effects of the backfill are not considered in determining the environment on the surface drip shield and waste package.
2. DOE has identified and considered the effects of ceramic coating on waste package lifetime, including negative consequences as a result of breakdown of the ceramic coating (cracking, spalling, or delamination) in response to the action of environment, manufacturing defects, mechanical impacts and stresses arising from a multiplicity of sources, and the potential for enhanced localized corrosion of the containers that might occur at cracks are perforations in the ceramic coating layers.	This criterion is no longer applicable, as the current design for the repository does not include ceramic coatings.
3. DOE has identified ceramic coating materials with outer overpack materials and the combined effect of ceramic coating with backfill on container lifetime.	See response to Criterion 2.
4. DOE has identified and considered the effects of DSs (with backfill) on waste package lifetime, including extension of the humid-air corrosion regime, environmental effects, breakdown of DSs and resulting mechanical impacts on waste package, the potential for crevice corrosion at the junction between the waste package and the DS, and the potential for condensate formation and dripping on the underside of the shield.	The effects of the drip shield have been considered and evaluated in the analysis of waste package performance. This aspect is discussed in Section 3.2.3 of this document. The analysis conservatively assumes that the environment on the surface of the waste package is not affected by the presence of the drip shield. Degradation model for the WP takes into account potential for crevice corrosion and degradation due to mechanical failure and assumes exposure to drift environment with no protection by DS against water dripping. The effects of the backfill with respect to changes in water chemistry are also not assumed since the current design does not include backfill.

Table 4-1. Issue Resolution Status Reports, Subissues, Technical Acceptance Criteria, and PMR Approach (Continued)

NRC Technical Acceptance Criteria	PMR Approach
5. DOE has evaluated the effect of design changes in container wall thickness that may increase γ-radiolysis of the water contacting waste packages and, therefore, enhance the possible occurrence of localized corrosion processes.	Experiments have been performed with Alloy 22 to accurately mimic the effects of gamma radiolysis. It is known that gamma radiolysis of aqueous electrolytes produces hydrogen peroxide, and that that hydrogen peroxide increases the open circuit corrosion potential of stainless steels. There has been concern that such effects could push the corrosion potential close to the threshold potential for the initiation of LC. Laboratory experiments have shown that the maximum increase in corrosion potential due to hydrogen peroxide in concentrated repository ground waters is approximately 200 mV, and insufficient to exceed the threshold for initiation of LC (See Section 3.1.6).
6. DOE has identified the chemical composition of the water in the environment surrounding the waste packages and its evolution with time.	This has been done through both evaporative concentration and thermodynamic calculation.
7. DOE has justified the use of test results for the DSs, ceramic coatings, and backfill materials not specifically collected for the Yucca Mountain site for the environmental conditions expected to prevail at the proposed Yucca Mountain repository	At the present time, the ceramic coating is not part of the DS or waste package design.
8. DOE has conducted a consistent, sufficient, and suitable corrosion testing program at the time of the LA submittal. In addition, DOE has identified specific plans for further testing to reduce any significant area(s) of uncertainty as part of the performance confirmation program.	Testing activities during performance confirmation period are not covered in this PMR. This acceptance criterion will be addressed as part of the Performance Confirmation Program currently under development.
IRSR: TOTAL SYSTEM PERFORMANCE ASSESSMENT AND INTEGRATION	
SUBISSUE 3- Model abstraction	
Element 1 - Waste package corrosion (covered in Waste Package Degradation PMR	
Criterion T1 - Sufficient data (field, laboratory and/or natural analog data) are available to adequately define relevant parameters and conceptual models necessary for developing the waste package corrosion abstraction in TSPA.	The TSPA model requires estimates of corrosion and threshold potentials, both of which are determined through electrochemical testing. Thus far, cyclic polarization has been done in a wide variety of repository-relevant test solutions, including SDW, SCW, SAW, SCMW, SSW, and BSW. Cyclic polarization tests are now being conducted in these media with artificial crevices. Experiments have been performed to quantify the extent that pH can be lowered inside crevices, formed between the Alloy 22 WPOB and the 316NG SSSM. The TSPA model also requires estimates of GC rates. Testing in the LTCTF is continuing. Two-year test data has become available and is included in this PMR. These two-year test data are an integral part of the WAPDEG simulation (Sections 3.1.5 and 3.2).
Criterion T2 - Parameter values, assumed ranges, probability distributions, and/or bounding assumptions used in the waste package corrosion abstraction, such as the critical RH, material properties, pH, and chloride concentration are technically defensible and reasonably account for uncertainties and variabilities.	Model abstractions for various corrosion modes include the aspects of this criterion and documented in the supporting AMRs and Section 3-2 of this PMR.

Table 4-1. Issue Resolution Status Reports, Subissues, Technical Acceptance Criteria, and PMR Approach (Continued)

NRC Technical Acceptance Criteria	PMR Approach
Criterion T3 - Alternative modeling approaches consistent with available data and current scientific understanding are investigated and results and limitations appropriately factored into the waste package corrosion abstraction.	Where possible, alternative models are considered. For example, consider methods A and B in the SCC model. Method A is based upon the concept of a threshold stress intensity factor. Method B is based upon the slip dissolution or film rupture model used in the BWR industry. Both are accounted for in the PMR and TSPA calculation. Also consider methods A and B in the LC model. Method A is based upon the concept of exceeding a threshold electrochemical potential for the initiation of LC (crevice corrosion). Method B is based upon the concept of exceeding a threshold temperature of the initiation of LC (crevice corrosion).
Criterion T4 - waste package corrosion abstraction output is verified through comparison to output of detailed process models and/or empirical observations (laboratory testing or natural analogs, or both.).	Output from WAPDEG is being compared to experimental measurements used as the basis of calculations to verify that correct and reasonable results are obtained.
Criterion T5 - Important design features, physical phenomena and couplings, and consistent and appropriate assumptions are incorporated into the waste package corrosion abstraction.	The WP degradation model assumes conservative environmental and exposure conditions. WAPDEG code incorporates bounding conditions for the various corrosion modes that envelop effects of design features and couplings.
Element 2 - Mechanical disruption (covered in Disruptive Events PMR)	
Element 3 - Water contacting waste packages and waste forms	
Criterion T4 – Mechanical disruption of WPs abstraction output is verified through comparison to output of detailed process models, and/or empirical observations (laboratory testing or natural analogs, or both).	Abstraction of mechanical failure of Waste Package due to disruptive events is not in the scope of this PMR. However, will be addressed in addressed in the Disruptive Events PMR.
Criterion T5 – Important design features, physical phenomena and couplings, and consistent and appropriate assumptions are incorporated into the mechanical disruption of waste packages abstraction.	Abstraction of mechanical failure of Waste Package due to disruptive events is not in the scope of this PMR. However, will be addressed in addressed in the Disruptive Events PMR.
SUBISSUE 4 – Model abstraction	
Element 1 - Identification of initial FEPs	
T1 - DOE has identified a comprehensive list of processes and events that: (1) are present or might occur in the Yucca Mountain region and (2) includes those processes and events that have the potential to influence repository performance	Section 1.6 of this PMR describes the features, events, and processes in this PMR. The AMR supporting this section (CRWMS M&O 2000l) provides a list of the processes and events applicable to this PMR. The AMR provides a description of the screening arguments and dispositions for the FEPs and has been thoroughly reviewed by subject matter experts. In addition, the AMR describes the development of the FEPs database, including a description of the FEPs process in sufficient detail to demonstrate the comprehensiveness of the database.

Table 4-1. Issue Resolution Status Reports, Subissues, Technical Acceptance Criteria, and PMR Approach (Continued)

NRC Technical Acceptance Criteria	PMR Approach
Element 2 - Classification of FEPs	
T1 - DOE has provided adequate documentation identifying how its initial list of processes and events has been grouped into categories.	Section 1.5 of this PMR describes the features, events, and processes in this PMR. The AMR supporting this section (CRWMS M&O 2000l) provides documentation and justification for screening arguments and dispositions. Documentation is maintained of all mapping of FEPs into primary and secondary categories. For comprehensiveness, traceability is maintained from the secondary to the related primary FEPs. The AMR also describes the development of the FEPs database, including identifying and classifying relevant FEPs.
T2 - Categorization of processes and events is compatible with the use of categories during the screening of processes and events.	Section 1.5 of this PMR describes the features, events, and processes in this PMR. The AMR supporting this section, (CRWMS M&O 2000l), provides documentation and justification for screening arguments and dispositions. Documentation is maintained of all mapping of FEPs into primary and secondary categories. For comprehensiveness, traceability is maintained from the secondary to the related primary FEPs. The AMR also describes the development of the FEPs database, including identifying and classifying relevant FEPs.
Element 3 - Screening	
T1 - Categories of processes and events that are not credible for the Yucca Mountain repository because of waste characteristics, repository design, or site characteristics are identified and sufficient justification is provided for DOE's conclusions	Section 1.5 of this PMR describes the features, events, and processes in this PMR. The AMR supporting this section (CRWMS M&O 2000l) provides documentation and justification for screening arguments and TSPA dispositions. Documentation includes a statement of the screening decision for each FEP. Justification is provided for each excluded FEP including the criterion on which it was excluded and the technical basis for the screening argument.
T2 - The probability assigned to each category of processes and events is consistent with site information, well documented, and appropriately considers uncertainty.	Section 1.5 of this PMR describes the features, events, and processes in this PMR. The AMR supporting this section (CRWMS M&O 2000l) provides documentation and justification for screening arguments and dispositions. Probability estimates for FEPs are based on technical analysis of the past frequency of similar events consistent with site information, well documented, and appropriately considers uncertainty.
T3 - Processes and events may be screened from the performance assessment on the basis of their probability of occurrence, provided DOE has demonstrated that they have a probability of less than one chance in 10,000 of occurring over 10,000 years.	Section 1.5 of this PMR describes the features, events, and processes in this PMR. The AMR supporting this section (CRWMS M&O 2000l) provides documentation and justification for screening arguments and TSPA dispositions. Justification is provided for each excluded FEP including the criterion on which it was excluded and the technical basis for the screening argument. For excluded FEPs, documentation includes the criterion on which it was excluded and the technical basis for the screening argument. The probability assigned to FEPs may be one of the screening criteria. FEPs may be excluded only if they can be shown to have a probability of occurrence of less than 10^{-8}/year.

Table 4-1. Issue Resolution Status Reports, Subissues, Technical Acceptance Criteria, and PMR Approach (Continued)

NRC Technical Acceptance Criteria	PMR Approach
T4 - Categories of processes and events may be omitted from the performance assessment on the basis that their omission would not significantly change the calculated expected annual dose, provided DOE has demonstrated that excluded categories of processes and events would not significantly change the calculated expected annual dose.	Section 1.5 of this PMR describes the features, events, and processes in this PMR. The AMR supporting this section (CRWMS M&O 2000l) provides documentation and justification for screening arguments and TSPA dispositions. For omitted categories, documentation includes the criterion on which it was excluded and the technical basis for the screening argument.
Element 4 – Formation of scenarios	
T1 - DOE has provided adequate documentation identifying: (1) whether processes and events have been addressed through consequence model abstraction or scenario analysis and (2) how the remaining categories of processes and events have been combined into scenario classes.	Section 1.5 of this PMR describes the features, events, and processes in this PMR. The AMR supporting this section (CRWMS M&O 2000l) provides documentation and justification for screening arguments and TSPA dispositions. FEPs that have not been excluded are identified as either expected FEPs or disruptive FEPs. Expected FEPs will be included in the TSPA-SR nominal scenario, which is simulated by the base case model described in the TSPA-SR documentation. Disruptive scenarios are constructed from expected FEPs and combinations of disruptive FEPs.
T2 - The set of scenario classes is mutually exclusive and complete.	Section 1.5 of this PMR describes the features, events, and processes in this PMR. The AMR supporting this section (CRWMS M&O 2000l) provides documentation and justification for screening arguments and TSPA dispositions. In addition, the AMR describes the development of the FEPs database including a description of the construction and screening of scenarios.
Element 5- Screening of scenario classes	
T1 - Scenario classes that are not credible for the Yucca Mountain repository because of waste characteristics, repository design, or site characteristics, individually or in combination, are identified and sufficient justification is provided for DOE's conclusions.	TSPA provides justification for screening arguments and TSPA disposition. Scenarios are screened using the same regulatory, probability, and consequence criteria used for screening individual FEPs. Documentation of this process includes identification of any scenarios that have been screened from the analysis and the technical basis for that screening decision.
T2 - The probability assigned to each scenario class is consistent with site information, well documented, and appropriately considers uncertainty.	TSPA provides justification for screening arguments and TSPA disposition. Probability estimates for scenario classes are based on analyses similar to probabilities assigned for individual FEPs.
T3 - Scenario classes that combine categories of processes and events may be screened from the performance assessment on the basis of their probability of occurrence, provided: (1) the probability used for screening the scenario class is defined from combinations of initiating processes and events and (2) DOE has demonstrated that they have a probability of less than one chance in 10,000 of occurring over 10,000 years.	TSPA provides justification for excluding scenario classes. The probability assigned to scenario classes is one of the screening criteria. Scenario classes may be excluded from the TSPA only if they can be shown to have a probability of occurrence of less than 10^{-8}/year. Justification is provided for each excluded scenario class, including the criterion on which it was excluded and the technical basis for the screening argument. In addition, the AMR describes the development of the FEPs database including a description of screening and specifying scenarios for TSPA analysis.

Table 4-1. Issue Resolution Status Reports, Subissues, Technical Acceptance Criteria, and PMR Approach (Continued)

NRC Technical Acceptance Criteria	PMR Approach
T4 - Scenario classes may be omitted from the performance assessment on the basis that their omission would not significantly change the calculated expected annual dose, provided DOE has demonstrated that excluded categories of processes and events would not significantly change the calculated expected annual dose.	TSPA provides justification for excluding scenario classes. For excluded scenario classes, documentation includes the criterion on which it was excluded and the technical basis for the screening argument. In addition, the AMR describes the development of the FEPs database including a description of screening and specifying scenarios for TSPA analysis.

5. SUMMARY AND CONCLUSIONS

Performance of a potential Yucca Mountain high-level radioactive waste repository depends on both the natural barrier system and the engineered barrier system and on their interactions. As a major component of the engineered barrier system, the waste package contributes to isolation of high-level radioactive waste during the postclosure period and reduces the uncertainties associated with the performance of the repository. It is expected that the waste package protected by a drip shield will be exposed to processes and conditions in the repository environment that will eventually have an impact on its postclosure performance. Some of the important conditions contributing to waste package degradation include: humidity and temperature in the emplacement drift, chemistry of the water dripping on the waste package, corrosion properties of the waste package outer barrier. As part of the performance-based risk-informed evaluation of postclosure repository performance, it is important to understand and account for degradation processes that will impact the waste package lifetime. This document describes how waste package and drip shield degradation processes are modeled, analyzed, and combined into an overall degradation model; the results from the model are incorporated into the assessment of the postclosure repository total system performance. This PMR also addresses Key Technical Issues and Issue Resolution Status Reports of the NRC and the approach to the resolution of the issues. In addition, issues on repository performance raised by other agencies such as NWTRB are also addressed.

A variety of anticipated modes of waste package degradation under the most important environmental conditions including thermal, hydrological, and geochemical conditions have been considered and analyzed as part of an integrated degradation process model. The waste package degradation process model consists of individual process models or analyses and associated abstraction models. These models address the environment on the degradation of the waste package and drip shield and consider various degradation modes including early material failure due to manufacturing and fabrication defects, phase stability and aging, general corrosion, localized corrosion, stress corrosion cracking, and hydrogen-induced cracking. A generic integrated model constructed based on abstracted results from individual component models is then applied to the waste package and drip shield materials to determine their overall performance. A detailed discussion of the waste package and drip shield degradation processes within the near field environment and the analytical results from the process-level models are documented in the individual AMRs. Following is a list of the process-level models:

- Environment on the Surface of Drip Shield and Waste Package Outer Barrier
- Mechanisms for Early Failures
- Aging and Phase Stability of Waste Package Outer Barrier
- General Corrosion and Localized Corrosion of Waste Package Outer Barrier
- General corrosion and Localized Corrosion of Drip Shield
- Stress Corrosion Cracking of the Drip Shield, the Waste Package Outer Barrier and the Stainless Steel Structural Material

- Hydrogen Induced Cracking (HIC) of Drip Shield
- Degradation of Stainless Steel Structural Material.

Abstraction of Models–Abstraction results from the detailed process-level models listed above are used as input to the waste package degradation (WAPDEG) model for evaluation of the performance of the waste package outer barrier and drip shield materials. These abstractions include thresholds for corrosion initiation and degradation rate with the associated uncertainty and variability. The WAPDEG analysis results are further abstracted as input to the TSPA-SR analysis. The abstractions include the time-histories of waste package failures including the number of penetrations on waste packages and the size distribution of penetration openings on waste packages including the associated uncertainties. The TSPA-SR uses the results of the abstraction and synthesis of waste package degradation information in performance assessment to determine waste package lifetime and potential impact on long-term repository performance.

Analysis Results–Abstracted results from the process models described above, along with abstracted results for the drift environment were used as input in the integrated degradation model, WAPDEG. The WAPDEG model, an integrated degradation model, is used for waste package and drip shield degradation analysis and to determine the failure time. This integrated model is based on a stochastic simulation approach and provides a description of waste package and drip shield degradation, as a function of time and repository location for specific design and thermal-hydrologic modeling assumptions. Each WAPDEG realization corresponds to a complete WAPDEG run for a given number of waste packages. Accordingly, the WAPDEG analysis outputs are reported as a group of "curves" that represent the potential range of the output parameters. The nominal case analysis for waste package and drip shield degradation constitutes 100 realizations of WAPDEG simulation that uses 100 input vectors for uncertain corrosion model parameters and simulation parameters that were sampled from their respective ranges.

Except for the relative humidity (RH) threshold for corrosion initiation, the temperature and RH do not affect waste package and drip shield degradation. For this reason, representative sets of temperature and RH histories were used in the analysis. Also, the analysis does not distinguish between different waste packages for different waste forms (i.e., waste packages for commercial spent nuclear fuel, high-level waste, etc.), which could give rise to varying thermo-hydrologic conditions to the drip shield and waste packages. In addition, the threshold for localized corrosion initiation of the drip shield and waste package outer barrier requires the presence of drips and is much higher than the conditions expected in the repository. Therefore, localized corrosion is not expected. The analysis assumed waste package failure when the Alloy 22 outer barrier has breached. Therefore, the stainless steel inner structural layer of waste package was not considered in the analysis, as this component is not viewed as a corrosion barrier.

The waste package and drip shield degradation analyses have shown that based on the current corrosion model abstractions and assumptions presented in this PMR, both the drip shields and waste packages do not fail within the regulatory time period (10,000 years). In particular, the waste package service lifetime is predicted to extend far beyond the regulatory time period (failure beginning at about 50,000 years). The materials selected for the drip shield (Titanium Grade 7) and the waste package outer barrier (Alloy 22) are highly corrosion resistant and, under

the repository exposure conditions, are expected to be immune to the degradation processes that, if initiated, could lead to failure in a shorter time period. Those degradation modes are localized corrosion (pitting and crevice corrosion), stress corrosion cracking (SCC), and hydrogen induced cracking (HIC) (applicable to the drip shield only). Both the drip shield and waste package degrade by general corrosion at very low passive dissolution rates. The current experimental data and detailed process-level analyses, upon which the model abstractions incorporated in the WAPDEG analysis are based, have also indicated that the candidate materials would not be subject to those rapidly penetrating corrosion modes under the expected repository conditions, except for possibly the closure-lid welds of the waste package, if SCC were to occur there. To preclude SCC, weld stress mitigation will be implemented on a dual lid waste package closure weld design.

The estimated long life-time of the waste packages in the current analysis is attributed mostly to 1) the depth of the stress mitigation in the dual closure-lid welds and 2) the very low general-corrosion rate of the closure-lid welds which requires a very long time to corrode away the compressive stress zones, thus providing a very long delay time before initiating SCC crack growth.

This document may be affected by technical product input information that requires confirmation. Any changes to the document that may occur as a result of completing the confirmation activities will be reflected in subsequent revisions. The status of the input information quality may be confirmed by review of the Document Input Reference System database.

INTENTIONALLY LEFT BLANK

6. REFERENCES AND INPUTS

6.1 DOCUMENTS CITED

Budnitz, B.; Ewing, R.C.; Moeller, D.W.; Payer, J.; Whipple, C.; and Witherspoon, P.A. 1999. *Peer Review of the Total System Performance Assessment-Viability Assessment Final Report.* Las Vegas, Nevada: Total System Performance Assessment Peer Review Panel. ACC: MOL.19990317.0328.

Cohon, J.L. 1999a. Reaction to Information Presented by the DOE, September 14-15, 1999 Nuclear Waste Technical Review Board Meeting. Letter from J.L. Cohon (NWTRB) to L.H. Barrett (DOE/OCRWM), November 10, 1999. ACC: MOL.20000321.0152.

Cohon, J.L. 1999b. Comments on the Scientific Program, June 1999 Nuclear Waste Technical Review Board Meeting. "Letter from J.L. Cohon (NWTRB) to L.H. Barrett (OCRWM), August 3, 1999." ACC: MOL.20000317.0405.

CRWMS M&O 1998. *Total System Performance Assessment - Viability Assessment Base Case.* B00000000-01717-0210-00011 REV 01. Las Vegas, Nevada: CRWMS M&O. ACC: MOL.19981202.0279.

CRWMS M&O 1999a. *Monitored Geologic Repository Project Description Document.* B00000000-01717-1705-00003 REV 00 DCN 01. Las Vegas, Nevada: CRWMS M&O. ACC: MOL.19991117.0160.

CRWMS M&O 1999b. *Development Plan for Waste Package Degradation Process Model Report.* TDP-WIS-MD-000030 REV 00. Las Vegas, Nevada: CRWMS M&O. ACC: MOL.19991220.0375.

CRWMS M&O 1999c. *Classification of the MGR Uncanistered Spent Nuclear Fuel Disposal Container System.* ANL-UDC-SE-000001 REV 00. Las Vegas, Nevada: CRWMS M&O. ACC: MOL.19990928.0216.

CRWMS M&O 1999d. *1101213PM7 Waste Package Analyses & Models - PMR.* Activity Evaluation, September 21, 1999. Las Vegas, Nevada: CRWMS M&O. ACC: MOL.19991012.0219.

CRWMS M&O 2000a. *Environment on the Surface of the Drip Shield and Waste Package.* ANL-EBS-MD-000001. Las Vegas, Nevada: CRWMS M&O URN-0125. Submit to RPC

CRWMS M&O 2000b. *Aging and Phase Stability of Waste Package Outer Barrier.* ANL-EBS-MD-000002 REV 00. Las Vegas, Nevada: CRWMS M&O URN-0133. Submit to RPC

CRWMS M&O 2000c. *General Corrosion and Localized Corrosion of Waste Package Outer Barrier.* ANL-EBS-MD-000003 REV 00. Las Vegas, Nevada: CRWMS M&O. ACC: MOL.20000202.0172.

CRWMS M&O 2000d. *General Corrosion and Localized Corrosion of the Drip Shield.* ANL-EBS-MD-000004 REV 00. Las Vegas, Nevada: CRWMS M&O URN-0135. Submit to RPC

CRWMS M&O 2000e. *Degradation of Stainless Steel Structural Material.* ANL-EBS-MD-000007 REV 00. Las Vegas, Nevada: CRWMS M&O URN-0137. Submit to RPC

CRWMS M&O 2000f. *Analysis/Model Report (AMR) REV 00D on Stress Corrosion Cracking of the Drip Shield, the Waste Package Outer Barrier and the Stainless Steel Structural Material.* Input Transmittal 00139.T. Las Vegas, Nevada: CRWMS M&O. ACC: MOL.20000317.0389.

CRWMS M&O 2000g. *WAPDEG Analysis of Waste Package and Drip Shield Degradation.* Input Transmittal 00133.T. Las Vegas, Nevada: CRWMS M&O. ACC: MOL.2000316.0265.

CRWMS M&O 2000h. *Hydrogen-Induced Cracking of Drip Shield.* ANL-EBS-MD-000006 REV 00. Las Vegas, Nevada: CRWMS M&O URN-0136. Submit to RPC

CRWMS M&O 2000i. *Calculation of General Corrosion Rate of Drip Shield and Waste Package Outer Barrier to Support WAPDEG Analysis.* CAL-EBS-PA-000002 REV 00. Las Vegas, Nevada: CRWMS M&O URN-0134. Submit to RPC

CRWMS M&O 2000j. *Abstraction of Models of Stress Corrosion Cracking of Drip Shield and Waste Package Outer Barrier and Hydrogen Induced Corrosion of Drip Shield.* Input Transmittal 00134.T. Las Vegas, Nevada: CRWMS M&O. ACC: MOL.20000316.0266.

CRWMS M&O 2000k. *Calculation of Probability and Size of Defect Flaws in Waste Package Closure Welds to Support WAPDEG Analysis.* Input Transmittal 00143.T. Las Vegas, Nevada: CRWMS M&O. ACC: MOL.20000317.0476.

CRWMS M&O 2000l. *FEPs Screening of Processes and Issues in Drip Shield and Waste Package Degradation.* Input Transmittal 00150.T. Las Vegas, Nevada: CRWMS M&O. ACC: MOL.20000317.0480.

CRWMS M&O 2000m. *Analysis of Mechanisms for Early Waste Package Failure.* ANL-EBS-MD-000023 REV 01. Las Vegas, Nevada: CRWMS M&O. ACC: MOL.20000223.0878.

CRWMS M&O 2000n. *Abstraction of Models For Pitting And Crevice Corrosion Of Drip Shield And Waste Package Outer Barrier.* Input Transmittal 00141.T. Las Vegas, Nevada: CRWMS M&O. ACC: MOL.20000317.0474.

CRWMS M&O 2000o. *Abstraction of Models for Stainless Steel Structural Material Degradation.* Input Transmittal 00140.T. Las Vegas, Nevada: CRWMS M&O. ACC: MOL.20000317.0477.

CRWMS M&O 2000p. *Incorporation of Uncertainty and Variability of Drip Shield and Waste Package Degradation in WAPDEG Analysis.* Input Transmittal 00142.T. Las Vegas, Nevada: CRWMS M&O. ACC: MOL.20000317.0478.

CRWMS M&O 2000q. *Performance Confirmation Plan.* TDR-PCS-SE-000001 REV 01. Las Vegas, Nevada: CRWMS M&O URN-0138.

DOE (U.S. Department of Energy) 1995. *The Nuclear Waste Policy Act, As Amended. With Appropriations Acts Appended.* DOE/RW-0438, Rev. 1. Washington, D.C.: U.S. Department of Energy, Office of Civilian Radioactive Waste Management. ACC: HQO.19950124.0001.

DOE (U.S. Department of Energy) 1998. *Total System Performance Assessment.* Volume 3 of *Viability Assessment of a Repository at Yucca Mountain.* DOE/RW-0508. Washington, D.C.: U.S. Department of Energy, Office of Civilian Radioactive Waste Management. ACC: MOL.19981007.0030.

DOE (U.S. Department of Energy) 2000. *Quality Assurance Requirements and Description.* DOE/RW-0333P, Rev. 9. Washington, D.C.: U.S. Department of Energy, Office of Civilian Radioactive Waste Management. ACC: MOL.19991028.0012.

Dyer, J.R. 1999. "Revised Interim Guidance Pending Issuance of New U.S. Nuclear Regulatory Commission (NRC) Regulations (Revision 01, July 22, 1999), for Yucca Mountain, Nevada." Letter from Dr. J.R. Dyer (DOE/YMSCO) to Dr. D.R. Wilkins (CRWMS M&O), September 3, 1999, OL&RC:SB-1714, with enclosure, "Interim Guidance Pending Issuance of New NRC Regulations for Yucca Mountain (Revision 01)." ACC: MOL.19990910.0079.

Kotra, J.P.; Lee, M.P.; Eisenberg, N.A.; and DeWispelare, A.R. 1996. *Branch Technical Position on the Use of Expert Elicitation in the High-Level Radioactive Waste Program.* NUREG-1563. Washington, D.C.: U.S. Nuclear Regulatory Commission. TIC: 226832.

NRC (U.S. Nuclear Regulatory Commission) 1998. *Issue Resolution Status Report Key Technical Issue: Total System Performance Assessment and Integration.* Rev. 1. Washington, D.C.: U.S. Nuclear Regulatory Commission. ACC: MOL.19990105.0083.

NRC (U.S. Nuclear Regulatory Commission) 1999. *Issue Resolution Status Report Key Technical Issue: Container Life and Source Term.* Rev. 2. Washington, D.C.: U.S. Nuclear Regulatory Commission. TIC: 245538.

YMP (Yucca Mountain Project) 1998. *Disposal Criticality Analysis Methodology Topical Report.* YMP/TR-004Q, Rev. 0. Las Vegas, Nevada: Yucca Mountain Site Characterization Office. ACC: MOL.19990308.0035.

YMP (Yucca Mountain Project) 1999. *Repository Safety Strategy: U.S. Department of Energy's Strategy to Protect Public Health and Safety After Closure of a Yucca Mountain Repository.* YMP/96-01, Rev. 03. Las Vegas, Nevada: Yucca Mountain Site Characterization Office. ACC: MOL.19990406.0237.

6.2 CODES, STANDARDS, REGULATIONS, AND PROCEDURES

64 FR 46976. 40 CFR 197: Environmental Radiation Protection Standards for Yucca Mountain, Nevada; Proposed Rule. Readily Available

ASTM C 1174-97. 1997. *Standard Practice for Prediction of the Long-Term Behavior of Materials, Including Waste Forms, Used in Engineered Barrier Systems (EBS) for Geological Disposal of High-Level Radioactive Waste.* West Conshohocken, Pennsylvania: American Society for Testing and Materials. TIC: 246015.

ASTM G 1-90 (Reapproved 1999). 1990. *Standard Practice for Preparing, Cleaning, and Evaluating Corrosion Test Specimens.* West Conshohocken, Pennsylvania: American Society for Testing and Materials. TIC: 238771.

ASTM G 5-87. 1992. *Standard Reference Test Method for Making Potentiostatic and Potentiodynamics Anodic Polarization Measurements.* Philadelphia, Pennsylvania: American Society for Testing and Materials. TIC: 245311.

ASTM G 61-86 (Reapproved 1998). 1987. *Standard Test Method for Conducting Cyclic Potentiodynamic Polarization Measurements for Localized Corrosion Susceptibility of Iron-, Nickel-, or Cobalt-Based Alloys.* West Conshohocken, Pennsylvania: American Society for Testing and Materials. TIC: 246716.

ASTM G1-81. 1987. *Standard Practice for Preparing, Cleaning, and Evaluating Corrosion Test Specimens.* Philadelphia, Pennsylvania: American Society for Testing and Materials. TIC: 246089.

AP-2.14Q, Rev. 0, ICN 0. *Review of Technical Products.* Washington, D.C.: U.S. Department of Energy, Office of Civilian Radioactive Waste Management. ACC: MOL.19990701.0616.

AP-3.10Q, Rev. 02, ICN 0. *Analyses and Models.* Washington D.C.: Office of Civilian Radioactive Waste Management. ACC: MOL.20000217.0246.

AP-3.11Q, Rev. 0, ICN 1. *Technical Reports.* Washington, D.C.: U.S. Department of Energy, Office of Civilian Radioactive Waste Management. ACC: MOL.19991130.0149.

AP-3.15Q, Rev. 1, ICN 1. *Managing Technical Product Inputs.* Washington, D.C.: U.S. Department of Energy, Office of Civilian Radioactive Waste Management. ACC: MOL.20000218.0069.

AP-SIII.2Q, Rev. 0, ICN 2. *Qualification of Unqualified Data and the Documentation of Rationale for Accepted Data.* Washington, D.C.: U.S. Department of Energy, Office of Civilian Radioactive Waste Management. ACC: MOL.19991214.0625.

QAP-2-0 Rev. 5, ICN 1. *Conduct of Activities*. Las Vegas, Nevada: CRWMS M&O. ACC: MOL.19991109.0221.

QAP-2-3, Rev. 10. *Classification of Permanent Items*. Las Vegas, Nevada: CRWMS M&O. ACC: MOL.19990316.0006.

INTENTIONALLY LEFT BLANK